Compressive Strength and Behavior of 8H C3000/PMR15 Woven Composite Material

by

Farshad Mirzadeh

Dissertation submitted to the Faculty of the

Virginia Polytechnic Institute and State University

in partial fulfillment of the requirements for the degree of

Doctor of Philosophy

in

Engineering Mechanics

APPROVED:

Kenneth L. Reifsnider, Chairman

Daniel Frederick

Charles W. Smith

Daniel Post

Robert L. Wheeler

December 1988

Blacksburg, Virginia

Compressive Strength and Behavior of 8H C3000/PMR15 Woven Composite Material

by

Farshad Mirzadeh

Kenneth L. Reifsnider, Chairman

Engineering Mechanics

(ABSTRACT)

Center-notched and unnotched specimens cut from Celion 3000/PMR15 woven composite panels with 60% fiber volume fraction were tested under quasi-static compressive load to failure at room temperature. Micrographic evidence clearly identifies the mode of compressive failure as fiber kinking. Each fiber in the kink fractures because of a combination of compressive and shear stresses. A post failure mechanism follows the local fiber bundle failures, which completely deforms the material by large cracks. In center notched specimens, fiber kinks start from the notch and propagate to some distance from the notch before the post failure takes place. The effect of bundle interactions on stresses and strains was clearly distinguished by comparing the results of the finite element analysis of a bundle surrounded by other plies to the results of the Moire interferometry on the edge of a laminate. A model was introduced which incorporated the micromechanical geometry as well as the constituent properties to predict the notched and unnotched compressive strengths of the woven material. For notched strength predictions, the Average Stress Criterion was used, and the characteristic distance was found to be a function of laminate thickness. Predicted notched and unnotched strengths correlate very well with the experimental results.

Acknowledgements

The author would like to thank Professor Kenneth L. Reifsnider for his guidance and advice during the course of the student's studies at Virginia Tech. Thanks are also due to professors Charles W. Smith, Daniel Post, Daniel Frederick, and Robert L. Weeler for serving on his advisory committee. Additionally, the author would like to thank for his help on running the Moire interferometry tests, and Dr. William B. Avery for allowing the author to use his finite element code.

Most of all, the author would like to thank his parents for their support and encouragement throughout his educational carrier, and his wife for her patience during the last months of his research.

The author would also like to show his appreciation to his former adviser and friend, , for directing the author toward the area of mechanics and composite materials.

Table of Contents

List of Illustrations

List of Tables

1.0 Introduction and Literature Review

1.1 Introduction

Woven fabrics have recently become an important form of reinforcement in composite materials. They provide bidirectional reinforcement in a single layer, have better impact resistance than tape laminates, and provide more balanced in-plane properties in the lamina than do unidirectional fibers. Although fabrics do not have the structural efficiency of unidirectional fibers, their easy application and economical fabrication have made them more attractive to industry. In composite aircraft structures, recent design policy requires that woven composites be used for complicated or curved parts. In the lay-up process of those parts, it is much easier to handle fabrics than unidirectional laminae. The compressive behavior of these materials has not been carefully investigated and is not well understood. This research program has analyzed the behavior and failure mode of a woven material under compressive load.

1.2 Literature Review

In the past two decades, several papers have been devoted to studying micro-buckling as a failure mode of multilayered materials and unidirectional composites subjected to compressive stresses in the direction of laminae or fibers.

The compressive strength of fibrous composites formed by the set of parallel fibers imbedded in a homogeneous matrix was first considered by Rosen [1]. He found that the buckle wave length is proportional to the fiber diameter. Two possibilities for the buckling were then considered. The first was that the fibers might buckle in opposite directions, and the so-called extension mode would occur. The second was that the fibers might buckle in the same direction, called the shear mode. Using energy methods, Rosen derived the compressive strength σ_c, for the extension mode as

$$\sigma_c = 2V_f \sqrt{\frac{V_f E_f E_m}{3(1 - V_f)}} \tag{2.1.a}$$

For the shear mode, he found that

$$\sigma_c = \frac{G_m}{1 - V_f} \tag{2.1.b}$$

where

$E_f =$ modulus of elasticity of fiber

$E_m =$ modulus of elasticity of matrix

$G_m =$ shear modulus of matrix

$V_f =$ fiber volume ratio

In his energy equations, Rosen ignored the effects of axial and shear deformation of fibers, and eventually for the shear mode he assumed that the buckle wave length is much larger than the fiber thickness, and therefore ignored a second term in the equation for that mode. His model gives much larger failure stresses than do experimental results. One of the

important reasons for this behavior is that his model is a two dimensional one, while in actual composites, fiber buckling may be three dimensional. Because of the higher degree of freedom, actual failure stresses are much lower than predicted.

Lanir and Fung [2] studied fiber composite columns under compression. They used a hexagonal array of fibers and divided the behavior into two parts, prebuckling and post buckling behavior. In their model they included the effect of separation between fiber and matrix at the interface. For the buckling of fibers in the matrix using energy method, they derived the famous formula

$$P = \frac{E_f I \pi^2}{l^2} \left(m^2 + \frac{2kl^4}{m^2 E_f I \pi^4}\right) \tag{2.2}$$

where

E_f = modulus of elasticity of the fiber

m = mode shape number

I = moment of inertia of the fiber

The second term in equation (2.2) is the contribution of the matrix. In the study of post-buckling behavior, they also considered the integrity of the fiber-matrix system. For the case when fiber and matrix remain integral, they gave the equation

$$P(e_z) = \frac{E_f I \pi^2 (m+1)}{l^2} + \frac{2kl^2}{\pi^2 (m+1)^2} - \frac{2kl^2}{\pi^2 m^2} \tag{2.3}$$

where

e_z = axial strain

The case for a separated fiber system is more involved, since it is not a simple plane strain situation; the reader should refer to reference 2. Lanir and Fung concluded that in composites subjected to longitudinal compressive loads, the fiber may buckle inside the ma-

trix, under loads which are lower than the ultimate strength. They also concluded that prebuckling debonding decreases the buckling load, and in common composites, buckling of the fibers will have no significant effect on the overall behavior of the composite in the linear elastic range.

Herrmann and Mason [3] investigated the compressive response of a wire embedded in an elastic matrix. First, the beam-column behavior of an initially crooked wire embedded in a matrix and subjected to a state of uniaxial stress was studied. Second, the possibility of buckling within the matrix of a compressively loaded straight wire was considered. They considered a case in which an infinite elastic medium is subjected to periodic loads applied at the surface of a cylindrical cavity. Two types of three dimensional elasticity solutions were used to characterize the lateral support of the wire by matrix in both cases: 1) an exact foundation model which satisfied all interface conditions between the wire and the matrix and 2) an approximate foundation model which satisfied only a portion of three conditions. They concluded that the approximate foundation model gave acceptable results when G_m/G_f was less than about .03, and that the effect of transverse shear deformation of wire was important when G_m/G_f exceeded about 0.01. The numerical results of reference 3 show that only for small ratios of shear moduli (less than 0.0001) is there a possibility of wire buckling within the matrix; since most conventional composites have shear moduli ratio of about .01 or higher, the failure occurs before the buckling occurs. Another important conclusion is that if the shear moduli ratio is sufficiently low, the tensile and compressive stress-strain curves will be quite different.

Hanasaki and Hasegawa [4] later studied the compressive strength of unidirectional fibrous composites. They assumed that fibers were initially curved and that their curvatures were parallel to each other. Therefore, three basic assumptions were made: 1) the deformation is two dimensional; 2) the influence of normal strain of matrix parallel to fibers and its Poisson's ratio could be neglected; 3) deflections and moments at both ends of a certain length of fibers were neglected. Based on the above assumptions, they derived the strength of composite material as follows:

$$\sigma = \left[1 - \frac{a\pi}{\gamma_{max}(1 - V_f)l + a\pi}\right]\left[\frac{E_f\pi^2}{12w^2l^2} + \frac{G_m}{(1 - V_f)V_f}\right]\left[V_f + (1 - V_f)\frac{E_m}{E_f}\right] \qquad (2.4)$$

where

V_f = volume fraction of fiber

l = half wavelength

a = amplitude

w = width of fiber

The maximum value of σ at γ_{max} becomes the compressive strength of the composite material, while G_m is a function of γ_{max}.

The compressive strength of Boron-Epoxy composites was studied by Lager and June [5]. Rosen's model for shear mode (2.1.b) and transverse mode (2.1.a) with an influence coefficient of .63 were used to fit the data obtained from Boron-Epoxy composites with fibers in a nearly square array.

$$\sigma_c = \frac{.63G_m}{1 - V_f} \qquad \text{shear mode} \qquad (2.5.a)$$

$$\sigma_c = 2V_f\sqrt{\frac{.63\,V_f E_m E_f}{3\,(1 - V_f)}} \qquad \text{transverse mode} \qquad (2.5.b)$$

The use of a so-called influence coefficient was justified because of the observation of out-of-plane buckling for cylinders in square array, while the idealized model assured a two dimensional effect.

Experimental data of reference 5 shows that up to a fiber volume fraction of about .08 the transverse mode dominated, and for higher fiber volume fractions, the shear mode dominated.

It was concluded that the initial shear modulus of the matrix material could be used for all axial strain levels within the useful volume fraction range of 0.10 to 0.60 because of the apparent anisotropy of the elastic properties of epoxy under a uniaxial plastic stress-strain condition. The authors also emphasized that equations (2.5.a) and (2.5.b) should not be expected to be applicable to all other composite materials such as Graphite-Epoxy.

Chung and Testa [6] investigated the problem of elastic stability of fibers in a composite plate. The spacing between fibers was assumed to be large in comparison to the plate thickness. In this investigation, beam theory was used to characterize the behavior of fibers, and a generalized plane stress formulation was used for the matrix. The analysis led to a set of complicated equations for symmetric and anti-symmetric (extensional and shear) modes of fiber buckling. If the wavelength of the buckled fibers is large in comparison to the fiber spacing, and simultaneously the matrix Poisson's ratio is set equal to zero, for large fiber-matrix moduli ratio the equations of reference 6 will collapse into equations given by Rosen [1], namely equations (2.1.a) and (2.1.b). Chung and Testa also reported experimental data on specimens made of epoxy and two grades of glass sheets. In all of the test specimens, buckling occurred within the elastic range of the materials. The critical values measured in the tests agree quite well with theoretical predictions.

Compressive strength of unidirectional composites and factors influencing it were discussed by Foy [7]. The energy method was used to show that the compressive strength was equal to the composite shear modulus when the composite was treated as a macroscopic, homogeneous, orthotropic material. That is,

$$\sigma = G \tag{2.6}$$

where

G = shear modulus of composite

Foy showed that the Reuss estimate or a "stiffness in series" model

$$\sigma = G = \frac{G_m}{(1 - V_f) + V_f \frac{G_m}{G_f}} \tag{2.7}$$

would result in equation (2.5.a) as the ratio of G_m/G_f approaches zero; for most composites,this is true. The reason is that Rosen's model neglects the strain energy due to shear deformation of fibers. However, as the fiber volume fraction approaches unity, the second term in the denominator of equation (2.7) becomes important. Foy also discusses the effect of voids, fillers and whiskers on the shear modulus and compressive strength of composites and notes that voids reduce and fillers increase the compressive strength.

Compressive strength of Boron-Metal matrix composites was investigated by Schuerch [8]. He apparently derived Rosen's equations (2.1.a) and (2.1.b) with the exception that for the symmetric case he multiplied the fiber crippling stress by the factor

$$\frac{1}{E_f}[V_f E_f + (1 - V_f)E_m]$$

to obtain the composite strength, while Rosen simply multiplied it by fiber volume fraction. Schuerch also discussed micro-stability domain and limits on elastic and inelastic crippling failure. He also proposed that the tangent shear modulus be used in the strength equations to include the effects of nonlinear behavior of matrix. Shuerch assumed isotropic behavior in the nonlinear portion of the stress-strain curve for the matrix material, that

$$G_{mt} = \frac{E_{mt}}{2(1 - \nu)} \tag{2.8}$$

where

G_{mt} = tangent shear modulus for the matrix

E_{mt} = Tangent modulus for the matrix

Theoretical and experimental results on the compressive of strength of Boron- Magnesium composite specimens were shown to agree with each other.

Sadowski et al. [9] studied the basic phenomenon of buckled fibers in composites qualitatively. Their analysis lead to a relation between the pertinent elastic and thermal characteristics of the matrix and fiber, and the compressive force along the axis of the fiber at the critical moment of incipient buckling.

De Ferran and Harris [10] in a study of the compressive strength of steel wire reinforced polyester resin showed that most of the above analyses are inadequate for predicting the compressive strength of composites. Their experimental data show that the strength can be calculated by the rule of mixtures using the tensile strength of the steel wire. For specimens containing cold-drawn wire the yield stress was used, whereas the ultimate strength was used in calculations for specimens reinforced with an unnealed wire.

Argon [11] considered a region of initial element misalignment, where the reinforcing element made an angle ϕ_0 with the compression axis. Then, he developed a simple relation for the shear collapse mode of failure in composites by analogy with kink bands in metal crystals. By setting equal to zero the total energy obtained by adding the external work, the change in elastic energy outside the band and the plastic work done inside the band, and the energy due to the double bending of the lamellae, he arrived at the following relation for the compressive strength.

$$\sigma = \frac{K}{\phi_0} \tag{2.9}$$

where K is the interlaminar shear strength. Apparently this relation is independent of the properties and fiber volume ratio of the composite.

Greszczuk [12] studied microbuckling of perfectly straight fibers in unidirectional composites. Using energy methods, he obtained the compressive strength of the composite as

$$(\sigma)_{cr} = G_{TL} + \pi^2 E_f k\,(r/l)^2 \tag{2.10}$$

where

$G_<$ = Shear modulus of composite

k = Fiber volume fraction

r = Radius of fibers

l = Buckle wave length

Comparison of the experimental results with theoretical values obtained from equation (2.10) showed an overestimate of the compressive strength by this equation.

Weaver and Williams [13] observed fiber kink formations in unidirectional carbon-epoxy specimens under hydrostatic pressure, and proposed a model for kinking in the composite based on the initiation of fracture in buckled fibers. They obtained the fiber failure load using Euler's equation without consideration of the matrix contribution in supporting the fibers; the theoretical values calculated were 50% higher than the experimental ones.

Chaplin [14] studied the shear mode of compressive failure in unidirectional composites. He explained the relationship between the orientation of the kink band and the limiting shear deformation in the band in terms of volumetric strains. However, he was unsuccessful in understanding the conditions which govern the initiation of the kink band.

A detailed analysis of the kinking as a mode of failure in carbon fiber composites and the process of kinking was presented by Evans and Adler [15]. The key micro-structural parameters that dictate kinking under both axial compression and shear were studied and their correlation to the process of kinking was determined.

In their study, Evans and Adler used three dimensional carbon-carbon composites with bundles of rectangular cross-section. Three principal modes of kinking were observed: kinking due to longitudinal compression, lateral compression, and lateral displacement or *shear*. The kink morphologies for longitudinal compression and lateral displacement were noticed to be very similar. To account for the observed kink morphologies, a thermodynamic analysis of kinking in terms of the strain energy and plastic work associated with the matrix was also performed. Evans and Adler suggested that inclination of the kink is controlled by

minimization of the plastic work, while minimization of the elastic strain energy determines the kink boundary orientation.

Using fracture and deformation parameters, an approximate expression for the critical kink formation stress was obtained as

$$\tau_{Ac} = \frac{\pi C \sigma_c}{3d_s(2 + \frac{d_f}{C})^2(\frac{d_s}{d_b} + 1)^2} \tag{2.11}$$

for shear kinks, where

C = fiber radius

d_s = separation between bundles

d_f = separation between fibers

d_b = bundle diameter

σ_c = critical remote stress causing unstable crack growth in a fiber

No formula was given for the critical compressive stress that initiates compressional kinks. However, it was mentioned that the critical compressive stress for the elastic buckling of a fiber or a fiber bundle can be an upper bound in the kink initiation condition for this type of loading.

Parry and Wronski [16] examined the compression failure of uniaxially aligned carbon fiber composites under superposed hydrostatic pressure, and suggested that the failure process involved kinking with eventual separation along one or both of the kink boundaries. They also suggested that the group of micro-buckled fibers failed by a tensile mechanism. This statement may be subject to criticism because of the high compressive stresses in the fibers at the onset of failure.

Hahn and Williams [17] studied the compressive behavior of unidirectional graphite/epoxy composites using two different fibers and four different resin systems. These authors identified the predominant macroscopic failure mode as shear crippling when the resin is stiff. When the resin is soft, however, the microbuckling can replace kinking.

Compressive failure of anisotropic plates with cutouts under compressive and shear loads was studied by Gurdal and Haftka [18]. Their failure model was based on the kinking failure of fibers and included the effects of local compressive and shearing stresses near a cutout on the fibers. Fibers were modeled as beams on an elastic foundation. Using the energy method they arrived at the fiber buckling load

$$P_{f,c} = 2cG_m(1 + \frac{h}{2c})^2 + \frac{\pi^2 E_f I_f}{l^2} \tag{2.12}$$

where

h = width of fiber

$2c$ = clear distance between fibers

l = fiber length

Comparison of the model predictions with the available experimental results for quasi-isotropic and orthotropic plates showed a good agreement for the kinking failure model. The results of this model were also compared to the results of a point-stress model; in some cases, e.g. for quasi-isotropic laminates, there are large differences between the two predictions. However, for 0° dominated laminates the two predictions agree quite well.

Among the researchers who studied the effect of holes and notches on the behavior of composite materials, the most distinguished are Whitney and Nuismer [19]. They introduced two stress fracture criteria for laminated composites containing stress concentrations. The two criteria based on the laminate normal stress distribution near the discontinuity were developed for predicting the residual strength of laminated composites. In the first approach (the point stress criterion), it was assumed that failure would occur when the stress at some distance, d_0, away from the discontinuity is equal to or greater than the strength of the unnotched material. In the second approach (average stress criterion), it was assumed that failure would occur when the average stress over some distance a_0 away from the discontinuity is equal to the unnotched laminate strength. Both approaches show capability of predicting discontinuity size effects without application of LEFM. Comparison of theory and experimental data for

quasi-isotropic Glass/Epoxy and $(0, \pm 45)_s$ Graphite/Epoxy showed good correlation. It was concluded that the characteristic lengths a_0 and d_0 may be material constants independent of laminate geometry and stress distribution. It was also shown that a relationship existed between mode I fracture toughness and crack length by using the exact stress distribution ahead of the crack tip for an isotropic plate.

Tan [20] applied the first ply failure (FPF) criterion to predict the notched tensile and compressive strength of the PEEK matrix composite laminates under quasi-static uniaxial loading for different hole sizes. His test specimens consisted of both quasi-isotropic and orthotropic laminates containing a circular center hole. Two strength prediction models were used. In model A, the ratio of the notched FPF strength at the point $(0,b_1)$ over the unnotched FPF strength was assumed to be equal to the ultimate strength reduction. Hence the strength reduction factor was defined as

$$SRF = \frac{\sigma_N^{\infty}}{\sigma_0} = \frac{FPF\ (notched)\ at (0, b_1)}{FPF(unnotched)} \tag{2.13a}$$

where

σ_N^{∞} = Ultimate notched strength

σ_0 = Ultimate unnotched strength

In (2.13a) b_1 is a characteristic distance away from the discontinuity on the axis normal to the applied load.

In model B, a characteristic curve concentric to the opening at a distance b_0 from its boundary was considered. The stress reduction factor was defined as

$$SRF = \frac{\overline{\sigma}_N^{\infty}}{\overline{\sigma}_0} = \frac{FPF\ (Notched)\ at\ \dfrac{X^2}{(a+b_0)^2} + \dfrac{Y^2}{(b+b_0)^2} = 1}{FPF\ (Unnotched)} \tag{2.13b}$$

where $\overline{\sigma}_N^{\infty}$ and $\overline{\sigma}_0$ are defined the same as σ_N^{∞} and σ_0. The gross failure stresses were then computed for an infinite width laminate with circular hole and center crack, respectively, using the following formulas.

$$\frac{K_t}{K_t^{\infty}} = \frac{2 + (1 - \frac{2a}{W})^3}{3(1 - \frac{2a}{W})} \tag{2.14.a}$$

$$\frac{K_t}{K_t^{\infty}} = \sqrt{(\frac{W}{\pi a}) \tan(\frac{\pi a}{W})} \tag{2.14.b}$$

where

$W =$ Width of the specimen

$2a =$ Effective normal crack length or hole diameter

FPF model B correlated quite well with the experimental data, and the predicted strength using model A agreed with the data generally. However, in some cases the characteristic distances b_1 and b_0 had to be modified. The modification suggested had the forms

$$b_1 = m_1(\frac{a}{a_r})^e \tag{2.15.a}$$

$$b_0 = m_0(\frac{a}{a_r})^n \tag{2.15.b}$$

where m_1, e, m_0, and n are constants to be determined from a minimum of two data points, and a_r is the reference hole radius which can be taken as unity.

Tan observed that generally the notched strength predicted using a constant characteristic length was more accurate in the tension case than in the compression case. For both notched compressive and notched tensile strengths the modified model A resulted in the best fit over experimental data for both quasi-isotropic and cross-ply laminates. Model B was used for the strength prediction of laminates with slanted cracks and the modified model B gave the best fit over experimental data.

Tan also derived approximate solutions for the normal stress distribution of orthotropic laminates containing elliptical holes [21]. A notch sensitivity study revealed that the effect of the opening aspect ratio upon the notched strength is more significant for larger openings.

In another paper [22], Tan conducted an experimental program to check the accuracy of his extended point stress and average stress criteria for laminates containing a circular hole, an elliptical hole, and a center crack. Although the comparisons were quite good, he found that the characteristic lengths, d_0 and a_0, were functions of the opening aspect ratio. Therefore, he presented a modified criterion that expressed the characteristic lengths as functions of the opening length and aspect ratio.

Mikulas Jr. [23] conducted a study to investigate the notch sensitivity of graphite epoxy material in compression. He suggested that there are two ideal cases which are called notched sensitive (brittle) and notch insensitive. The fact that the data points of the above material system fell above the notch sensitive curve indicated that the material was not ideally brittle and some load redistribution had occurred around the hole. Comparison with idealized limiting failure cases showed that the degree of notch sensitivity was dependent upon the hole size. Graphite epoxy laminates with a hole greater than 5 cm were found to behave as ideally brittle material in compression, and failure could be predicted using a classical stress concentration factor. Mikulas found that for smaller holes, the point stress failure criterion of reference 15, considering finite width effects, would provide reasonable compressive failure predictions.

Although the authors mentioned in the above literature review have made considerable contributions to the understanding of compressive behavior and strength of composites, none of them has worked on the compressive behavior of composites made from woven bundles of Celion 3000 graphite fibers and PMR15 matrix or any other woven constituents. In the past few years, however, a few researchers have worked on the theoretical prediction of the elastic moduli of satin weave fabric composites. Among those, Ishikawa and Chou have been the most active in this area. The anti-symmetry in this type of composite was investigated by Ishikawa [24] and closed form solutions of the upper and lower bounds of the stiffness and compliance were obtained by a series model assuming constant stresses and strains. Also, three-dimensional finite element analyses were carried out, the results of which fell between the upper and lower bound obtained by closed form solutions.

Elastic behavior of woven fabric composites was investigated by Ishikawa and Chou [25]. They obtained the lower and upper bounds of elastic properties using the mosaic model regarding the fabric composite as an assemblage of asymmetrical cross-ply laminates. These authors also introduced two other models, the fiber undulation and bridging models [26,27] in an attempt to analyze the composite threadwise and obtain the stiffness properties. The stiffness prediction of eight-harness satin composites by the bridging model showed good correlation with experimental data. Ishikawa and Chou have also worked on the analysis of woven hybrid composites [28], experimental confirmation of elastic moduli [29], thermoelastic properties [30], and nonlinear behavior of fabric composites [31].

1.3 Objective

In this study our attention is directed toward the damage and failure mode of a woven material in compression. The literature is very incomplete in this area. In fact, compressive mechanistic models of strength are not available for laminates, especially laminates made of woven materials. To provide the basis for such a model, we had to establish the precise micro-failure mechanism for compressive load, and investigate the local stresses associated with that mechanism.

The objective of this research program was to develop a mechanistic model which can predict the compressive strength of woven composite laminates under quasi-static loading environments. To create such a model, it was necessary to establish a correct mechanical representation of the micro-failure mechanism in terms of micro-geometry and material properties. Then we attempted to relate the global compressive strength to constituent properties, and local geometry and stresses, which will enable us to improve laminate strength by material design for these material types. The following steps were taken in the course of this study.

a) Compression testing of at least five specimens of each lay-up, notched and unnotched, were performed on MTS load frames in the Materials Response Group laboratory. The average test data for each laminate was compared to the predicted values by the model.

b) Investigation of local failure mode and failure process was necessary for damage identification. Several destructive and nondestructive techniques, such as C-scan, X-ray analysis, and deply of laminates for fiber observations under SEM, were used to detect damaged areas, delaminations, and modes of fiber failure. Edge and surface replicates were also made during and after load application to identify any damage occurrence.

c) Finite element modeling of a lamina embedded in the surrounding material was performed using finite element analysis, we obtained important information about bundle deformations, strains, and stress distributions across the bundle, which were helpful in understanding material behavior.

d) Moire interferometry was performed to examine the true micro-behavior of the material, displacement and strain distributions, and interactions between the bundles.

The importance of this research program lies in understanding the behavior of woven composites in relation to the type of weave, bundle geometry, and material properties, which is the key to better design of woven composite laminates and prediction of their strength and stiffnesses.

2.0 Experimental Investigation

2.1 Introduction

The experimental characterization of composite materials is generally more complicated than for homogeneous, isotropic materials, because composites behave in a much more complicated fashion, due to macroscopic anisotropic effects such as orientation dependency and coupling effects as well as microscopic deformation and damage process.

A researcher studying the compressive behavior of composite materials frequently encounters difficulties associated with the proper interpretation of data, which generally have scatter. There are various failure modes that are suspected of inducing compressive failure such as fiber kinking, symmetric or nonsymmetric microbuckling of fibers, and delamination. The scatter in compression data becomes worse due to the sensitivity of compression testing to global Euler buckling, specimen misalignment in the grips, bending/stretching coupling, temperature or moisture in the laminate, quality of the material, or uneven loading.

2.2 Material System

2.2.1 Matrix System

The matrix material in the present study is PMR-15. PMR polyimides are gaining acceptance as high temperature resistant matrix resins for aerospace applications. Composite and bonded materials fabricated from PMR polyimide resins offer end use temperatures up to 600°*F*(316°*C*), nearly twice the end use temperatures of epoxy resins. PMR polyimide resins offer processing advantages over condensation polyimides since they avoid using high boiling solvents which often lead to void formation. Thermally stable polyimides are prepared by condensing an aromatic polyamine, an aromatic dianhydride and a specific monoanhydride for capping the polymer chain. The reaction is carried out in a solution of dimethyl formidide and toluene. High molecular weight solid prepolymers are dispersed in low molecular weight prepolymers dissolved in solvent, then applied to carbon cloth and cured in the range of 450°*F*(232°*C*) to 600°*F*(316°*C*) under pressure. By this means products of high heat resistance are obtained.

The concept of using polymerizable monomer reactants (PMR resins) dissolved in easily evaporable solvents, such as methyl alcohol, led to better controls and processing. At this time, aerospace and aircraft components are being made from graphite fibers in a PMR resin matrix. The number 15 in PMR-15 designates 1500 molecular weight [32].

2.2.2 Fiber System

The fiber material is Celion 3000, which is one of a family of high strength carbon fibers used as reinforcement in high performance composites. Celion 3000 is suggested for making thin ply prepreg, where uniformity of fiber distribution is important, and for weaving fabrics

of moderate thickness. Excellent oxidative stability permits use in polyimide or other high temperature matrix systems. Celion 3000 is suitable for reinforcement of structural composites for aerospace applications, or recreational and industrial products.

2.2.3 Composite System

Fabrics are formed by interlacing two sets of threads. The pattern of interlacing can be understood from figures 1a and 1b, where the horizontal and vertical fibers in figure 1a are called the fill and warp fibers respectively. Each ply of the laminate is actually a combination of 0° and 90° fibers interwoven, and the fill fibers are considered to be in the 0° direction. Likewise, a 45° ply contains fibers in both 45° and $-45°$ directions. In this investigation we used an eight-harness satin with three types of laminates. For simplicity of terminology, henceforth we will call the 0° laminate *unidirectional* , the fibers in the 0° direction, the *fill* fibers; and the ones perpendicular to those, the *warp* fibers. We will also call the laminates made of stacks of (0,45,0,45,0) *orthotropic*, and the ones made of stacks of (0,45) *quasi – isotropic*. In all laminates, plies are stacked without symmetry about the midplane; therefore on one side of the laminate mostly fill fibers (and on the other side mostly warp fibers) are visible. Since each ply consists of two perpendicular fiber directions, one may assume that there are no geometric differences between the two directions. But because of the weave geometry, the fiber volume fractions in the two directions are slightly different such that fill direction has a slightly higher fiber volume fraction of about 65%. The fiber volume fraction in the bundle was determined to be 80% using microscopic pictures and fiber geometry; therefore there are regions of pure matrix between the fiber bundles as shown in figure 2.

2.3 Specimen Preparation

Before cutting each panel, the modulus of elasticity of the laminate was evaluated by the classical lamination theory. Then the modulus was used to estimate the maximum unsupported length needed between the two grips such that global buckling would not take place. Because of these limitations, specimens cut from different panels had slightly different lengths.

Notched and unnotched specimens shown in figure 3 were cut from six panels with different layups (table 1) using a round diamond saw in the work shop of the Engineering Science and Mechanics Department. Specimens which were supposed to be investigated during the test, or after failure took place, were polished along their edges by 600 grit sand paper to make the saw scratches disappear. Then, the specimens were further polished using 5 micron aluminum oxide powder. Polishing the edges enabled us to make edge replica during and after the tests.

2.4 Test Methods and Equipment

Several tests have been conducted to investigate the triggering mechanism in the failure and its process. Notched and unnotched test specimens were tested using two MTS servo hydraulic load frames with 50 and 20 kip capacities. The choice of load frame depended on the type of laminate used, specimen geometry, and compressive strength. Hydraulic grips were used to hold the specimens without any fixtures , except for two alignment plates which were used to align each specimen with the load direction. Sand paper was used as tabs to protect the specimens from surface damage in the grip zones. All specimens were loaded to failure under quasi-static loading, in displacement control mode, and in the fill direction. Figures 4a and 4b show the 20 kip MTS load frame and the grip configuration respectively.

2.5 Test Results

2.5.1 Unnotched Specimens

The configuration of any notched or unnotched specimen after post failure consists of a wide center-crack denoted by B along the length of specimen, and two other cracks denoted by A as shown in figures 5a and 5b. It seems that cracks A opened first; then, because of the wedge shape of one side of the specimen, crack B propagated down and away from cracks A. In a well-aligned grip situation these cracks can form more easily in the middle of the unnotched specimen because of a smaller constraint imposed by the grips. But if the grips are not aligned properly, the intersection of cracks A and B will be closer to one of the grips.

As shown in figure 6, the load-displacement graph of an unnotched unidirectional specimen under quasi static loading showed slight nonlinearity as the load increased. Failures in the unnotched specimens were quite sudden, and their Young's moduli in the load direction had positive values at failure.

The load-displacement graph of the same type of specimen tested under incremental compressive loading is also shown in figure 6. At low load, the material did not show considerable viscoelastic behavior. But at higher loads, quick load relaxation was noticed; most of the load relaxation took place in the first two minutes of each sustained displacement increment. The graphs of both specimens followed the same path closely, but the incrementally loaded specimen showed slightly lower strength. This type of loading was not pursued to determine whether it would result in a lower or a higher compressive strength. However, during the course of this experimental investigation we found that initiation and propagation of damage explained in the next section is a time-dependent phenomenon for stresses near ultimate strength. Therefore it is possible that incremental loading would generally result in lower compressive strength. The halted test whose graph is shown in figure 6 will be explained in the next subsection.

Back-to-back 1″ extensometers were used as shown in figure 7 to obtain the stress-strain response of 22-ply unidirectional and 15-ply orthotropic unnotched specimens. Because compressive failure of specimens would damage extensometers, these tests were stopped before the failure occurred. The stress-strain graphs in figure 8 show that at low tensile and compressive stresses, the strains on both sides of the specimens were almost equal. At higher compressive stresses, however, the curves diverged from each other, and the warp side showed somewhat higher strains. Each ply of a woven fabric is unsymmetric and when stacked on top of each other, they produce an unsymmetric laminate, although the stacking sequence may seem to be symmetric with respect to the mid-plane. This lack of symmetry in the laminates results in the divergence of the stress-strain curves as mentioned above. As the ratio of 0° to 45° plies decreases, the degree of unsymmetry will increase proportionately. This is the reason for the large divergence in the curves of the orthotropic laminate.

2.5.2 Kink Observations

Since our search for the failure mode after the catastrophic failures of specimens was inconclusive, we tried to stop one of the tests at the onset of failure. After a few trials, the test was halted before the propagation of damage took place. The load-displacement graph obtained from the test (figure 6) indicates that the specimen lost its load-carrying capacity at 94.33 ksi (650 MPa). At this point, the specimen was considered to be failed since further increase in the displacement would only have triggered the post-failure mechanism, which would change the specimen configuration to the ones shown in figure 5. The five load drops noticed in this graph are due to the halts in the test to make edge replicates of the specimens. Although this graph may look like the graph of an incrementally loaded specimen, the time durations in which the displacements were held constant were very short. Therefore, we do not consider this test to be an incremental test.

Examination of the specimen during and after the halted test revealed that fiber bundle kinking was the mode of failure of the material at hand. Figure 9 (an edge replicate) shows a kink in the second ply, formed during the test under a compressive stress of 83 ksi (572 MPa). Fiber kinks and following matrix cracks were also observed on the edge of the specimen at loads as low as 86% of the ultimate strength. However, these fiber fractures were only found near the edge, and may be called *edge effect* kink failures. These failures, such as the one shown in figure 9, were not found to occur at any place far from the edge at such low loads as 86% of the ultimate. The same kink after removal of the load is shown in figure 11a.

Examination of the surfaces after the test revealed several fiber kinks on the fill surface which resulted in an area of delamination under the fill surface ply near one of the grips, spread over almost the entire width of the specimen. The damage consisted of kinks in the fill fiber bundles, extending across two neighboring bundles. The kinks occur because of high compressive stresses in the exposed parts of the fill fiber bundles on the fill side of the specimen. Figure 10 shows the delaminated area of the specimen between the first and the second ply, detected by an ultrasonic C-scan. The delamination seen is the result of the propagation of the cracks emanated from the surface fiber fractures. Other small areas of delamination were also noticed, some near the grip area.

When internal fiber kinking was determined as a possible mode of failure in the material, other failed specimens were investigated for fiber kinks. Kinks were found to be abundant and spread along the length and across the thickness of failed specimens. Most of the kinks had a shear-kink configuration consisting of two parallel cracks causing lateral displacement of fibers similar to the configurations shown in figures 11a and 11b. But some of them consisted of only one crack which completely split the fiber bundle (figure 12a), or a partial kink such as shown in figure 12b. We believe that the *post failure* mechanism starts with propagation of the kink boundary cracks into the matrix material parallel to the plies and perpendicular to the loading direction toward the closest region of high stress, which is susceptible to kink failure in the neighboring bundles, causing premature fracture of those bundles. This process results in the formation of cracks of type A in figure 5. These fractures, along with the longi-

tudinal matrix cracks, will eventually cause the catastrophic failure of the entire specimen, and will give the specimen the configurations shown in figure 5.

It is important to distinguish between the failure itself and the post failure phenomena. The failure occurs when many fiber bundle kinks form and result in the loss of the load carrying capacity of the material. Further straining will result in the quick propagation of cracks emanating from the kinks; this is the post failure phenomenon.

2.5.3 Kink Morphology

Figure 13 shows a fiber bundle kink formed by the rotation of a group of fibers of equal length away from their original position. The geometry of the kink is a function of the strain energy of the system [14]. Because of these geometrical constraints, the line which is formed by the points of fiber fracture called the kink boundary, bisects the angle between the original direction of the fibers and the kinked direction. The kink morphology in the failed specimens was similar to that observed in many other systems by others such as noted in reference 15.

From the principal kinks mentioned in reference 15, a combination of compressive and shear modes was detected here which showed up in the curved portions of the fiber bundles, between the peak and the maximum slope locations of the bundles. The kink boundaries were almost parallel, and all kinks were of out-of-plane type. The average kink width was approximately equal to 0.0025 -in., which is 9 to 10 times the fiber diameter, and about 0.46 times the bundle thickness. The kink orientation angle α, defined in figure 13, is not known exactly. But from figure 11a, the measured values of the kink boundary orientation β is 20°. The angle β in another fiber kink (figure 11b) has a value of approximately 20°. Since β was constant in all of the kinks observed, it may be considered as a characteristic of the material. The compressive strength data of the unnotched specimens are listed in table 1.

Because of the constraints imposed by the strain energy of the system during the kink formation, the angle α must be twice the angle β [13]. However, it is almost impossible to

measure α at the time of kink formation, and its values are quite different under load and after removal of the load.

2.5.5 Notched Specimens

Notched specimens cut from all six types of laminates listed in table 1 were tested under quasi-static compressive load. Smaller scatter was noticed in the compressive strengths of center-notched specimens compared to those of unnotched ones, because damage in notched specimens always starts in the stress concentration region near the notch and propagates away until the specimen fails completely. Therefore, in the notched specimens, failure always occurs in the middle of the specimen, although in the unnotched ones this is not usually the case.

The experimental observations show that the 0° plies are the first plies that fail. The 45° plies, however, do not fail until all the 0° plies have lost their load- carrying capacity. Therefore, the mode of failure in the 45° plies is different from the 0° plies, because of the existence of in-plane shear stresses in the local directions of the 45° plies.

Individual plies of an unnotched and a notched specimen obtained by the deplying technique which is explained in the next section are shown in figures 14 and 15 respectively. Splits in the 0° plies were caused by the post failure mechanism. The failure boundary is straight and perpendicular to the load direction at every point. The failure boundary in the 45° plies , however, has a zigzag shape splitting the ply along and perpendicular to each bundle. Failure in these plies was obviously caused by in-plane shear stresses in the 45° direction. Failure of the quasi-isotropic laminates (notched and unnotched) were not as sudden as unidirectional laminates. This was apparently because of the support provided by the unfailed 45° plies after the 0° plies fail.

In all of the laminates tested, fiber bundle failures started from the surface ply and propagated through the thickness of the laminate. Therefore, one may claim that if two specimens

of the same type of laminate but different thicknesses are tested, the thicker one will have a higher strength because propagation of damage through the thickness would require increase in the applied compressive stress. We know definitely that in unnotched specimens damage propagates through the thickness in fractions of a second. As table 1 indicates, the 8-ply quasi-isotropic laminate shows unnotched and notched strengths slightly smaller than those of its twelve-ply counterpart. More interesting is the behavior of the orthotropic 15-ply and 20-ply laminates. The 20-ply laminate shows a higher unnotched , but a lower notched strength than the 15-ply laminate. The unidirectional laminate also shows such a *reverse behavior* similar to orthotropic laminates. We do not know the definite reason behind this reverse behavior. However, we know that different panels of the same laminate type might have gone through slightly different cure processing, and this may be the reason for the scatter in the test data and the behavior explained above. Other factors such as test procedure, alignment, and type of loading device might have affected the results.

To examine the initiation and propagation of damage, several notched specimens were loaded to a value estimated to be near the failure load, until a few bundle kinks occurred in the surface plies. Then the specimens were examined under a microscope, and X-rays were taken to determine the amount of damage. They were then loaded again very slowly to cause propagation of damage, and were subsequently deplied and examined. Unidirectional laminates and thin quasi-isotropic laminates did not show considerable growth of damage before complete failure. But thick quasi-isotropic and orthotropic laminates showed more damage growth before failure. This can be noticed in the X-ray radiographs of a 12-ply unidirectional, a 15-ply orthotropic, and a 12-ply quasi-isotropic laminate in figure 16. The dark lines in the radiographs are the tracer lines in the fiber directions.

2.6 Deplying Technique

One of the most effective destructive techniques available for examination of the type, extent, and location of fiber damage inside a material is the deplying technique. The specimen under investigation is placed in an oven, and the temperature is raised to a level which vaporizes the matrix material. To prevent oxidization of fibers, an inert gas such as Argon passes through the oven, and fumes are sucked out by a hood on top of the oven. Once the matrix is evaporated, delaminations take place, and plies can be separated very easily. This must be performed cautiously to prevent any alteration of fiber fractures caused by the compression test.

The above mentioned three specimens were kept at 1290°*F*(700°*C*) for six hours, and were deplied subsequently. Each ply was then kept at 1470°*F*(800°*C*) separately for one minute to allow the excess matrix material which had remained on the surface of the ply to evaporate.

Figure 17 shows the first three kinks formed in the surface ply of a 12-ply unidirectional specimen (N03). The kink on the right side of the hole arrested, but the one on the left side propagated and caused another kink in the neighboring bundle. This phenomenon is similar to the propagation of the tensile fiber breaks in a unidirectional lamina and the concept of shear lag. Once a kink occurs in a bundle, the bundle loses its load-carrying capacity in the vicinity of the kink. Thus the load will be transferred to the neighboring bundles through shear stresses. This happens not only in the plane of the ply, but also through the thickness of the laminate. Damaged areas of this specimen seen in the X-ray radiograph of figure 16a correspond well to the location of the fiber fracture in the surface ply. The other eleven plies in this specimen did not have any fiber fractures.

In the 15-ply orthotropic specimen (NB3) almost all of the 0° plies contained fiber kinks near the notch, but no kinks were found in the 45° plies. Figure 18 shows the fiber fractures near the notch in two plies of this specimen. The kinks in the 0° plies extended as far as the

fifth bundle from the notch on one side, and as far as the third bundle on the other side of the notch. Each bundle is approximately 0.05 -in. wide. The extent of damage shown in figure 18 also corresponds well to the X-ray radiograph of this specimen shown in figure 16b.

Figure 19 shows the first and the tenth ply of specimen NB8, cut from the 12-ply quasi-isotropic laminate. Fiber kinks extended to the fourth bundle on one side and to the second bundle on the other side in the surface ply. The extent of damage seen corresponds to the X-ray radiograph of this specimen, shown in figure 16c.

In observing the failure of compression loaded specimens with holes, it was frequently noted that in approaching the failure load, local fiber kinking occurred near the edge of the hole, although not necessarily at the location of maximum stress factor. For example, the kink on the right side of the notch in figure 17 formed exactly at the location of highest stress concentration of the notch, but the ones on the left side of the notch started from the crimp part of the first bundle.

2.7 Scanning Electron Microscopy

Several plies of a post-failed unidirectional laminate were deplied and examined under a Scanning Electron Microscope. Lengths of fibers in the kink band shown in figure 20 vary between five to eight times the fiber diameter. However, in figure 11, we observed that the fibers in the kink were much longer as was mentioned before. It is possible that short fiber kinks are the consequences of a dynamic behavior, namely the post-failure of the material. Short fiber kinks of reference 13 were called the *artifacts* of post-failure by the authors of reference 16. Short kinks were usually noticed in the straight portions of bundles. During the post failure phenomenon, delaminations which appear on the edge as cracks B (figure 5) would cause sudden increase of compressive stress in the unfailed bundles next to the delamination. It is possible that these unsupported bundles buckle at their higher modes, and result in short fiber kinks which were observed under SEM.

Figure 21 shows the fracture surfaces of the fibers in the kink band, some of which on the left side of the picture have two fracture surfaces. However, this phenomenon cannot be explained at this point. Some of the fracture surfaces in other kink bands shown in figure 22 were found to have 45° angles, which implies failure by a maximum shear stress state caused by axial compressive stresses.

3.0 Finite Element Analysis

3.1 Introduction

Among the researchers who have investigated the mechanical behavior of woven composite materials, only a few have used finite element methods. Ishikawa et al. [24] used FEM to examine their bound theories for the *mosaic model*. Later, they checked the applicability of their approximate theories by finite element analysis of the *fiber undulation model* [25]. Kriz [33,34] used FEM to study the response of plain weave glass-epoxy laminates to cryogenic temperatures. Stiffness and stress distributions were calculated for an undamaged and a damaged composite under thermal-mechanical loading. Other researchers such as Kimpara et al. [35], Jortner [36], and Stanton et al. [37] have also used FEM to investigate woven composites. Walrath and Adams [38] have done a literature review of the use of finite elements on composite materials.

Our purpose of using FEM here is not to investigate the mechanical behavior of the woven composite at hand in detail such as done by Avery [39], but rather to get an insight into the local behavior, and to compare the strain distributions in the bundles to the ones obtained from photomechanics.

3.2 Finite Element Code

The code (NVT3), used here, is a linear elastic finite element code developed under the assumption of generalized plane strain by Avery [39]. This assumption allows the user to study the response of an infinitely long body of arbitrary cross section to various mechanical loadings with the restriction that all quantities except axial displacement are independent of the axial coordinate z. Global and local coordinates and their situations with respect to the body are shown in figure 23.

3.3 Finite Element Mesh

The mesh was generated on a bundle the geometry of which was obtained from micrographic pictures. Two types of elements were used in the analysis: the 6-node triangular isoparametric element and the 8-node quadrilateral isoparametric element. These elements are standard orthotropic elements. The orientation angle of these elements with respect to the x axis can be input for the purpose of transformation of local material properties. Due to the geometrical symmetry which exists in bundles, we only needed to model a ply containing half of the repeating length of a bundle. Figure 24 shows the undeformed mesh of a ply of the material. The mesh plot in this figure does not have the same scale in both x and y directions. This way, the element and node numbers can be read easily. Elements 1 through 76 are elements of the fill fiber bundle under examination along the x direction, elements 77 through 201 are elements of warp fiber bundles along the z direction, and finally elements 201 through 257 are elements of pure matrix. The other plies which surround this ply are modeled as homogeneous orthotropic elements 258 through 485, shown in figure 25.

3.4 Material Properties

3.4.1 Matrix Properties

The tensile modulus E_m of PMR15 was obtained from General Electric Company, and the compressive modulus was assumed to be equal to the tensile modulus. The Poisson's ratio of 0.42 obtained from GE was much higher than 0.36 given by [41] and did not result in reasonable bundle properties once calculated. Therefore 0.36 was chosen as a matrix Poisson's ratio. The shear modulus G was then calculated from the tensile modulus and the Poisson's ratio. These values are tabulated in table 2. The information provided by GE also indicates that matrix material remains linearly elastic up to its tensile strength at room temperature. There was no information on the isotropy or anisotropy of PMR15. Therefore, we assumed that the matrix remained isotropic at all load levels.

3.4.2 Fiber Properties

Properties of C3000 graphite fibers used to calculate the bundle properties were obtained from Celanes and reference 40. A tensile modulus of 34 msi (234 GPa) reported was obtained from an impregnated strand test method. A tensile strength of 515 ksi (3550 MPa) was also reported by GE. The compressive modulus was assumed to be equal to the tensile modulus. However, the compressive strength was assumed to be equal to 90% of the tensile strength [40]. Since other properties such as E_2 , ν_{12}, and G_{12} for C3000 fibers were not found in the literature, properties of T300 graphite fibers were used instead. Although T300 fibers have a lower tensile strength than C3000 fibers, the two fibers have almost equal tensile moduli. A value of 1.65 msi (11.4 GPa) used for G_{12} is an average of 1.3 msi (9 GPa) for T300 and 2.0 msi (13.8 GPa) for AS fibers given by Chamis [40]. The reason for this choice is that 1.3 msi would

result in a shear modulus G_{12} for bundles, which is smaller than the shear modulus of C6000/PMR15 unidirectional material. Since the fiber volume ratio of the bundle is higher than the fiber volume ratio of the unidirectional composite, 1.3 msi would underestimate the shear modulus of the bundle. Other fiber properties were obtained from reference 40, and appear in table 2.

3.4.3 Bundle Properties

The best estimate of the bundle properties may be obtained experimentally from a unidirectional material. However, the only unidirectional material available, C6000/PMR15, has a lower fiber volume fraction of about 60% compared to 80% for the fiber bundle. The fiber volume fraction for the bundle was obtained using the cross-sectional area of C3000 fibers available from Celanese and the average of cross-sectional areas of bundles obtained experimentally from micrographic pictures.

The elasticity solution given by Hashin [41,42], was used to calculate the elastic properties of the bundle except G_{23} and ν_{23}. Since Hashin's equations resulted in the Poisson's ratio ν_{23} , which was higher than the Poisson's ratio of the matrix, ν_{23} was obtained using the approximate equations given in reference 40. Examination of cross sections of bundles was convincing enough to support the assumption of a transversely isotropic bundle. With such an assumption in the 2-3 plane, the following equations hold.

$$E_2 = E_3$$

$$\nu_{13} = \nu_{12}$$

$$G_{23} = \frac{E_2}{2(1 + \nu_{23})}$$

Bundle properties are also tabulated in table 2.

3.5 Boundary Conditions and Loading

The choice of boundary conditions is not a trivial one in this case, since they must closely simulate the real situation. Analyses such as the one performed in reference 39, although very detailed, may not be realistic because of the unreal boundary conditions imposed on a 2-ply laminate. Such an analysis would only yield stress and strain resultants in a 2-ply laminate because of the free surfaces existing on the top and bottom of such a laminate. As will be discussed in the next chapter, photomechanics reveals that the behavior of each bundle is affected by the neighboring bundles which surround it. Although it is impossible to analyze an 8-ply or 12-ply laminate with a random arrangement of the bundles because of computer memory and time limitations, it is possible to simulate the surrounding plies as a homogeneous material possessing smeared laminate properties.

The boundary and loading conditions are shown in figure 25. The nodes at the left-hand side of the mesh have zero displacements in the X direction, and the bundle was fixed in the Y direction at its middle node on the left end. Displacements equal to $-8.5x10^{-4}$ -in. and $-2x10^{-3}$ -in. which correspond to stresses of -44 ksi (-303 MPa) and -96 ksi (-662 MPa) respectively were applied at each node on the right-hand side boundary. These displacements were calculated from the strains at -44 and -96 ksi using an average of the warp and fill side stress-strain curves of figure 8 for the unidirectional laminate. The laminate was free to displace in the z direction with no load. The 96 ksi load is approximately equal to the mean compressive strength of the unidirectional laminate, and the 44 ksi load is equal to the load used in the Moire experiment explained in the next chapter.

3.6 Results and Discussion

The results of the finite element analysis of a bundle under a displacement of $-8.5x10^{-4}$-in. are given here. Figure 26 shows the deformed finite element mesh. However, the displacements are exaggerated. The change in the bundle configuration is quite obvious. Since we assumed that the constituents behavior is linearly elastic at all load levels according to the available information, stresses are proportional to the strains everywhere in the bundle. Therefore, stress and strain distribution patterns are similar. Figures 27 and 28 show the graphs of normal compressive stress (σ_1) distributions across the bundle in global and local directions respectively. The abscissa of each graph is the normal stress and the ordinate is the global y coordinate of each Gauss point at which stresses were calculated. Each curve shows a spline fit, and the four points shown in each curve are the stresses at the second and the third Gauss points of two neighboring elements across the bundle. The element numbers of each pair are shown in the figures. Existence of bending moments in the bundle is proved by large differences between the stresses near the lower and the upper interfaces. The graphs imply that bending moments are present near elements number 1 and 2, and also near element numbers 43 and 44.

Around the inflection point of the bundle where the slope has its largest value, normal stresses are almost constant across the bundle with slightly higher stresses near the boundaries of the bundle. This is observed in the pair of elements (19,20), and (25,26). The stress distribution in elements 13 and 14 is somewhat erratic; the reason for this behavior is that the triangular elements under element number 13 change from pure matrix to bundles in the z direction. This change in the stiffness of elements causes local disturbances in the analysis. Shapes of the curves in both global and local coordinates are almost the same, and stresses at the Gauss points are only slightly different. The maximum difference between the local and global values occurs in the vicinity of the highest slope of the bundle because of the higher shear stresses.

Graphs of global shear stress distributions across the bundle plotted in figure 29 show almost uniform stress distributions everywhere. As may be expected, shear stresses in elements 1 and 2 and at the straight portions of the bundle almost vanish. Shear stress distributions and their quantities in the local directions are quite different from those of the global directions.

Displacements and strains may be obtained by finite element analysis of a bundle embedded in a surrounding material which possesses the laminate properties, as was discussed in the previous section. However, understanding the effects of bundles on each other requires changing the relative locations of bundles with respect to each other for each analysis. Since bundles are randomly located through the thickness of the laminate, finite element analysis may give only a limited insight to the problem. In the next chapter we will discuss the use of photomechanics to further investigate the behavior of bundles and their interactions.

4.0 Moire Interferometry

4.1 Introduction

A correct modeling of the behavior of woven composite laminates or unidirectional composites with curved fibers may require an understanding of the effects of the bundles on each other, and also on the stress or strain distributions within a fiber bundle and the material which surrounds it.

Another method which can present the strain distributions at the bundle level is Moire interferometry. Moire interferometry has recently been used to examine local deformations and strain fields in composite laminates. One of the aspects which makes Moire interferometry attractive for composite materials is its sensitivity to the high deformation gradients that exist in places such as the resin rich areas of laminates.

In the past decade, Post and co-workers [43-51] have performed a series of investigations on composites using Moire methods. However, based on our knowledge, this sophisticated technique has never been used to investigate the mechanical behavior of bundles in woven composites.

4.2 Test Method and Specimens

A detailed explanation of the method may be found in references 49 and 51. However, a summary of the method will be given here.

Test specimens were cut from a 22-ply unidirectional and a 20-ply orthotropic laminate, and were examined under a microscope prior to the application of the grating to detect possible saw scratches which may interfere with the fringes. High frequency diffraction gratings with 2400 lines per millimeter were replicated on to the specimens (figure 31), which deformed with the specimen during the load application. The unidirectional specimen was tested under 7.35 ksi (50.66 MPa), 14.7 ksi (101.33 MPa), 29.4 ksi (202.66 MPa), 44.0 ksi (303.3 MPa) , 48.8 ksi (336 MPa), and 73.5 ksi (507.64 MPa), and the orthotropic specimen was tested under 15.0 ksi (103 MPa), 30.0 ksi (207 MPa), and 45.0 ksi (310 MPa) compressive stresses in the fill direction. The highest stress levels were chosen to be well below the ultimate stresses so that local bundle failures would not occur. The specimen geometry and loading condition is shown in figure 32. The bottom end of the specimen was centered on a ball joint to prevent any application of bending moments, and the load was applied to the top of the specimen by a moving wedge. The applied load was calculated by measuring the strain in the loading device through a strain gauge.

A collimated beam of laser light (figure 33) was divided by a screen into four parts A, B, C, and D. To measure the U displacement field, beams C and D were blocked, and beam A (after being reflected from a mirror) interfered with beam B to create a virtual reference grating. The reference and specimen gratings interacted to create the U-field Moire fringe pattern. In the same way, by blocking beams A and B, beams C and D created the V-field fringe pattern.

4.3 Results and Discussion

4.3.1 Fringe Patterns

Figures 34 and 35 show the U and V-field fringe patterns obtained from the unidirectional specimen under 44 ksi and the orthotropic specimen under 45 ksi respectively. To obtain information on the strain distributions in a bundle, one must follow a chosen bundle. Although the U-field fringes do not allow us to see the bundles and their boundaries, it is possible to find some of the bundles in the V-field fringe patterns. Therefore, to read the U-field fringe numbers along the bundles, the two fields must be superposed on each other. Fringe patterns of the orthotropic specimen are illustrated in figure 35 only to show the complexity of the U-field fringes only. No analysis was performed for this specimen.

Since fringes correspond to the relative displacements of all points with respect to each other on the edge of the laminate, fringe numbering is arbitrary as long as increase in the fringe numbers is compatible with displacements of the points on the edge, i.e in the positive Y direction fringe numbers must decrease. This is illustrated in figure 36. Also, we must emphasize that bundles lie along the Y direction in this experiment, contrary to FEM where the bundle was modeled along the X axis.

Large gradients are noticed along the boundaries of the bundles in the V-field. This implies the large contribution of $\frac{\partial v}{\partial x}$ to shear strain. The signs and values of $\frac{\partial v}{\partial x}$ also defer in various bundles. The irregularities of both V and U-field fringes clearly shows the interaction of randomly placed bundles through the thickness.

To eliminate possible end effects, a bundle near the center of the unidirectional specimen (shown by an arrow in figure 34 and blown up in figure 36) was chosen, and the fringes were read using a digitizer board. Since bundles are curved, coordinates of each point must be recorded along with its corresponding fringe number (order). Figures 37 and 38 show the coordinates of the points at which the fringe numbers were read. For curve fitting purposes,

two extra sets of data above and below the bundle were collected. To obtain the shear and normal strain distributions across the bundle, seven locations along the bundle were chosen as shown in figure 39. These locations are at $Y = 0$, $Y = \pm 0.02$, $Y = \pm 0.04$, and $Y = \pm 0.08$ inches from the center of undulation. Figures 40 and 41 show the variation of U and V-field fringe numbers *along* the bundle. U-field fringe numbers increase in the crimped part of the bundle, and their maximum value is at $Y = 0$, which implies larger displacements of the bundle in the crimped part compared to the rest of the bundle. V-field fringe numbers, however, do not show much variation along the bundle, implying small changes in the slope $\frac{\partial v}{\partial y}$.

Figures 42 and 43 show the U and V-field fringe numbers *across* the bundle at the designated points along the Y axis. V-field fringe numbers have little variation in the X direction while U-field fringe numbers increase slightly, implying that small strains $\frac{\partial u}{\partial x}$ exist in most parts of the bundle.

4.3.2 Normal and Shear Strains

Curves of normal strain $\frac{\partial u}{\partial x}$ distribution across the bundle are plotted in figure 44. These curves do not show any similar patterns at similar locations at the two sides of the bundle. Short horizontal lines on each curve indicate the upper and lower bundle interfaces. Otherwise, the second point from each end of every curve represents the interface. Curves of $\frac{\partial v}{\partial x}$ shown in figure 45 exhibit larger variations than $\frac{\partial u}{\partial y}$ shown in figure 46. Also the contribution of $\frac{\partial v}{\partial x}$ to the shear strain is almost 3.5 times the contribution of $\frac{\partial u}{\partial y}$. The addition of $\frac{\partial v}{\partial x}$ to their corresponding $\frac{\partial u}{\partial y}$ will result in shear strain distributions shown in figure 47. The most notable characteristic of these curves is that they all have a general *S* shape, which extends from a negative value to a positive value. However, this characteristic was not noticed in the results of the finite element analysis.

Although the V-field fringe patterns shown in figure 41 do not vary considerably along the bundle, there are small variations in the slope from point to point which result in the scatter

noticed in figure 48. Therefore, quadratic regressions were used to smooth out the scatter rather than spline fits which were used in all of the previous graphs. From figure 48, utilizing the curves of figure 38, we obtain the normal strain $\frac{\partial v}{\partial y}$ distributions across the bundle (figure 49). Almost all of the curves in this graph show the same trend, and maximum change in the value of normal strain is found at $Y = 0.08$ -in., and is equal to 6.4%, which is quite small.

4.3.3 Comparison With Finite Element Results

It was mentioned previously that Moire interferometry reveals the interaction of bundles, while the finite element analysis only shows the behavior of a ply resting on an orthotropic medium which possesses the smeared properties of the laminate. Although it is interesting to compare the results of the two techniques as far as the strain distributions are concerned, because of time limitations, strain distributions were only calculated for certain locations in the bundle. Figures 50 and 51 show the shear strain distributions at the four locations $Y = 0.0$, $+0.02$, $+0.04$, and $+0.08$ -in. from the center of undulation in global and local directions respectively. Notice that the coordinate system is similar to the one used in the Moire interferometry. Solid lines and dotted lines are the results of spline fits over Moire and FEM results at the nodal points respectively. From the mechanics of the problem, we expect the shear strain to vanish at $Y = 0$. At this location the curve of FEM results is very close to zero at all points, but the Moire curve starts from approximately $+0.003$ in/in at the lower interface and ends with -0.004 in/in at the upper interface. Although curves of the two methods do not lie on each other, the averages of the two curves are close, and the same is true for the other three graphs. The difference arises when we examine the Moire results in the negative Y direction. Shear strain curves of figure 47 indicated that all strain distributions had the same *S* shape trend at both positive and negative bundle locations. But, FEM results for shear strain are symmetric with respect to the center of undulation. For example, at $Y = -0.02$ -in., shear

strain given by FEM is positive every where across the bundle, while Moire results are negative.

Normal compressive strain distributions in the bundle which were obtained by Moire and FEM are compared to each other in figures 52 and 53. We observe that at $Y = 0.0$ -in., Moire shows almost no bending moment in the bundle, while FEM indicates the presence of a bending moment in global directions. Similar behavior is observed at $Y = 0.04$ -in. too. At $Y = 0.02$-in. large differences are observed between the strain distributions resulted from the two methods. But, at $Y = 0.08$-in. the curves almost coincide. Transformation of stresses from global to local directions has a considerable effect on the strain distributions obtained from Moire interferometry. This effect is especially observed at $Y = 0.02$ and $Y = 0.04$ -in., where the slope of the bundle is highest.

4.3.4 Discussion

So far, from the results of photomechanics, we have found that the stress distributions have complex forms, and they generally do not have the same pattern in every bundle in the material. Furthermore, looking at the V-field fringe patterns of figure 34, one may wonder which bundle or bundles must be analyzed, and if a grating with 2400 lines per inch is sensitive enough for a sound analysis. These questions can not be answered without further investigation. What is obvious, of course, is that the randomness of bundles causes a random behavior revealed by the Moire interferometry. But whether the results are useful for modeling purposes is questionable because of the large scatter in the fringe patterns of bundles. The results of finite element analysis are consistent and easy to follow. In figures 50 to 53, we have compared the results of a generalized plane strain finite element analysis to the results obtained from a plane stress physical situation on the edge of the laminate. Although theoretically there is a conflict, there will be little difference between the results of a plane stress and a generalized plane strain finite element analysis because of very small values of

the stress σ_z which exist in the generalized plane strain solution. Therefore, in the following section we impose the stress distributions observed in the FEM analysis on the analytical model.

5.0 Micromechanical Model

5.1 Introduction

Compression tests were conducted with sufficient care, and an extensive effort was made, to determine the precise nature of the micro-failure process that controls the compressive strength of notched and unnotched laminates. A description of some of those results follows.

The micro-failure mechanism in Celion 3000/PMR15 woven material was determined as fiber kink mechanism, which is often observed in graphite fibers. It occurs at the crimped parts of the fiber bundles and is assisted by the presence of out-of-plane shear stresses at those locations.

Knowing the micro-failure mechanism and its process, and assuming that the bundle is a unidirectional composite material, it is possible to derive micro-material properties such as moduli and Poisson's ratios of the bundle from the constituent properties by the available elasticity and/or strength of materials approaches. Models such as the *bridging model* introduced by Ishikawa et al. [26] are available for estimating the laminae properties. This will enable us to use the classical lamination theory to obtain laminae stresses and strains. Having laminae stresses, it is possible to calculate the force applied to a bundle. Then, the

micro-mechanical model will result in the stresses induced in the fibers at any point in a bundle.

The key step in going from bundle stresses to fiber stresses is the normal and shear stress distributions in the bundle. These stress distributions were examined by finite element analysis and Moire interferometry in the previous sections, and we decided that the results of FEM would be imposed to determine the normal and shear stress distributions.

The design process is opposite of the analysis. Starting with the fiber compressive strength, loads resisted by the bundles, laminae, and eventually the laminate can be obtained. In this process, all constituent properties and micro-geometries such as the weave type, the cross-sectional shape and dimensions of the bundle, fiber diameter, and fiber and matrix volume ratios must be considered. Altering these parameters, makes it possible to investigate the behavior of a laminate before it is manufactured.

5.2 Formulation

5.2.1 Bundle Analysis

To evaluate the behavior of the fiber bundles quantitatively under the load, a model is proposed, which allows us to examine pointwise a representative fiber bundle. The material is assumed to be composed of repeating segments which include a fill fiber bundle HL long with its middle $2L$ curved and supported by H_w warp fiber bundles as well as the matrix material. H_w is the harness number, and for the material at hand, it is equal to eight. The micro-geometry of this material requires that

$$H = 0.75H_w = 6$$

This model simulates a fill bundle as an initially bent beam column member, supported entirely by a two- parameter elastic foundation, which includes the warp bundles and the matrix. Force equilibrium, accounting for the effect of shear deformation, will be imposed to obtain the governing differential equation for this problem. Solution of the differential equation and imposition of boundary conditions will result in the final shape of the bundle under compressive load. For simplicity of formulation, the linear elastic beam theory was assumed to govern the solution.

To represent the shape of the fiber bundle mathematically, the origin of the coordinate system is placed at the center of undulation (figure 54), and the shape of the fiber bundle can be represented approximately by the following expressions.

$$y_0 = a\,(1 + \cos\frac{\pi x}{L}) \qquad -L < x < L \tag{5.1.a}$$

$$y_0 = 0 \qquad L < |x| < \frac{HL}{2} \tag{5.1.b}$$

The Fourier series representing expressions 5.1.a and 5.1.b is written as:

$$y_0 = \frac{a_0}{2} + \sum_{n=1}^{\infty}\left[a_n \cos(\frac{2n\pi x}{HL}) + b_n \sin(\frac{2n\pi x}{HL})\right] \tag{5.2}$$

where

$$a_0 = \frac{4a}{H}$$

$$a_n = \frac{2a}{H}\left[\frac{H}{n\pi}\sin(\frac{2n\pi}{H}) + \frac{\sin(1-\frac{2n}{H})\pi}{(1-\frac{2n}{H})\pi} + \frac{\sin(1+\frac{2n}{H})\pi}{(1+\frac{2n}{H})\pi}\right]$$

and

$$b_0 = b_n = 0$$

The bundle is assumed to be subjected to a pair of equilibrating compressive axial forces P_b, acting at the centroid of the end cross sections. If we cut an infinitesimally small element dx of the bundle (figure 55), the equilibrium of moments leads to

$$(M_b + dM_b) - M_b - P_b dy - S_b dx + m dx = 0 \tag{5.3}$$

where

$$y = y_0 + y_1 \tag{5.4}$$

and y_1 is the change in the shape of the fiber bundle. Substitution of (5.4) in (5.3) and division by dx will result in

$$\frac{dM_b}{dx} - P_b\left(\frac{dy_1}{dx} + \frac{dy_0}{dx}\right) - S_b + m = 0 \tag{5.5}$$

The magnitude of bending moment at any point on the elastic curve of the bundle consists of the contributions of change in the curvature and shear deformation, which can be represented by the following expression.

$$\frac{M_b}{E_b I_b} = -\frac{d^2 y_1}{dx^2} + \frac{\alpha}{A_b G_b}\frac{dS_b}{dx} \tag{5.6}$$

The factor α is called the *shear correction factor* [52], which is a function of the cross-sectional shape , and for a cantilever beam of elliptical cross-section with a quadratic shear stress distribution on its cross-section, it is equal to 10/9. The bundle is embedded in surrounding material, and therefore the shear stress distribution in the bundle may not be similar to a quadratic distribution everywhere along the bundle as the results of finite element and Moire analyses proved. However, at the locations of interest to us, where kinks occur in a bundle, shear stress distributions in the local directions resemble quadratic distributions (fig-

ure 30 elements (1,2), (7,8) , and (13,14)). Therefore, we may choose 10/9 as the shear correction factor if we desire.

Differentiating (5.6) twice and (5.5) once, knowing that $\frac{dS_b}{dx} = K_1 y_1$,and $m = K_2 \frac{dy_1}{dx}$, and dividing by $E_b I_b$, we obtain the governing differential equation for this problem.

$$\frac{d^4 y_1}{dx^4} + \left(\frac{P_b}{E_b I_b} - \frac{\alpha K_1}{A_b G_b} - \frac{K_2}{E_b I_b} \right) \frac{d^2 y_1}{dx^2} + \frac{K_1}{E_b I_b} y_1 = - \frac{P_b}{E_b I_b} \frac{d^2 y_0}{dx^2} \tag{5.7}$$

The solution to this differential equation includes a homogeneous and a particular part. Here we are not interested in the homogeneous part of the solution, since it is related to the state of bifurcation in the stability problem. It is well known that in an initially bent beam column under compression such as we have here, lateral displacement increases without bound as the axial load increases, and the axial load becomes asymptotic to the Euler buckling load. Besides, all the unknown coefficients of the homogeneous solution will be equal to zero if such a solution is attempted. Therefore, only the particular solution is considered here.

The boundary conditions for this problem are

$$\left(\frac{dy_0}{dx} \right)_{\frac{-HL}{2}} = \left(\frac{dy_0}{dx} \right)_{\frac{HL}{2}} = 0 \tag{5.8.a}$$

$$(S_b)_{\frac{-HL}{2}} = (S_b)_{\frac{HL}{2}} = 0 \tag{5.8.b}$$

Since the right hand side of (5.2) includes only a cosine series, the particular solution must have a cosine form.

$$y_1 = y_1^p = \sum_{n=1}^{\infty} c_n \cos\left(\frac{2n\pi x}{HL}\right) \tag{5.9}$$

This form of particular solution will automatically satisfy the boundary condition (5.8.a). Therefore, we must check the boundary condition (5.8.b) on the shear force. Substituting y_1 in the differential equation of (5.7), will result in

$$c_n = \frac{P_b a_n}{(\frac{2n\pi}{HL})^2 E_b I_b + \frac{\alpha K_1 E_b I_b}{A_b G_b} - P_b + (\frac{HL}{2n\pi})^2 K_1 + K_2} \tag{5.10}$$

The shape of the bundle y_b under axial load is obtained by adding the deflection y_1 to the initial shape y_0.

$$y_b = \frac{2a}{H} + \sum_{n=1}^{\infty} \frac{(\frac{2n\pi}{HL})^2 E_b I_b + \frac{\alpha K_1 E_b I_b}{A_b G_b} + (\frac{HL}{2n\pi})^2 K_1 + K_2}{(\frac{2n\pi}{HL})^2 E_b I_b + \frac{\alpha K_1 E_b I_b}{A_b G_b} - P_b + (\frac{HL}{2n\pi})^2 K_1 + K_2} a_n \cos(\frac{2n\pi x}{HL}) \tag{5.11}$$

Initially there are no moments or shear forces along the bundle; it is only after the application of the axial compressive force, P_b , that bending moments and shear forces appear. Therefore, bending moments and shear forces are the consequences of deformations y_1. Let's recall that inclusion of shear deformation in the statement for moment and shear force will give

$$M_b = - E_b I_b \frac{d^2 y_1}{dx^2} + \frac{\alpha K_1 y_1 E_b I_b}{A_b G_b} \tag{5.12}$$

But we also have from (5.5):

$$S_b = \frac{dM_b}{dx} - P_b \frac{dy}{dx} + K_2 \frac{dy_1}{dx} \tag{5.13}$$

Substituting (5.12) in (5.13), vertical shear force can be obtained as

$$S_b = -E_b I_b \frac{d^3 y_1}{dx^3} + \left(\frac{\alpha K_1 E_b I_b}{A_b G_b} - P_b + K_2 \right) \frac{dy_1}{dx} - P_b \frac{dy_0}{dx} \tag{5.14}$$

By inserting the first, the second, and the third derivatives of y_1 in the expressions of moment and shear, namely (5.12) and (5.13), we arrive at

$$S_b = \sum_{n=1}^{\infty} \frac{\frac{HL}{2n\pi} K_1}{(\frac{2n\pi}{HL})^2 E_b I_b + \frac{\alpha K_1 E_b I_b}{A_b G_b} - P_b + (\frac{HL}{2n\pi})^2 K_1 + K_2} P_b a_n \sin(\frac{2n\pi x}{HL}) \tag{5.15}$$

$$M_b = \sum_{n=1}^{\infty} \frac{E_b I_b (\frac{2n\pi}{HL})^2 + \frac{\alpha K_1 E_b I_b}{A_b G_b}}{(\frac{2n\pi}{HL})^2 E_b I_b + \frac{\alpha K_1 E_b I_b}{A_b G_b} - P_b + (\frac{HL}{2n\pi})^2 K_1 + K_2} P_b a_n \cos(\frac{2n\pi x}{HL}) \tag{5.16}$$

Equations 5.15 and 5.16 are the final forms of the shear force and bending moment in the bundle in terms of the material constants. Obviously boundary condition (5.8.b) is also satisfied by (5.15). Therefore, the shape function (5.11) satisfies all boundary conditions.

At this point, we have all the equations which determine the shape of a fiber bundle under compressive load, and values of shear forces and moments at any point of the fiber bundle. Any short segment of a fiber bundle can be assumed to be a unidirectional composite in equilibrium under compressive axial forces, shear forces and bending moments.

Stresses in global directions at any cross-section may be obtained from

$$\sigma_x = \frac{P_b \cos\theta}{A_b} + \frac{M_b y \cos^3\theta}{I_b} \tag{5.17a}$$

$$\tau_{xy} = \frac{S_b \cos\theta}{A_b} \tag{5.17b}$$

Where θ is the slope angle shown in figure 54.

We have linearly distributed these stresses over the cross-section of the bundle following the results of the finite element analysis for normal and shear stress distributions in global directions shown in figures 27 and 29. Now we can transform these stresses into the local directions (x',y') using the slope of the bundle at every point along the bundle.

$$\sigma_{x'} = \sigma_x \cos^2\theta + 2\tau_{xy} \sin\theta \cos\theta \tag{5.18a}$$

$$\tau_{x'y'} = -\frac{\sigma_x}{2} \sin 2\theta + \tau_{xy} \cos 2\theta \tag{5.18b}$$

Stresses σ_y and $\sigma_{y'}$ are small compared to the other stresses, and any significant contribution of these stresses to the process of failure is doubtful. Therefore, they are ignored.

To obtain the fiber stresses which cause fiber failure, we need the forces applied to a single fiber, located at a critical point of the fiber bundle and embedded in the matrix. Using strength of materials approach, the compressive axial force in a fiber is

$$P_f = \sigma_{x'} A_f \frac{E_{lf}}{E_b} \tag{5.19}$$

Again, according to the simple strength of materials approach [53], shear stresses in the fiber and matrix may be assumed to be equal, yielding the shear force in the fiber as

$$S_f = \tau_{x'y'} A_f \tag{5.20}$$

When shear forces such as S_b are applied to an orthotropic bar such as the bundle, small shear stresses in the direction perpendicular to the direction of S_b will be induced because of the orthotropy of the material [54]. These relatively small shear stresses have opposite

signs on the two sides of the semi-minor axis, and do not contribute to the kink formation due to the inability of the fibers to deform in these directions. Therefore, these shear stresses are ignored in this analysis.

5.2.2 Fiber Analysis

Each fiber is modeled as a straight beam on an elastic foundation (figure 56). The approach used to determine the stresses in the fibers as they deform is an energy approach similar to to the one used in reference 18 with the difference that reference 18 considers the fibers and the matrix as plates, continuous in the third direction, and uses the strain energy of the matrix sandwiched between the plates to obtain the governing differential equation. Here, as will be shown later, the volume of the matrix corresponding to one fiber in a hexagonal array is used in the energy calculations. The analysis is carried out under the following assumptions:

(1) The deformation is two dimensional. This is, in fact, proved to be true by the experimental results and by the kink formations.

(2) Because of the shear kink formation, all fibers deform in phase. Therefore, small normal strains in the matrix material are ignored.

(3) There is no rotation at the ends of certain lengths of fibers. This assumption is enforced due to uncertainty in the values of bending rigidities at the two ends of a fiber.

(4) Matrix and fiber remain elastic up to failure. This is not an assumption, and results of the tests performed by GE support this fact.

A hexagonal array of fibers is assumed here because of its resemblance to a random arrangement. Another reason is that a square array can only have a maximum of 78.5% fiber volume fraction and would limit the fiber volume fraction in the model. Knowing V_f, the radius R of a hexagonal array is obtained from the geometry of the array as

$$R = r\sqrt{\frac{2\pi}{V_f\sqrt{3}}} \tag{5.21}$$

Neglecting shear deformations of the fiber and the extensional deformations of the matrix, the strain energy of the system of one fiber and its corresponding volume of matrix is equal to

$$\bar{U} = \frac{E_f I_f}{2}\int_0^l \left(\frac{d^2v}{dx^2}\right)^2 dx + \frac{1}{2}\int_0^l V_m^f \tau_{xy}\gamma_{xy} dx \tag{5.22}$$

Where

$$V_m^f = \frac{\sqrt{3}}{2}R^2 V_m$$

$$\tau_{xy} = G_m \gamma_{xy}$$

$$\gamma_{xy} = (1 + \frac{r}{c})\frac{dv}{dx}$$

V_m^f is the volume of matrix corresponding to one fiber, and is shaded in figure 57. The work done by the external forces is

$$\bar{V} = \frac{P_f}{2}\int_0^l \left(\frac{dv}{dx}\right)^2 dx + S_f\int_0^l \frac{dv}{dx} dx \tag{5.23}$$

The following differential equation and corresponding boundary conditions are derived by taking the first variation of the total energy.

$$\frac{d^2}{dx^2}(E_f I_f \frac{d^2v}{dx^2}) + \left[p_f - V_m^f G_m(1 + \frac{r}{c})^2\right]\frac{d^2v}{dx^2} = 0 \tag{5.24}$$

$$\text{at } x = 0 \qquad v = 0 \quad \text{and} \quad \frac{dv}{dx} = 0$$

$$\text{at } x = l \qquad \frac{dv}{dx} = 0 \quad \text{and} \quad \frac{d^3v}{dx^3} = -\frac{S_f}{E_f I_f}$$

Solution of the above differential equation and boundary conditions consists of three situations as follows:

For $P_f \leq V_m^f G_m (1 + \frac{r}{c})^2$

$$v = -\frac{S_f}{E_f I_f (B_1)^3}\left[\sinh B_1 x - B_1 x - \frac{(\cosh B_1 l - 1)}{\sinh B_1 l}\ (\cosh B_1 x - 1)\right] \tag{5.25.a}$$

Where

$$(B_1)^2 = \frac{\left[V_m^f G_m (1 + \frac{r}{c})^2 - P_f\right]}{E_f I_f} \tag{5.25.b}$$

For $P_f = V_m^f G_m (1 + \frac{r}{c})^2$

$$v = \frac{S_f x^2}{2E_f I_f}\left(\frac{l}{2} - \frac{x}{3}\right) \tag{5.26}$$

For $P_f \geq V_m^f G_m (1 + \frac{r}{c})^2$

$$v = \frac{S_f}{E_f I_f (B_2)^3}\left[\sin B_2 x - B_2 x + \frac{(\cos B_2 l - 1)}{\sin B_2 l}\ (\cos B_2 x - 1)\right] \tag{5.27.a}$$

Where

$$(B_2)^2 = \frac{\left[P_f - V_m^f G_m (1 + \frac{r}{c})^2\right]}{E_f I_f} \tag{5.27.b}$$

For a circular fiber, the maximum bending stress on its cross-section is

$$\sigma = \frac{M_f r}{I_f}$$

Where the bending moment , neglecting the shear deformations is defined by

$$M_f = E_f I_f \frac{d^2 v}{dx^2}$$

The maximum compressive stress includes both contributions of fiber axial force and bending moment. Therefore from equations (5.25), (5.26) , and (5.27) we have

For $P_f \leq V_m' G_m (1 + \frac{r}{c})^2$

$$\sigma_f^{max} = \frac{P_f}{A_f} + \frac{S_f r}{I_f B_1} \quad \frac{(cosh\, B_1 l - 1)}{sinh\, B_1 l} \tag{5.28}$$

For $P_f = V_m' G_m (1 + \frac{r}{c})^2$

$$\sigma_f^{max} = \frac{P_f}{A_f} + \frac{S_f l r}{2 I_f} \tag{5.29}$$

For $P_f \geq V_m' G_m (1 + \frac{r}{c})^2$

$$\sigma_f^{max} = \frac{P_f}{A_f} - \frac{S_f r}{I_f B_2} \quad \frac{(cos\, B_2 l - 1)}{sin\, B_2 l} \tag{5.30}$$

Equations 5.28 to 5.30 give the maximum stresses induced in a fiber. These stresses can be compared to the compressive strength of graphite fibers. In the equations presented in this chapter all but two of the parameters are readily available from the micro-geometry or material properties except K_1 and K_2. In the next chapter we will attempt to derive these parameters using an approximate elasticity solution.

6.0 Foundation Parameters

6.1 Introduction

When load is applied to the surface of a linearly elastic half-space, the surface deflects both under the load and in the unloaded areas adjacent to the load, with displacements diminishing with distance. This occurs because the material is a connected continuum. The Winkler model [56] which is the simplest one we found, however, does not perform this way; only the loaded region deflects while the adjacent surface remains unchanged. A linearly elastic isotropic continuum can be described by two material properties E and ν. But the Winkler material is described by only one parameter, the spring constant K_1 , which is not sufficient to characterize the foundation. The Vlasov and Leontiev [57] approach has provided the additional property to the basic Winkler model. Various improvements along this line have been suggested by a number of authors, including Filonenko-Borodich [58], Hetenyi [59,60], Pasternak [61], and Zhaohua [62]. Among the proposed models, the most convenient mathematically is the one in which the tops of the Winkler springs forming the ground surface are tied together by a stretched elastic string, or membrane, or shear beam. The tension in this string is the second foundation property. The effect of the stretched string on the mathematics is to modify the surface reaction of the foundation from the simple

$$P = K_1 V$$

of the Winkler spring to

$$P = K_1 V - K_2 \frac{d^2 V}{dx^2}$$

Displacements of the unloaded areas may be found by setting P=0 in the above differential equation. This equation appears implicitly in the fourth order differential equation 5.7. Therefore, the concept of distributed moments which we have used is equivalent to the concept of a stretched string. When the foundation is an orthotropic continuum, K_1 and K_2 may be functions of up to nine independent material constants, compared to two for an isotropic foundation.

6.2 Elasticity Solution

Let's suppose that the bundle is resting on top of an orthotropic homogeneous foundation, infinitely thick and infinitely deep (half space). For simplicity of formulation, the bundle is assumed to be straight and to have a rectangular cross section so that a uniform state of stress exists in the thickness direction of the foundation, and the foundation is in the state of plane strain. When the bundle deforms due to axial compressive force, there will be normal and shear stresses induced along the contact surface. Therefore, we may consider a half space with loads applied at its boundary as shown in figure 58 , and use compatibility relations between the bundle and the foundation to derive K_1 and K_2.

Determination of the corresponding deflection V of the top of the foundation is a two-dimensional elasticity problem in which the boundary conditions for the foundation are

$\sigma_x = \sigma_y = \tau_{xy} = 0$ for $y = \infty$

$-2a\sigma_y = K_1 y_1 = K_1 V_{y=0}$

$$2a\tau_{xy}b = K_2 \frac{dy_1}{dx} = K_2\left(\frac{dv}{dx}\right)_{y=0}$$

where y_1 is deflection of the curved bundle due to application of an axial compressive load.

Displacement compatibility relations between the beam and the foundation at y=0 as shown in figure 59 are

$$V = -\int_0^{\infty} \varepsilon_y dy = y_1$$

$$U = -\frac{dy_1}{dx} b$$

A stress function which satisfies the boundary conditions of the foundation at $y = \infty$ has the form

$$\phi = \frac{1}{2a} \sum_{n=1}^{\infty} \left(\frac{D_1}{\lambda} y + \frac{D_2}{\lambda^2}\right) e^{-\lambda y} \cos \lambda x \tag{6.1}$$

where $\lambda = \frac{2n\pi}{HL}$ and D_1 and D_2 are constants to be determined. From (6.1) the stresses in the foundation are

$$\sigma_x = \frac{1}{2a} \sum_{n=1}^{\infty} [D_1(\lambda y - 2) + D_2] e^{-\alpha y} \cos \lambda x \tag{6.2}$$

$$\sigma_y = \frac{-1}{2a} \sum_{n=1}^{\infty} (D_2 + D_1 \lambda y) e^{-\alpha y} \cos \lambda x \tag{6.3}$$

$$\tau_{xy} = \frac{1}{2a} \sum_{n=1}^{\infty} (D_1 - D_2 - D_1 \lambda y) e^{-\alpha y} \sin \lambda x \tag{6.4}$$

The stress-strain relationship in the foundation is

$$\begin{Bmatrix} \varepsilon_x \\ \varepsilon_y \\ \gamma_{xy} \end{Bmatrix} = \begin{bmatrix} S_{11} & S_{12} & 0 \\ S_{12} & S_{22} & 0 \\ 0 & 0 & S_{66} \end{bmatrix} \begin{Bmatrix} \sigma_x \\ \sigma_y \\ \tau_{xy} \end{Bmatrix}$$

where S's are the compliances of the foundation. From the above stress-strain relationship together with (6.2) and (6.3), the strains in the two directions may be obtained as

$$\varepsilon_x = \frac{1}{2a} \sum_{n=1}^{\infty} \{S_{11}[D_1(\lambda y - 2) + D_2] - S_{12}[D_2 + D_1 \lambda y]\} e^{-\alpha y} \cos \lambda x \tag{6.5}$$

$$\varepsilon_y = \frac{1}{2a} \sum_{n=1}^{\infty} \{S_{12}[D_1(\lambda y - 2) + D_2] - S_{22}[D_2 + D_1 \lambda y]\} e^{-\alpha y} \cos \lambda x \tag{6.6}$$

Integrating ε_y along the depth of the foundation and utilizing the first compatibility relation, we obtain

$$\sum_{n=1}^{\infty} \frac{1}{2a} \left[-\frac{S_{12}}{\lambda} (D_2 - D_1) + \frac{S_{22}}{\lambda} (D_2 + D_1) \right] \cos \lambda x = \sum_{n=1}^{\infty} c_n \cos \lambda x \tag{6.7}$$

where y_1 has been replaced by the corresponding summation in (5.9). There is a cosine series on each side of (6.7). Therefore, the coefficients of both series are equivalent, and c_n is

$$c_n = \frac{1}{2a\lambda} [-S_{12}(D_2 - D_1) + S_{22}(D_2 + D_1)] \tag{6.8}$$

From the second compatibility relation, after differentiating both sides with respect to x and equating the coefficients of the series, we obtain

$$c_n = \frac{1}{2ab\lambda^2} [S_{11}(D_2 - 2D_1) - S_{12}D_2] \tag{6.9}$$

D_2 can be determined from (6.8) and (6.9) in terms of the material properties.

$$D_2 = \frac{2a\lambda c_n(b\lambda S_{12} + b\lambda S_{22} + 2S_{11})}{-S_{11}S_{12} + 3S_{11}S_{22} - S_{12}^2 - S_{12}S_{22}} \tag{6.10}$$

From the second boundary condition, by substituting for y_1 and σ_y, K_1 may be written in terms of the material properties and λ as

$$K_1 = \frac{2a\lambda(b\lambda S_{12} + b\lambda S_{22} + 2S_{11})}{-S_{11}S_{12} + 3S_{11}S_{22} - S_{12}^2 - S_{12}S_{22}} \tag{6.11}$$

Finally from the third boundary condition, by substituting for τ_{xy} and y_1' , a relationship for K_2 may be obtained in terms of the two parameters D_1 and D_2, which can be substituted for using (6.9) and (6.10).

$$K_2 = \frac{2ab(2b\lambda S_{22} + S_{12} + S_{11})}{-S_{11}S_{12} + 3S_{11}S_{22} - S_{12}^2 - S_{12}S_{22}} \tag{6.11}$$

It is not surprising that K_1 and K_2 are functions of λ also. The implication is that the resistance of the foundation to load is a function of the periodicity of the surface load distribution itself. This was also suggested by Biot [63].

7.0 Analysis and Design

7.1 Analysis

7.1.1 Introduction

The computer code FMAN, shown in appendix A, is an analysis code able to analyze any notched or unnotched hybrid laminate. The code incorporates the classical lamination theory and Lekhnitskii's solution to compute stresses anywhere in a laminate containing an elliptical hole as shown in figure 60. However, the major purpose of this code is to determine the characteristic distances for the average stress and point stress criteria introduced by Whitney and Nuismer [15]. A detailed explanation of the code and its flow chart are given in appendix A.

7.1.2 Average Stress Criterion (ASC)

To determine the characteristic distance d and its possible dependency on the laminate thickness, three cases have been considered for the average stress criterion.

(A) The local compressive stresses in the first ply to fail were averaged over the distance *d* along a line perpendicular to the maximum compressive stress in that ply, and the average was set equal to the average compressive strength of the unidirectional unnotched laminate which is 96.83 ksi (668 MPa). In our case the first ply to fail is the 0° ply, and the stresses were thus averaged along a line which is perpendicular to the loading direction and passes through the center of the hole. Figures 61, 62, and 63 show the stress distributions in various laminates and in their 0° plies. Obviously, for the case of 12-ply and 22-ply unidirectional laminates, the laminate and ply stresses are identical. Although laminate stresses do not really exist, they may be thought of as being the stresses which correspond to the strains induced in a notched laminate, and are related to those strains through the [A], [B], and [D] matrices of CLT. These stresses are the direct result of the Lekhnitskii's solution. Values of *d* obtained from case A are tabulated in table 3 and are shown in figure 64. Using linear regression, a line was fit over the data and shows almost a linear correlation of *d* with laminate thickness.

(B) Compressive stresses in the 0° ply were averaged over *d* and were set equal to the compressive stress in the 0° ply of the unnotched laminate of the same type. The unnotched ply stresses are tabulated in table 4 along with the ratio R which is proportional to the Tsai-Wu failure criterion for the first ply to fail. When $R > 1$, the laminate is safe and the applied load may be multiplied by R to make the first ply fail. Values of R were obtained with the assumption that the ply tensile strength is equal to its compressive strength, and confirm that compressive and tensile strengths are close if not equal. For the quasi-isotropic and orthotropic laminates, the compressive and tensile strengths were assumed to be equal to 96.83 ksi, which is the average of the compressive strengths of the unidirectional laminates. The shear strength of 18.22 ksi (126 MPa) used in the failure criteria was obtained from GE. Values of *d* in this case have a large scatter as shown in figure 64.

(C) In this case the laminate stresses obtained directly from Lekhnitskii's solution were averaged over a distance *d* and the average was set equal to the corresponding unnotched

laminate strength. Notice that this case shows even greater scatter. Characteristic distances for cases B and C are also tabulated in table 3. Although the lines which fit over the data of cases B and C show smaller slopes leading to an almost constant d in case C, because of smaller coefficients of correlation, these cases will result in large errors in the prediction of the notched strength.

At locations near the hole and at the hole boundary where high stress concentrations exist, compressive stresses in the 0° plies will somewhat decrease due to the reduction in the modulus E_2 of the ply. This is noticed in plots of figures 62 and 63 where curves of laminate stresses are parallel to the curves of 0° ply stresses away from the hole. But, immediately near the hole, they become closer because of the reduction in the 0° ply stresses. This is explained with more detail in the next section.

7.1.3 Point Stress Criterion (PSC)

To check the point stress criterion, the characteristic distances d_0 corresponding to case A of ASC were obtained and tabulated in table 3 as case D (figure 64) along with the equivalent number of bundles which fail. Although the line for case D seems to be a better fit than the other cases, the point stress criterion shows large scatter due to a small coefficient of correlation (table 3), and is not suitable for design purposes. It also does not correlate to the experimental observations of the number of failed bundles.

7.1.4 Modification of Lamina Properties

We discussed the nonlinearity of stress-strain curves shown in figure 8, and the cause of this nonlinearity was postulated to be the waviness of fiber bundles. Because of this nonlinear behavior, the apparent elastic moduli of the material became functions of the load level. When an orthotropic or a quasi-isotropic laminate is under compression, both compressive

and tensile stresses are induced in the individual plies, with the highest compressive stresses in the 0° plies in the load direction. Since the moduli of each ply are functions of the stresses in that individual ply, in the laminate analysis, these moduli must be modified according to the induced stresses. The modification of moduli E_1 and E_2 of each ply was performed using the empirical curve of the unidirectional laminate in figure 8. E_1 and E_2 were modified at several stages in the analysis of both unnotched and notched laminates. In the case of notched laminates, moduli were modified to obtain correct laminate properties for computing stresses around the hole, and later they were modified at every individual point of interest around the hole. G_{12} and ν_{12}, however, were not modified because of the lack of information on their load dependencies. We expect that small changes in G_{12} and ν_{12} have negligible effect on the analysis.

If stress-strain curves of figure 8 are extrapolated in the compression side, eventually the elastic modulus becomes small. This behavior will cause a disturbance in the modification and analysis when moduli calculated from those curves tend to zero or become negative. Therefore, there must exist a limit on when and how much the moduli can be modified. Unfortunately this limit can not be measured experimentally. As an example, analytically, very high stresses are induced near an elliptical hole with $\frac{a}{b} = 2$. In such a case, although it was not experimentally observed, it is predicted that bundles in the 0° plies near the hole fracture and loose almost all of their load carrying capacities. Therefore, using very small moduli in those regions is not far from reality.

7.1.5 Finite Width Correction

Lekhnitskii's solution [55] is given for stresses in an infinite anisotropic plate containing an elliptical hole. Therfore, to correctly calculate the characteristic distances, stresses around the circular hole were modified to take into account the effect of finite specimen width using equation 2.14.a given here.

$$\frac{K_t}{K_t^{\infty}} = \frac{2 + (1 - \frac{2a}{W})^3}{3(1 - \frac{2a}{W})} \qquad (2.14.a)$$

where

W = Width of the specimen

$2a$ = Hole diameter

The above equation is for an isotropic plate with a circular hole and gives reasonable results for orthotropic plates [20,21,22].

7.2 Design

7.2.1 Introduction

The design procedure is opposite of the analysis, with the difference that the bundle compressive strength is first calculated using the formulation given in chapter 5. Once the bundle strength is known, we can work our way up to ply, unnotched, and notched laminate strengths. A detailed explanation of the code and its flow chart are given in appendix B. Since the design procedure is a trial and error one, we need to know beforehand the ply properties to be used in the classical lamination analysis. Determination of such properties has been the work of Ishikawa et al. [38-45] for several years. The Bridging Model introduced in his papers is the key to the calculation of ply properties. However, a code for the Bridging Model is not provided here, and we assume that lamina properties are available

7.2.2 Strength Predictions

To make certain that the assumed cosine Fourier series for the bundle shape is a good approximation of the real shape, the two were compared. The curves of initial bundle shapes shown in figure 65 indicate that the assumed Fourier series is a reasonable approximation to the real bundle shape.

In using the equations of chapter five given for the kink stress prediction, a compressive strength of 463 ksi (3196 MPa) which is roughly 90% of the tensile strength of the graphite fiber [40] was considered to be the limit stress in the fibers. This resulted in a ply compressive strength of 89.53 ksi (617 MPa), which is lower than the average experimental quantities for the unidirectional laminate. Figure 66 shows the calculated maximum compressive stresses in graphite fibers along the bundle. Maximum fiber stress occurs at 0.15*L* from the canter of undulation, and matches quite well with the kink locations observed in the failed specimens.

Micro-geometry such as the semi-major and semi-minor axes of the bundle and its cross-sectional area, the unit length *l*, and etc. were obtained from the micrographic pictures of the material. Although the cross-section of each bundle is different in size from another one, using average values for these important parameters may serve the purpose.

Notched and unnotched compressive strength values predicted by FMD are tabulated in table 5 with their percent differences from experimental values. The maximum difference between the predicted and experimental strengths occurs for the 12-ply unidirectional laminate. The reason is that this laminate showed a rather high unnotched experimental strength as was shown in table 1. However, the overall differences are low for all practical purposes. The predicted notched and unnotched strength values are also shown in figures 67 to 69 along with their experimental data to give a better feeling of the overall differences and scatter.

8.0 Conclusions

The present investigation has established that the failure process of notched and unnotched graphite/PMR15 laminates constructed from eight-harness satin plies with several stacking sequences is controlled by the kinking of fiber bundles resulting in fiber fracture at the local level, matrix cracking along fiber directions, and growth of the regions of fiber kinking across the width and through the thickness of the specimens. It has also been shown that this process is progressive, and is influenced strongly by both the local and global stresses.

The compressive behavior of the material is also influenced by the geometry of the weave. Thus, values such as the oscillation amplitude, slope, cross-sectional shape, and fiber volume fraction of the bundles influence the compressive strength of the material. Moreover, the surface of the material provides the initiation point for the initiation and growth of the final failure event. Hence, the nature of the surface and the specimen thickness influences the compressive strength as well, especially in the notched material.

The nonlinear behavior of this material under compressive loading is caused by the curved fiber bundles which behave similarly to initially bent beams on an elastic foundation. Compressive stresses cause an increase in the curvatures of the crimped sections of the fiber bundles which then result in the reduction of bundle stiffnesses in the loading direction. This kind of behavior causes smaller failure stresses than would be expected in 0° plies, especially in the vicinity of notches.

In an unnotched laminate, where compressive stresses are uniform in each ply, fiber kinks occur in the crimped parts of the bundles because of the presence of out-of-plane shear stresses and bending moments.

The relative locations to the notch of the crimped parts in the bundles which are next to the notch determine the locations of the kinks. The kink boundary angles observed, did not follow the constraints imposed by the laws of energy as stated in reference 13. Although many details concerning the compressive failure of these materials remained undetermined, especially in the presence of damage induced by cyclic loading, the experimental investigation provided a firm foundation for the analysis and modeling of the compression failure process.

Normal strain distributions obtained from the finite element analysis of a bundle showed consistence with what would be expected from a beam on an elastic foundation model. Shear strain distributions in global directions were almost constant across the bundle. Strain distributions obtained from the Moire interferometry, however, showed larger variations across the bundle, and also showed randomness along the bundle because of the appearance of bundle interactions in this type of test.

Analysis of notched laminates by Lekhnitskii's solution for circular holes showed the dependency of the characteristic distances of the point stress and the average stress criteria on the laminate thickness. The average stress criterion correlated better with the experimental results.

Using the overall patterns of the finite element analysis in the micromechanical model, the predicted notched and unnotched strengths using the beam on an elastic foundation model and the average stress criterion correlate very well with the experimental results for the material at hand. Unfortunately other material types and geometries were not available for us to check their behavior with predicted results.

References

1. Rosen, B. W., "Mechanics of Composite Strengthening," Chapter 3, *Fiber Composite Materials,* S. H. Bush (Ed.), American Society of Metals, (1964).

2. Lanir, Y. and Fung, Y. C. B., "Fiber Composite Columns Under Compression," J. Composite Materials, Vol. 6 (July 1972), p. 387.

3. Herrmann, L. R. and Mason, W. E., "Response of Reinforcing Wires to Compressive State of Stress," J. Composite Materials, Vol. 1 (1967), p. 212.

4. Hanasaki, S. and Hasagawa, Y., "Compressive Strength of Unidirectional Fibrous Composites," J. Composite Materials, Vol. 8 (July 1974), p. 306.

5. Lager, J. R. and June, R. R., "Compressive Strength of Boron-Epoxy Composites," J. Composite Materials, Vol. 3 (January 1969), p.48.

6. Chung, W. Y. and Testa, R. B., "The Elastic Stability of Fibers in a Composite Plate," J. Composite Materials, Vol .3 (January 1969), p. 58.

7. Foye, R. L., "Compression Strength of Unidirectional Composites," AIAA Paper, No. 66-143, 1966.

8. Schuerch, H., "Prediction of compressive Strength in Uniaxial Boron Fiber-Metal Matrix Composite Materials," AIAA Journal, Vol. 4 (January 1966), p. 102.

9. Sadowsky, M. A., Pu, S. L., and Hussain, M. A., "Buckling of Fibers," Journal of Applied Mechanics, Vol. 34, Ser. C, Dec 1967, pp.1011-1016.

10. De Ferran, E. M. and Harris, B., "Compression Strength of Polyester Resin Reinforced with Steel Wires" J. Composite Materials, Vol. 4 (January 1970), p. 62.

11. Argon, A. S., "Fracture of Composites," Treatise on Materials Science and Technology, Vol. 1, p.79. Academic Press, New York, 1972.

12. Greszczuk, L. B., "Microbuckling Failure of Circular Fiber-Reinforced Composites" AIAA Journal, Vol. 13, No. 10, October 1975.

13. Weaver, C. R. and Williams, J. G., "Deformation of a Carbon-Epoxy Composite Under Hydrostatic Pressure," Journal of Materials Science 10, (1975), p.1323.

14. Chaplin, C. R., "Compressive Fracture in Unidirectional Glass-Reinforced Plastics," Journal of Materials Science and Technology 12, (1977), p.347.

15. Evans, A. G. and Adler, W. F., "Kinking as a Mode of Structural Degradation in Carbon Fiber Composites," Acta Metallurgica, Vol. 26. pp.725-738, Pargamon Press. 1978.

16. Parry, T. V. and Wronski, A. S., "Kinking and Compressive Failure in Uniaxially Aligned Carbon Fiber Composite Tested Under Superposed Hydrostatic Pressure," J. Materials Science 17 (1982), p. 893.

17. Hahn, T., and Williams, J. G., "Compression Failure Mechanisms in Unidirectional Composites," Composite Materials: Testing and Design (Seventh Conference), ASTM STP 893, J. M. Whitney, Ed., American Society for Testing and Materials, Philadelphia, 1986, pp. 115-139.

18. Gurdal, Z. and Haftka, R. T., "Compressive Failure Model For Anisotropic Plates With a Cutout," AIAA Journal, Vol. 25, No. 11, Nov.1987.

19. Whitney, J. M. and Nuismer,R. J., "Stress Fracture Criteria for Laminated Composites Containing Stress Concentrations," J. Composite Materials, Vol. 8 (July 1974), p. 253.

20. Tan, S. C., "Notched Strength prediction and Design of Laminated Composites Under In-Plane Loadings," J. Composite Materials, Vol. 21, August 1987.

21. Tan, S. C., "Laminated Composites Containing an Elliptical Opening. I. Approximate Stress Analyses and Fracture Models," J. Composite Materials, Vol. 21, October 1987.

22. Tan, S. C., "Laminated Composites Containing an Elliptical Opening. II. Experiment and Model Modification," J. Composite Materials, Vol. 21, October 1987.

23. Mikulas, M. Jr., "Failure Prediction Techniques for Compression Loaded Composite Laminates with Holes," Selected NASA Research in Composite Materials and Structures, NASA CP 2142, Seattle, WA., Aug. 1980.

24. Ishikawa, T., "Anti-Symmetric Elastic Properties of Composite Plates of Satin Weave Cloth," Fib. Sci. Tech., Vol. 15 (1981).

25. Ishikawa, T and Chou, T. W., "One-Dimensional Micromechanical Analysis of Woven Fabric Composites," AIAA Journal, Vol. 21 No. 12 (1983).

26. Ishikawa, T and Chou, T. W., "Stiffness and Strength Behavior of Woven Fabric Composites," J. Materials Science, Vol. 17 (1982).

27. Ishikawa, T and Chou, T. W., "Stiffness and Strength Properties of Woven Fabric Composites," Proceedings of ICCM 4 (Tokyo), (1982).

28. Ishikawa, T and Chou, T. W., "Elastic Behavior of Woven Hybrid Composites," J. Composite Materials, Vol. 16 (1982).

29. Ishikawa, T., Matsushima, M., Hayashi, Y., and Chou, T. W., "Experimental Confirmation of the Theory of Elastic Moduli of Fabric Composites," J. Composite Materials, Vol.19, Sep. 1985.

30. Ishikawa, T and Chou, T. W., "In-Plane Thermal Expansion and Thermal Bending Coefficients of Fabric Composites," J. Composite Materials, Vol. 17, March 1983.

31. Ishikawa, T and Chou, T. W., "Nonlinear Behavior of Woven Fabric Composites," J. Composite Materials, Vol. 17, Sept. 1983.

32. Delmonte, J., *Technology of Carbon and Graphite Fiber Composites,* Robert E. Krieger Publishing Company, 1987, p.134.

33. Kriz, R. D., "Stiffness and Internal Stresses of Woven-Fabric Composites at Low Temperatures," Advances in Cryogenic Engineering, Vol. 30 (1983).

34. Kriz, R. D., "Influence of Damage on Mechanical Properties of Woven Composites at Low Temperatures," Journal of Composites Technology and Research, Vol. 7, No. 2, Summer 1985, pp. 55-58.

35. Kimpara, I., Hamamoto, A., and Takehana, M., "Analysis of First Knee Behavior of Woven Roving Composites," Trans. JSCM, Vol. 3, No. 1/2, Dec. 1977.

36. Jortner, J., "A Mechanistic Model For Delamination of @-D Carbon-Carbon," 7th JANNAF Rocket Nozzle Technology Meeting, Monterey, Nov. 1985.

37. Stanton, E. L., and Kipp, T. E., "Nonlinear Mechanics of Two-Dimensional Carbon-Carbon Composite Structures and Materials," AIAA Journal, Vol. 23, No. 8, August 1985, pp. 1278-1284.

38. Walrath, D. E., and Donald F. A., *Finite Element Micromechanics and Minimechanics Modeling of a Three-Dimensional Carbon-Carbon Composite Material,* University of Wyoming, UWME-DR-501-106-1, Dec. 1985.

39. Avery, W, B., *A Study of the Mechanical Behavior of a 2-D Carbon-Carbon Composite,* Ph.D. Dissertation, Virginia Tech, Blacksburg, Va. 1987.

40. Chamis, C. C., "Simplified Composite Micromechanics Equations For Strength, Fracture, Toughness and Environmental Effects," SAMPE Quarterly, July 1984.

41. Hashin, Z. and Rosen, B. W., "The Elastic Moduli of Fiber-Reinforced Materials," ASME Journal of Applied Mechanics, Vol. 31, 1964.

42. Hashin, Z., "Analysis of Properties of Fiber Composites With Anisotropic Constituents," ASME Journal of Applied Mechanics, Vol. 64, September 1979.

43. Daniel, L. I., Rowlands, R. E., and Post, D., "Strain Analysis of Composites by Moire Methods," Experimental Mechanics, Vol. 13, No. 6, June 1973.

44. Bowles, D. E., Post, D., Herakovich, C. T., and Tenney, D. R., "Moire Interferometry for Thermal Expansion of Composites," Experimental Mechanics, 21(12), Dec. 1981.

45. Hyer, M. W., Herakovich, C. T., and Post, D., "Thermal Expansion of Graphite Epoxy," 1982 Advances in Aerospace Structures and Materials, ASME, New York, 1982. Ii.Nemeth, M. P., Herakovich, C. T., and Post, D., "On the Off-Axis Tensile Test for Unidirectional Composites," Composites Technology Review, 5(2), summer, 1983.

46. Herakovich, C. T., and Post, D., Buczek, M. B., and Czarnek, R., "Free Edge Strain Concentrations in Real Composite Laminates: Experimental-Theoretical Correlation," J. Appl. Mech., Vol. 52, Dec. 1985.

47. Post, D., Czarnek, R.,Joh, D., Jo, J., and Guo, Y., "Experimental Study of a Metal-Matrix Composite," Experimental mechanics, 27(2), June, 1987.

48. Post, D., Czarnek, R.,Joh, D., Jo, J., and Guo, Y., "Deformation of a Metal-Matrix Tensile Coupon with a Central Slot: an Experimental Study," J. of Composites Technology and Research (ASTM), Vol. 9, No. 1, Spring 1987.

49. Post, D., "Developments in Moire Interferometry," Optical Engineering, Vol. 21, No. 3, June 1982.

50. Basehore, M. L. and Post, D., "Moire Method for In-plane and Out-of-plane Displacement Measurements" Experimental Mechanics, Vol. 21, No. 9, Sept. 1981.

51. Post, D., "Moire Interferometry at VPI & SU," Experimental Mechanics, 23(2), June, 1983.

52. Oden, J. T. and Ripperger, E. A., *Mechanics of Elastic Structures,* McGraw-Hill Book Company, 1981. p. 173. .

53. Jones R. M., *Mechanics of Composite Materials,* McGraw-Hill Book Company, 1975. p. 95.

54. Lekhnitskii, S. G., *Theory of Elasticity of an Anisotropic Body,* Mir Publishers, Moscow, 1981.

55. Lekhnitskii, S. G., *Anisotropic Plates,* Translated from the Second Russian Edition by S. W. Tsai, and T. Cheron. Gordon and Breach, 1968.

56. Winkler, E., *Theory of Elasticity and Strength,* Prague: H. Dominicus, 1867 (in German).

57. Vlasov, V. Z., and Leontiev, N. N., *Beams, Plates, and Shells on Elastic Foundations,* Translated from Russian by Israel Program for Scientific Translations, NTIS No. N67-14238 (1966).

58. Filonenko-Borodich, M. M., "Some Approximate Theories of Elastic Foundation," Uch. Zap. Mosk. Gos., Univ. Mech. 46, 1940. pp. 3-18 (in Russian).

59. Hetenyi, M., *Beams on Elastic Foundation,* Ann Arbor: University of Michigan Press, 1946.

60. Hetenyi, M., "Series Solutions for Beams on Elastic Foundations," Journal of Applied Mechanics, 507-514 (June 1971).

61. Pasternak, P. L., "On a New Method of Analysis of an Elastic Foundation by Means of Tow Foundation Constants," Moscow: Gos. Izd. Lit. po Stroit i Arkh, 1954 (in Russian).

62. Zhaohua, F., and Cook, R. D., "Beam Elements on Two-Parameter Elastic Foundations," Journal of Engineering Mechanics, Vol. 109, No.6, December 1983.

63. Biot, M. A., "Bending of an Infinite Beam on an Elastic Foundation," Transactions ASME, Journal of Applied Mechanics, 59, A1-A7 (1937).

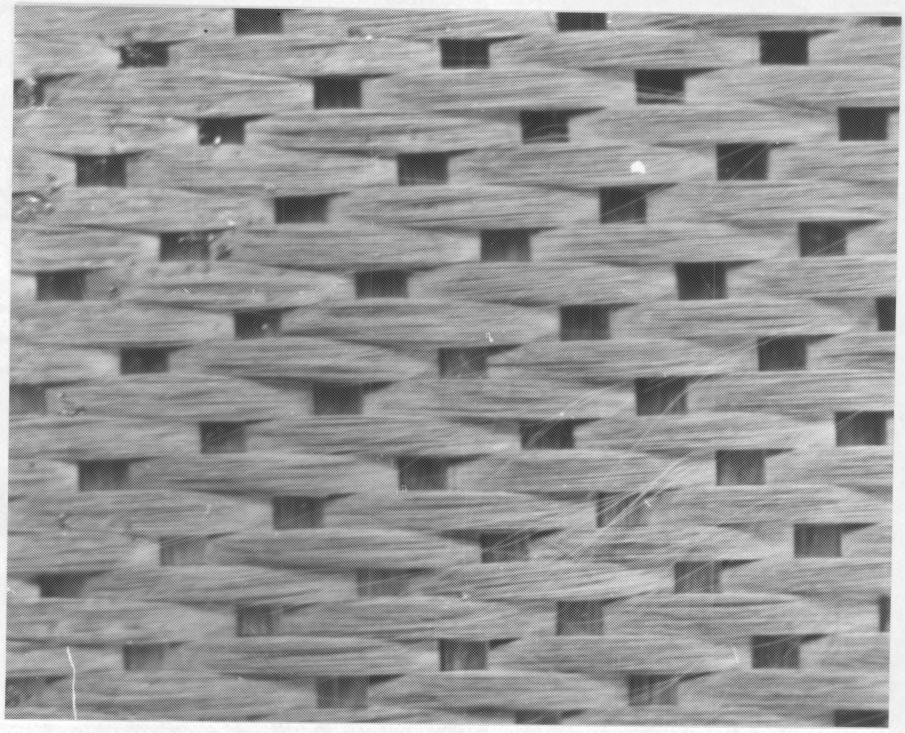

(a)

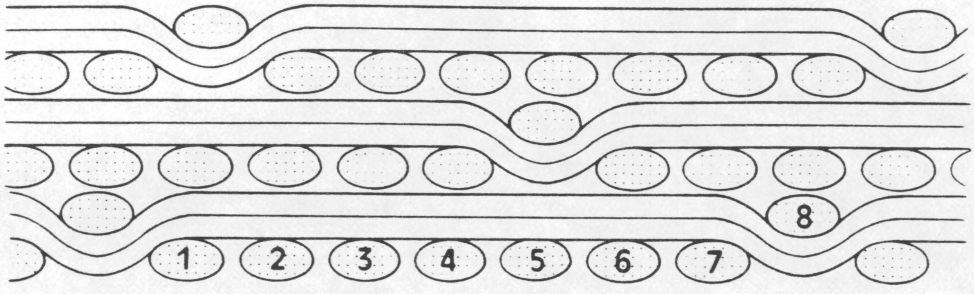

(b)

Figure 1. **Weave pattern of an eight-harness satin:** a) fill and warp bundles surface, b) idealized cross-section.

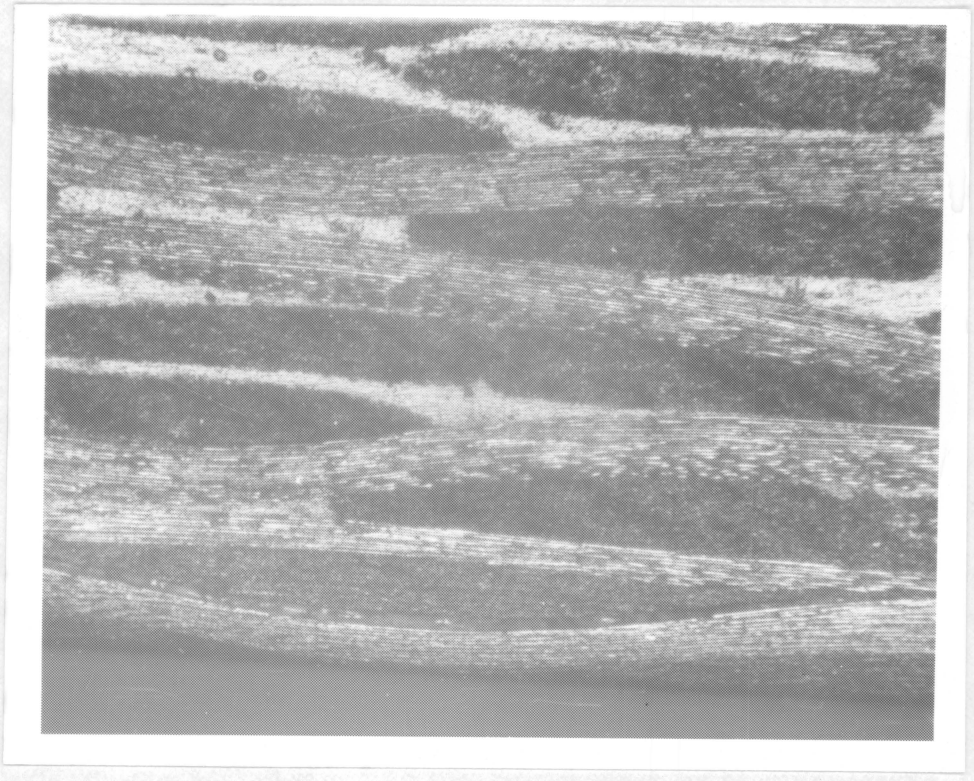

Figure 2. Micrographic view of the cross-section of 8H C3000/PMR15 composite laminate.

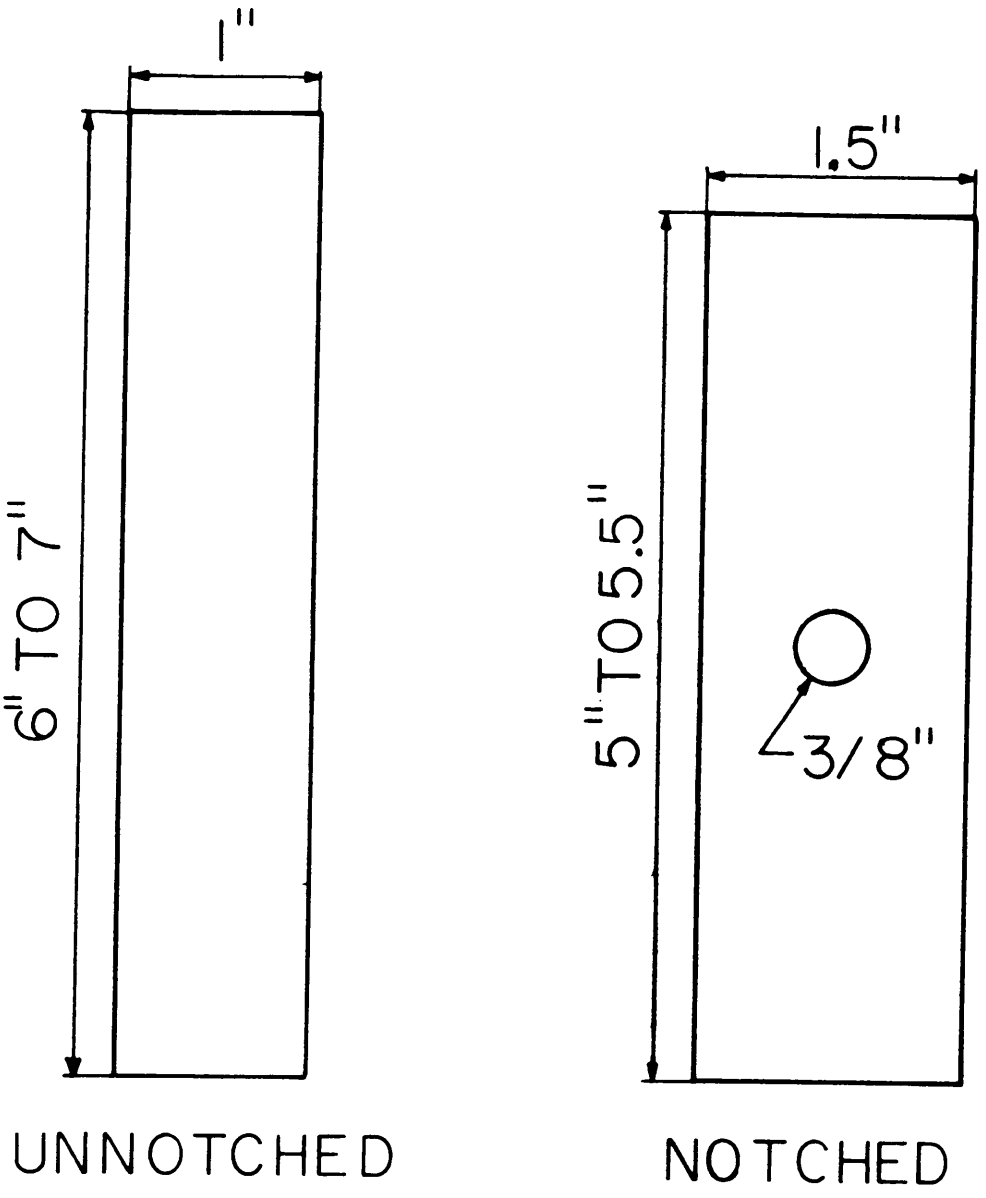

Figure 3. Center-notched and unnotched specimen geometries.

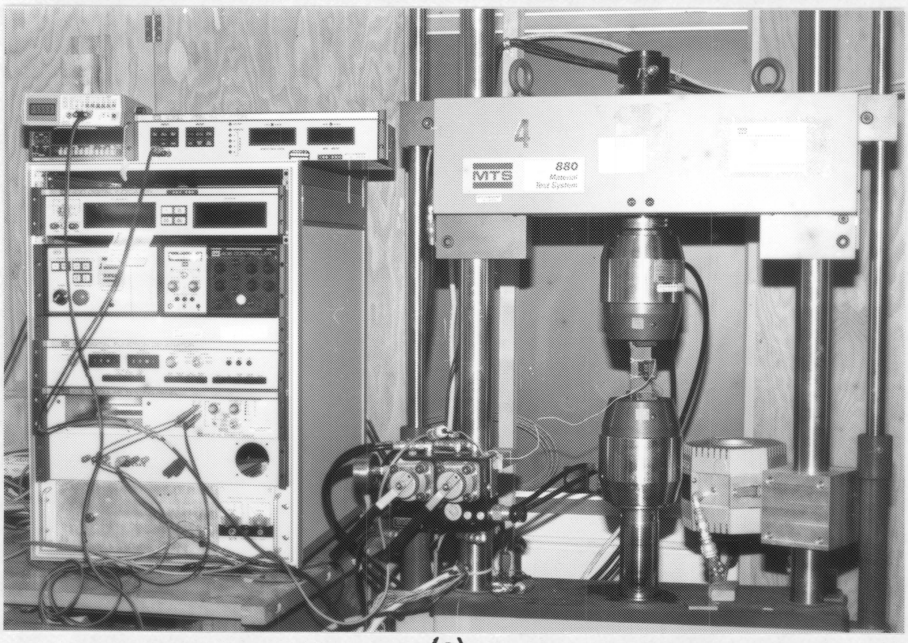

(a)

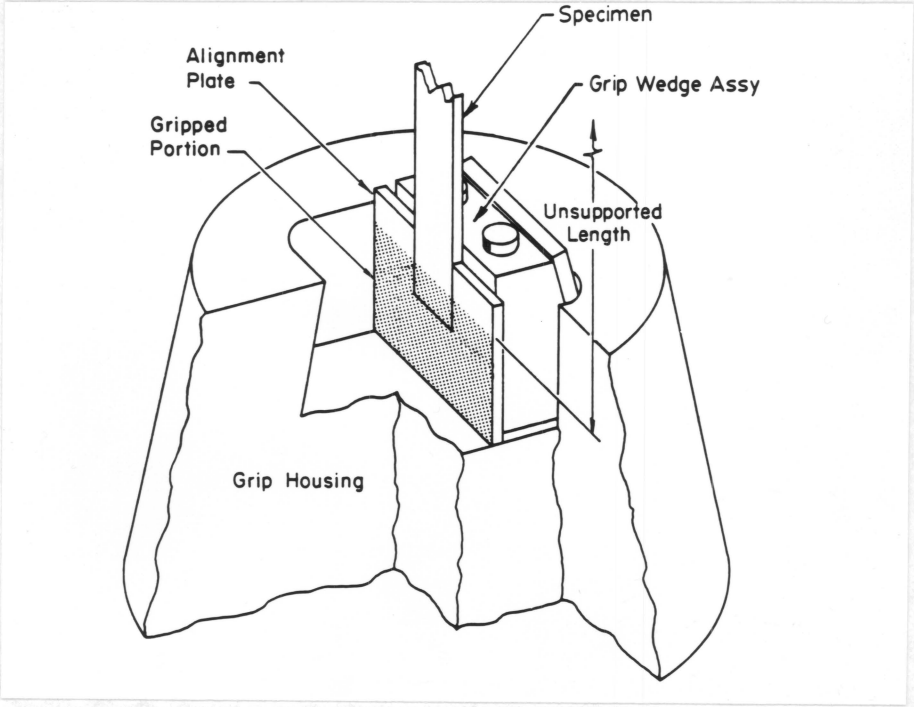

(b)

Figure 4. The 20-kip MTS hydraulic test frame: a)The overall figure b) Schematic of a specimen in the grips.

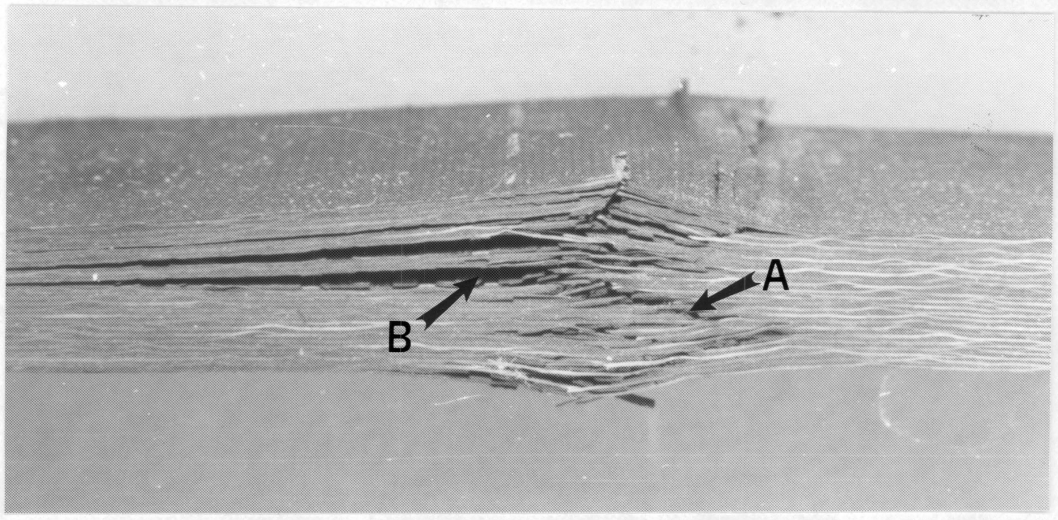

(a)

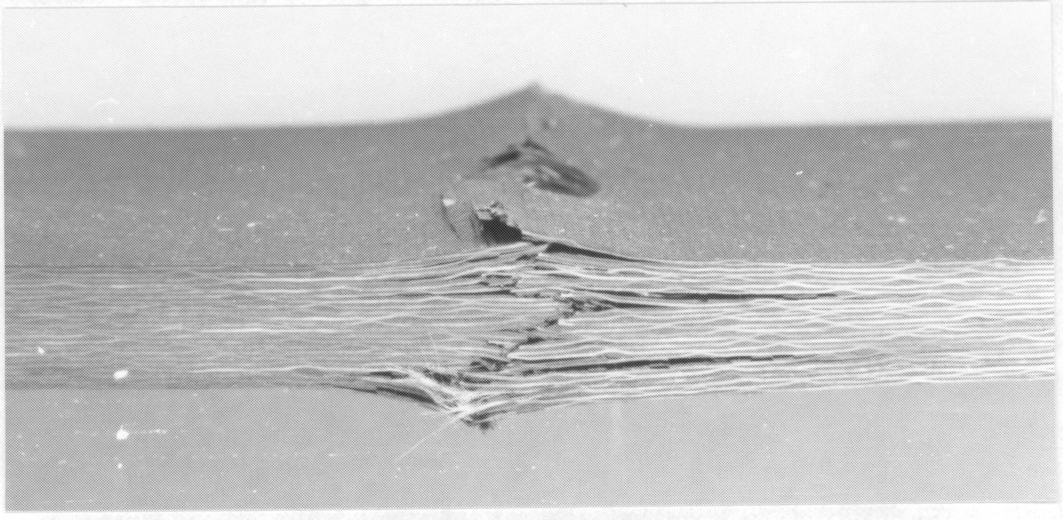

(b)

Figure 5. Post-failed configurations of specimens: a) unnotched, b) notched.

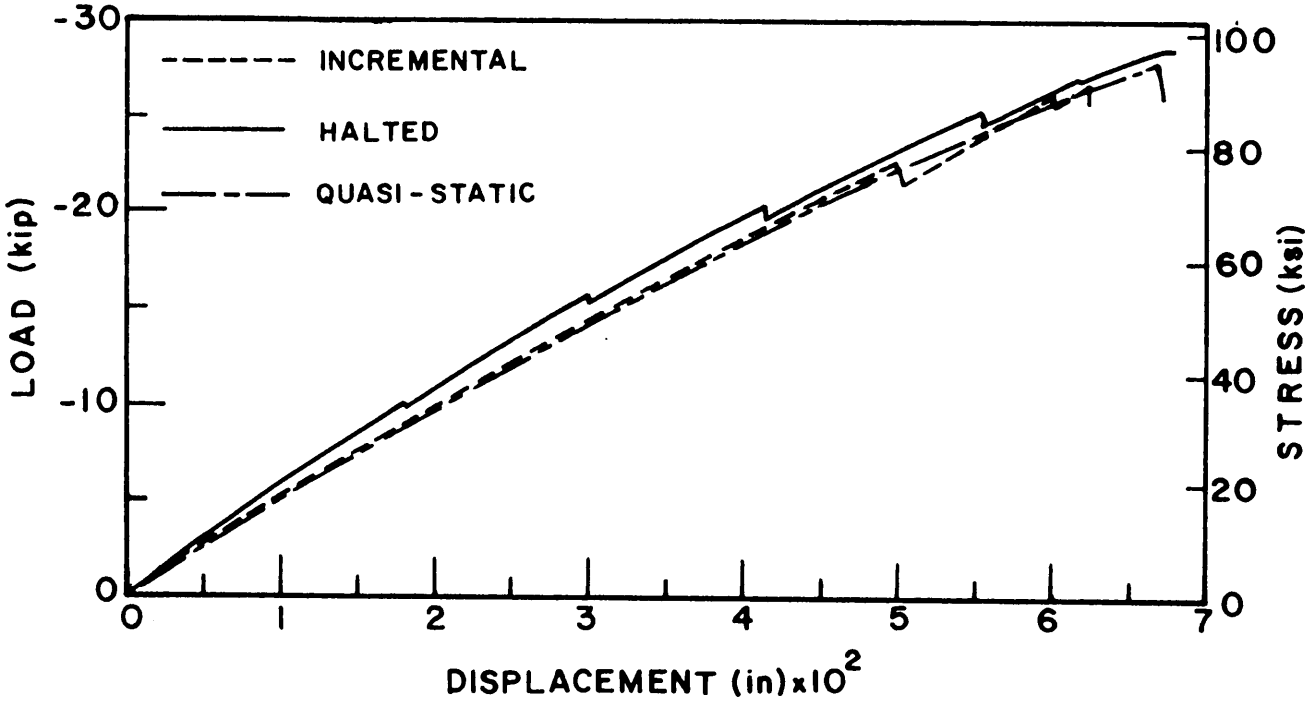

Figure 6. Load-displacement graphs of a 22-ply unidirectional specimen under different loading conditions.

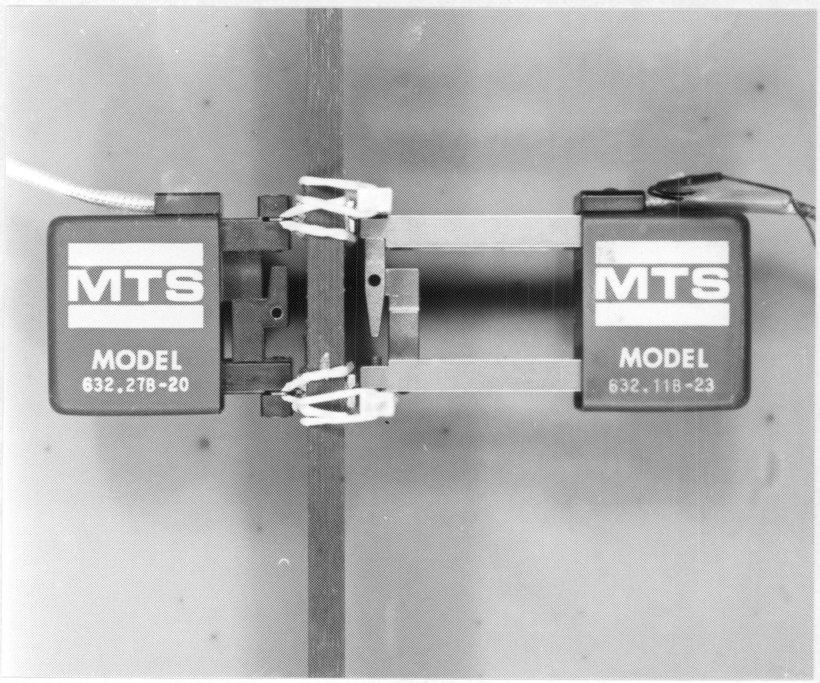

Figure 7. 1" extensometers attached to a specimen.

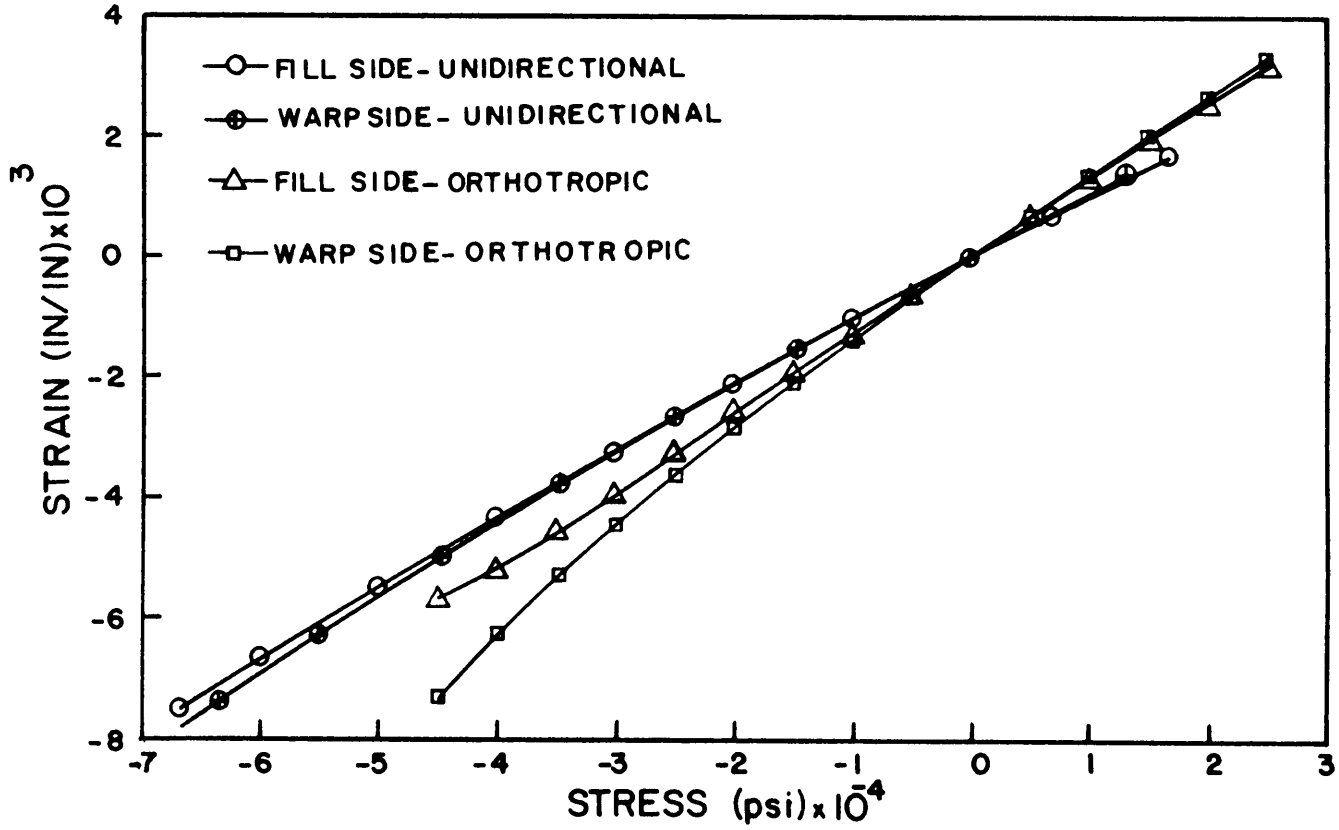

Figure 8. Stress-strain curves of a 22-ply unidirectional and a 15-ply orthotropic specimen.

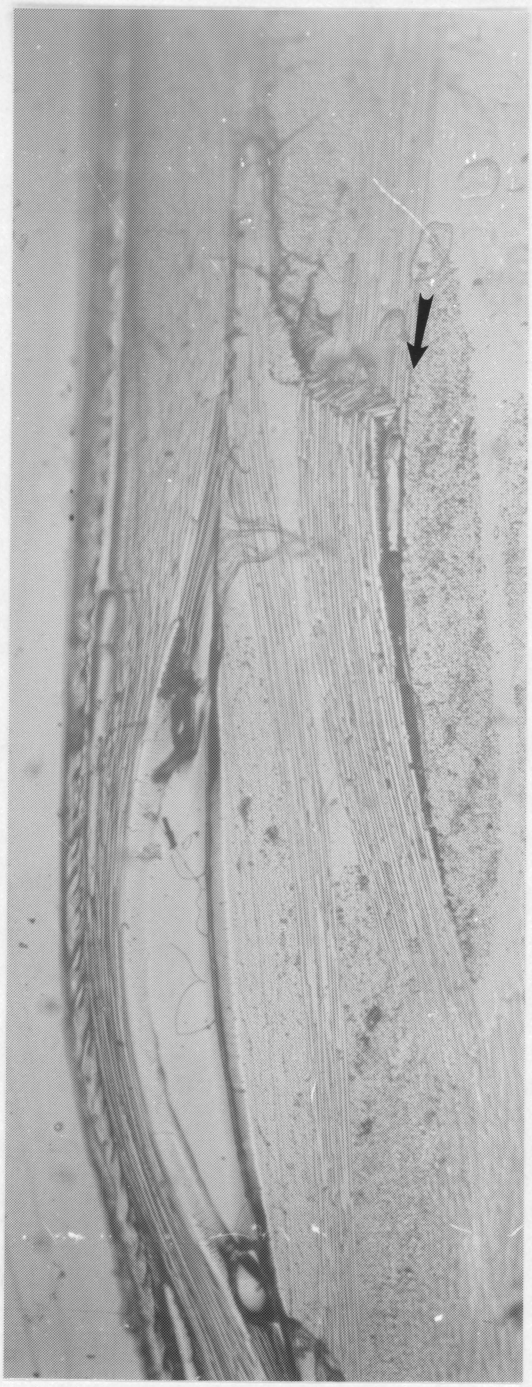

Figure 9. A fiber bundle kink in the second ply from the surface of a specimen under compression.

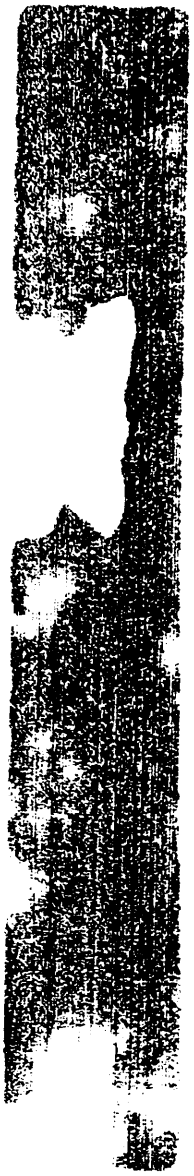

Figure 10. Ultrasonic C-scan of a failed specimen.

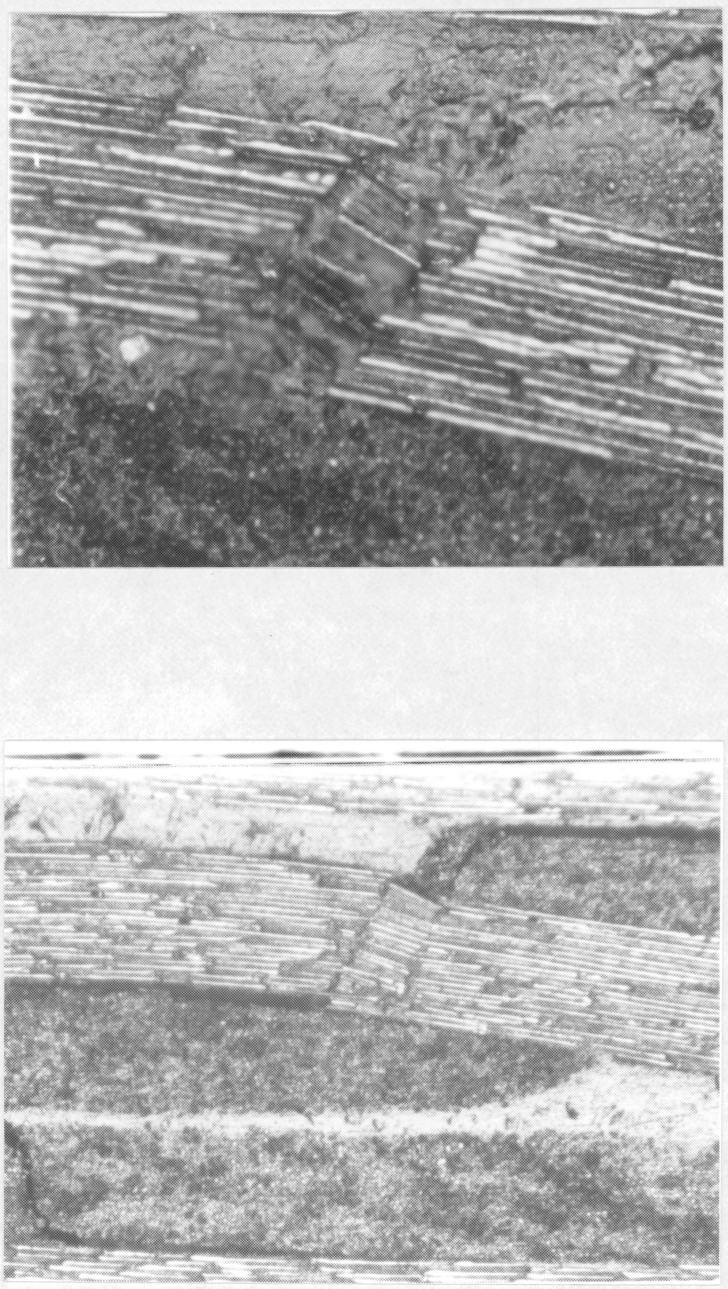

Figure 11. Typical fiber bundle kinks with parallel boundaries.

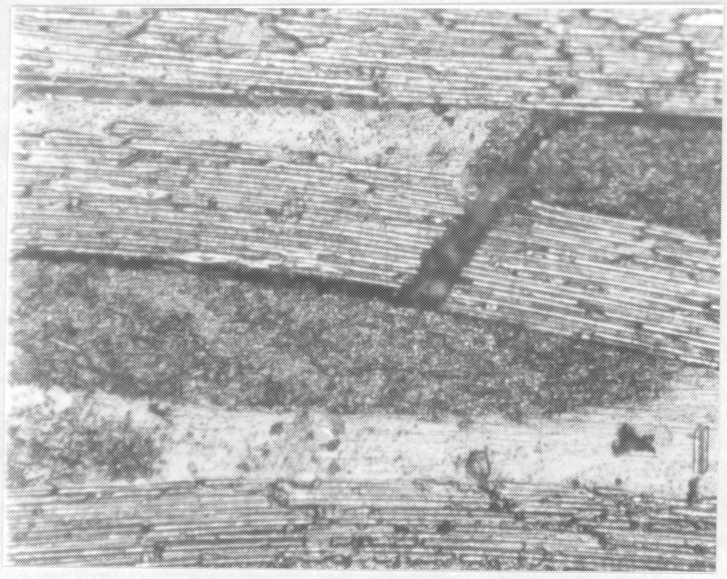

(a)

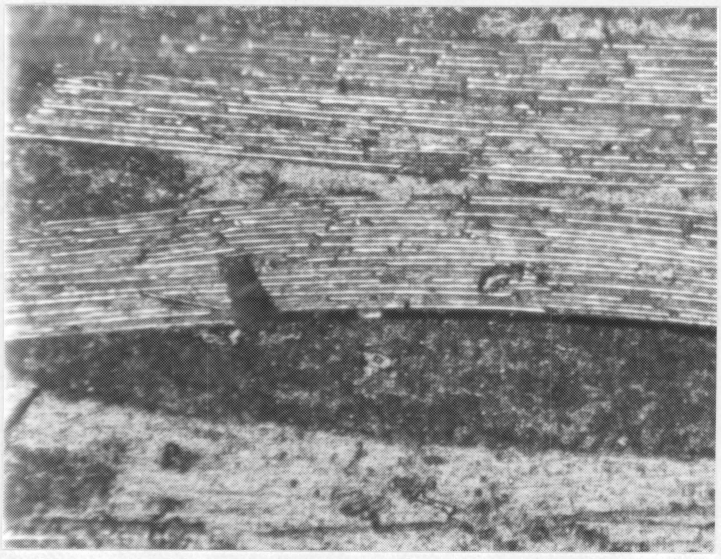

(b)

Figure 12. Fiber bundle kinks: a) single crack kink, b) partial kink.

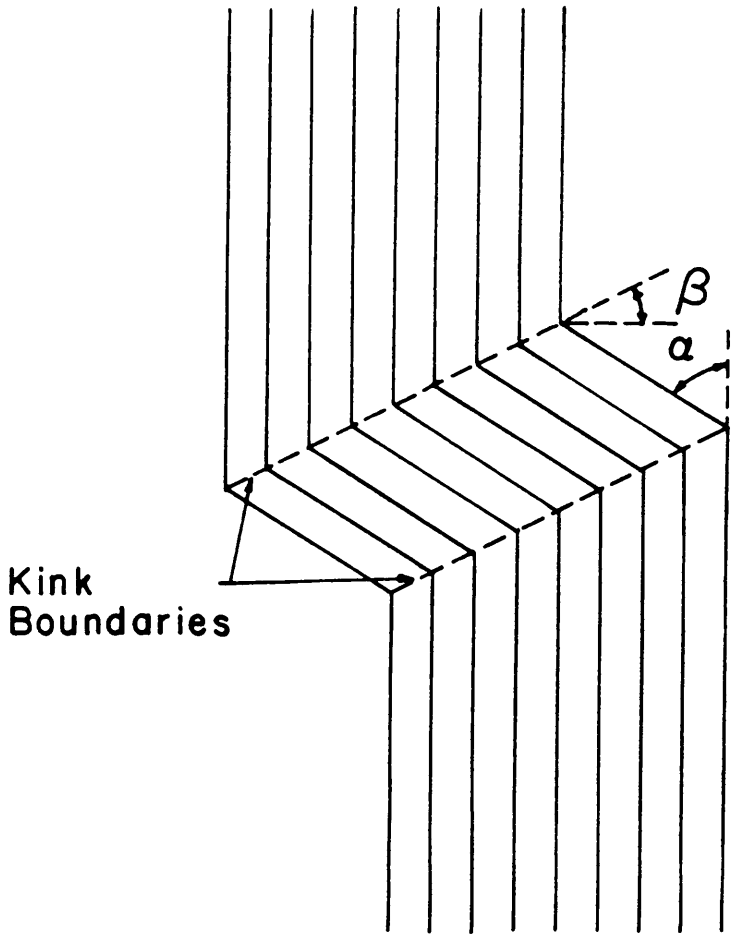

Figure 13. Fiber bundle kink geometry.

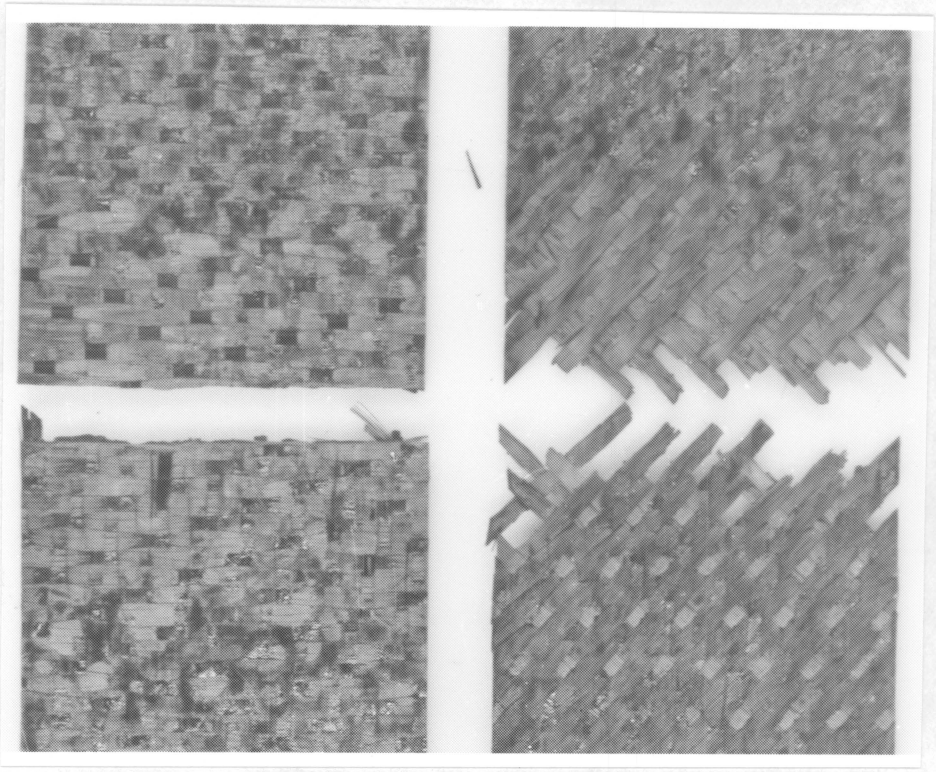

Figure 14. Typical failure boundaries in 0-deg and 45-deg plies of an unnotched specimen.

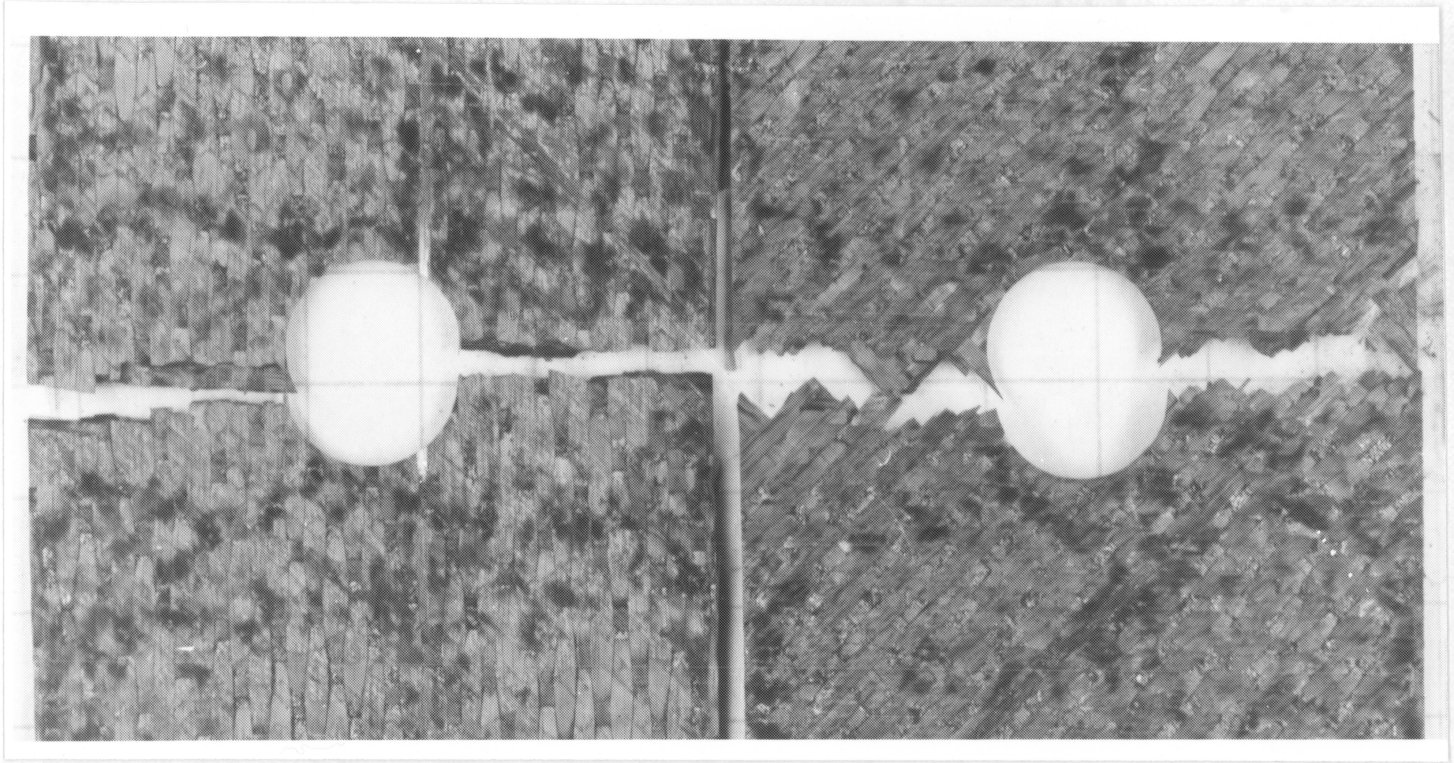

Figure 15. Typical failure boundaries in 0-deg and 45-deg plies of a notched specimen.

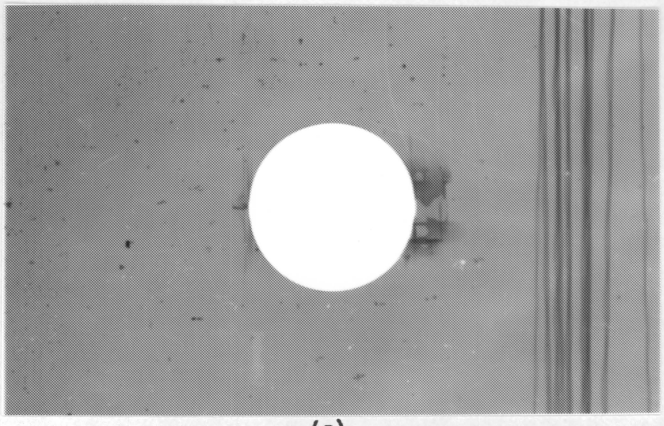

(a)

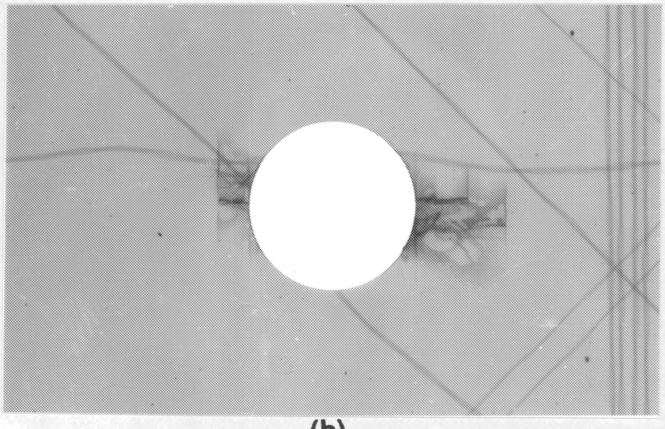

(b)

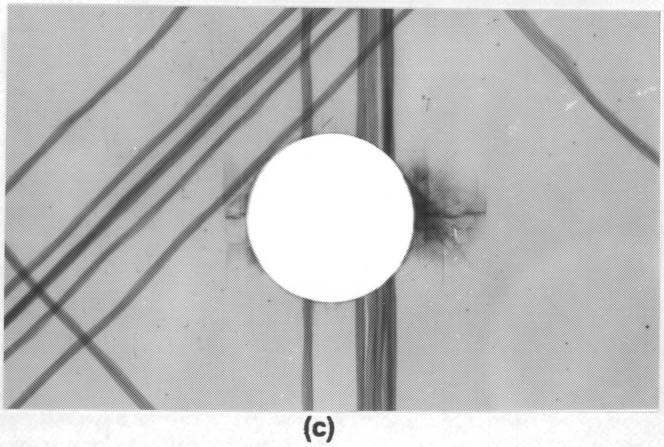

(c)

Figure 16. X-ray radiographs of specimens: a) N03, b) NB3, and c) NB8.

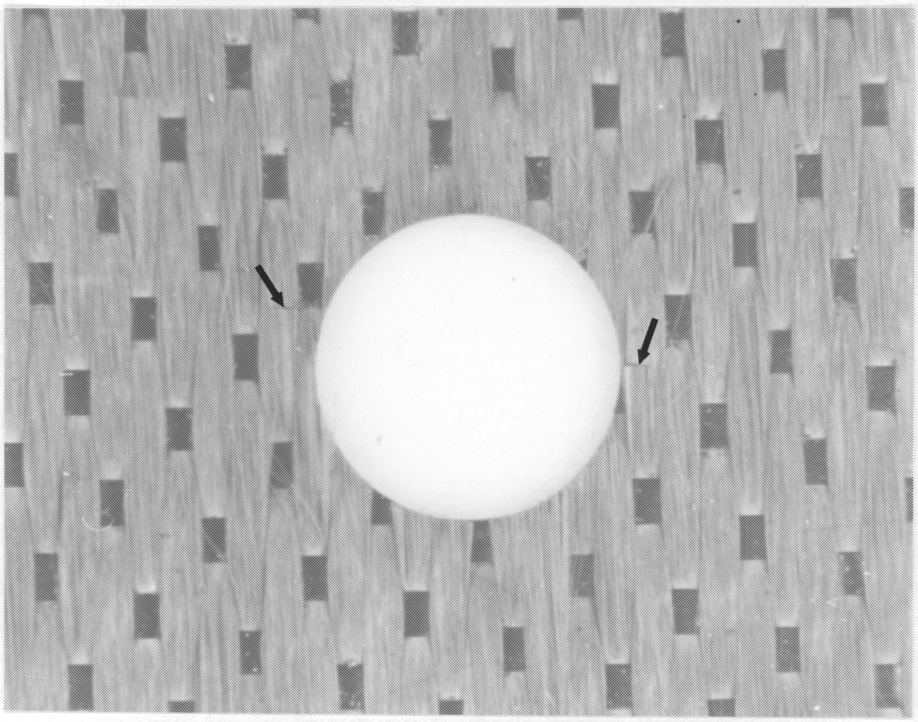

Figure 17. The surface ply of a 12-ply unidirectional specimen (N03).

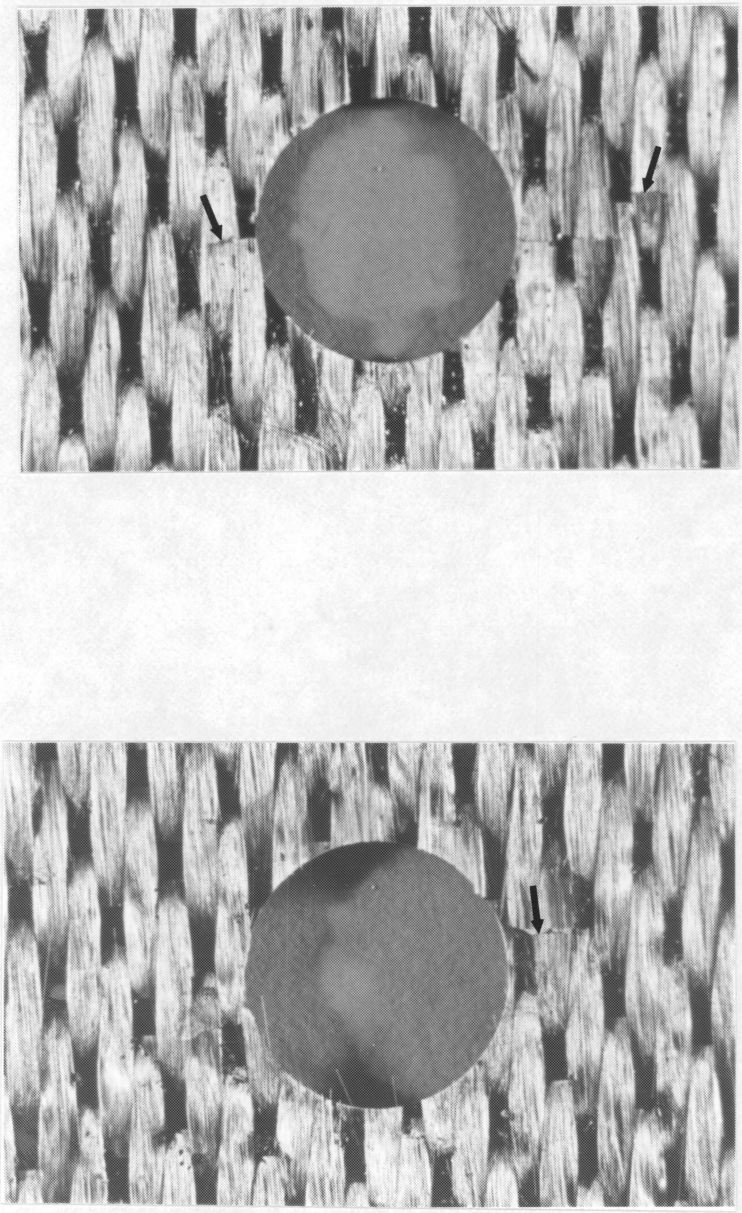

Figure 18. 1st and 3rd plies of a 15-ply orthotropic specimen (NB3).

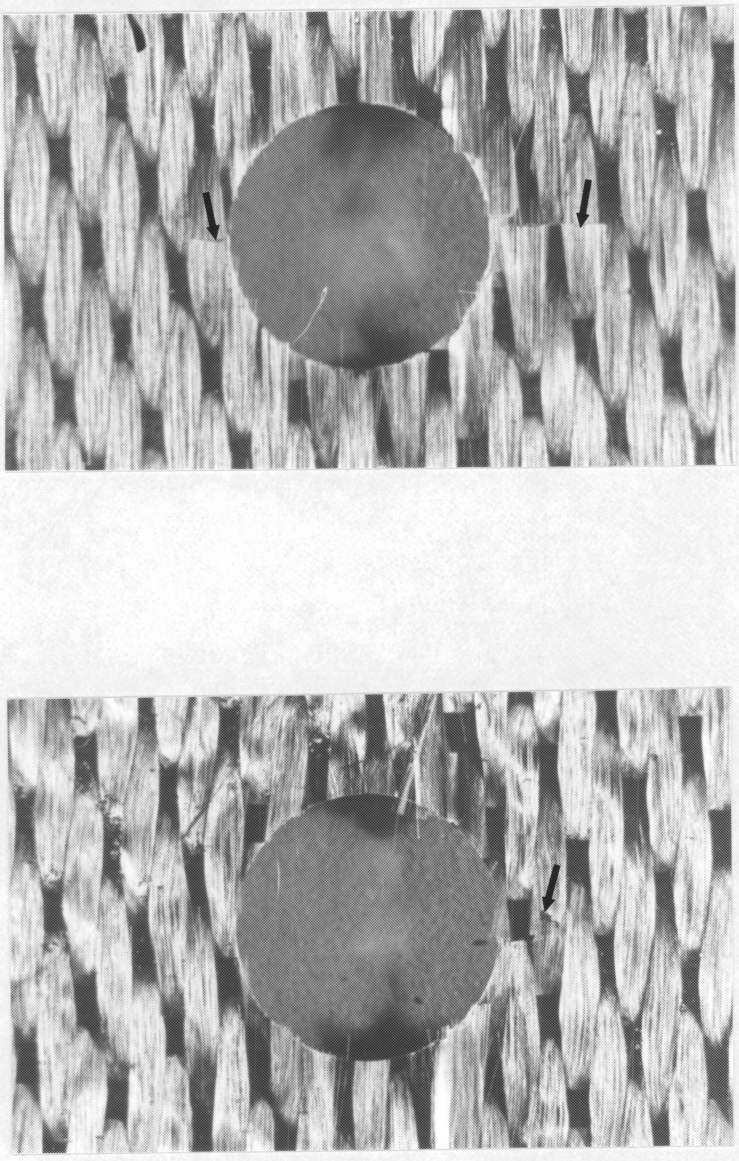

Figure 19. 1st and 10th plies of a 12-ply quasi-isotropic specimen (NB8).

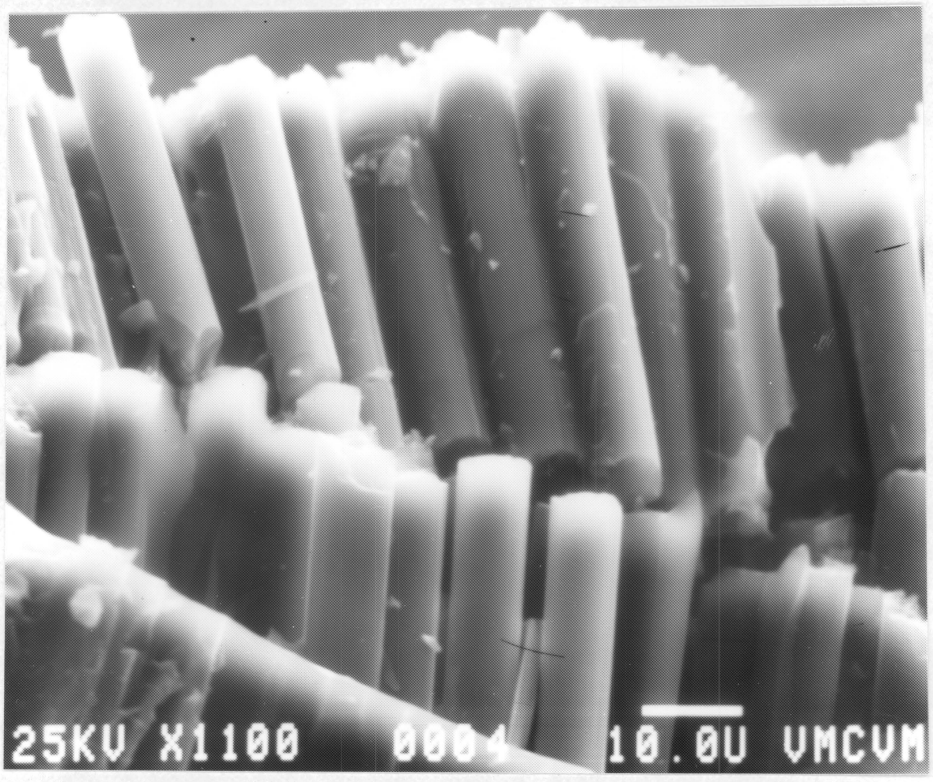

Figure 20. Portion of a kink band observed under SEM.

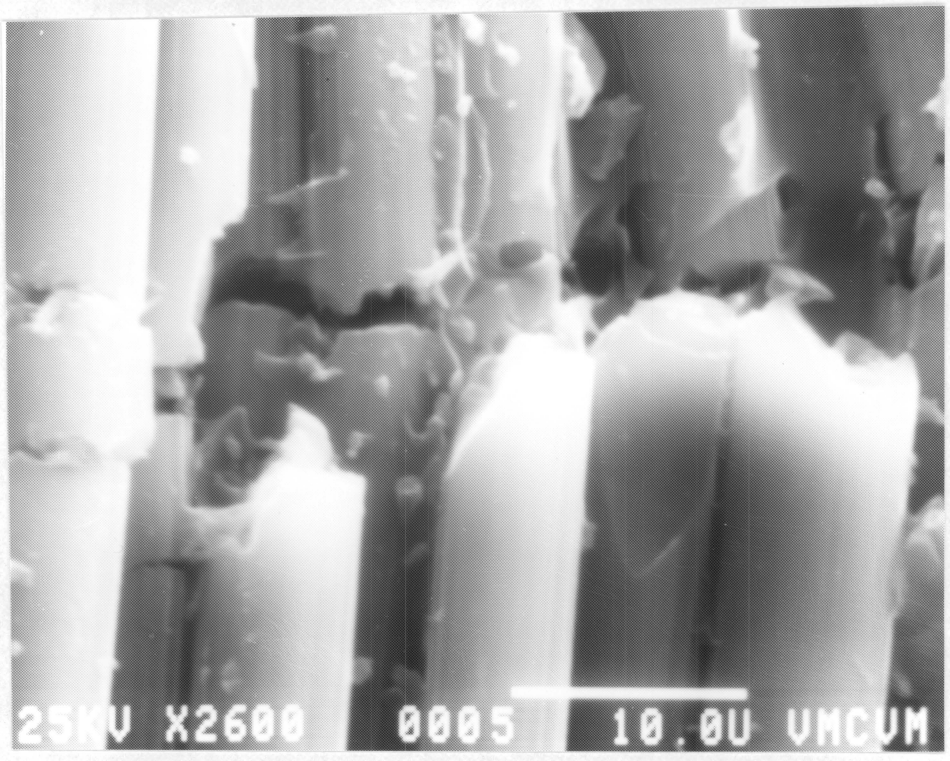

Figure 21. Fracture surfaces of the fibers in a kink band due to axial and bending stresses.

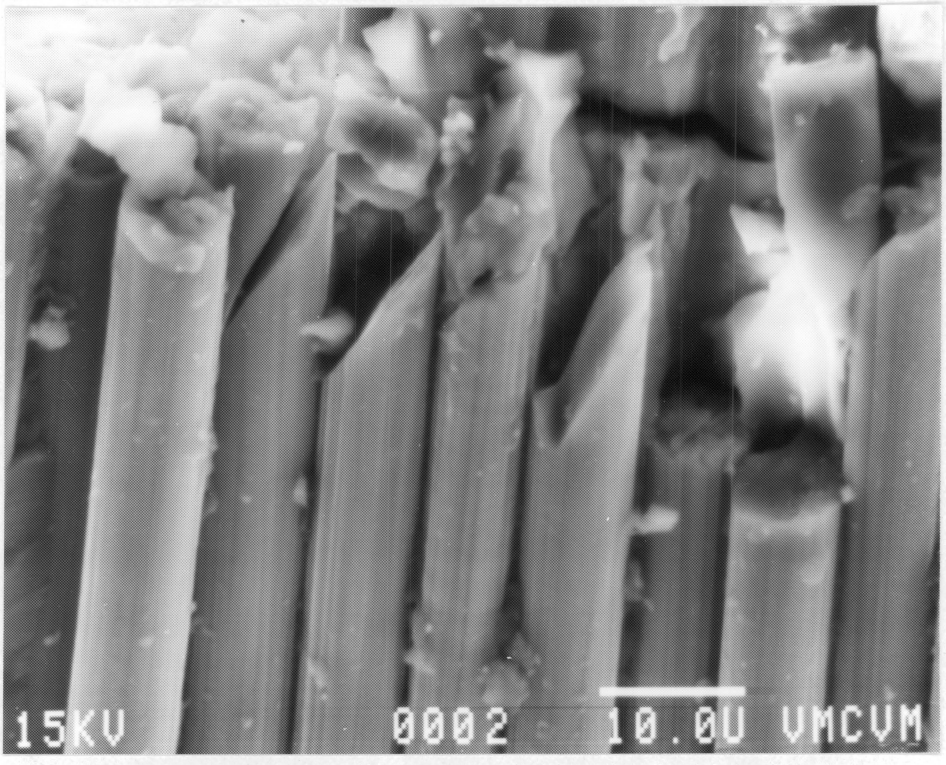

Figure 22. Fracture surfaces of the fibers in a kink band due to axial stresses only.

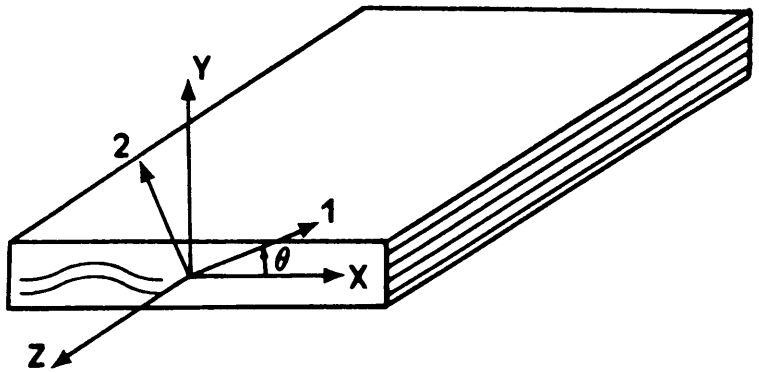

Figure 23. Finite element global and local coordinates in a long body.

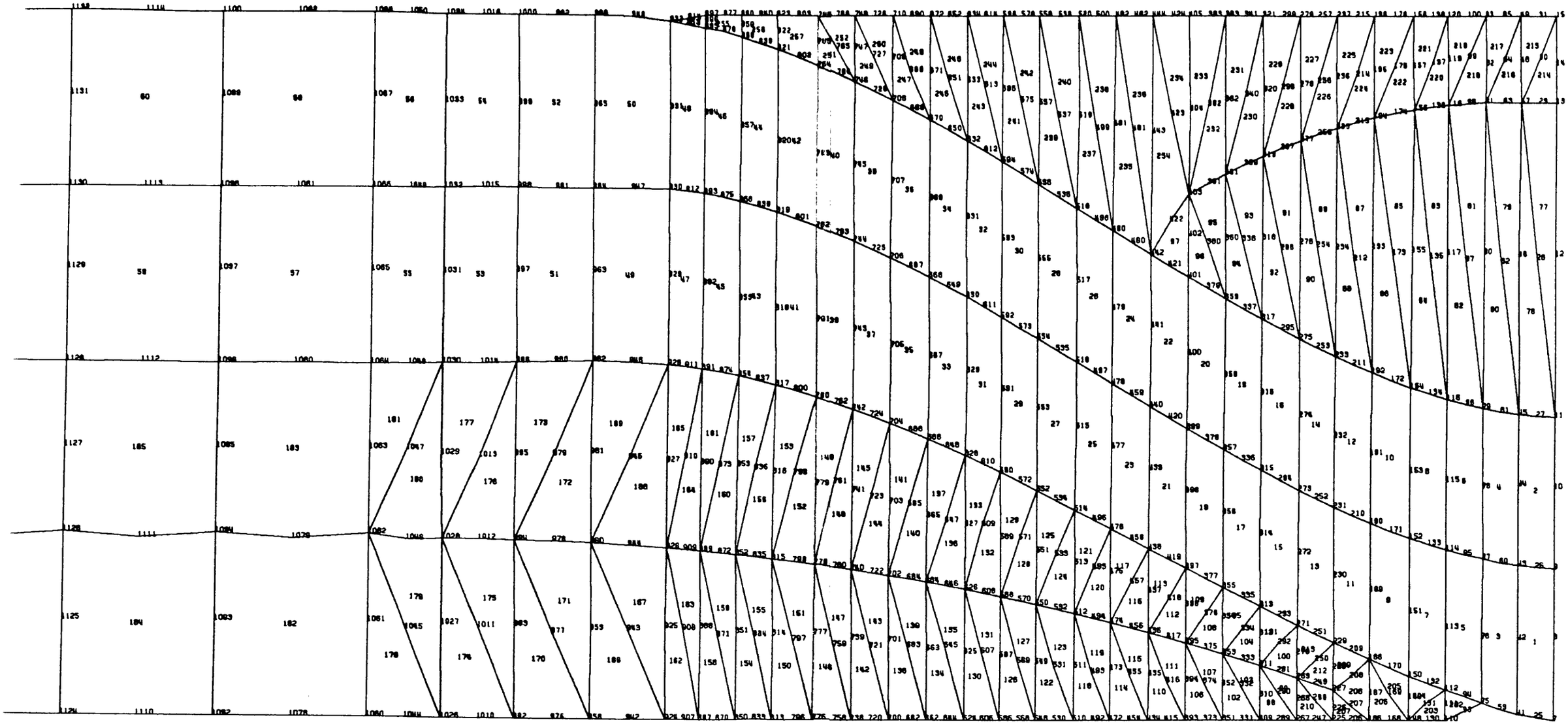

Figure 24. Undeformed finite element mesh plot of a lamina.

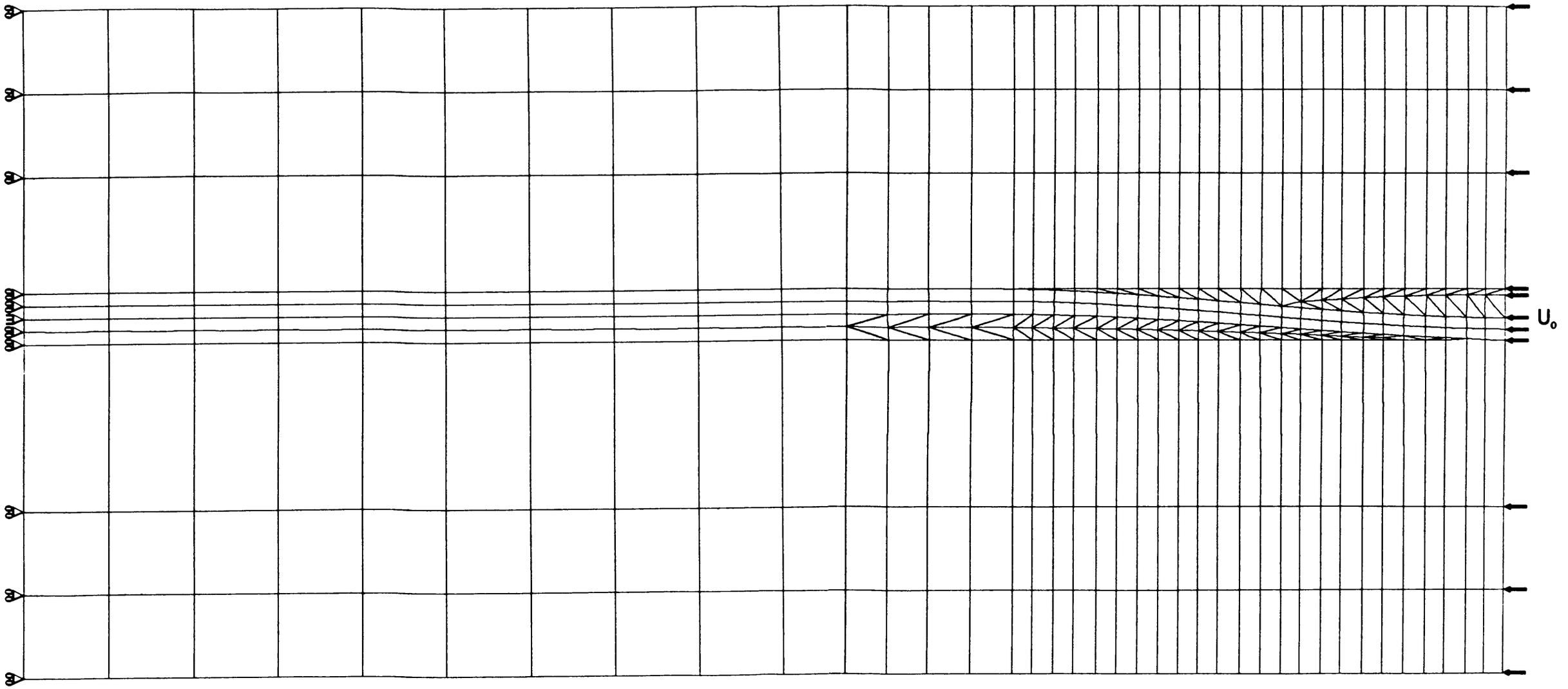

Figure 25. Undeformed finite element mesh plot of a unidirectional laminate with its boundary conditions.

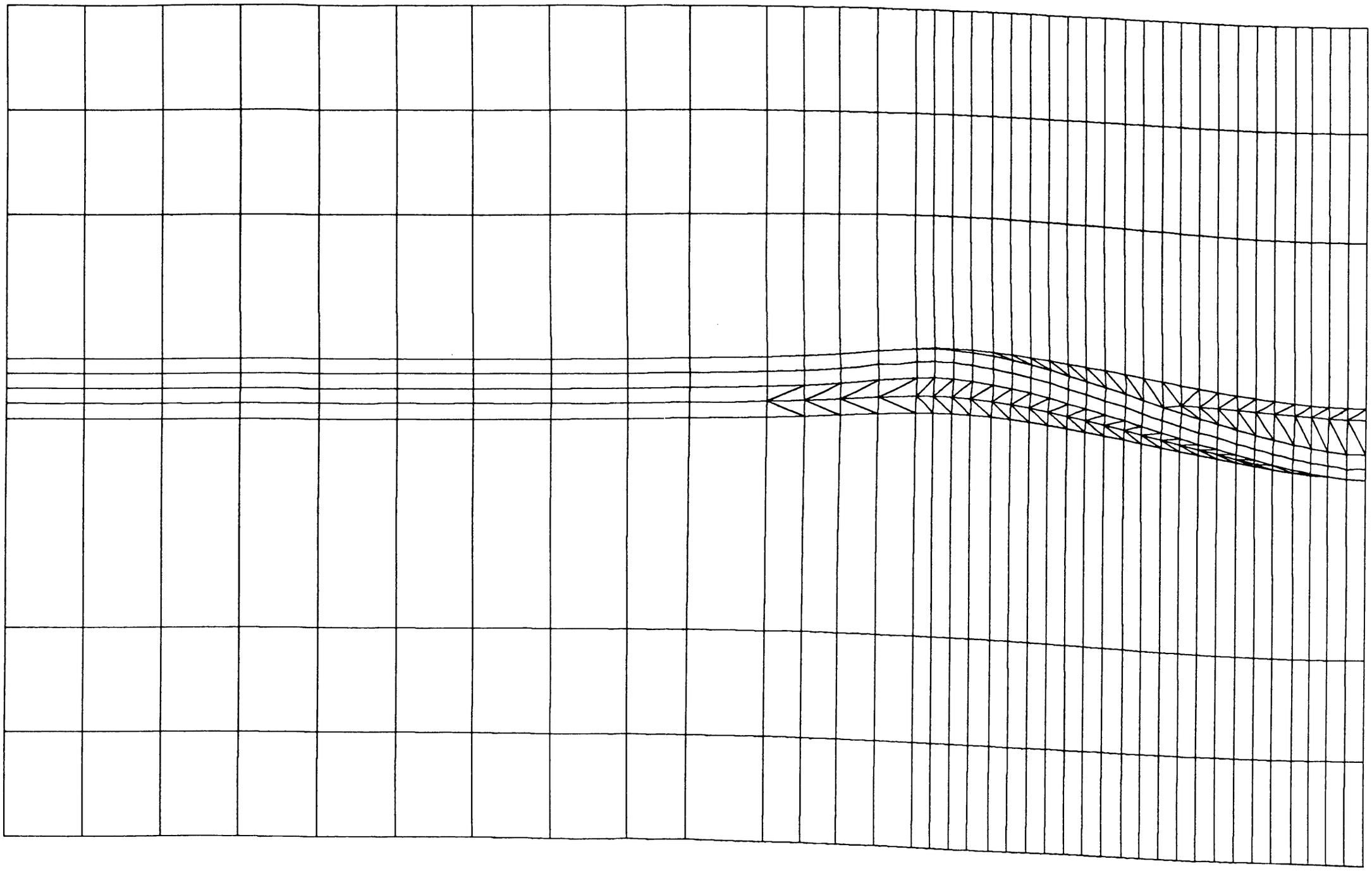

Figure 26. Deformed finite element mesh plot of a unidirectional laminate.

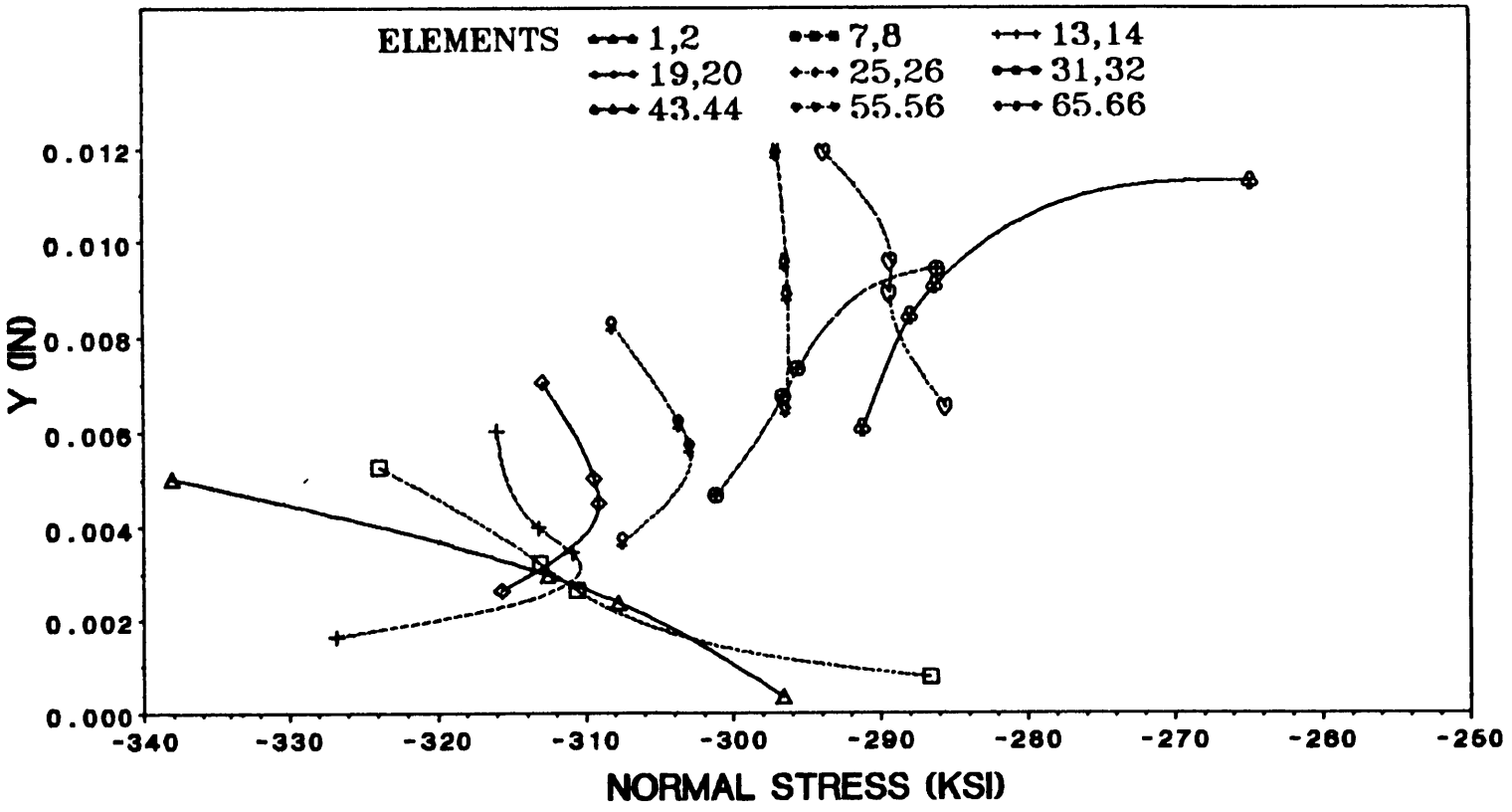

Figure 27. Distributions of σ_x across the bundle at the Gauss points.

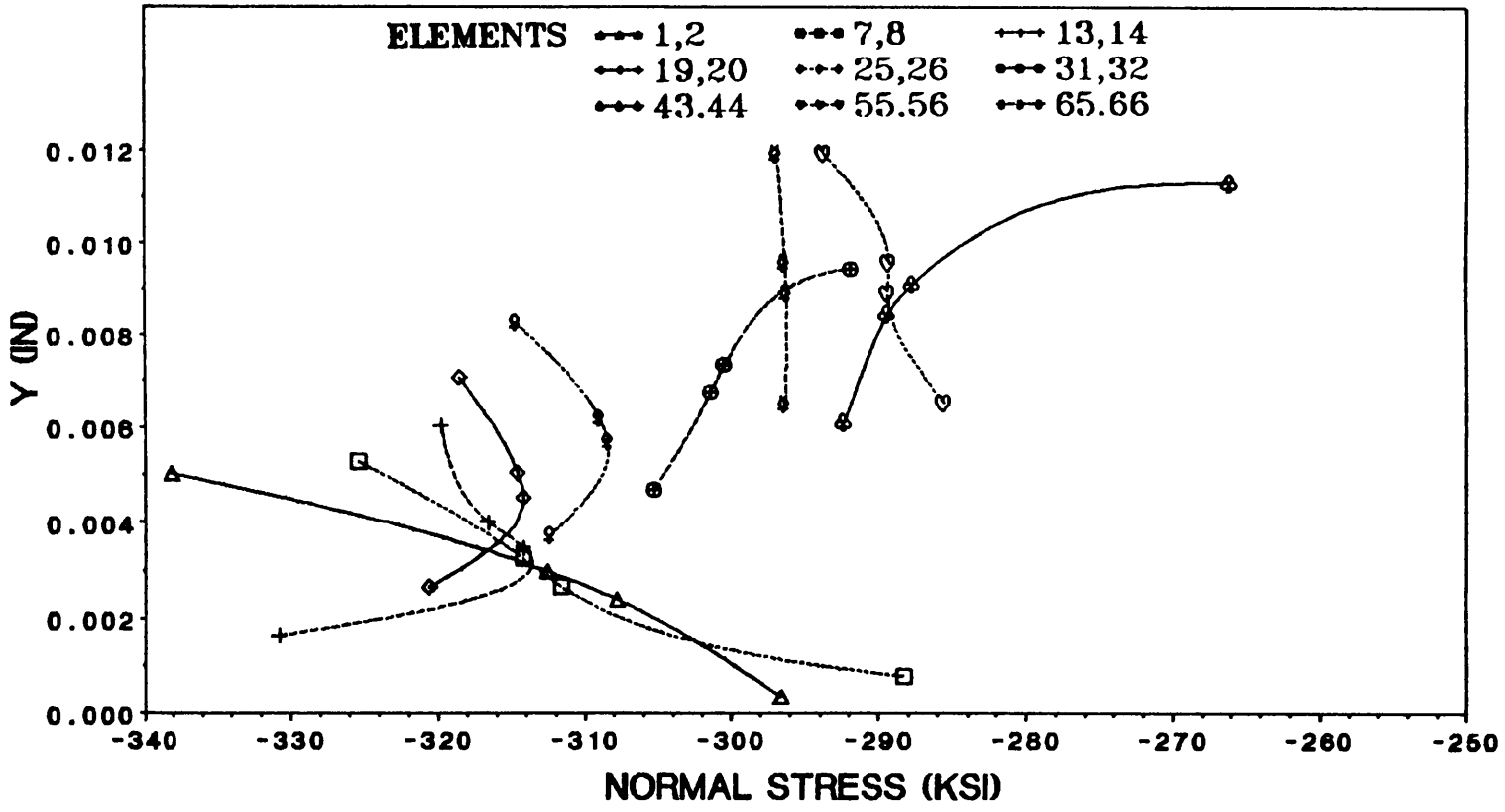

Figure 28. Distributions of σ_1 across the bundle at the Gauss points.

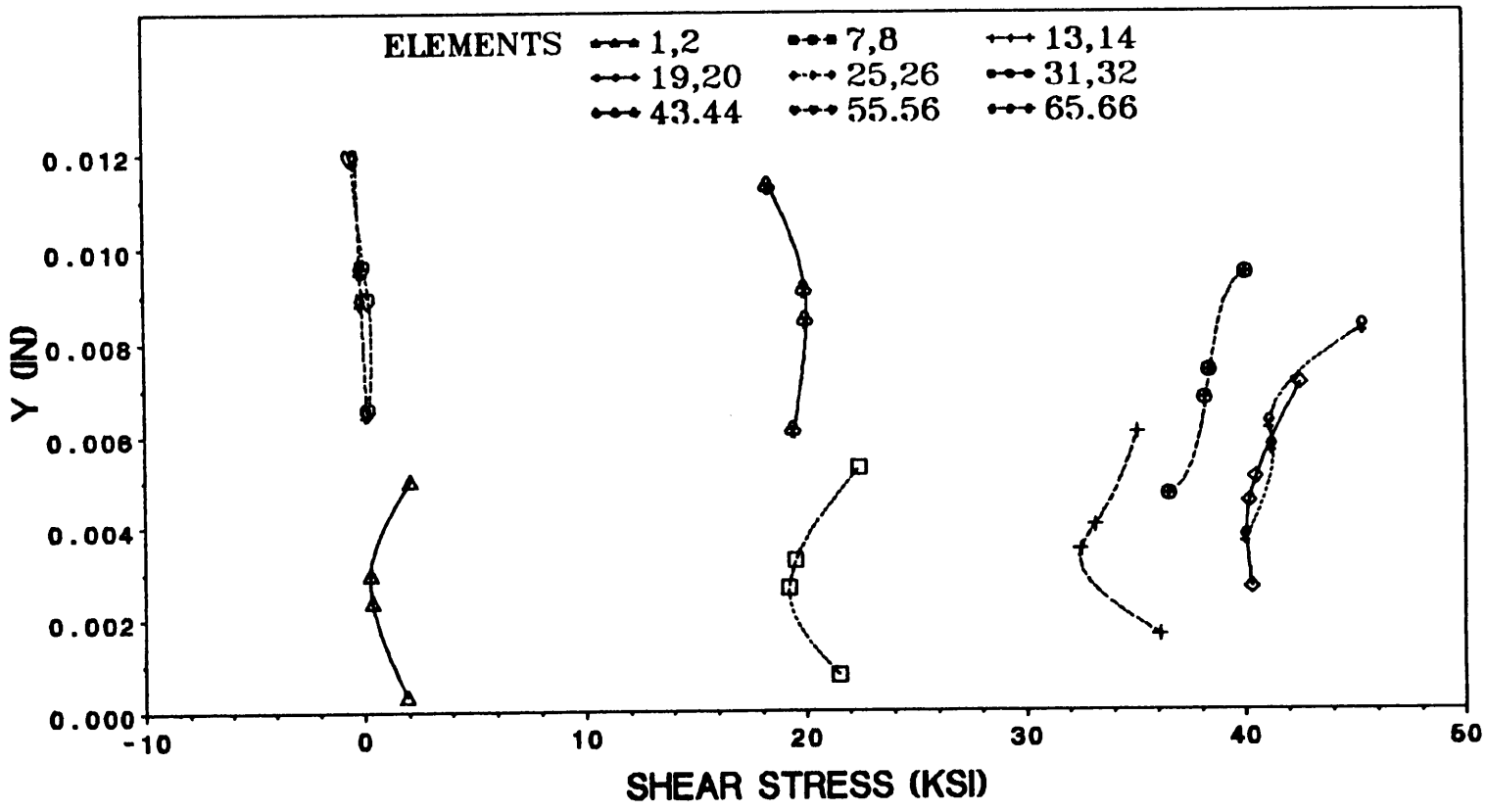

Figure 29. Distributions of τ_{xy} across the bundle at the Gauss points.

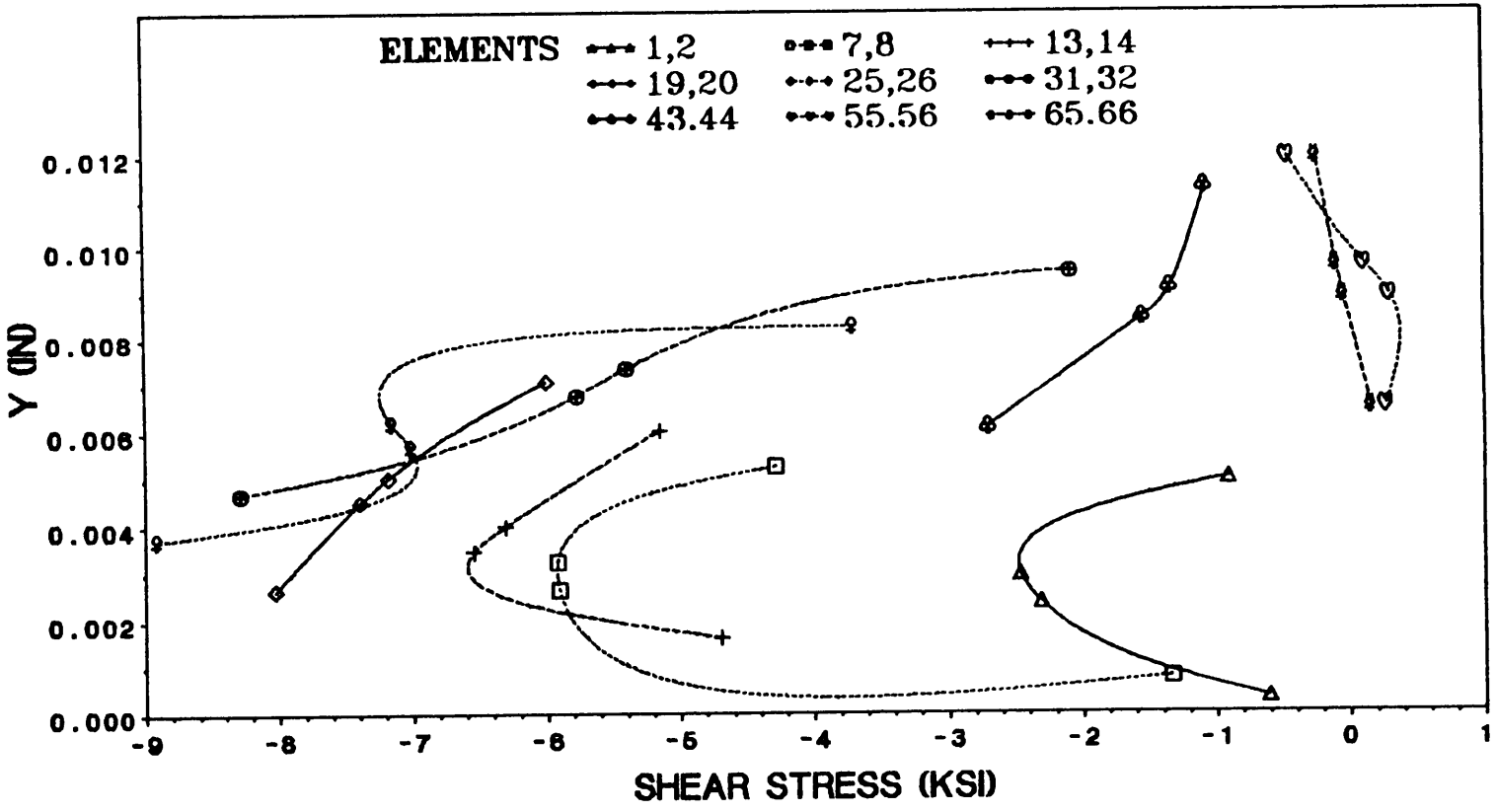

Figure 30. Distributions of τ_{12} across the bundle at the Gauss points.

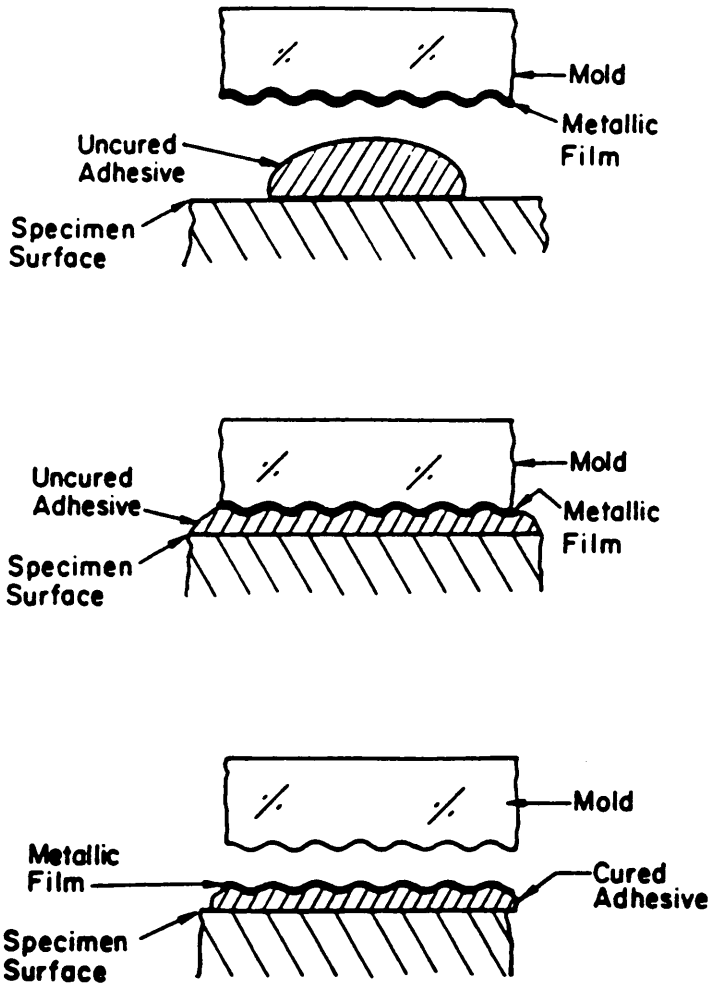

Figure 31. Procedure for molding grating onto specimens.

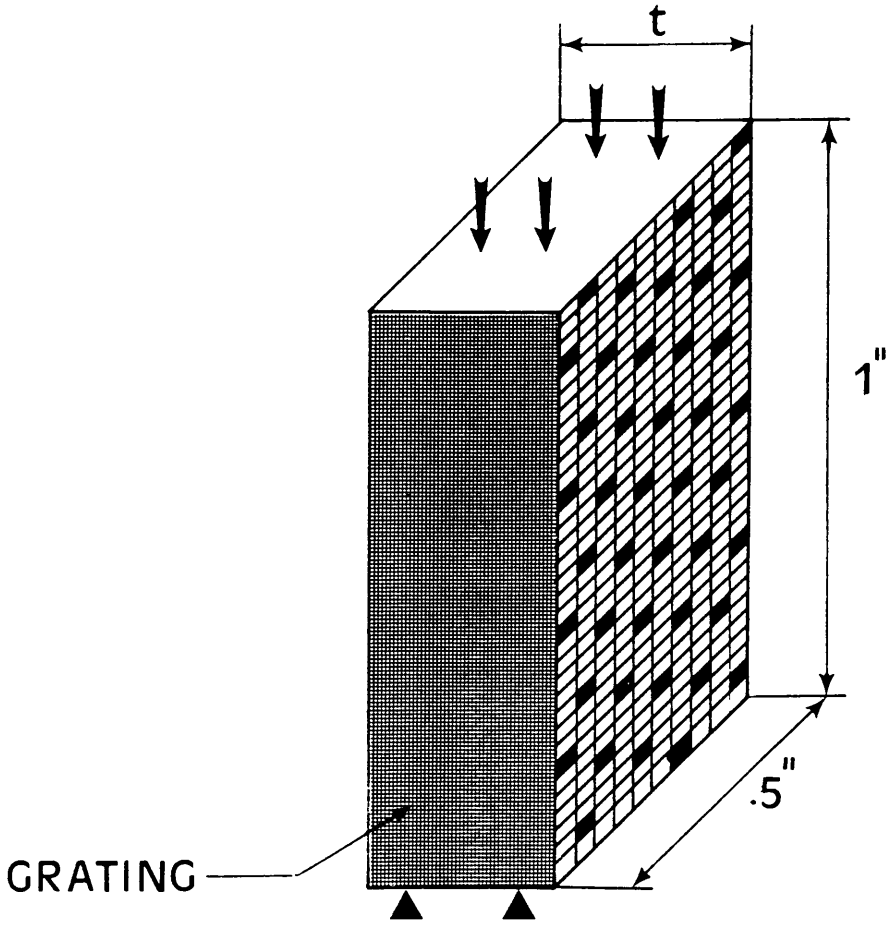

Figure 32. Specimen geometry and loading.

$\sin\alpha = f\lambda/2$; $f = 2400$ lines/mm

$U = N_x/f$; $V = N_y/f$

$\epsilon_x = \frac{\partial U}{\partial x}$; $\epsilon_y = \frac{\partial V}{\partial y}$

$\gamma_{xy} = \frac{\partial U}{\partial y} + \frac{\partial V}{\partial x}$

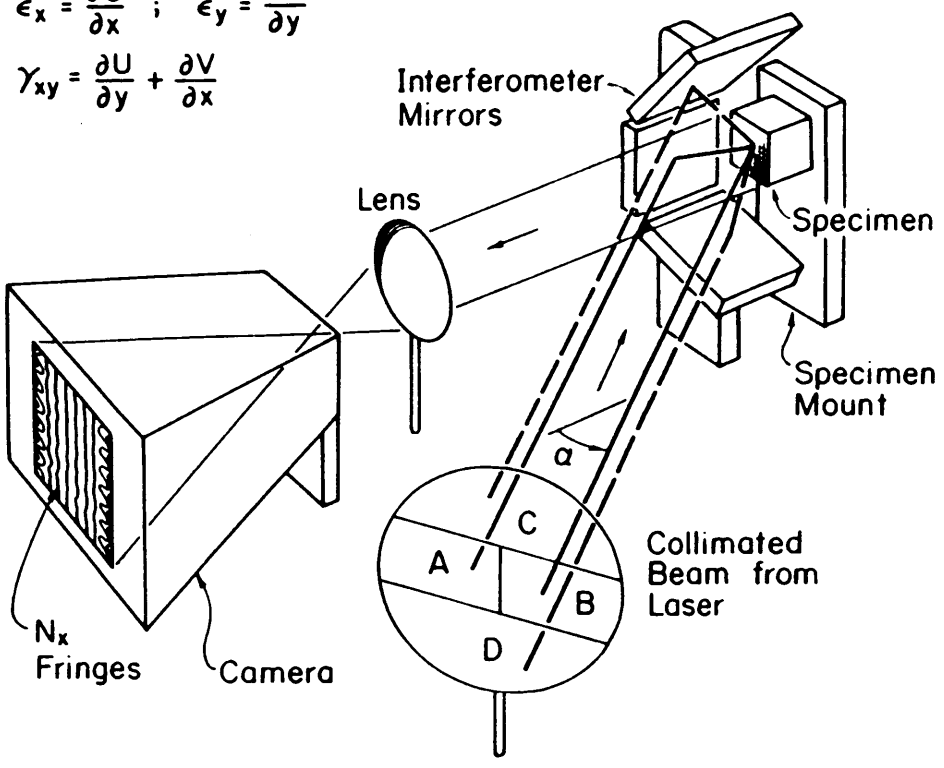

Figure 33. Schematic of the setup for the Moire interferometry test.

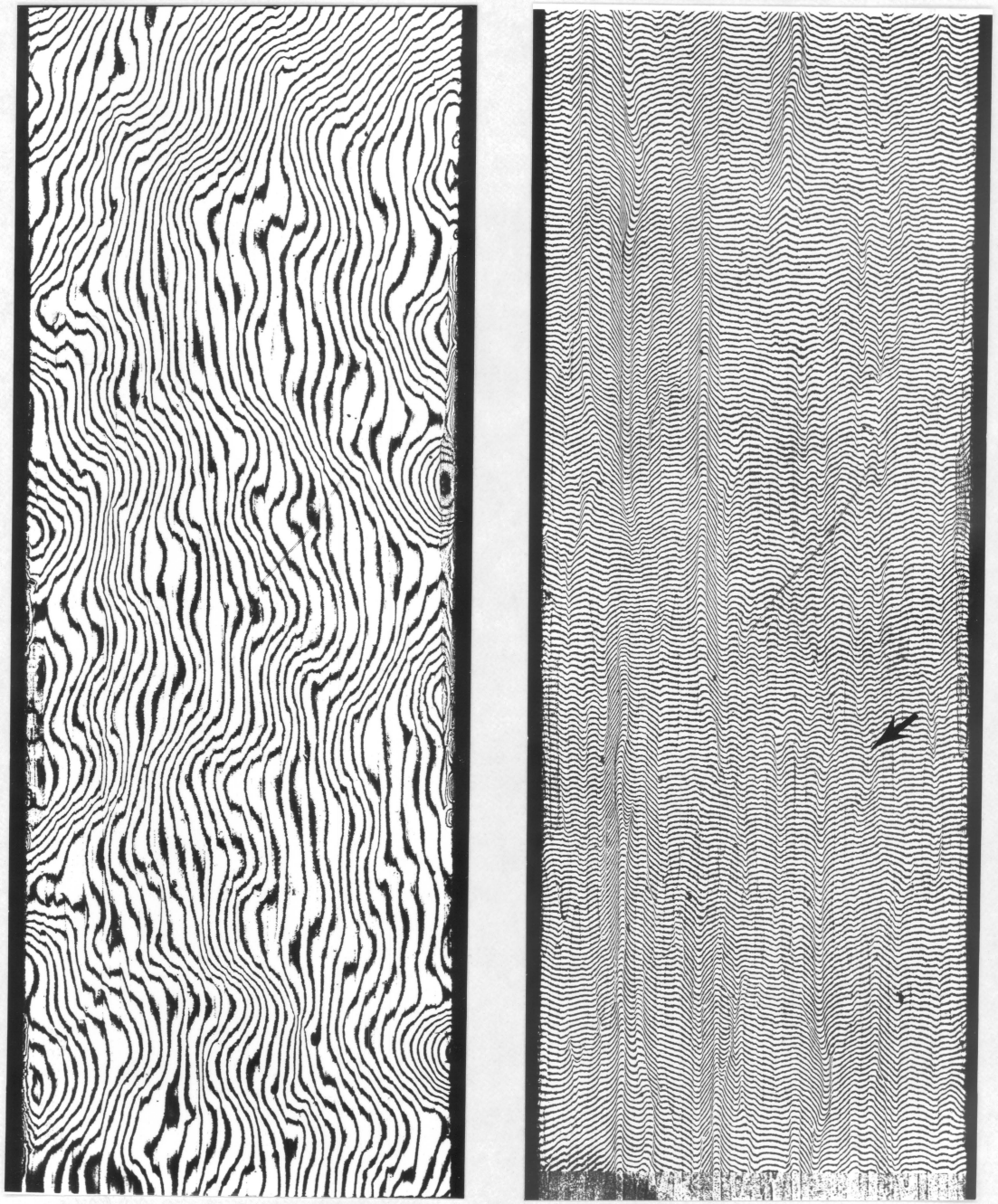

Figure 34. U and V-field Moire fringe patterns of a 22-ply unidirectional specimen under 44 ksi compression.

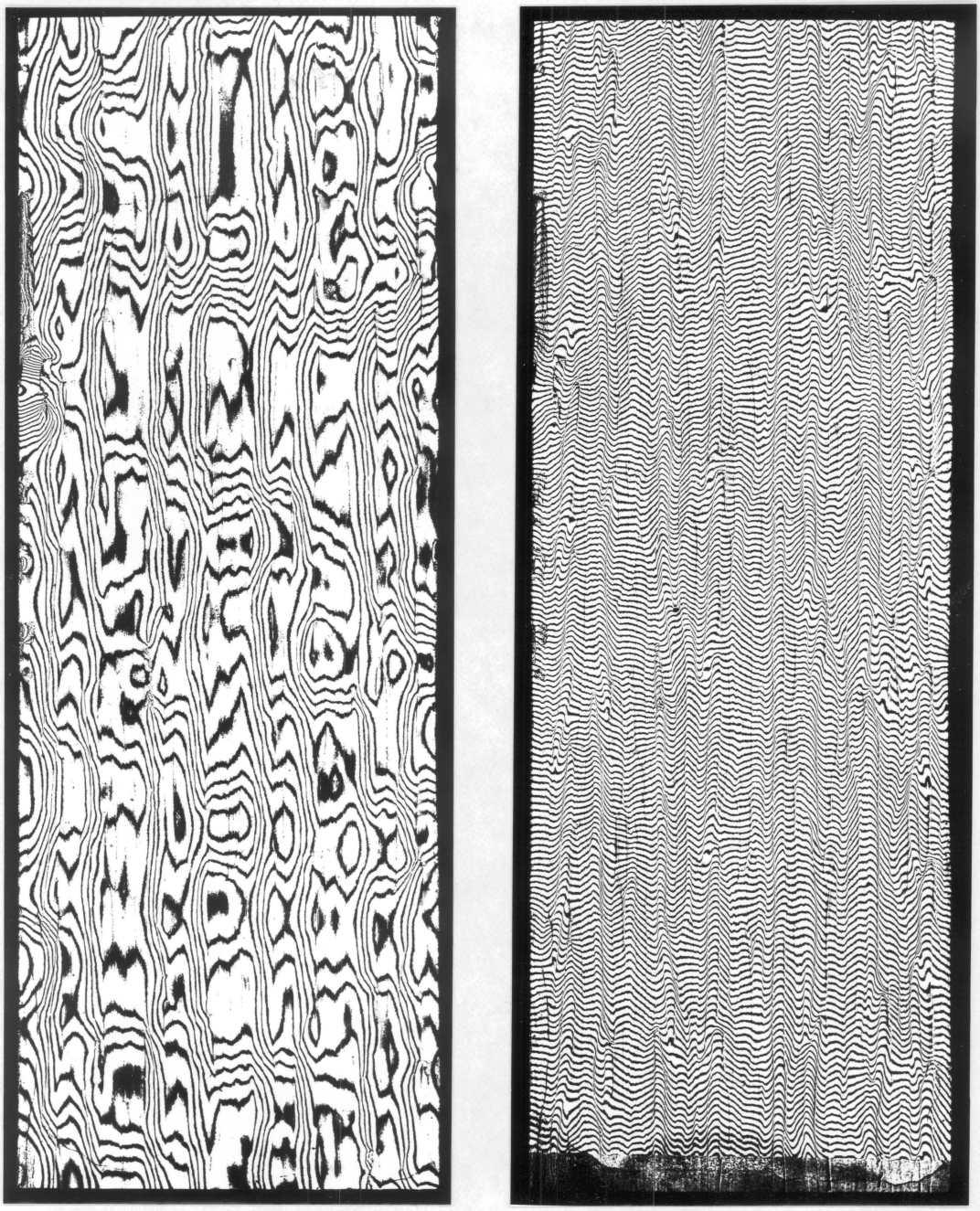

Figure 35. U and V-field Moire fringe patterns of a 20-ply orthotropic specimen under 45 ksi compression.

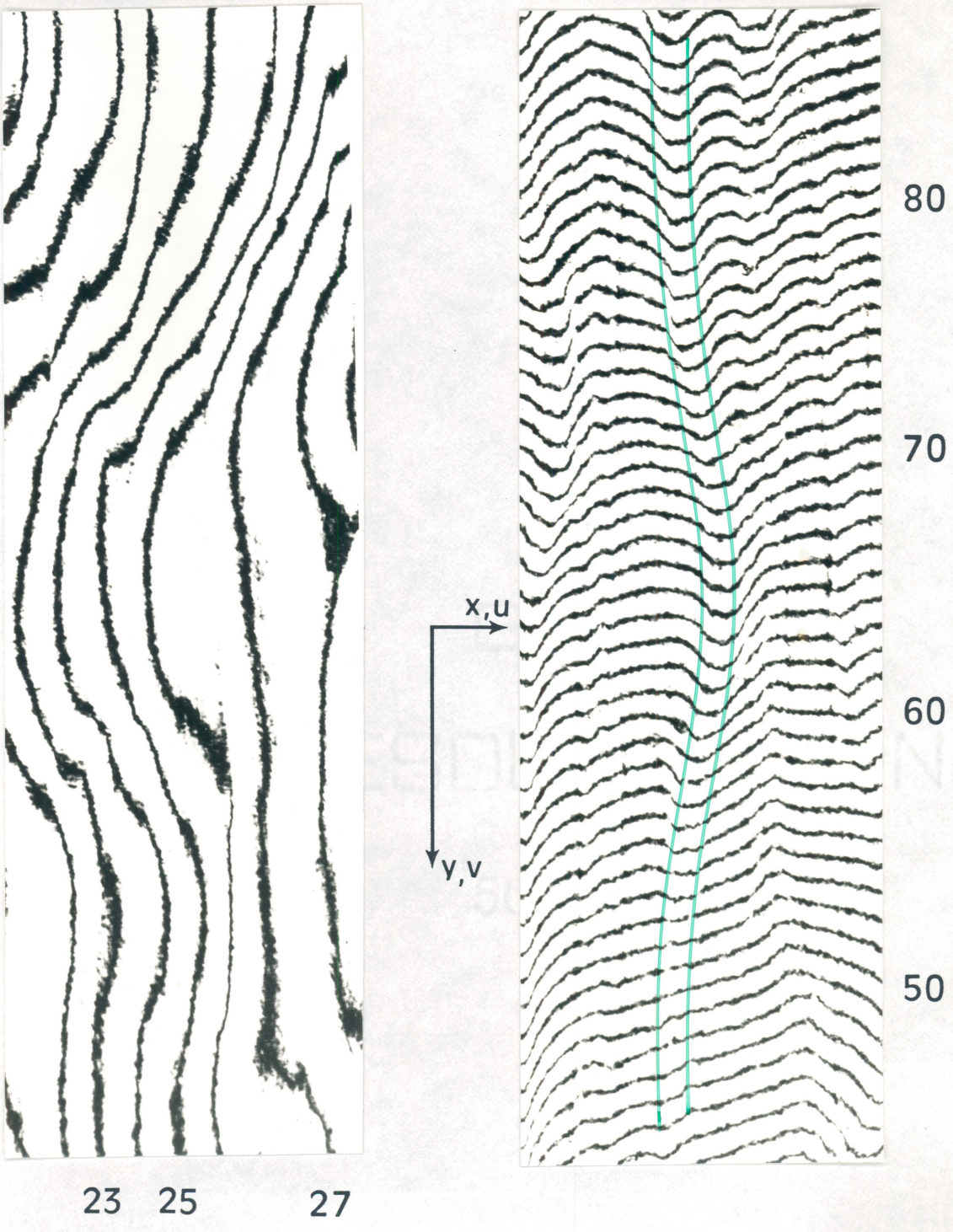

Figure 36. U and V-field Moire fringe patterns of the bundle under investigation.

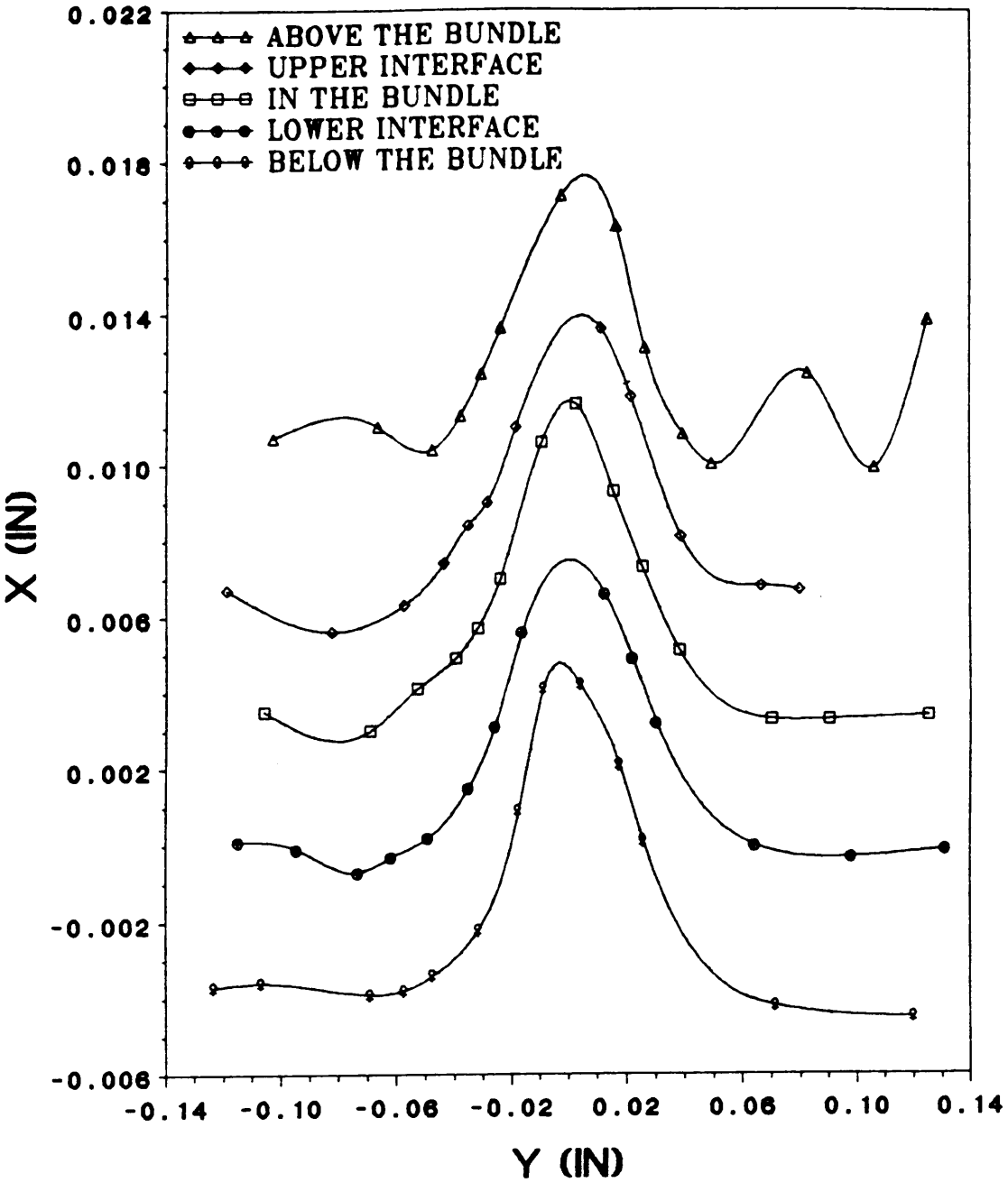

Figure 37. Coordinates of the points at which U-field Moire fringe numbers were read.

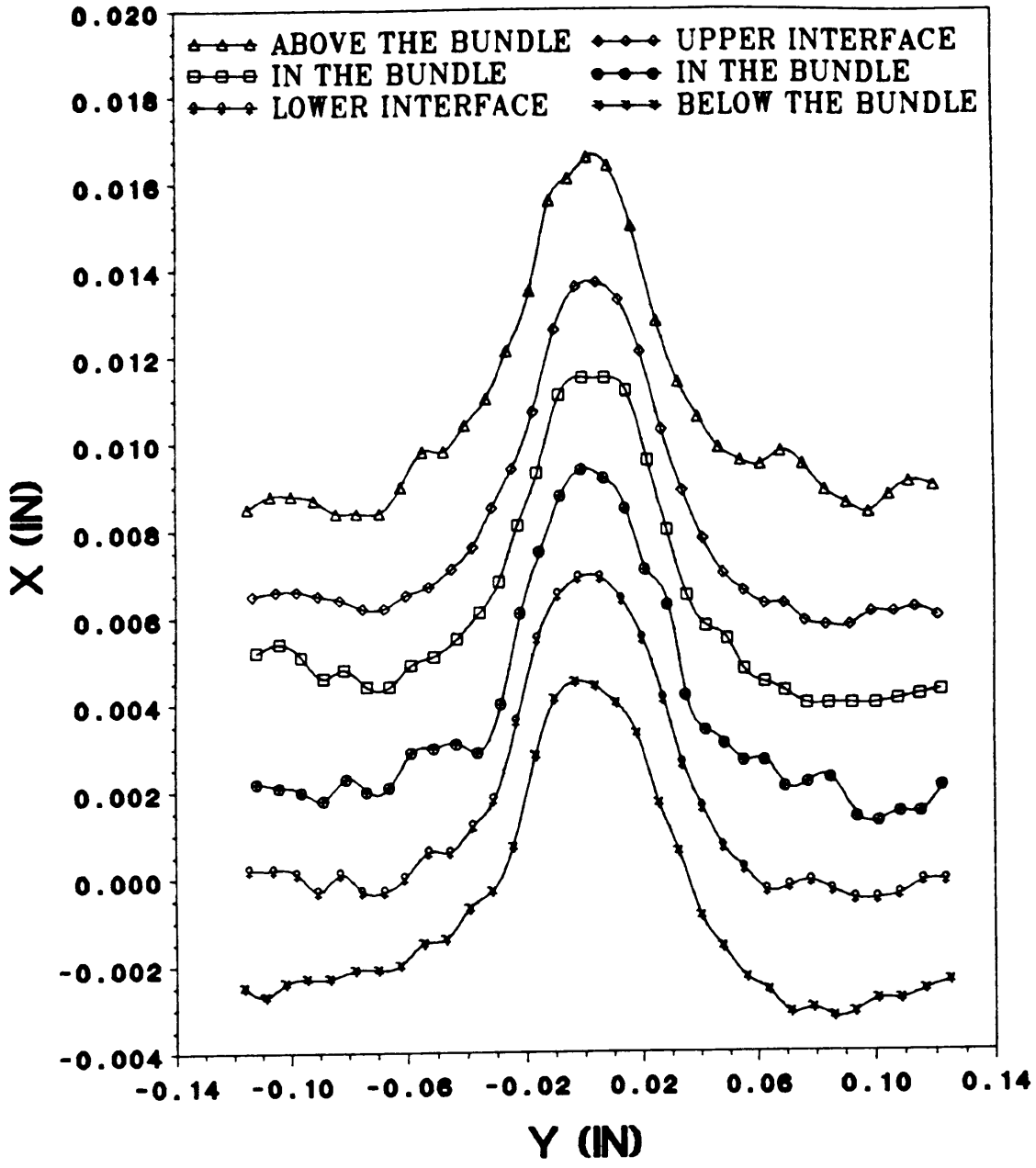

Figure 38. Coordinates of the points at which V-field Moire fringe numbers were read.

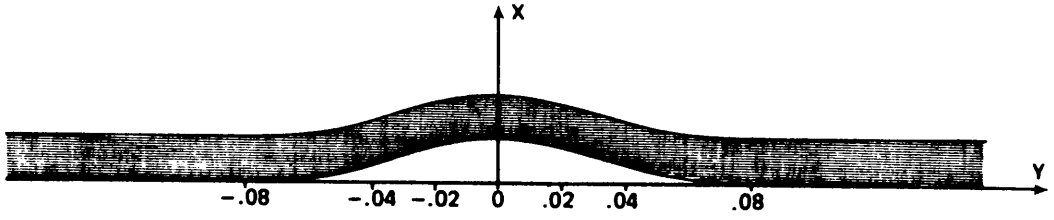

Figure 39. Relative locations of the points on the bundle where strains were calculated.

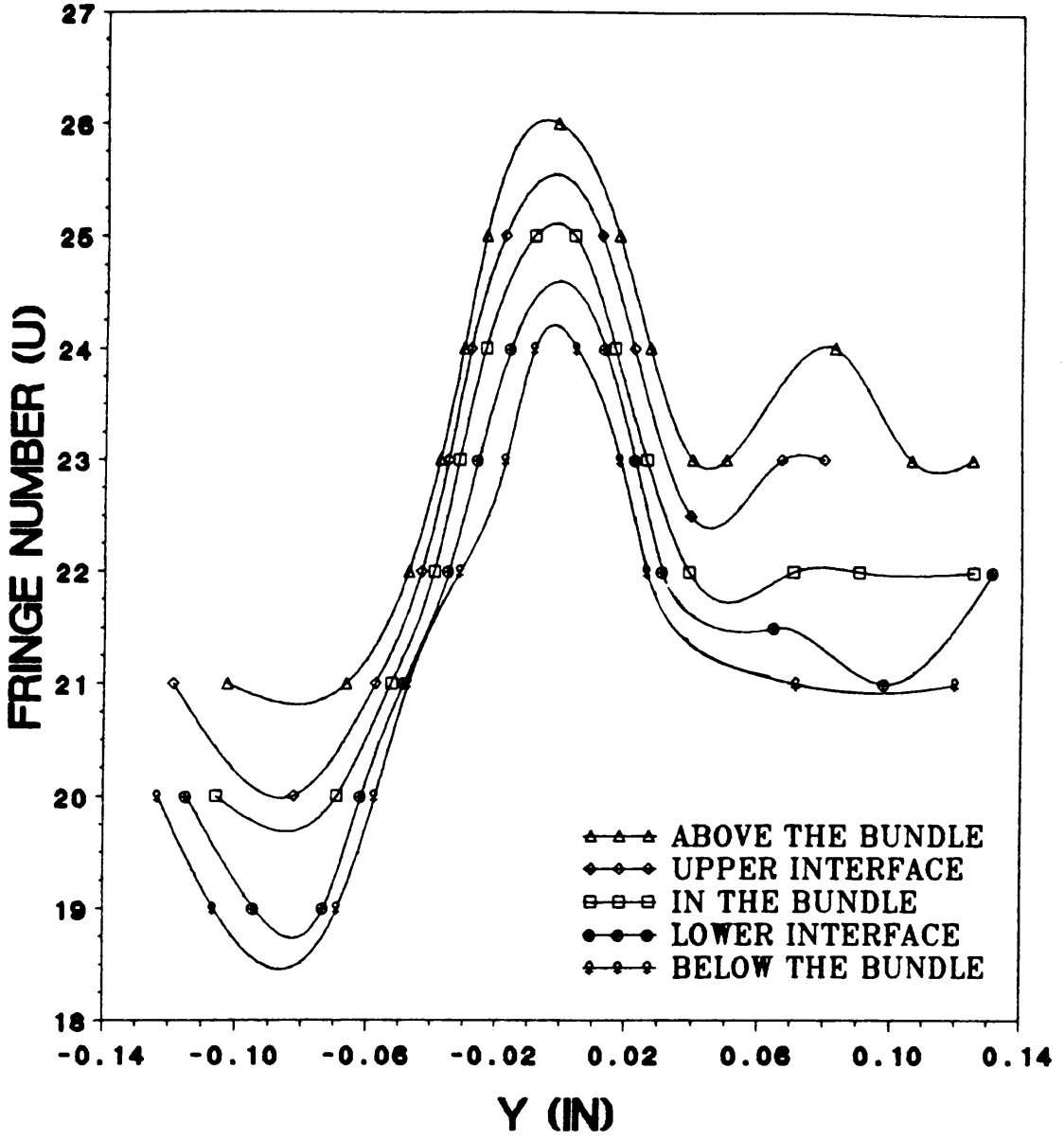

Figure 40. U-field fringe numbers along the bundle.

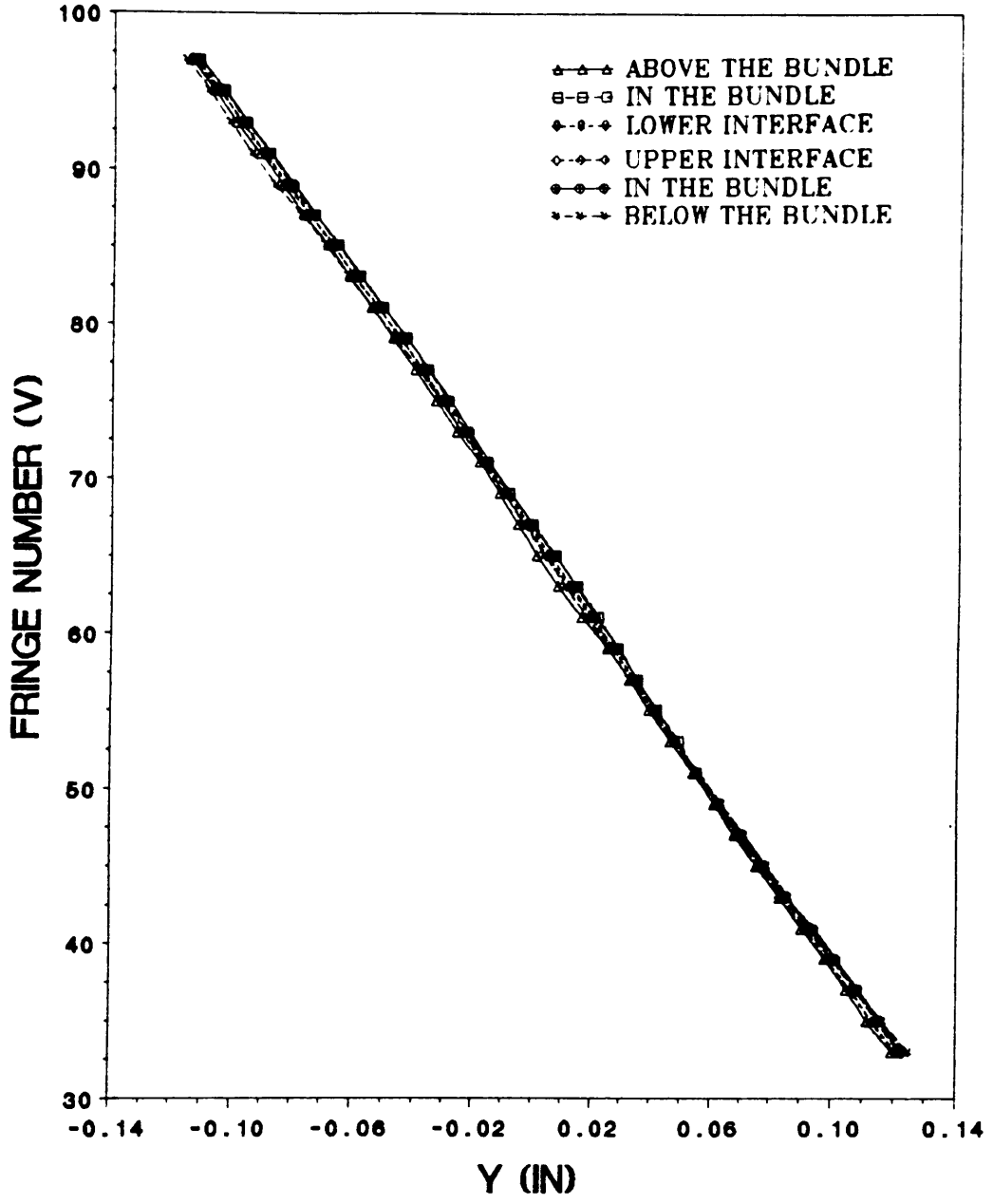

Figure 41. V-field fringe numbers along the bundle.

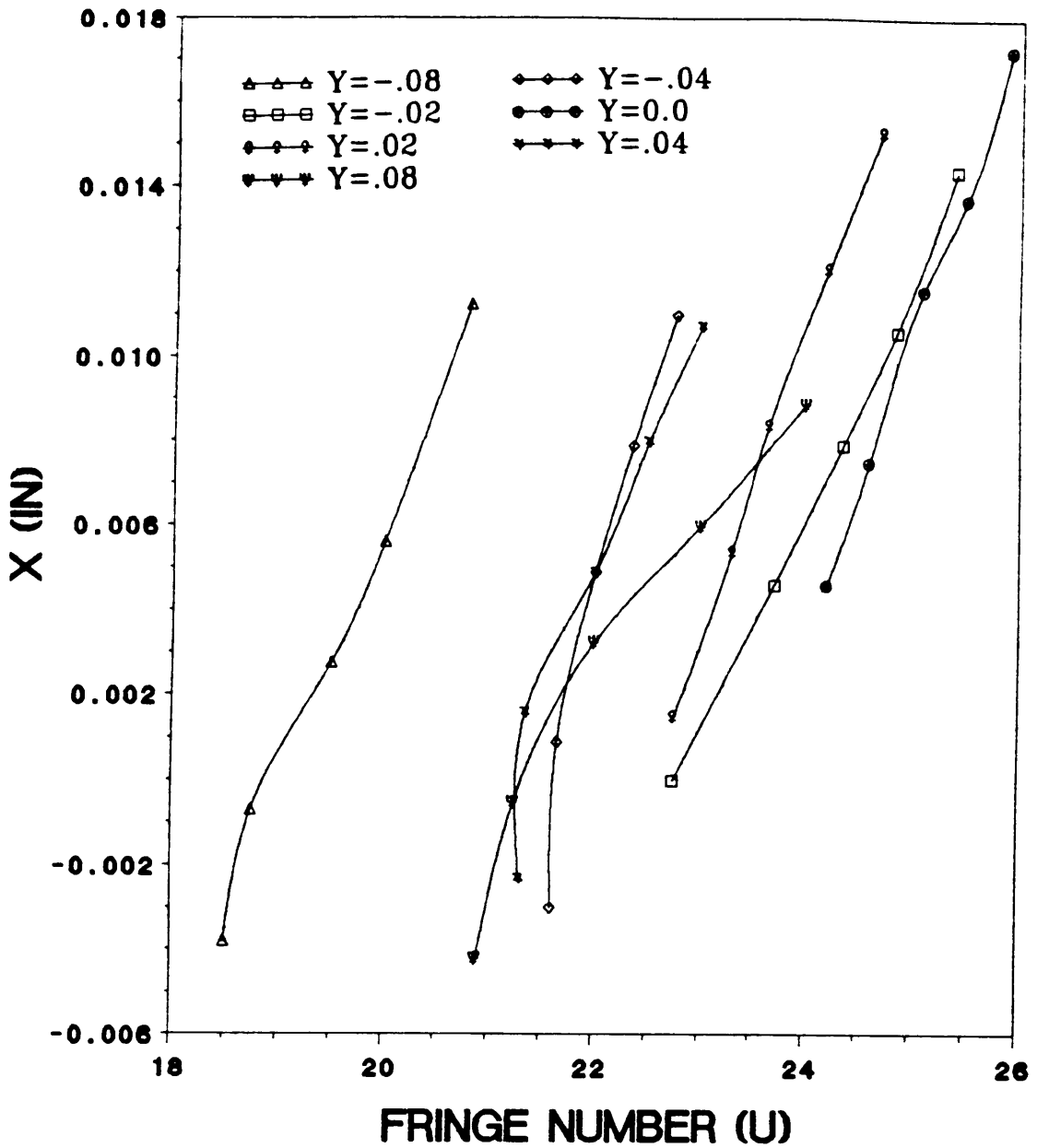

Figure 42. U-field fringe numbers across the bundle.

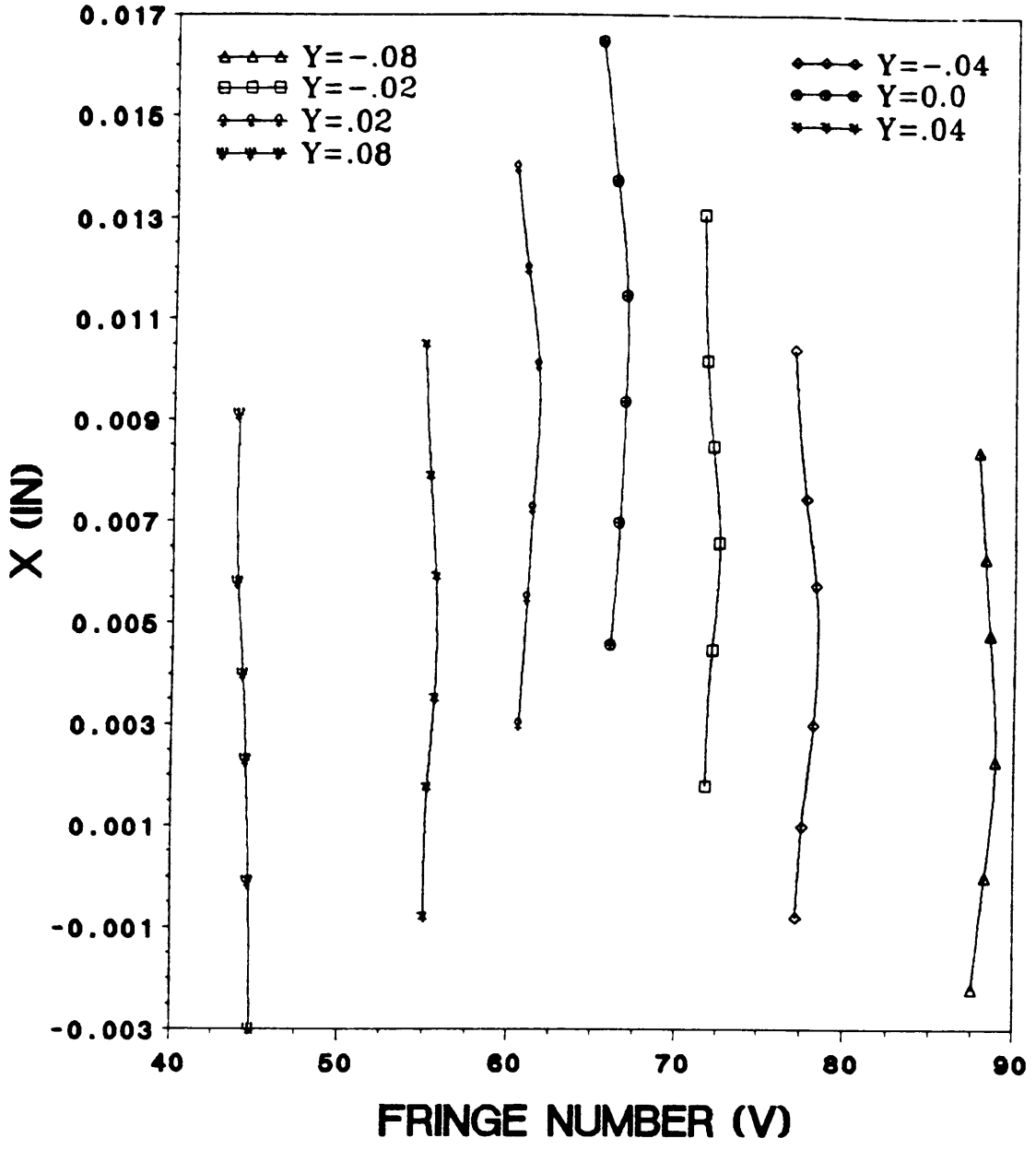

Figure 43. V-field fringe numbers across the bundle.

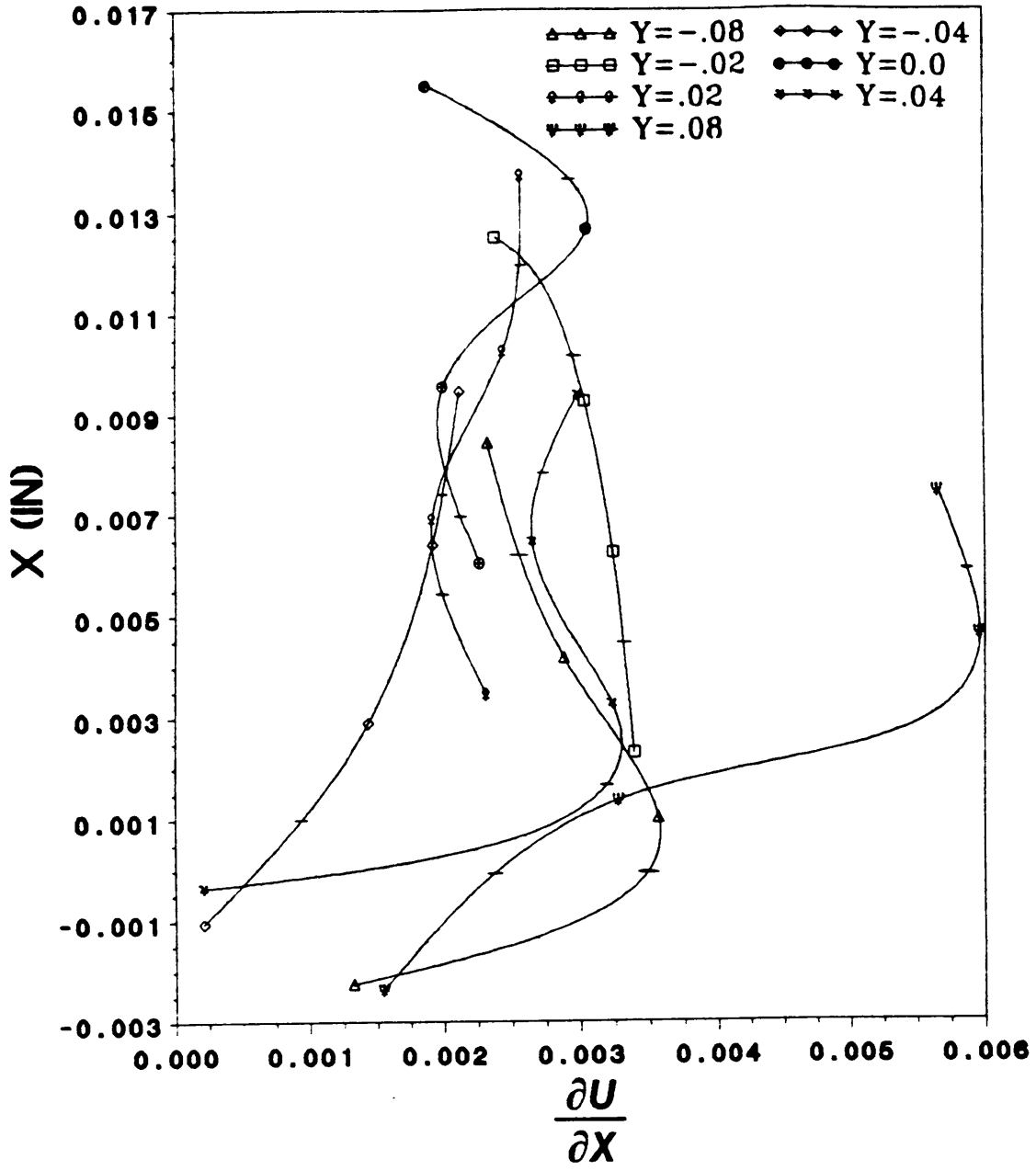

Figure 44. Normal strain ∂u/∂x distribution across the bundle.

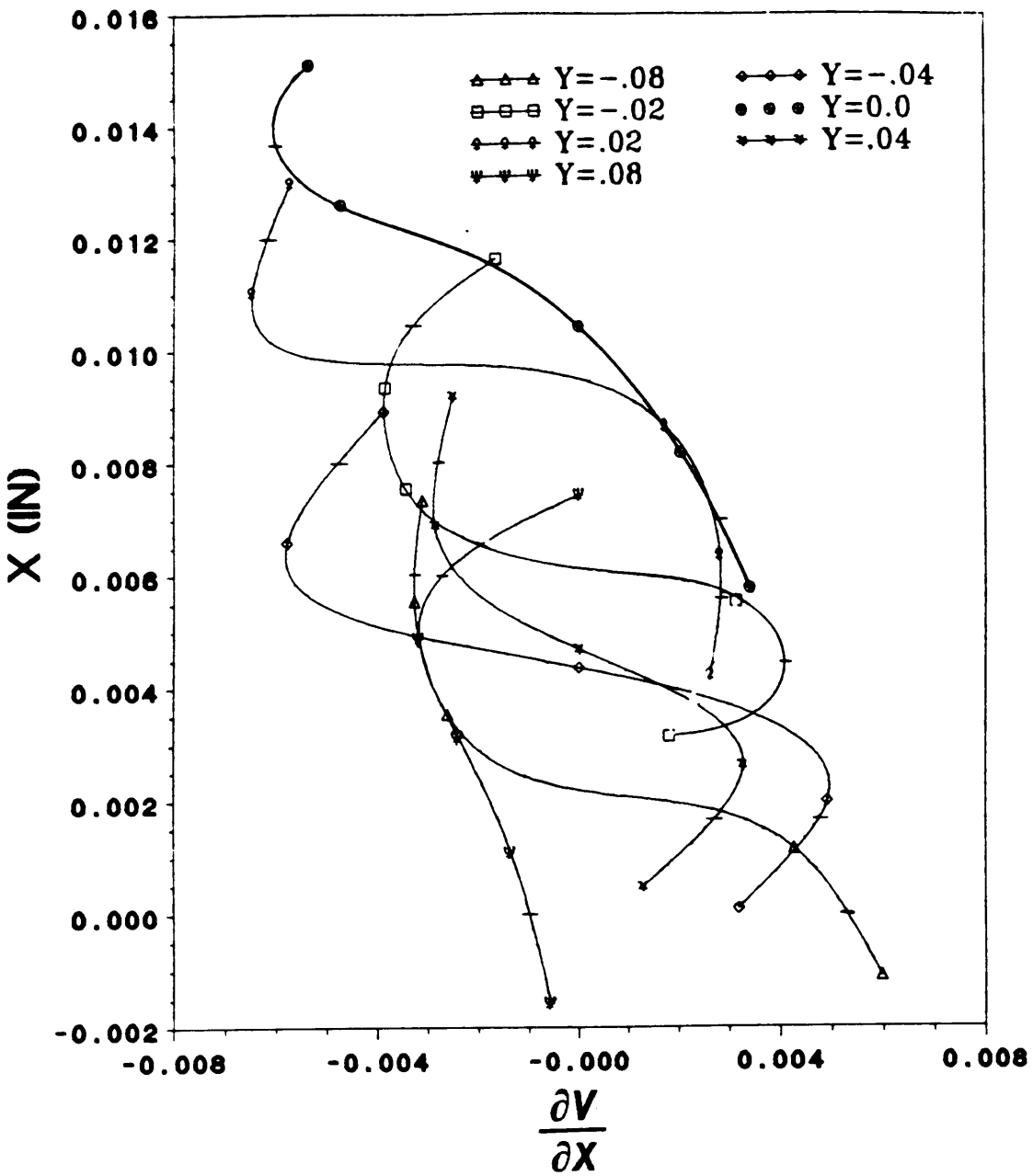

Figure 45. Distribution of $\partial v/\partial x$ across the bundle.

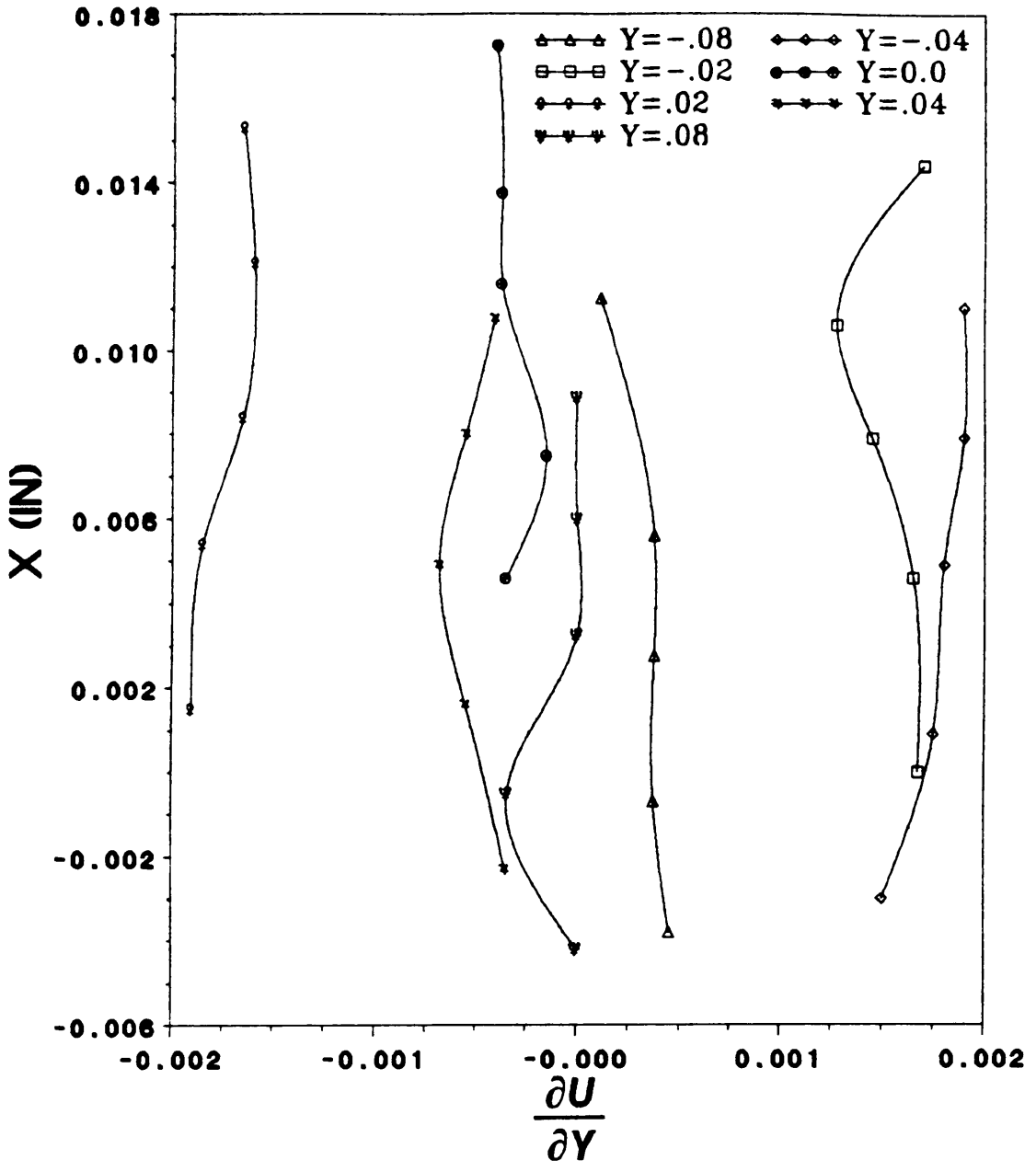

Figure 46. Distribution of ∂u/∂y across the bundle.

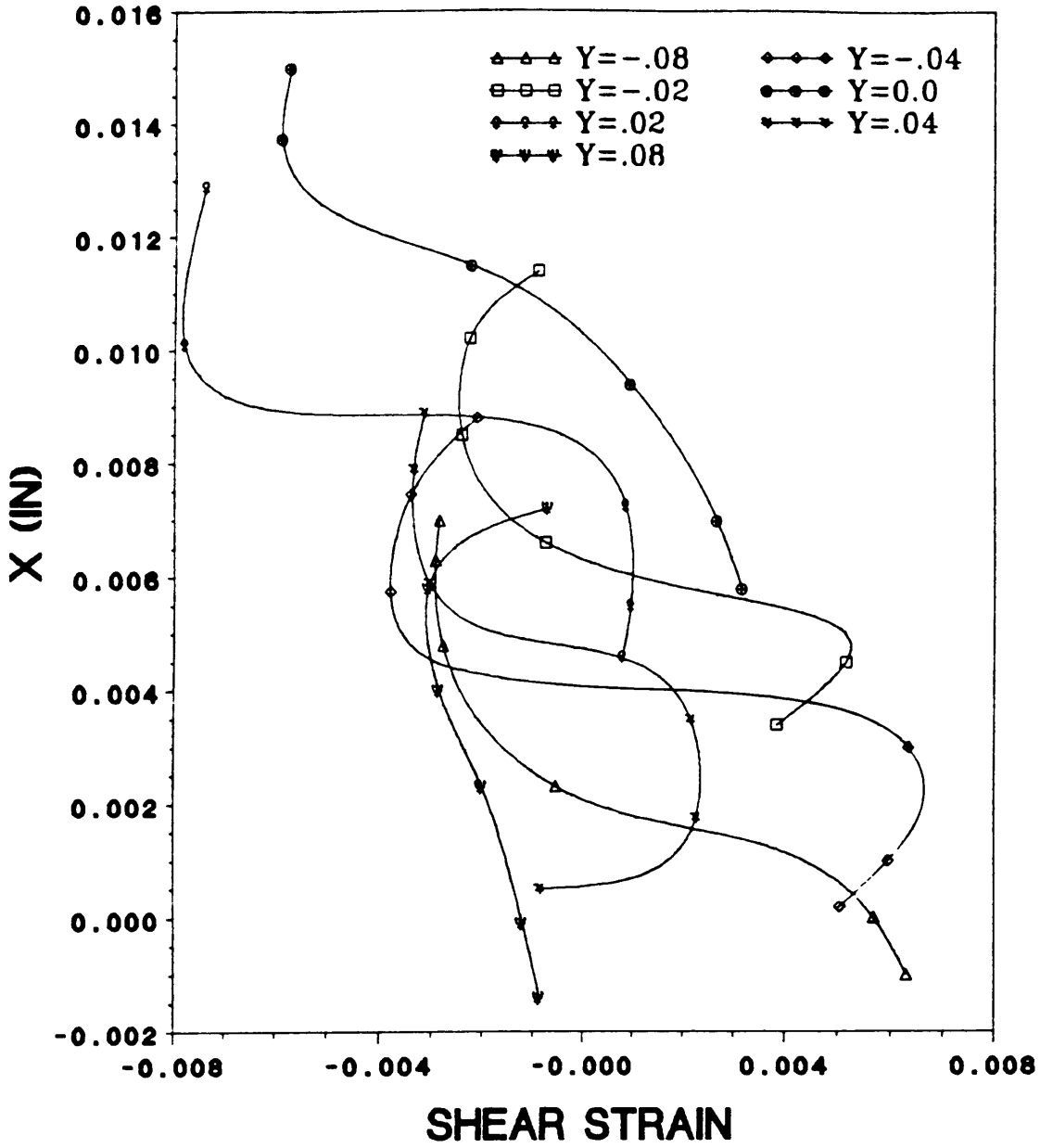

Figure 47. Shear strain distributions across the bundle.

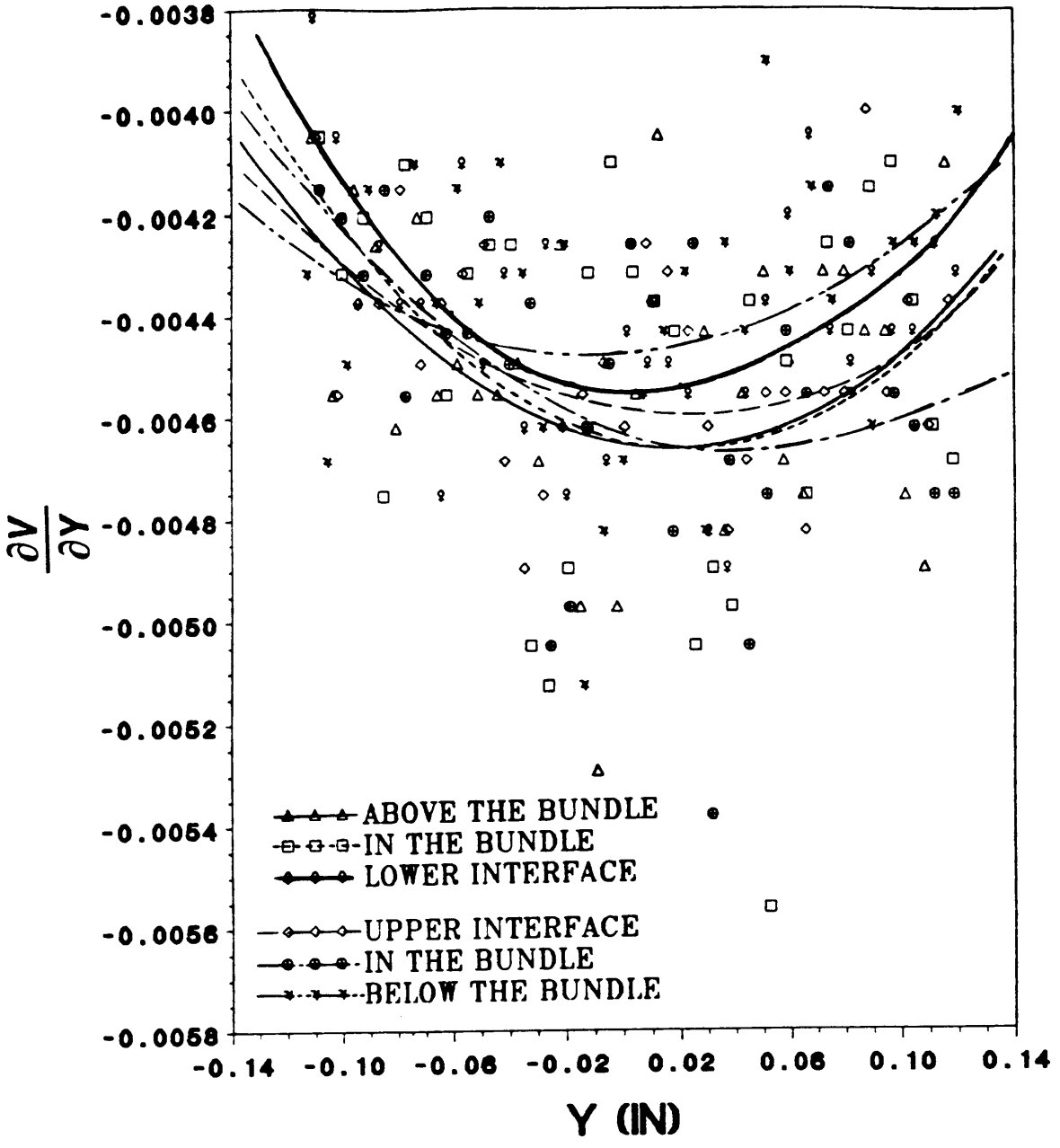

Figure 48. Normal strain ∂v/∂y distribution along the bundle.

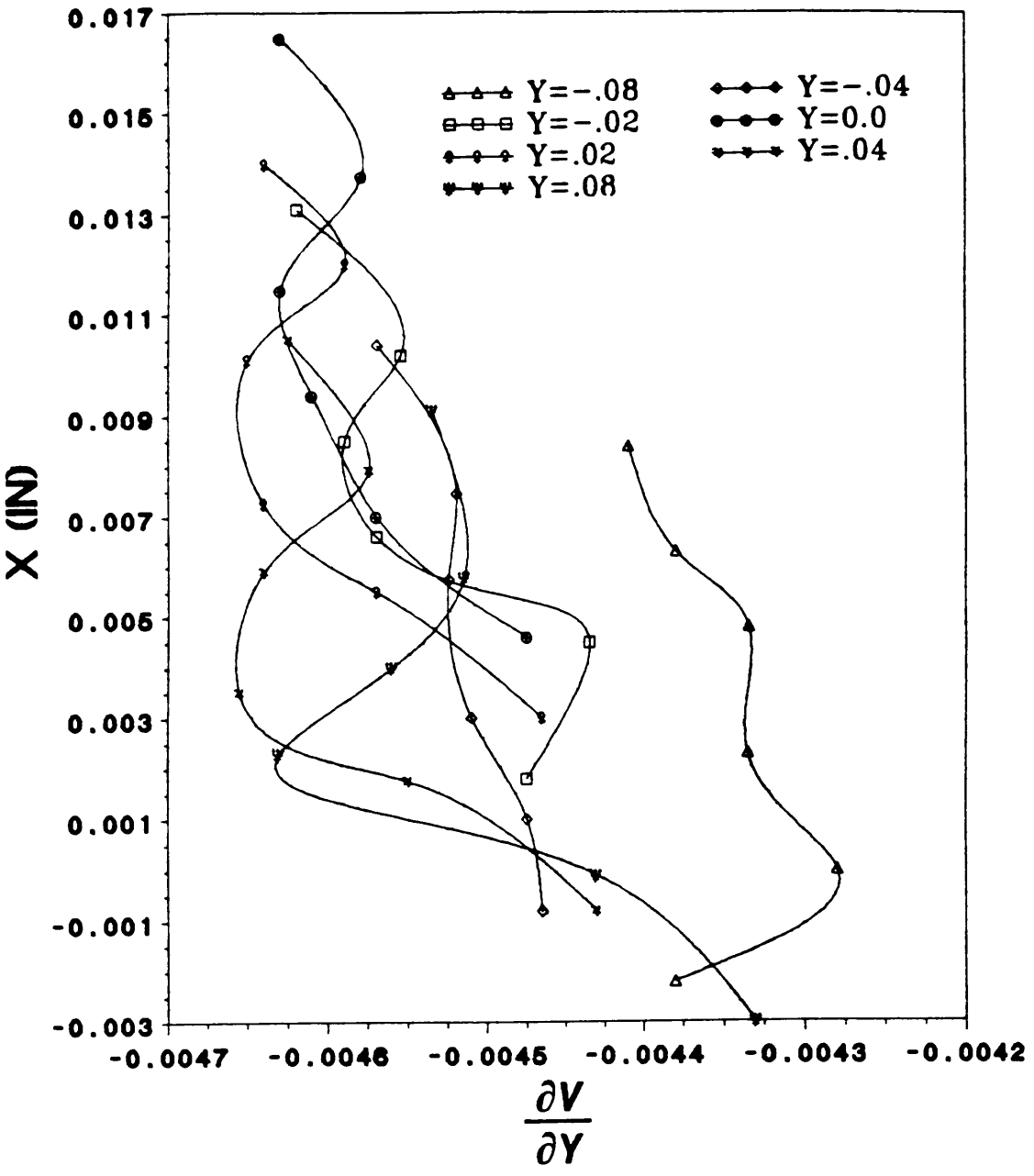

Figure 49. Normal strain $\partial v/\partial y$ distribution across the bundle.

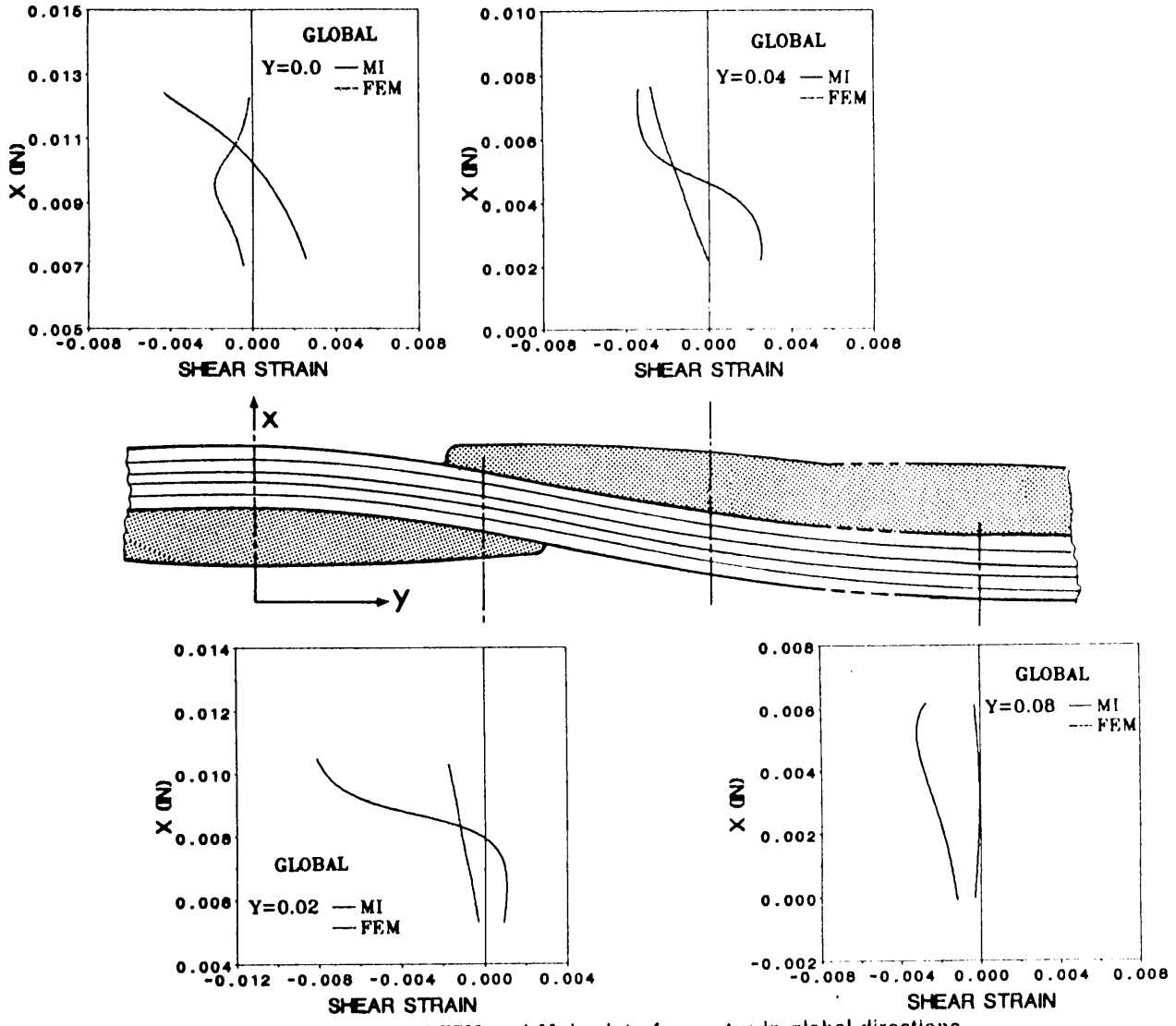

Figure 50. Comparison of shear strain distributions of FEM and Moire interferometry in global directions.

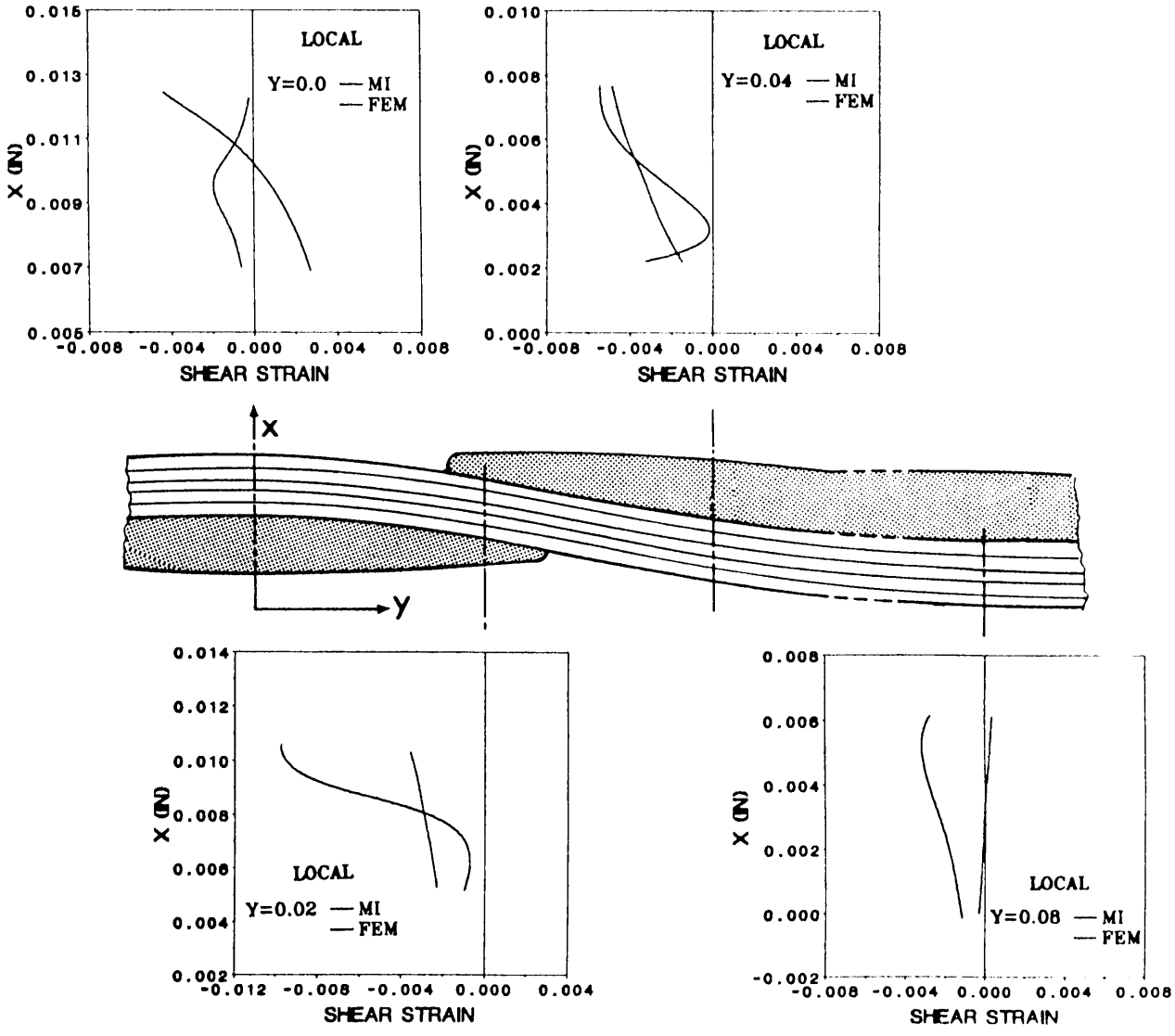

Figure 51. Comparison of shear strain distributions of FEM and Moire interferometry in local directions.

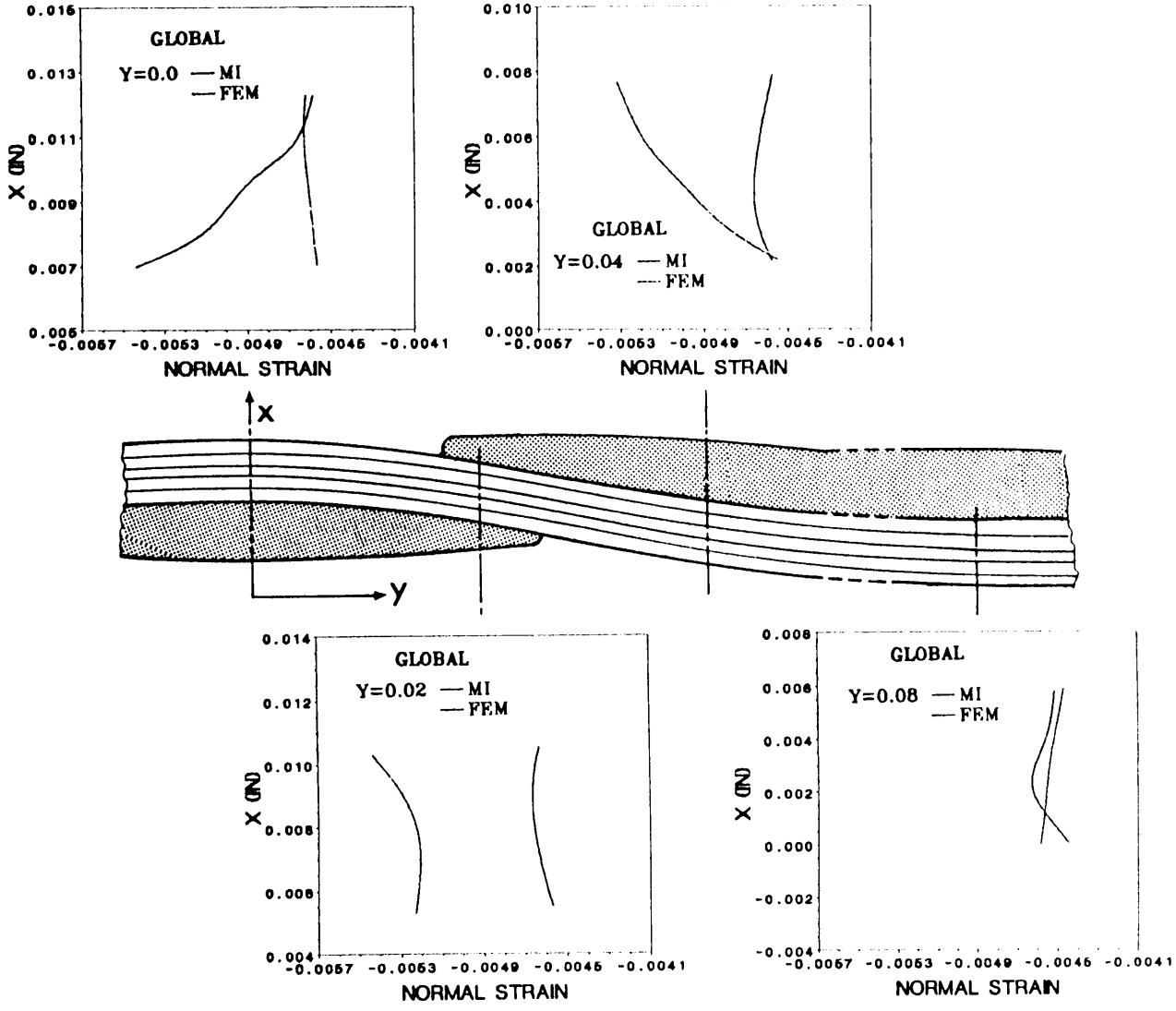

Figure 52. Comparison of normal strain σ_y distributions of FEM and Moire interferometry in global directions.

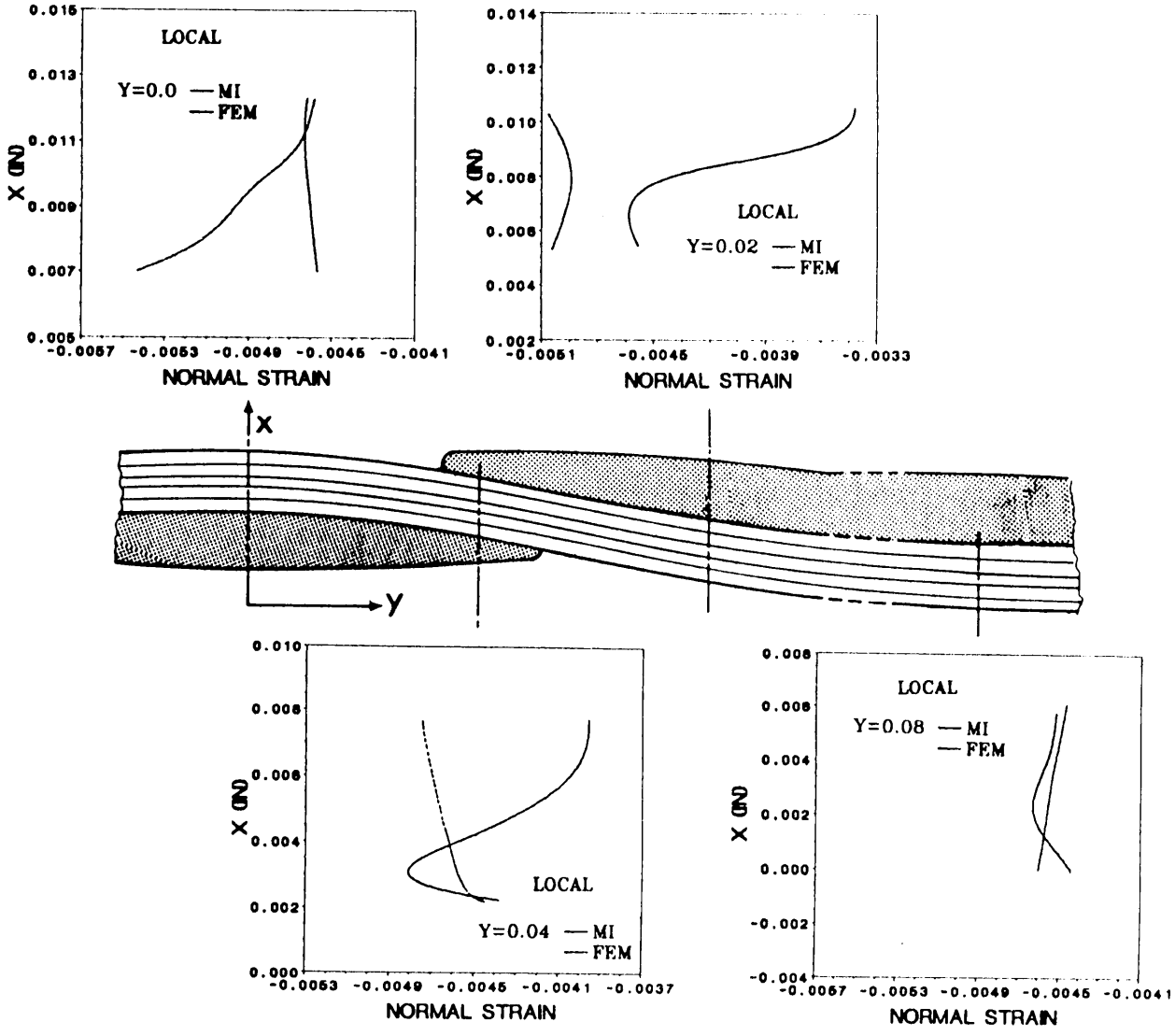

Figure 53. Comparison of normal strain σ_2 distributions of FEM and Moire interferometry in local directions.

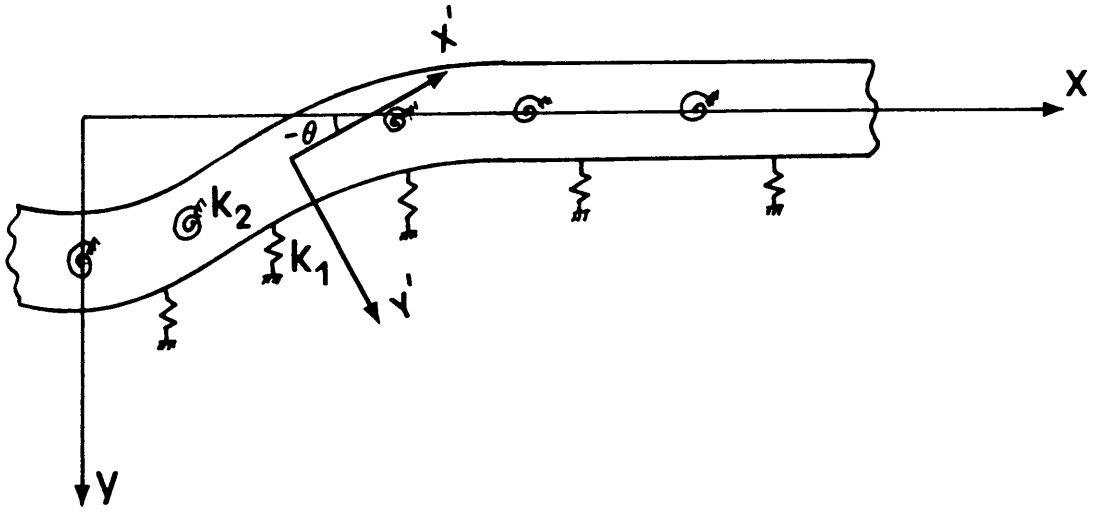

Figure 54. Beam model of a bundle on a two-parameter foundation.

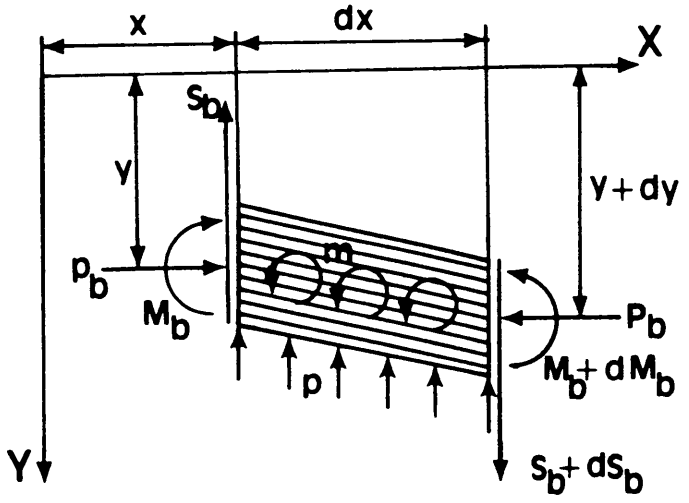

Figure 55. Free body diagram of an element dx of the bundle.

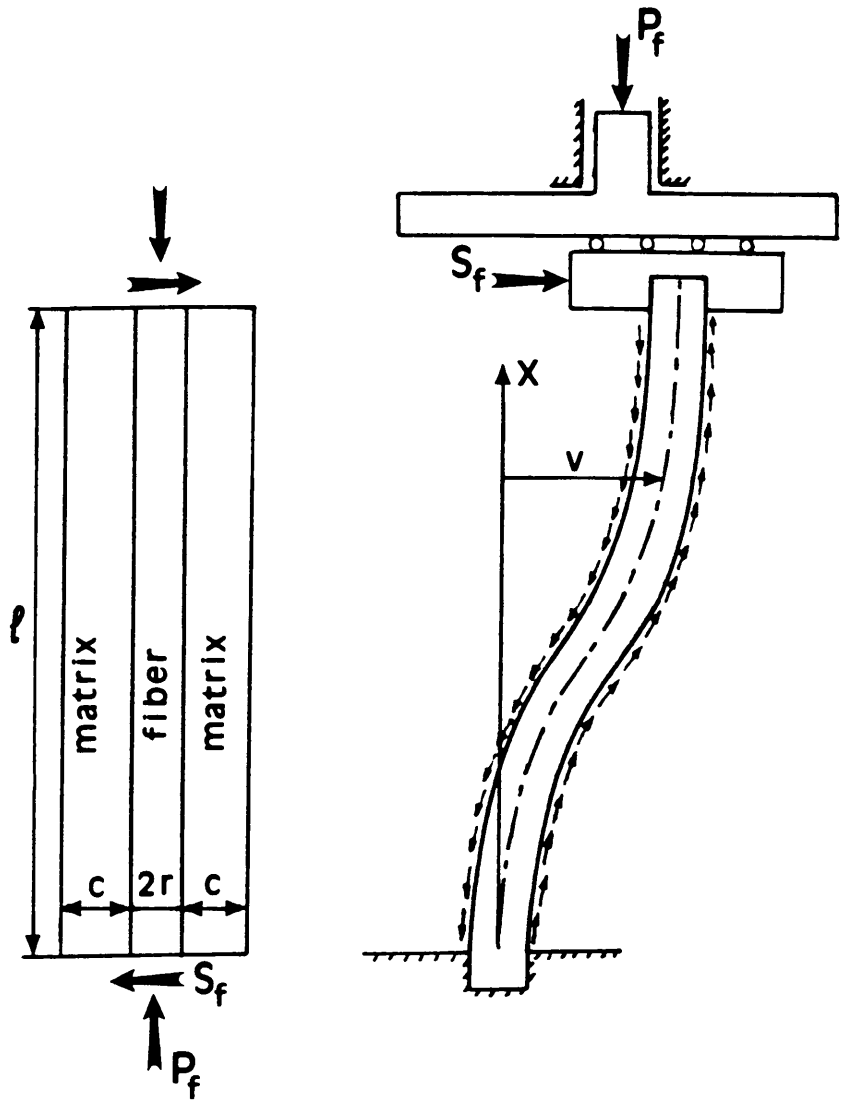

Figure 56. A single fiber, modeled as a beam on an elastic foundation.

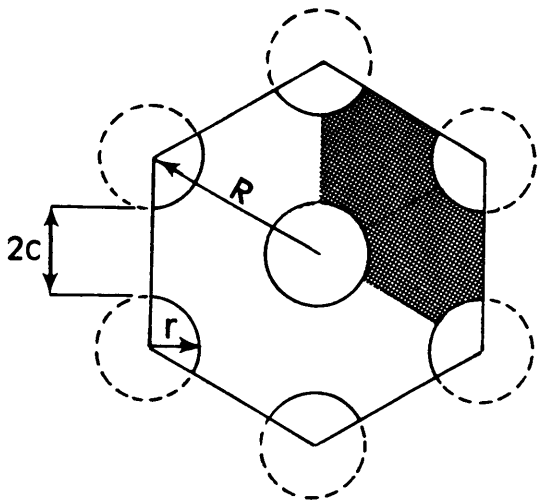

Figure 57. A hexagonal array of fibers with the volume of matrix corresponding to one fiber, shaded.

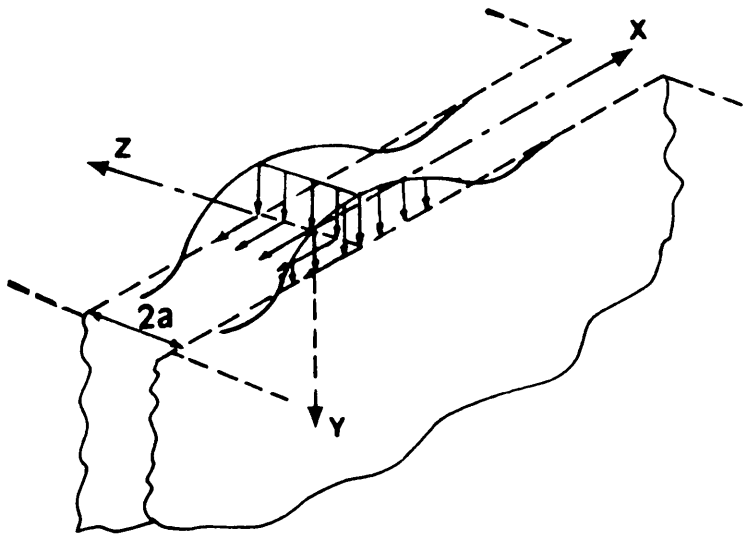

Figure 58. Half space foundation under surface tractions.

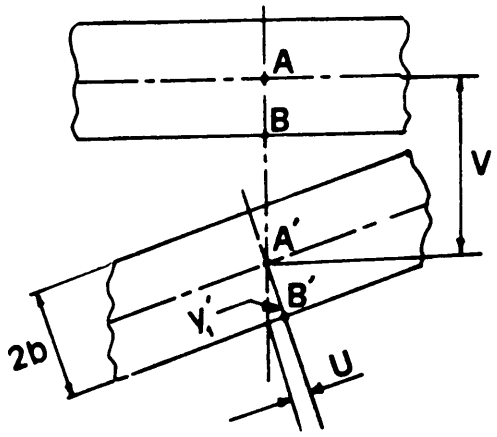

Figure 59. Displacements of the foundation surface due to beam deformation.

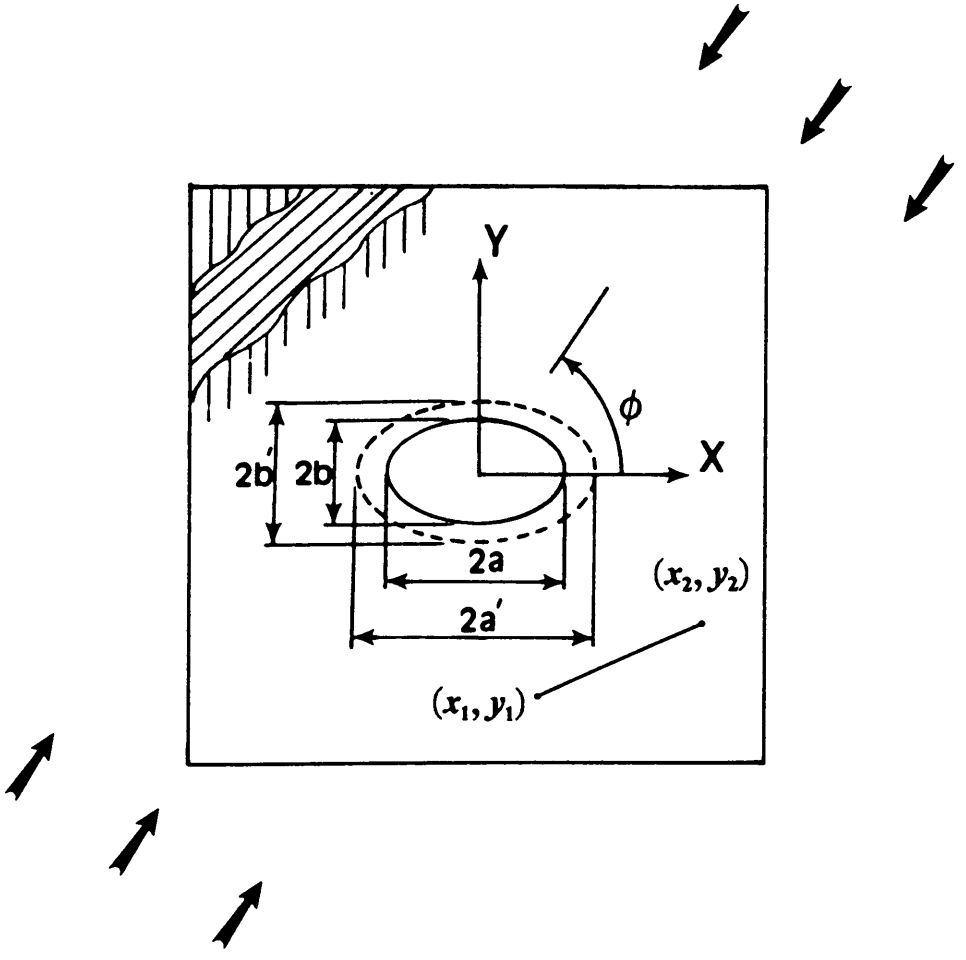

Figure 60. Composite laminate with an elliptical opening under compressive stress .

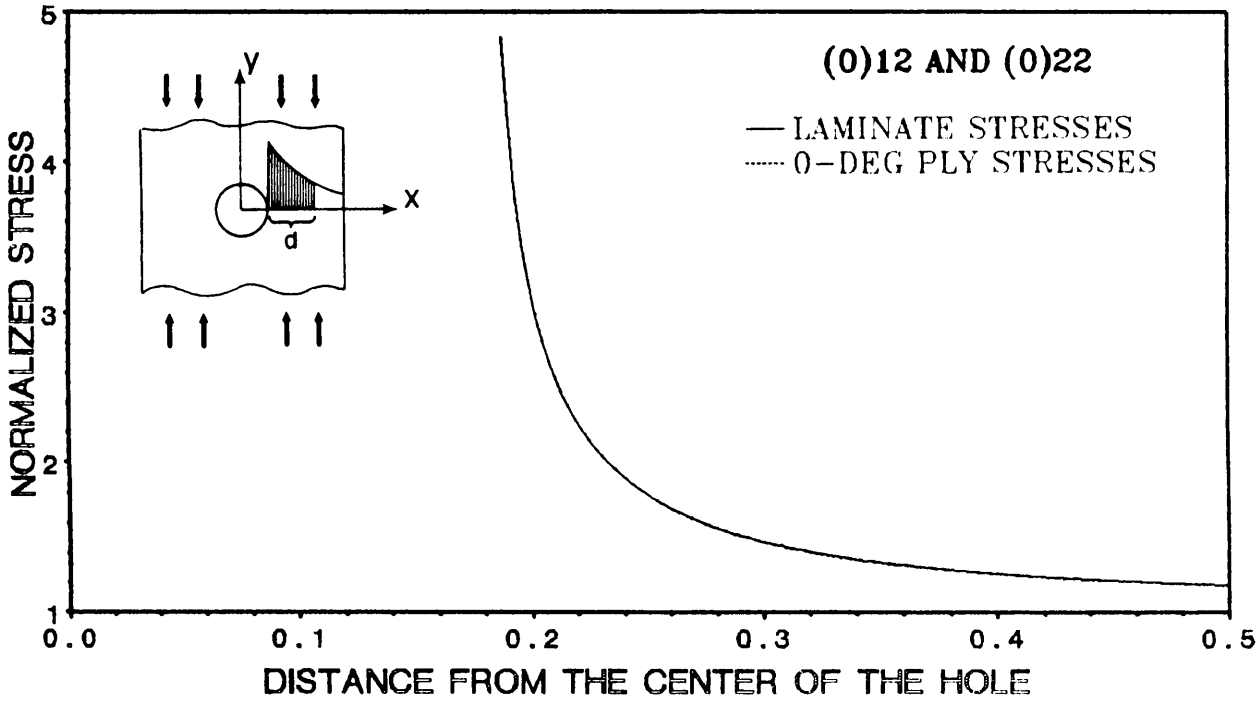

Figure 61. Normalized compressive stress distribution in notched 22-ply and 12-ply unidirectional laminates.

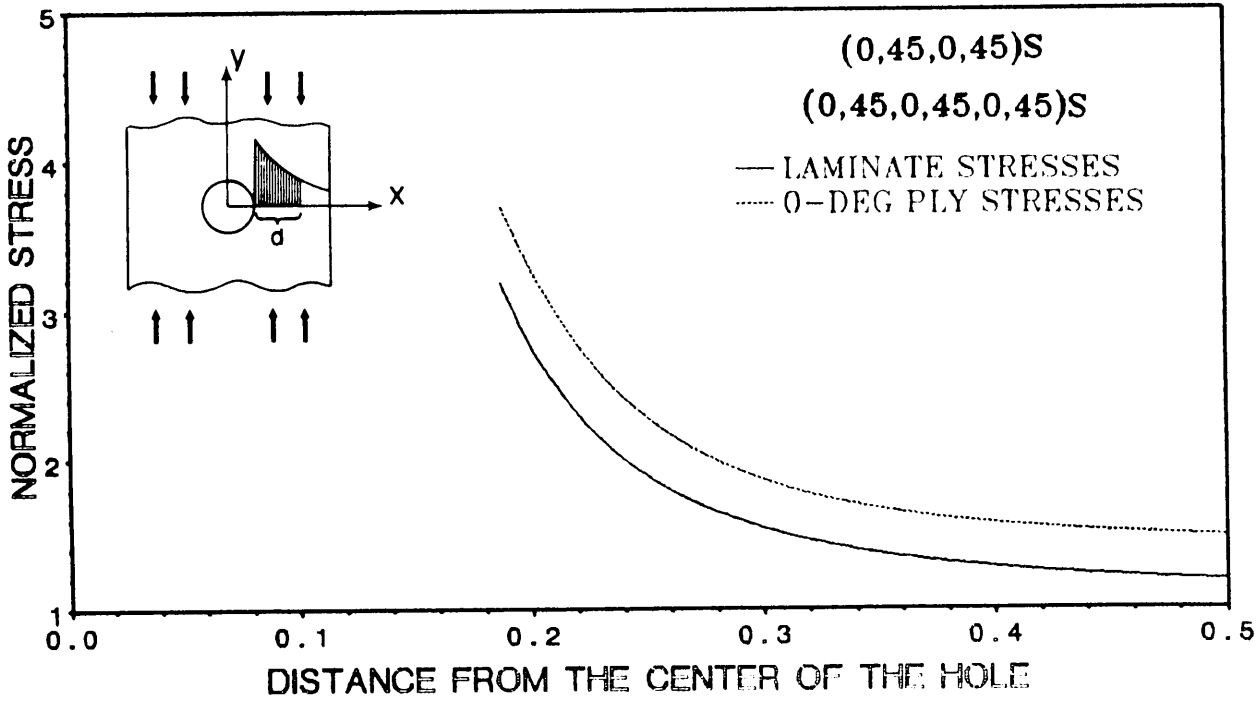

Figure 62. Normalized compressive stress distribution in notched 8-ply and 12-ply quasi-isotropic laminates.

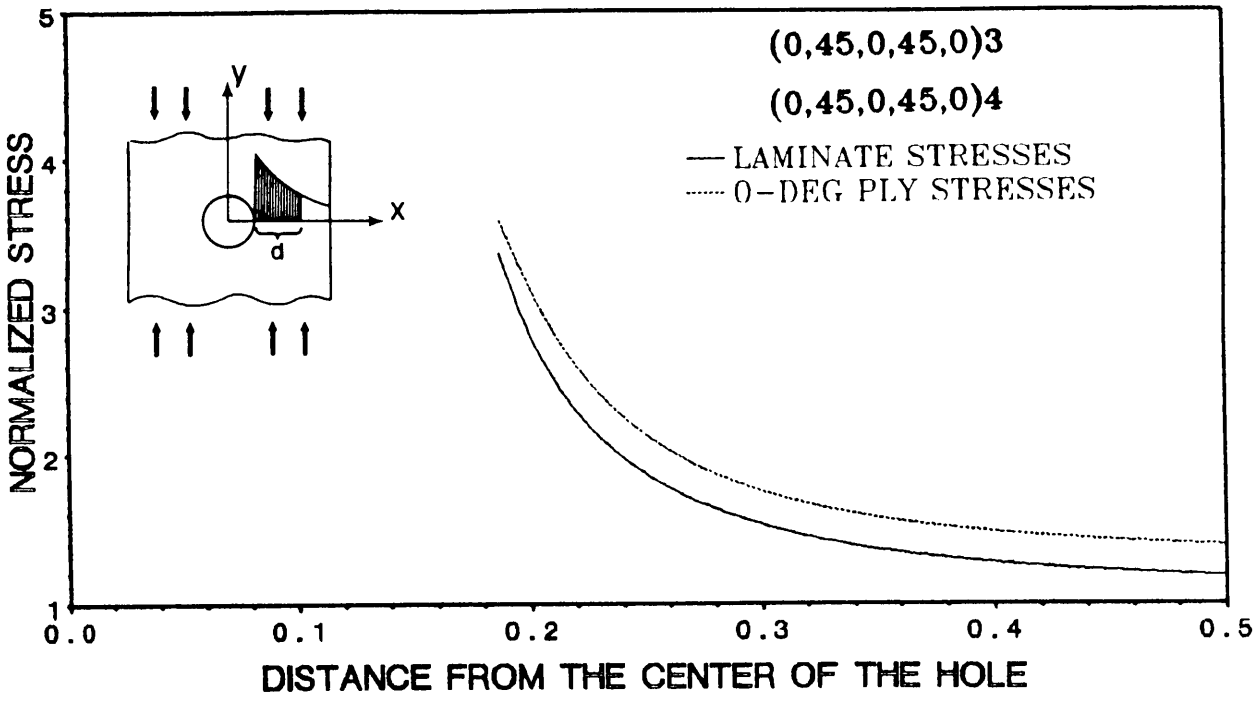

Figure 63. Normalized compressive stress distribution in notched 15-ply and 20-ply orthotropic laminates.

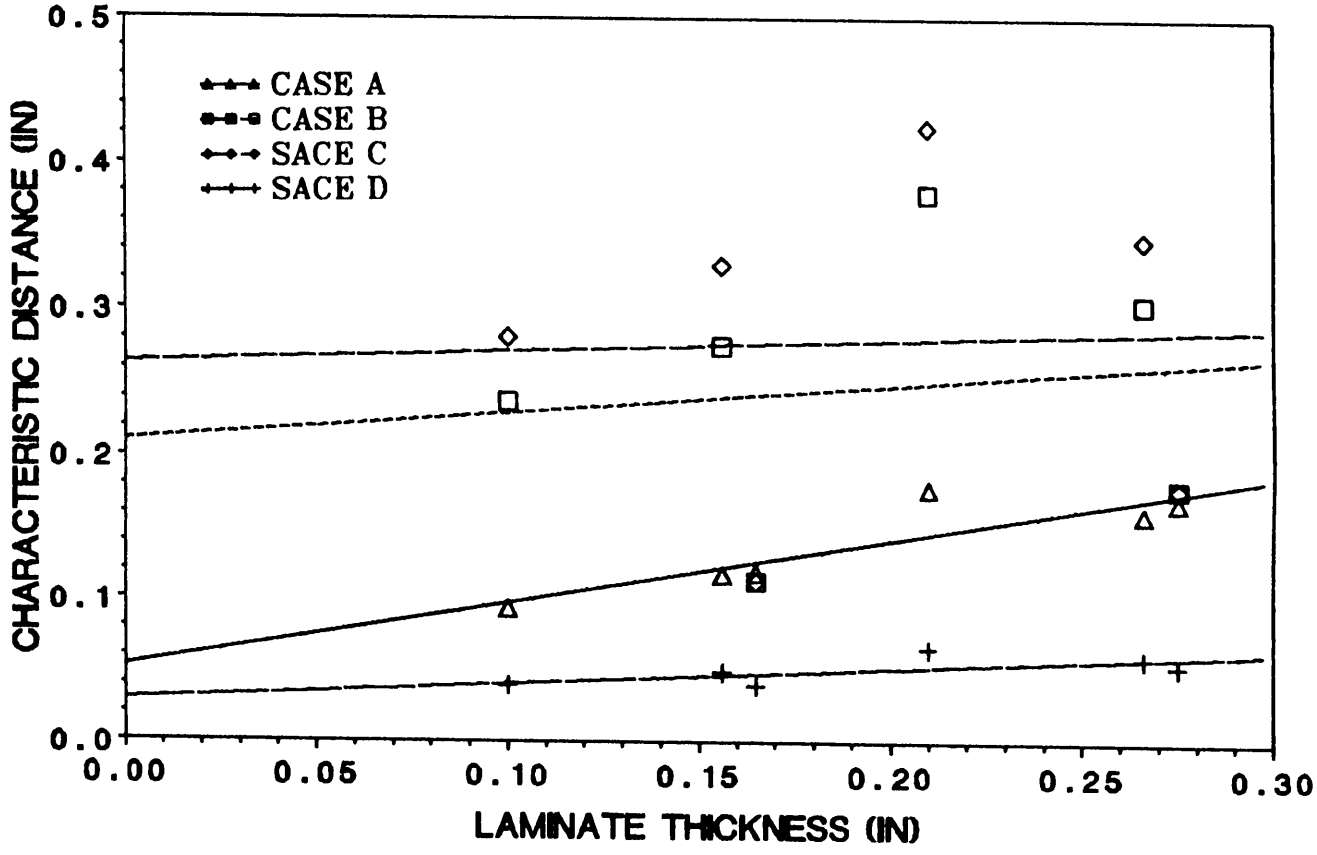

Figure 64. Characteristic distances for cases A, B, C, and D of different laminates.

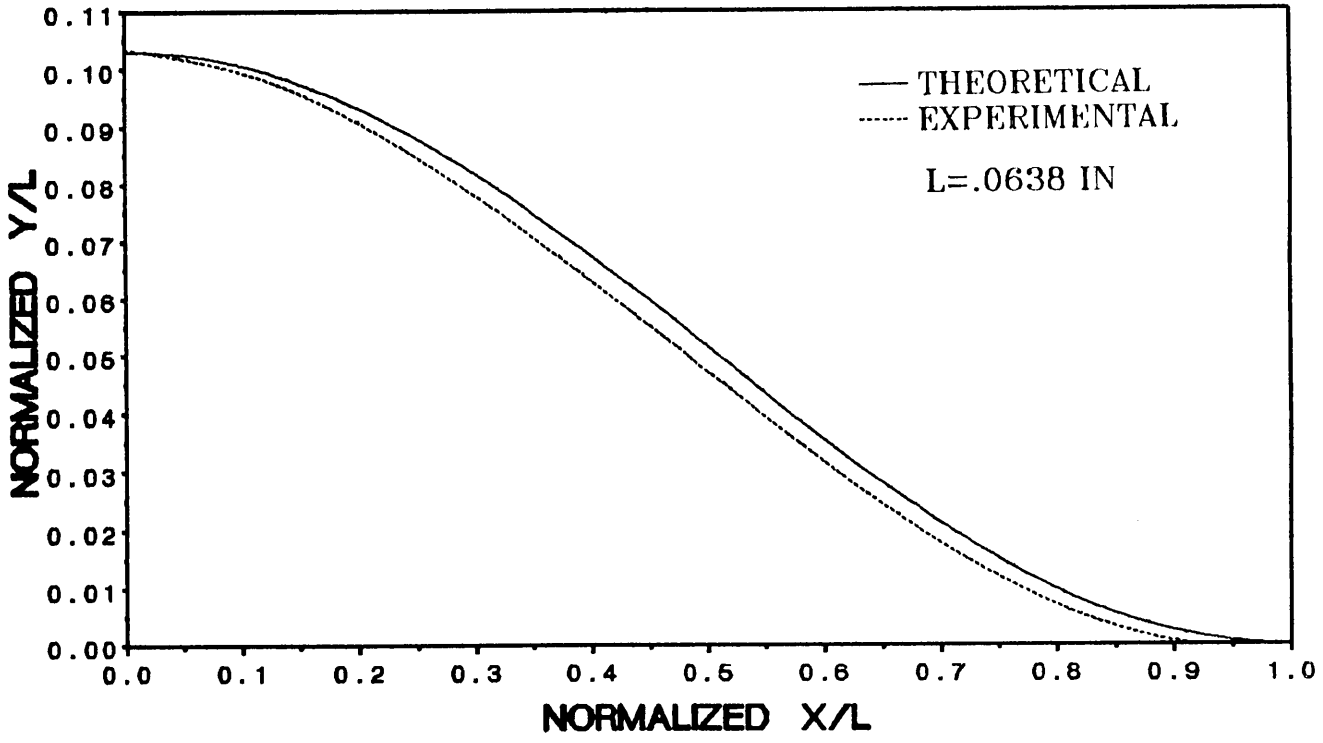

Figure 65. Comparison of the model with the actual bundle shape.

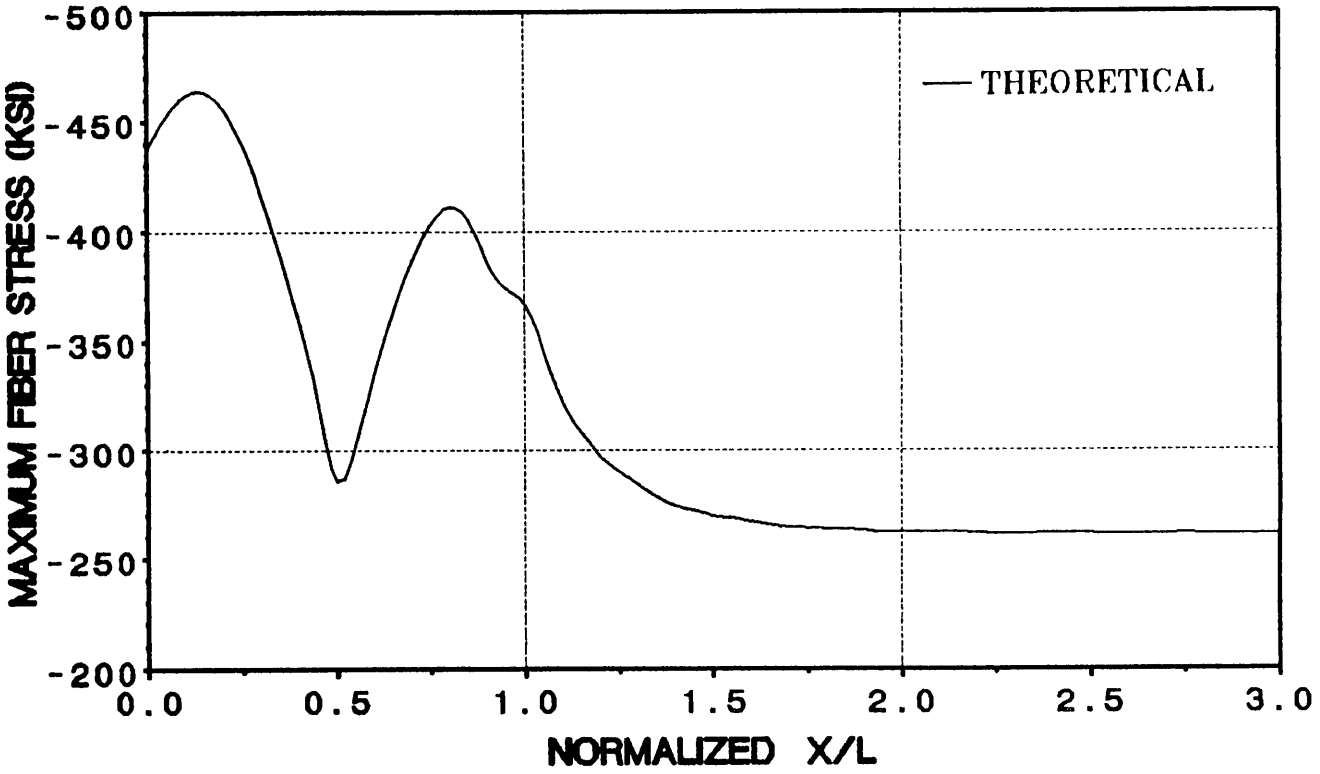

Figure 66. Maximum fiber compressive stresses along the bundle.

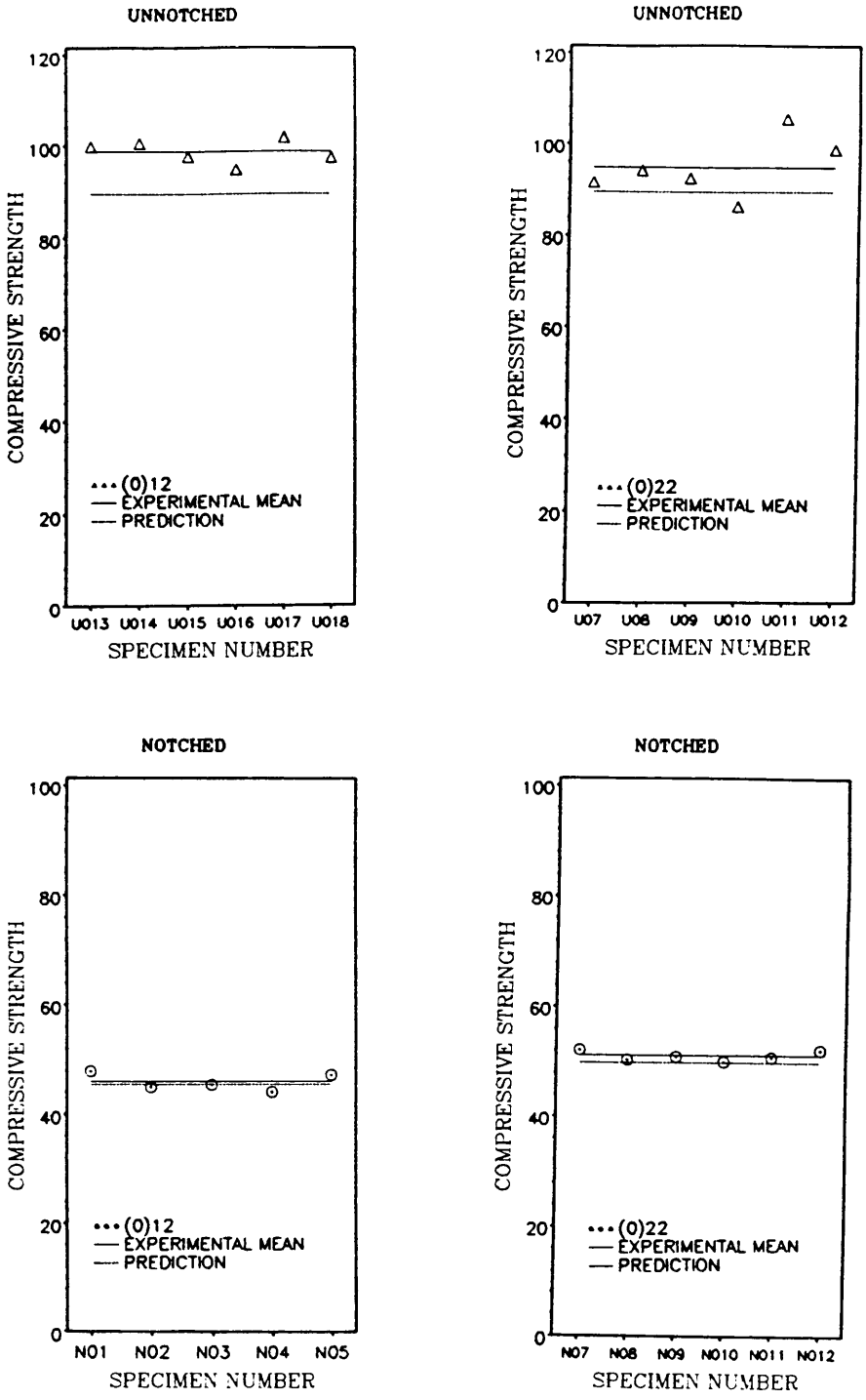

Figure 67. Comparison of experimental and predicted compressive strengths for unidirectional laminates.

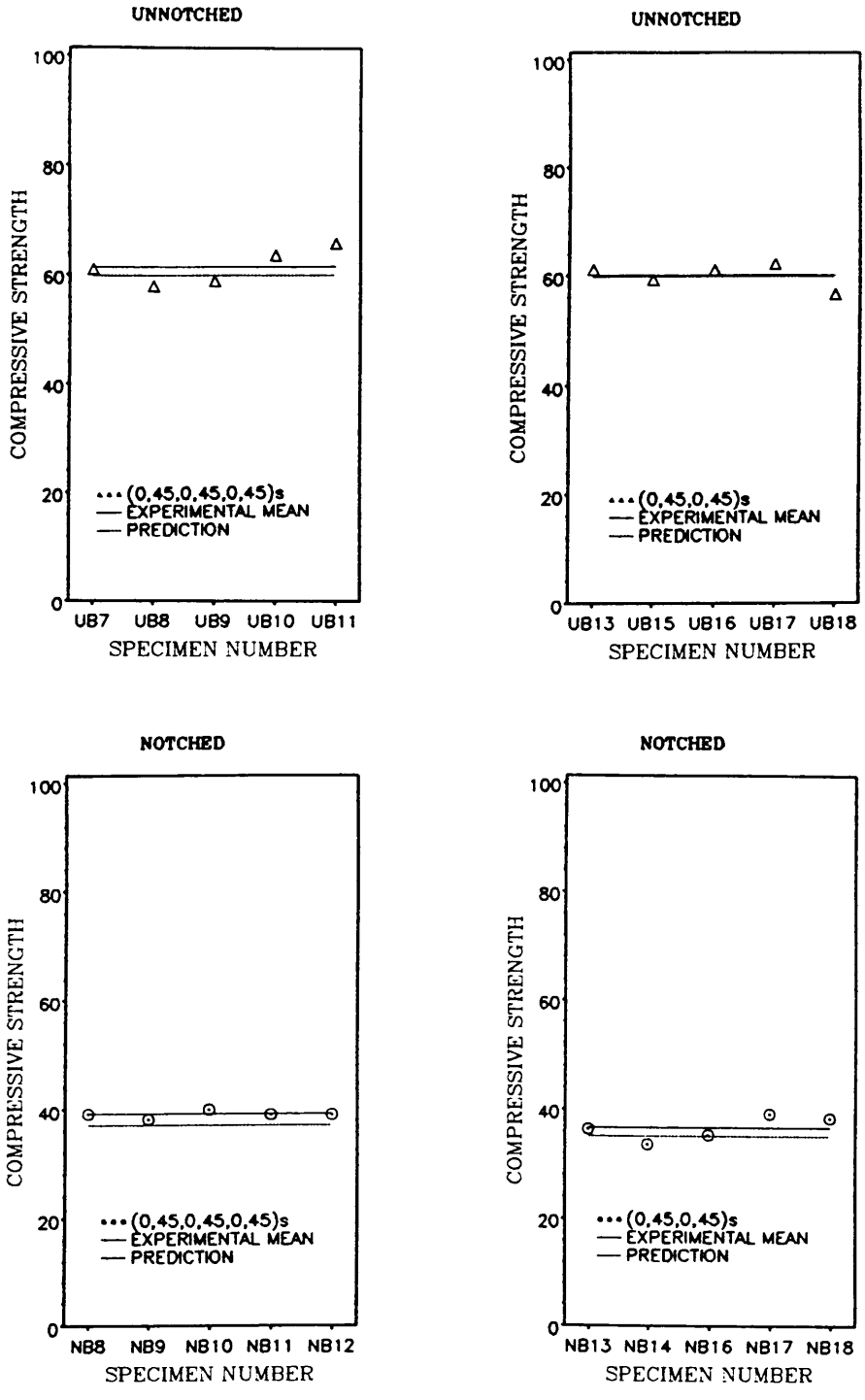

Figure 68. Comparison of experimental and predicted compressive strengths for quasi-isotropic laminates.

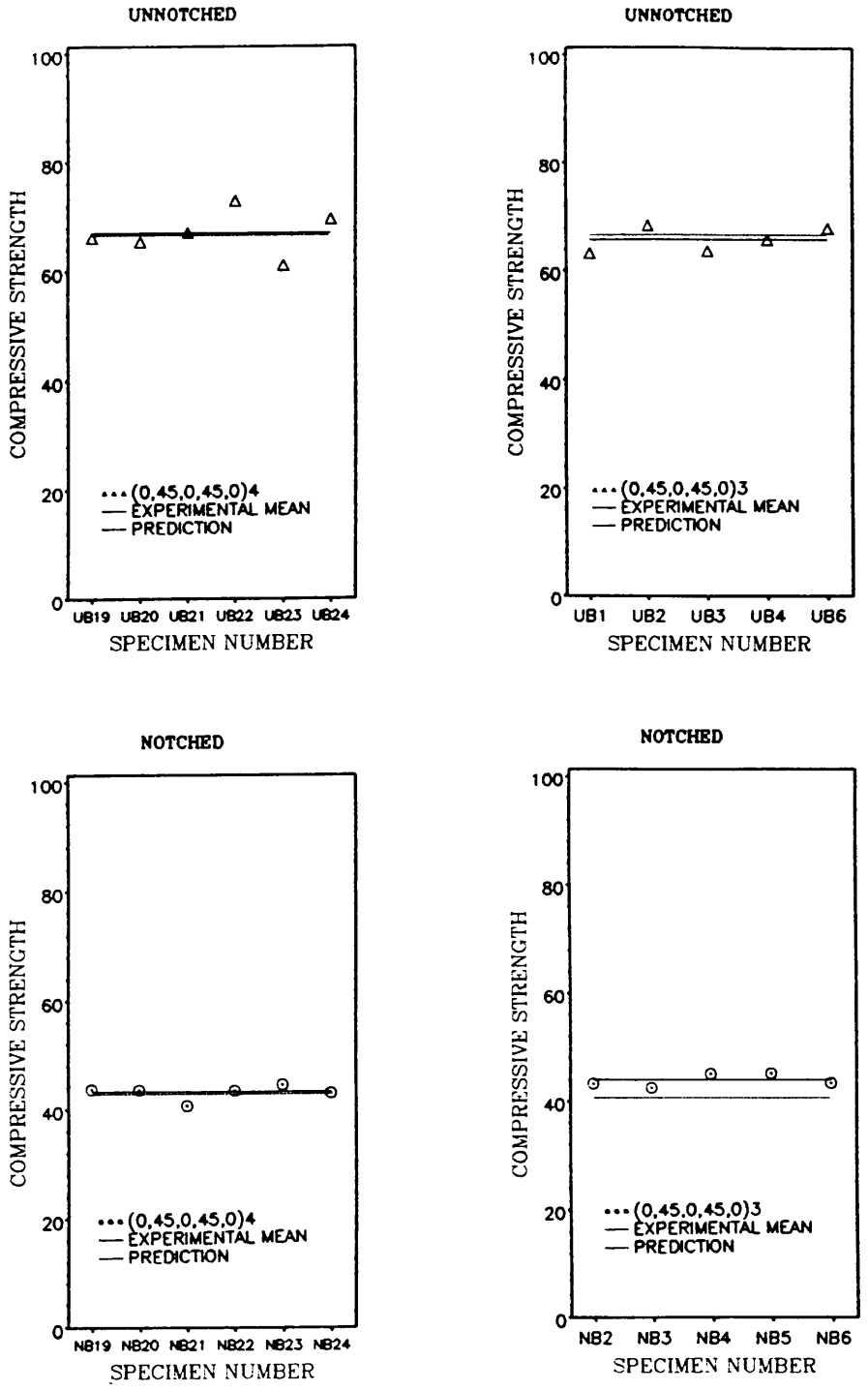

Figure 69. Comparison of experimental and predicted compressive strengths for orthotropic laminates.

Table 1. Laminate geometries and experimental data.

Lot number	Stacking sequence	Specimen number	Experimental strength KSI (MPa)	Standard deviation	Notched/ Unnotched	Specimen dimensions In.
19233	$(0,45,0,45)_s$	UB13,UB15 to UB18	-60.04 (-414)	2.19	0.6100	5x1x.1
		NB13,NB14	-36.61(-252)	2.26		5x1.5x.1
		NB16 to NB18				
6828	$(0,45,0,45,0,45)_s$	UB7 to UB11	-61.41 (-423)	3.18	0.6382	5.5x1x.156
		NB8 to NB12	-39.19 (-270)	.62		5.5x1.5x.156
6205-B	$(0,45,0,45,0)_3$	UB1 to UB4, UB6	-65.76 (-453)	2.35	0.6691	7x1x.21
		NB2 to NB6	-44.00 (-303)	1.17		5.5x1.5x.21
57-087	$(0,45,0,45,0)_4$	UB19 to UB24	-67.08 (-463)	3.99	0.6448	7x1x.266
		NB19 to NB23	-43.25 (-298)	1.30		5.5x1.5x.266
6205	$(0)_{12}$	U013 to U018	-98.78 (-681)	2.54	0.4655	6x1x.165
		N01, N02	-45.98 (-317)	1.57		5.5x1.5x.165
		N04 to N06				
57-106	$(0)_{22}$	U07 to U012	-94.88 (-654)	6.60	0.5387	6x1x.275
		N07 to N012	-51.11 (-352)	.89		5.5x1.5x.275

Table 2. Fiber, matrix, and bundle properties.

Property	Units	Graphite fiber	PMR15 matrix	Bundle
Longitudinal modulus	msi (GPa)	34 (234)	0.473 (3.32)	27.1 (190)
Transverse modulus	msi (GPa)	2 (14)	0.473 (3.32)	1.33 (9.34)
Longitudinal shear modulus	msi (GPa)	1.65 (11.5)	0.174 (1.2)	0.798 (5.6)
Transverse shear modulus	msi (GPa)	0.7 (4.9)	0.174 (1.2)	0.486 (3.35)
Longitudinal Poisson's ratio		0.2	0.36	0.229
Transverse Poisson's ratio		0.25	0.36	0.342
Tensile strength	ksi (MPa)	515 (3620)	4.5 (31.5)	

Table 3. Characteristic distances for various laminates.

Stacking sequence	Characteristic distances for A.S.C A In. (mm)	B In. (mm)	C In. (mm)	Characteristic distance for P.S.C D In. (mm)	Number of bundles
$(0,45,0,45)_s$	0.093 (2.36)	0.237 (6.02)	0.281 (7.14)	0.0392 (1.00)	1.59
$(0,45,0,45,0,45)_s$	0.117 (2.97)	0.275 (5.72)	0.330 (6.99)	0.0488 (1.24)	1.98
$(0,45,0,45,0)_3$	0.177 (4.50)	0.379 (9.63)	0.425 (10.80)	0.0654 (1.66)	2.65
$(0,45,0,45,0)_4$	0.159 (4.04)	0.304 (7.72)	0.348 (8.84)	0.0586 (1.49)	2.37
$(0)_{12}$	0.118 (3.00)	0.112 (2.84)	0.112 (2.84)	0.0392 (1.00)	1.59
$(0)_{22}$	0.168 (4.27)	0.177 (4.50)	0.177 (4.50)	0.0535 (1.36)	2.17
Coefficient of correlation	0.78	0.02	0.002	0.49	0.49

Table 4. Stresses induced in 0-deg plies of unnotched laminates at failure.

Stacking sequence	Unnotched strength ksi (MPa)	0-deg ply 2-direction ksi (MPa)	0-deg ply 1-direction ksi (MPa)	R
$(0,45,0,45)_s$	-60.04 (-414)	-76.48 (-527)	22.65 (156)	1.038
$(0,45,0,45,0,45)_s$	-81.41 (-423)	-77.71 (-536)	23.51 (162)	1.053
$(0,45,0,45,0)_3$	-65.76 (-453)	-78.48 (541)	17.44 (120)	1.056
$(0,45,0,45,0)_4$	-67.08 (-463)	-80.00 (-552)	17.83 (123)	1.035
$(0)_{12}$	-98.45 (-681)	-98.45 (-681)	0.00 (0.00)	1.000
$(0)_{22}$	-94.88 (-654)	-94.88 (-654)	0.00 (0.00)	1.000

Table 5. Predicted values of strength in various laminates and percent differences from experimental data.

Stacking sequence	Predicted strength			Difference from experiment	
	Ply ksi (MPa)	Unnotched ksi (MPa)	Notched ksi (MPa)	Unnotched %	Notched %
$(0,45,0,45)_s$	-89.53 (-617)	-59.81 (-412)	-53.00 (-241)	0.38	4.60
$(0,45,0,45,0,45)_s$	-89.53 (-617)	-59.81 (-412)	-37.10 (-256)	2.68	5.63
$(0,45,0,45,0)_3$	-89.53 (-617)	-66.64 (-459)	-40.60 (-280)	1.34	8.37
$(0,45,0,45,0)_4$	-89.53 (-617)	-66.64 (-459)	-42.80 (-295)	0.66	1.05
$(0)_{12}$	-89.53 (-617)	-89.53 (-617)	-45.40 (-313)	10.33	1.28
$(0)_{22}$	-89.53 (-617)	-89.53 (-617)	-49.80 (-343)	5.98	2.63

Appendix A. Analysis Code

A.1 FMAN Input Requirements

Title (20A4) = Title of the problem.

NOL (T50,F15.2) = Number of plies in the laminate.

P (T50,F15.2) = Applied compressive stress

P2 (T50,F15.2) = The load which the average stress of (ASC) is set equal to. (see cases A, B, and C in chapter 5).

NUMPLY (T50,I2) = Ply number in which stresses are averaged.

LCOUNT (T50,I2) = Number of plies for which results are printed.

Next NOL lines are ply properties for the classical lamination analysis, and have a free format.

E_1 E_2 G_{12} ν_{12} α_1 α_2 θ *thickness*

Next six lines are information about the hole in the laminate.

PHI (T50,F15.7) = Angle in which the global compressive stress is applied to the laminate with respect to the hole axes. (figure 60).

AA (T50,F15.7) = Semi-major axis of the hole.

BB (T50,F15.7) = Semi-minor axis of the hole.

W (T50,F6.2) = Specimen width.

PATH (T50,F3.0) = The path on which stresses are calculated.

If PATH=1, stresses are calculated on a line and the next line of input will consist of the free format information about the line.

X_1 Y_1 X_2 Y_2 *NOX* *NOY* *IDIR*

X1, Y1, X2, Y2 = Coordinates of the beginning and end points of the line path as shown in figure 60.

NOX = Number by which the X component of the line path will be divided. NOX must always be even because of the Modified Simpson's Rule used for the integration of stresses.

NOY = Number by which the Y component of the line path will be divided. NOY must always be even because of the Modified Simpson's Rule used for the integration of stresses.

Note: If NOX is none-zero, NOY will not be used.

Note: If NOX is zero, NOY will be used.

IDIR = Either equal to 1 or 2. It is the local direction of the stresses which are integrated in the NUMPLYth layer. If IDIR>2, then laminate stresses in the Y direction will be integrated instead.

If PATH=2, stresses are calculated on an elliptical path and the next input line will be the information about the ellipse.

THETA1 *THETA2* *DTHETA* *CAA* *CBB*

THETA1 and THETA2 = Starting and ending angles respectively.

DTHETA = Increments between THETA1 and THETA2

CAA = Semi-major axis of the elliptical path.

CBB = Semi-minor axis of the elliptical path.

A.2 Input Example

```
 CELION 3000/PMR15              (0,45,0,45)S
NOMBER OF PLIES IN THE LAMINATE            (NOL):  8
LOAD APPLIED TO THE LAMINATE (NOTCHED)       (P):-36600.
LOAD WHICH IS COMPARED TO THE AVERAGE STRESS(P2):-93440.
PLY NUMBER IN WHICH ST.ARE INTEGRATED   (NUMPLY): 1
# OF PLIES FOR WHICH INFO. IS PRINTED   (LCOUNT): 1
  E1          E2          G12      NU12    ALFA1 ALFA2  ANGLE    PLY TH.
9000000.    9000000.    850000.    .07      0.     0.     0.0      .013
9000000.    9000000.    850000.    .07      0.     0.    45.0      .013
9000000.    9000000.    850000.    .07      0.     0.     0.0      .013
9000000.    9000000.    850000.    .07      0.     0.    45.0      .013
9000000.    9000000.    850000.    .07      0.     0.    45.0      .013
9000000.    9000000.    850000.    .07      0.     0.     0.0      .013
9000000.    9000000.    850000.    .07      0.     0.    45.0      .013
9000000.    9000000.    850000.    .07      0.     0.     0.0      .013
DEGREE IN WHICH THE LOAD IS APPLIED          (PHI):90.
SEMI-MINOR AXIS OF THE HOLE                  (AA) :0.1875
SEMI-MINOR AXIS OF THE HOLE                  (BB) :0.1875
SPECIMEN WIDTH                                (W) :1.5
PATH IN WHICH ST. CALCULATED (1=LINE)(2=ELLIPSE):1.
  .1875    0.     .330    0.    20     10     2
```

A.3 FMAN Flow Chart

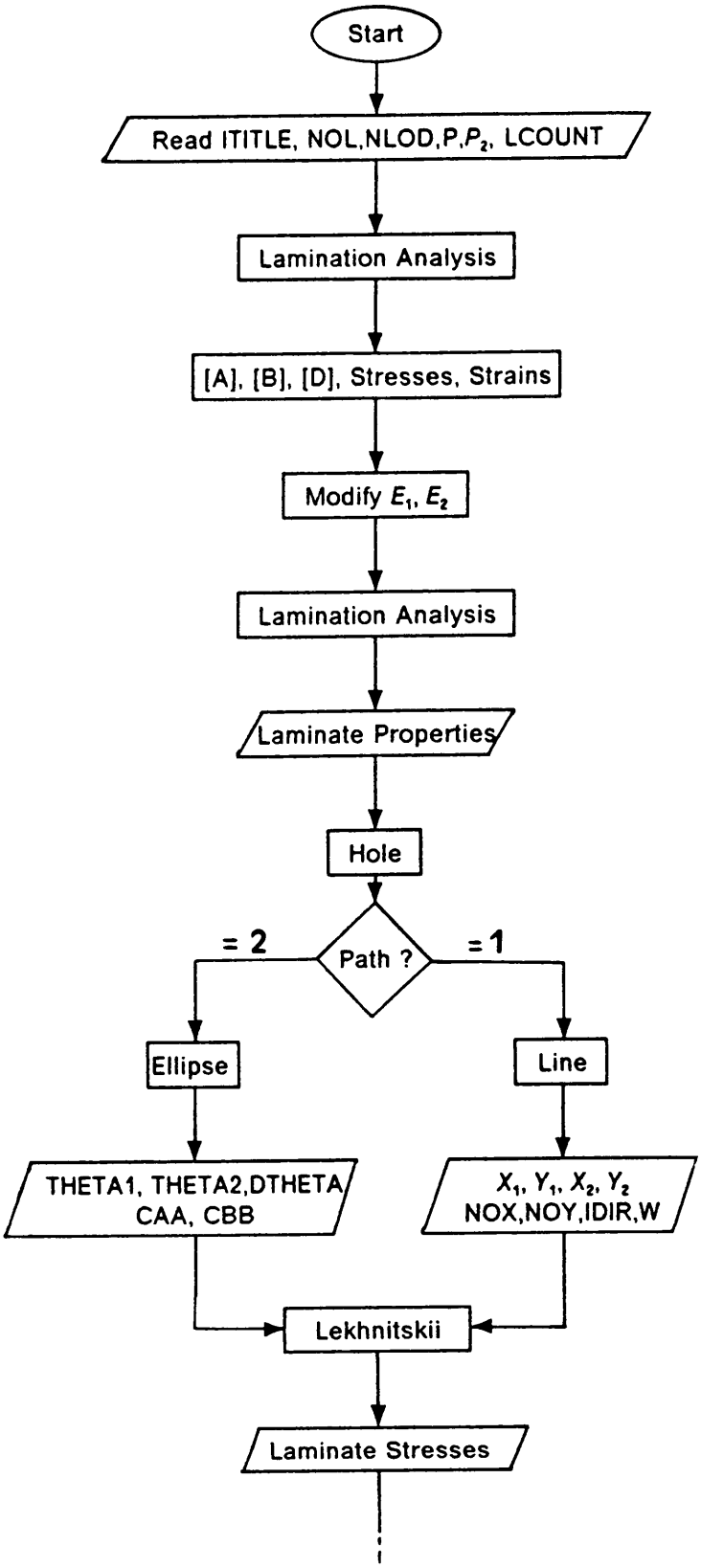

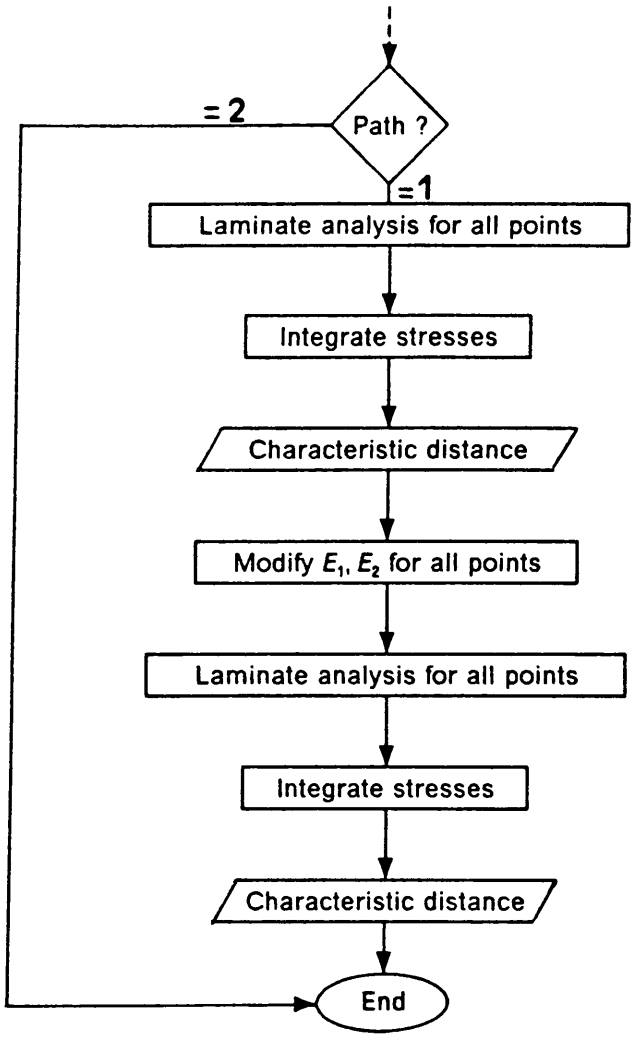
Path ?
=2
=1
Laminate analysis for all points
Integrate stresses
Characteristic distance
Modify E_1, E_2 for all points
Laminate analysis for all points
Integrate stresses
Characteristic distance
End

A.4 FMAN

```
C*************************************************************************
C                          F M A N                                       *
C                ANALYSIS OF COMPOSITE LAMINATES                         *
C                            BY                                          *
C                      FARSHAD MIRZADEH                                  *
C        VIGINIA POLYTECHNIC INSTITUTE AND STATE UNIVERSITY              *
C*************************************************************************
C
C     VERSION 2.  AUGUST 2, 1988
C     THE PROGRAM IS CAPABLE OF DOING THE FOLOWING:
C
C     INPUT
C  1- FIBER AND MATRIX PROPERTIES
C  2- BUNDLE GEOMETRY AND WEAVE GEOMETRY
C  3- APPLIED REMOTE LOAD AND ITS DIRECTION WITH RESPECT TO THE HOLE
C  4- HOLE GEOMETRY
C  5- PLY GEOMETRY AND PROPERTIES
C
C     COMPUTATIONS
C  1- CLASICAL LAMINATION ANALYSIS TO DETERMINE THE LAMINATE
C     PROPERTIES AND STRESSES.
C  1.B MODIFY PLY MODULY. USING AN IMPERICAL STRESS-STRAIN CURVE
C      NEW PLY PROPERTIES ARE DETERMINED.
C  1.C CLT TO DETERMINE LAMINATE GLOBAL PROPERTIES
C  2- USING LEKHNITSKII'S ELASTICITY SOLUTION LAMINATE STRESSES AROUND
C     THE HOLE ARE DETERMINED
C  3- STRESSES AT DEFINED POINTS ON 1) A LINE PATH OR  2) AN ELLIPTIC
C     PATH ARE CALCULATED BY LEKHNITSKII'S SOLUTION
C  4- CLT IS PERFORMED FOR EVERY SUCH POINT AND MIDPLANE STRAINS AND
C     PLY STRESSES ARE DETERMINED
C  5- USING AN IMPERICAL STRESS-STRAIN CURVE NEW PLY PROPERTIES ARE
C     DETERMINED FOR EVERY POINT AND PART FOUR IS REPEATED.
C  6- STRESSES IN EVERY SPECIFIED PLY ARE INTEGRATED BY MODIFIED SIMPSON
C     RULE (ON THE LINE PATH) TO DETERMINE THE CHARACTERISTIC DISTANCE.
C*************************************************************************
C
C****       THE FOLLOWING ARRAYS ARE USED
C
C A........ "A" MATRIX
C ABD...... COMBINATION OF A,B AND D MATRICES
C ABHD..... INVERSE OF ABD MATRIX
C ALF...... COEFFICIENT OF THERMAL EXPANSION
C ANG...... PLY ANGLE
C AST...... INVERSE OF "A" MATRIX
C B........ "B" MATRIX
C BETA..... ARRAY OR NUMBER OF PLIES X COEFFICIENT OF MOISTURE EXPANSION
C EE....... PLY MODULUS OF ELASTICITY (STRESS DIRECTION X POINT NUMBER
```

```
C EK....... ARRAY OF MIDPLANE STRAINS AND CURVATURES
C QB....... QBAR MATRIX
C QBAR..... QBAR MATRIX (JONES,S BOOK)
C QEBAR.... QE COLLECTED IN ONE MATRIX
C STSLAM... ARRAY OF NUMBER OF POINTS X LAMINATE STRESSES AND MOMENTS
C           (AT THIS POINT NO MOMENTS ARE PRESENT)
C SLAM..... LAMINATE STRESSES AND MOMENTS TAKEN OUT OF STSLAM
C SNTH..... THERMAL STRAIN (NOT USED)
C STSPLY... PLY STRESSES AT EACH POINT
C STNTH.... THERMAL STRAINS OF PLIES
C ST12..... PLY STRESSES IN 1-2 DIRECTION
C STN...... PLY STRAINS AT EACH INTERFACE
C STNMEC... MECHANICAL STRAINS
C STRG..... PLY STRENGTHS
C STS...... STRESSES ON TOP AND BOTTOM OF PLIES IN LAMINATE DIRECTIONS
C THICK.... PLY THICKNESS
C THLOD.... THERMAL LOAD
C X,Y...... COORDINATES OF POINTS
C Z........ DISTANCE OF PLY FROM THE MIDPLANE
C
C********  THE FOLLOWING SINGLE VARIABLES ARE USED
C
C A,B...... MAJOR AND MINOR SEMI AXESS OF THE BUNDLE CROSS-SECTION
C AMP...... AMPLITUDE OF BUNDLE
C ALPHA.... SHEAR CORRECTION FACTOR
C BL....... BUNDLE LENGTH
C CEL ..... TYPE OF CELION (3000 OR 6000 OR ....)
C DELX,DELY X AND Y INCREMENTS BETWEEN THE POINTS
C           X PLY NUMBER)
C DTHETA... INCREMENT OF THETA
C EM....... MATRIX YOUNG'S MODULUS
C ELF...... FIBER LONGITUDINAL MODULUS
C ETF...... FIBER TRANSVERS MODULUS
C EX....... LAMINATE MODULUS IN X DIRECTION
C EX....... LAMINATE MODULUS IN Y DIRECTION
C FRADI.... RADIUS OF FIBER
C FL ...... FIBER KINK LENGTH (EXPERIMENTAL)
C GF ...... FIBER SHEAR MODULUS
C GM ...... MATRIX SHEAR MODULUS
C GXY...... LAMINATE SHEAR MODULUS
C IDIR..... DIRECTION OF PLY STRESS WHICH IS INTEGRATED (1 OR 2) ONLY
C ICOUNT... COUNTER FOR DIFFERENT COMPUTATIONS
C IPOINT... NUMBER OF POINTS
C K1 ...... LINEAR SPRING CONSTANT
C K2 ...... TORSIONAL SPRING CONSTANT
C LCOUNT... PLY COUNTER FOR PRINTING PURPOSES ONLY
C NOX,NOY.. NUMBER OF INCREMENTS BETWEEN THE BEGINNING AND THE END POINT
C NNN ..... INTEGER VARIABLE FOR NUMBER OF POINTS
C NUF ..... FIBER POISSON'S RATIO
C NUM...... MATRIX POISSON'S RATIO
```

```
C P ....... APPPLIED STRESS TO THE NOTCHED MATERIAL
C TH ...... LAMINATE THICKNESS
C THETA1 .. STARTING ANGLE FOR ELLIPTICAL PATH
C THETA2 .. ENDING ANGLE FOR ELLIPTICAL PATH
C THETAA .. THETA COORDINATE OF EACH POINT
C TEMP..... TEMPERATURE DIFFERENCE FROM STRESS FREE TEMPERATURE
C STRGTU .. UNNOCHED STRENGTH OF THE MATERIAL
C VXY ..... LAMINATE POISSON'S RATIO
C X1,Y1 ... COORDINATES OF THE BEGINNING POINT OF THE LINE PATH
C X2,Y2 ... COORDINATES OF THE END POINT OF THE LINE PATH
C           IN LINE PATH. IF NOX IS NON ZERO THEN IT IS USED. IF NOX IS
C           ZERO THEN NOY IS OUTOMATICALLY USED.
C
C*****  M A I N   P R O G R A M
      IMPLICIT REAL*8 (A-H,O-Z)
      REAL*8 NUM,NUF,K1,K2,MODE
      DIMENSION  BETA(50,3),STNTH(50,3),ST12(102,3),STN(51,3),QEBAR(150)
     &,Z(51),QBAR(150,3),STNMEC(102,3),STS(102,3),ANG(50),THICK(50)
     &,ITITLE(20)
      COMMON/PROP/EX,EY,VXY,GXY,TEMP,TH
      COMMON/COUNT/ICOUNT,IPOINT,LCOUNT,NNN,NOX,NOY,IDIR
      COMMON/STIF/ALF(3),QB(3,3),EE(2,100,50)
      COMMON/FORC/STSLAM(100,6),SLAM(6),STSPLY(2,100,50),P,P2
     & ,STG(5),R1(50)
      COMMON/XY/X1,Y1,X2,Y2,DELX,DELY,THETA1,THETA2,DTHETA,X(361),Y(361)
     &,THETAA(361),W,AA,BB,PATH
      COMMON/BMPROP/ELF,ETF,GF,NUF,CEL,EM,GM,NUM,K2,K1,A,B,AMP,BL,
     &ALPHA,FRADI,FL,MODE,START,END,STEP
C ********** INPUT INFORMATOIN
      READ (5,250) (ITITLE(I),I=1,20)
 250  FORMAT(20A4)
      READ(5,300)NOL,P,P2,NUMPLY,LCOUNT
 300  FORMAT(T50,I3,/,2(T50,F15.2,/),2(T50,I2,/))
      STG(1)=-P2
      STG(2)=-P2
      STG(3)=-P2
      STG(4)=-P2
      STG(5)=18220.
      TEMP=0
      WRITE(6,350) (ITITLE(I),I=1,20)
 350  FORMAT(20A4)
      WRITE(6,150) NOL,TEMP
  150 FORMAT (5X,'NUMBER OF LAYERS=',I2,/,5X,'TEMPERATURE DIFFERENCE=',
     +F10.0,//)
      NOL3=NOL*3
      NOL22=NOL*2+2
      NOL1=NOL+1
C*****COMPUTE LAMINATE PROPERTIES ONLY
      LCNT2=LCOUNT*2
      NNN=1
```

```
      ICOUNT=1
      CALL CLT (NOL,NOL1,NOL3,NOL22,LCNT2,STNTH,ST12,STN,QEBAR,QBAR,
     &STNMEC,STS,ANG,THICK,BETA,Z)
      CALL MODIFY(NOL,ARG)
      ICOUNT=2
      CALL CLT (NOL,NOL1,NOL3,NOL22,LCNT2,STNTH,ST12,STN,QEBAR,QBAR,
     &STNMEC,STS,ANG,THICK,BETA,Z)
C**** PLAIN STRESS COMPLIANCES
      S11=1/EX
      S22=1/EY
      S12=-VXY/EX
      WRITE(6,160) S11,S12,S22
 160  FORMAT('PLAIN STRESS COMPLIANCES OF THE LAMINATE',/,
     &'S11=',E11.3,5X,'S12=',E11.3,5X,'S22=',E11.3)
C
C*****COMPUTE STRESS DISTRIBUTION AROUND THE HOLE IN THE LAMINATE
C
      CALL HOLE
C
C**** PERFORM CLT FOR EACH POINT OF INTEREST
C
      IF(PATH.EQ.2) GOTO 999
      ICOUNT=3
      DO 30 NNN=1,IPOINT
      CALL CLT (NOL,NOL1,NOL3,NOL22,LCNT2,STNTH,ST12,STN,QEBAR,QBAR,
     &STNMEC,STS,ANG,THICK,BETA,Z)
   30 CONTINUE
      IF(AA.EQ.0.0.AND.BB.EQ.0.0) GOTO 999
      CALL INTEG(NUMPLY,AVGSTS)
      IF(IDIR.GT.2) THEN
      WRITE(6,200)
  200 FORMAT(10X,'**** LAMINATE STRESSES ARE INTEGRATED ****')
      GOTO 999
      ENDIF
C
C    MODIFY THE PLY MODULI AT EVERY POINT OF INTEREST
C
   18 ICOUNT=4
      DO 10 NNN=1,IPOINT
      CALL MODIFY(NOL,ARG)
      IF(ARG.LE.0) GOTO 23
C
C**** PERFORM CLT FOR EACH POINT OF INTEREST USING NEW PROPERTIES
C
      CALL CLT (NOL,NOL1,NOL3,NOL22,LCNT2,STNTH,ST12,STN,QEBAR,QBAR,
     &STNMEC,STS,ANG,THICK,BETA,Z)
   10 CONTINUE
C
C***** INTEGRATION OF PLY STRESSES IS PERFORMED ONLY FOR IDIR=1 OR
```

```
C***** IDIR=2
C
   23 IF(AA.EQ.0.0.AND.BB.EQ.0.0) GOTO 999
      WRITE(6,26)
   26 FORMAT(3X,'X',8X,'PLY STRESS',8X,'LAMINATE STRESS')
      DO 25 JJ=1,IPOINT
      WRITE(6,555) X(JJ) , STSPLY(2,JJ,1),STSLAM(JJ,2)
  555 FORMAT(F10.6,10X,E15.5,10X,E15.5)
   25 CONTINUE
      CALL INTEG(NUMPLY,AVGSTS)
 999  STOP
      END
C
C*************** S U B R O U T I N E   C L T
C
      SUBROUTINE CLT(NOL,NOL1,NOL3,NOL22,LCNT2,STNTH,ST12,STN,QEBAR,QBAR
     &,STNMEC,STS,ANG,THICK,BETA,Z)
C     M A T R I C E S  N E E D E D  I N  L A M I N A T E  A N A L Y S I
C     M A X I M U M  5 0  L A Y E R S
      IMPLICIT REAL*8(A-H,O-Z)
      DIMENSION  BETA(150),A(3,3),B(3,3),STNTH(50,3),ST12(102,3)
     &,D(3,3),ABD(6,6),EK(6),ABHD(6,6),STN(51,3),WK(6),THLOD(6)
     &,QE(3),QEBAR(150),SNTH(3),AST(3,3),EOTH(6),STRG(5),Z(51)
     &,QBAR(150,3),STNMEC(102,3),STS(102,3),ANG(50),THICK(50)
      COMMON/PROP/EX,EY,VXY,GXY,TEMP,TH
      COMMON/FORC/STSLAM(100,6),SLAM(6),STSPLY(2,100,50),P,P2
     & ,STG(5),R1(50)
      COMMON/COUNT/ICOUNT,IPOINT,LCOUNT,NNN,NOX,NOY,IDIR
      COMMON/STIF/ALF(3),QB(3,3),EE(2,100,50)
      IF(ICOUNT.EQ.3) GOTO 7
C
C ****   ZERO ALL VARIABLES  ******************
C
      DO 1 J=1,3
      DO 1 I=1,NOL3
      QEBAR(I)=0
      QBAR(I,J)=0.
    1 CONTINUE
      DO 2 I=1,3
      DO 3 J=1,3
      QB(I,J)=0
      A(I,J)=0
      B(I,J)=0
      D(I,J)=0
    3 CONTINUE
      ALF(I)=0
      QE(I)=0
    2 SNTH(I)=0
      DO 4 I=1,6
      DO 5 J=1,6
```

```
      ABD(I,J)=0
    5 ABHD(I,J)=0
      EK(I)=0
      WK(I)=0
      THLOD(I)=0
    4 EOTH(I)=0
      IF (ICOUNT.EQ.4) GOTO 12
       DO 6 I=1,100
       DO 6 J=1,6
       STSLAM(I,J)=0.0
    6 CONTINUE
C*******************************************************************************
   12 WRITE (6,170)
  170 FORMAT(5X,'LAMINA  ANGLE(DEG)     THICKNESS          E1',
     +'          E2          G12       V12     V21      ALFA1      ALFA2',/)
      TH = 0
      DO 10 K=1,NOL
C
C**** COMPUTE STIFFNESS MATRIX FOR EACH PLY
C
      CALL XYPROP(K,MODE,NOL,NOL1,NOL3,NOL22,ANG,THICK)
      DO 8 I=1,3
    8 SNTH(I)=TEMP*ALF(I)
      CALL MULT (QB,SNTH,QE,3)
      DO 9 J=1,3
    9 STNTH(K,J)=SNTH(J)
      J=3*K-2
      K3=3*K
      DO 20 I=J,K3
      N=I-J+1
      DO 20 M=1,3
      QBAR(I,M)=QB(N,M)
      QEBAR(I)=QE(N)
   20 CONTINUE
      TH=TH+THICK(K)
   10 CONTINUE
C
C                G E N E R A T E  A,B,D  M A T R I C E S
C
      Z(1)=-TH/2
      DO 40 K=1,NOL
      L=K+1
      Z(L)=Z(K)+THICK(K)
      DO 30 II=1,3
      J=3*K-3+II
      II3=II+3
      THLOD(II)=THLOD(II)+QEBAR(J)*(Z(L)-Z(K))
      THLOD(II3)=THLOD(II3)+QEBAR(J)*(Z(L)*Z(L)-Z(K)*Z(K))/2
      DO 30 JJ=1,3
      A(II,JJ)=A(II,JJ)+QBAR(J,JJ)*(Z(L)-Z(K))
```

```
      B(II,JJ)=B(II,JJ)+QBAR(J,JJ)*(Z(L)*Z(L)-Z(K)*Z(K))/2
      D(II,JJ)=D(II,JJ)+QBAR(J,JJ)*(Z(L)**3-Z(K)**3)/3
   30 CONTINUE
C
C                G E N E R A T E  ABD  M A T R I X
C
      DO 40 I=1,3
      DO 40 J=1,3
      ABD(I,J)=A(I,J)
      N=3+I
      M=3+J
      ABD(I,M)=B(I,J)
      ABD(N,M)=D(I,J)
      ABD(N,J)=B(I,J)
   40 CONTINUE
      DO 55 I=1,6
      DO 55 J=1,6
   55 IF (ABS(ABD(I,J)).LT..001) ABD(I,J)=0.
C
C                P R I N T  ABD  M A T R I X
C
      IF(ICOUNT.EQ.2.OR.ICOUNT.EQ.4) GOTO 265
      WRITE (6,200)
  200 FORMAT (/,25X,'**** A MATRIX *****',35X,'**** B MATRIX ****',/)
      WRITE (6,220) (( ABD(I,J),J=1,6),I=1,3)
  220 FORMAT (6(5X,E14.7))
      WRITE (6,240)
  240 FORMAT( /,25X,'**** B MATRIX ****',35X,'**** D MATRIX ****'/)
      WRITE(6,260) (( ABD(I,J) ,J=1,6),I=4,6)
  260 FORMAT (6(5X,E14.7))
C
C***** ELASTIC PROPERTIES OF THE LAMINATE
C
  265 CALL INVERS(A,AST,3)
      DO 56 I=1,3
      DO 56 J=1,3
   56 AST(I,J)=AST(I,J)*TH
      EX=1/AST(1,1)
      EY=1/AST(2,2)
      VXY=-AST(1,2)/AST(1,1)
      VYX=-AST(1,2)/AST(2,2)
      GXY=1/AST(3,3)
      ETAXYX=AST(1,3)/AST(1,1)
      ETAXYY=AST(2,3)/AST(2,2)
      ETAXXY=AST(1,3)/AST(3,3)
      ETAYXY=AST(2,3)/AST(3,3)
C
C**** PRINT LAMINATE PROPERTIES
C
      WRITE(6,270)
```

```
  270 FORMAT(/,5X,'**********ELASTIC PROPERTIES OF LAMINATE**********')
      WRITE (6,280) EX,EY,GXY,VXY,VYX,ETAXYX,ETAXYY,ETAXXY,ETAYXY
  280 FORMAT(/,5X,'EX = ',E10.3,10X,'EY = ',E10.3,10X,'GXY = ',E10.3,
     *//,5X,'POISSON S RATIO XY = ',F10.6,10X,'POISSON S RATIO YX = ',
     *F10.6,//,5X,'ETA XY,X = ',F10.6,15X,'ETA XY,Y = ',F10.6,//,5X,
     &  'ETA X,XY = ',F10.6,15X,'ETA Y,XY = ',F10.6,//)
C
C ***** I N V E R T  ABD  M A T R I X
C
      CALL INVERS(ABD,ABHD,6)
C
C***** P R I N T  A'B'H'D'  M A T R I X
C
      IF(ICOUNT.EQ.2) GOTO 999
      IF(ICOUNT.EQ.4) GOTO 375
      WRITE (6,300)
  300 FORMAT(/,25X,'**** A PRIME MATRIX ****',35X,'**** B PRIME MATRIX
     +****',/)
      WRITE (6,320) ((ABHD(I,J),J=1,6),I=1,3)
  320 FORMAT (6(5X,E14.7))
      WRITE (6,350)
  350 FORMAT(/,25X,'**** H PRIME MATRIX ****',35X,'**** D PRIME MATRIX
     +****',/)
      WRITE (6,370) ((ABHD(I,J) ,J=1,6),I=4,6)
  370 FORMAT (6(5X,E14.7))
C
C**** CALCULATE THERMAL PROPERTIES
C
  375 CALL MULT(ABHD,THLOD,EOTH,6)
      IF (TEMP.EQ.0.0) GOTO 7
      ALF(1)=EOTH(1)/TEMP
      ALF(2)=EOTH(2)/TEMP
      ALF(3)=EOTH(3)/TEMP
      WRITE (6,290) (ALF(I),I=1,3)
  290 FORMAT (5X,'COEFF. OF THERMAL EXPANSION   X= ',E10.3,/,35X,'Y= '
     *,E10.3,/,35X,'XY= ',E10.3,//)
C
C*****  L O A D I N G
C
C**** C A L C U L A T E  M I D P L A N E  S T R A I N S
C**** A N D  C U R V A T U R E S
C
    7  IF(ICOUNT.LE.2) THEN
       NNN=1
       STSLAM(NNN,2)=P
       ELSE
       WRITE (6,400) NNN
  400 FORMAT (/,10X,'POINT # ',I3)
       ENDIF
       DO 65 J=1,3
```

```
   65 SLAM(J)=STSLAM(NNN,J)*TH
      DO 66 J=4,6
   66 SLAM(J)=0.
      CALL MULT (ABHD,SLAM,EK,6)
      WRITE (6,440)
  440 FORMAT (/,10X,'******* MIDPLANE STRAINS AND CURVATURES *******')
      WRITE (6,460) (EK(I),I=1,6)
  460 FORMAT (5X,'EPSX= ',E10.4,5X,'EPSY= ',E10.4,5X,'GAMAXY=',E10.4
     +,//,5X,'KX= ',E10.4,5X,'KY= ',E10.4,5X,'KXY= ',E10.4,/)
C
C*********** C A L C U L A T E  S T R A I N S
C
      DO 70 K=1,NOL
      KK=2*K-1
      N=K+1
      DO 70 I=1,3
      II=I+3
      STN(K,I)=EK(I)+Z(K)*EK(II)
      STN(N,I)=EK(I)+Z(N)*EK(II)
      STNMEC(KK,I)=STN(K,I)-STNTH(K,I)
      STNMEC(KK+1,I)=STN(N,I)-STNTH(K,I)
   70 CONTINUE
C
C*****C A L C U L A T E  S T R E S S E S
C
      CALL STRESS (NOL,NOL1,NOL3,NOL22,STRG,QBAR,LCNT2,STN,Z,ANG,STS
     &,ST12,THICK,STNMEC)
C
C 900 CONTINUE
  999 RETURN
      END
C
C            S U B R O U T I N E  X Y P R O P
C
C****  THIS SUBROUTINE WOULD CALCULATE PLY STIFFNESS AND COMPLIANCE
C****  MATRICES
      SUBROUTINE XYPROP (K,MODE,NOL,NOL1,NOL3,NOL22,ANG,THICK)
      IMPLICIT REAL*8(A-H,O-Z)
      DIMENSION ANG(50),THICK(50),SB(3,3),THETA(50)
      COMMON/STIF/ALF(3),QB(3,3),EE(2,100,50)
      COMMON/COUNT/ICOUNT,IPOINT,LCOUNT,NNN,NOX,NOY,IDIR
      IF(ICOUNT.EQ.2.OR.ICOUNT.EQ.4) GOTO 5
      READ (5,*) EE(1,NNN,K),EE(2,NNN,K),G12,V12,AL1,AL2,THETA(K)
     &,THICK(K)
C
C*****C A L C U L A T E  R E D U C E D  S T I F F N E S S
C
    5 V21=V12*EE(2,NNN,K)/EE(1,NNN,K)
      WRITE(6,100) K,THETA(K),THICK(K),EE(1,NNN,K),EE(2,NNN,K),
     &G12,V12,V21,AL1,AL2
```

```
  100 FORMAT (5X,I2,5X,F7.2,10X,F5.3,6X,3(E10.3,2X),2(F5.3,2X),2(E10.3))
      Q11=EE(1,NNN,K)**2/(EE(1,NNN,K)-V12**2*EE(2,NNN,K))
      Q12=V12*EE(2,NNN,K)*EE(1,NNN,K)/(EE(1,NNN,K)-V12**2*EE(2,NNN,K))
      Q22=EE(2,NNN,K)*EE(1,NNN,K)/(EE(1,NNN,K)-V12**2*EE(2,NNN,K))
      Q66=G12
      PI=4.*DATAN(1.DO)
      ANG(K)=THETA(K)/180.*PI
      SI=DSIN(ANG(K))
      CO=DCOS(ANG(K))
      QB(1,1)=Q11*CO**4+(2*Q12+4*Q66)*(SI*CO)**2+Q22*SI**4
      QB(1,2)=(Q11+Q22-4*Q66)*(SI*CO)**2+Q12*(SI**4+CO**4)
      QB(2,1)=QB(1,2)
      QB(2,2)=Q11*SI**4+(2*Q12+4*Q66)*(SI*CO)**2+Q22*CO**4
      QB(1,3)=(Q11-Q12-2*Q66)*SI*CO**3+(Q12-Q22+2*Q66)*SI*SI*SI*CO
      QB(3,1)=QB(1,3)
      QB(2,3)=(Q11-Q12-2*Q66)*SI*SI*SI*CO+(Q12-Q22+2*Q66)*SI*CO**3
      QB(3,2)=QB(2,3)
      QB(3,3)=(Q11+Q22-2*Q12-2*Q66)*(SI*CO)**2+Q66*(SI**4+CO**4)
      ALF(1)=AL1*CO**2+AL2*SI**2
      ALF(2)=AL1*SI**2+AL2*CO**2
      ALF(3)=(AL1-AL2)*CO*SI*2
C*****C A L C U L A T E  R E D U C E D  C O M P L I A N C E
      GOTO 999
  999 RETURN
      END
C
C*****************  S U B R O U T I N E  M U L T
C
      SUBROUTINE MULT (E,F,G,M)
      IMPLICIT REAL*8(A-H,O-Z)
      DIMENSION E(M,M),F(M),G(M)
      DO 5 II=1,M
    5 G(II)=0.
      DO 10 LL=1,M
      DO 10 JJ=1,M
      G(LL)=E(LL,JJ)*F(JJ)+G(LL)
   10 CONTINUE
      RETURN
      END
C
C*****************  S U B R O U T I N E  S T R E S S
C
      SUBROUTINE STRESS (NOL,NOL1,NOL3,NOL22,STRG,QBAR,LCNT2,STN,Z,ANG
     &,STS,ST12,THICK,STNMEC)
      IMPLICIT REAL*8(A-H,O-Z)
      DIMENSION   THICK(50),Z(51),ANG(50),STN(51,3)
     &,S1(3),S2(3),ST1(3),ST2(3),ST12(102,3),STS(102,3),
     &T(3,3),SL1(3),SL2(3),STRG(5),QBAR(150,3),STNMEC(102,3)
      COMMON/COUNT/ICOUNT,IPOINT,LCOUNT,NNN,NOX,NOY,IDIR
      COMMON/STIF/ALF(3),QB(3,3),EE(2,100,50)
```

```
      COMMON/FORC/STSLAM(100,6),SLAM(6),STSPLY(2,100,50),P,P2
     &  ,STG(5),R1(50)
      COMMON/XY/X1,Y1,X2,Y2,DELX,DELY,THETA1,THETA2,DTHETA,X(361),Y(361)
     &,THETAA(361),W,AA,BB,PATH
C
C**** CALCULATE PLY STRESSES IN THE LAMINATE DIRECTIONS
C
      DO 40 K=1,NOL
      KP1=K+1
      KK=2*K-1
      KK1=KK+1
      DO 10 I=1,3
      II=K*3-3+I
      DO 10 J=1,3
   10 QB(I,J)=QBAR(II,J)
      DO 20 I=1,3
      S1(I)=STNMEC(KK,I)
   20 S2(I)=STNMEC(KK1,I)
      CALL MULT (QB,S1,ST1,3)
      CALL MULT (QB,S2,ST2,3)
      DO 30 I=1,3
      STS(KK,I)=ST1(I)
   30 STS(KK1,I)=ST2(I)
C
C**** CALCULATE PLY STRESSES ON THE PLY DIRECTIONS
C
      CALL ROTATE (T,K,NOL,3,ANG)
      CALL MULT (T,ST1,SL1,3)
      CALL MULT (T,ST2,SL2,3)
      DO 50 I=1,3
      ST12(KK,I)=SL1(I)
      ST12(KK1,I)=SL2(I)
   50 CONTINUE
C
C**** BENDING MOMENTS ARE NOT PRESENT AND LAMINATE IS
C**** ASSUMED TO BE SYMMETRIC. THEREFORE STRESSES IN EACH PLY ARE THE
C**** AVERAGES OF STRESSES ON TOP AND BOTTOM OF EACH PLY
      STK1=ST12(KK1,1)/2+ST12(KK,1)/2
      STK2=ST12(KK1,2)/2+ST12(KK,2)/2
      STK3=ST12(KK1,3)/2+ST12(KK,3)/2
      STSPLY(1,NNN,K)=STK1
      STSPLY(2,NNN,K)=STK2
C**** CALCULATE MAX. PLY STRESS
      STMAX=STK1
      IF (STK2.LT.STK1) STMAX=STK2
   40 CONTINUE
C********** P R I N T  S T R A I N S  AND  S T R E S S E S
C
C     IF(ICOUNT.EQ.1.OR.ICOUNT.EQ.3) GOTO 999
      IF(ICOUNT.EQ.1) GOTO 999
```

```
      DO 60 K=1,LCOUNT
      KP1=K+1
      KK=2*K-1
      KK1=KK+1
      STK1=ST12(KK1,1)/2+ST12(KK,1)/2
      STK2=ST12(KK1,2)/2+ST12(KK,2)/2
      STK3=ST12(KK1,3)/2+ST12(KK,3)/2
      WRITE(6,100)
  100 FORMAT(5X,'TOTAL STRAINS IN X-Y SYSTEM',/,33X,'EX',12X,'EY',12X,
     +'GAMA XY')
      WRITE(6,150) K,(STN(K,I),I=1,3)
  150 FORMAT(5X,'TOP OF LAYER ',I2,3X,3(5X,E10.4))
      WRITE(6,200) K,(STN(KP1,I),I=1,3)
  200 FORMAT(5X,'BOTTOM OF LAYER ',I2,3(5X,E10.4),/)
      WRITE (6,250)
  250 FORMAT(5X,'MECHANICAL STRAINS IN X-Y SYSTEM',/,33X,'EX',12X,
     +'EY',12X,'GAMA XY')
      WRITE(6,150) K,(STNMEC(KK,I),I=1,3)
      WRITE(6,200) K,(STNMEC(KK1,I),I=1,3)
      WRITE(6,300)
  300 FORMAT(5X,'STRESSES IN X-Y SYSTEM',/,31X,'SIG X',12X,'SIG Y',12X,
     +'TAW XY')
      WRITE(6,350) K,(STS(KK,I),I=1,3)
  350 FORMAT(5X,'TOP OF LAYER ',I2,3X,3(5X,E11.5))
      WRITE(6,400) K,(STS(KK1,I),I=1,3)
  400 FORMAT(5X,'BOTTOM OF LAYER ',I2,3(5X,E11.5),/)
      WRITE (6,450)
  450 FORMAT(5X,'STRESSES IN 1-2 SYSTEM',/,31X,'SIG 1',12X,'SIG 2',10X
     +,'TAW 12')
      WRITE(6,350) K,(ST12(KK,I),I=1,3)
      WRITE (6,400) K,(ST12(KK1,I),I=1,3)
      CALL STRENG(STK1,STK2,STK3,K)
      WRITE(6,410)R1(K)
  410 FORMAT(5X,'SRENGTH RATIO IS',10X,'R=',F10.4)
   60 CONTINUE
  999 RETURN
      END
C
C******************  S U B R O U T I N E   I N V E R S E **********
C
      SUBROUTINE INVERS (AINV,BINV,NMAX)
      IMPLICIT REAL*8(A-H,O-Z)
      DIMENSION AINV(NMAX,NMAX),BINV(NMAX,NMAX)
      DO 20 N=1,NMAX
      D=AINV(N,N)
      DO 5 J=1,NMAX
    5 AINV(N,J)=-AINV(N,J)/D
      DO 10 I=1,NMAX
      IF(N-I.EQ.0) GOTO 10
      DO 15 K=1,NMAX
```

```
      IF(N-K.EQ.0) GOTO 15
      AINV(I,K)= AINV(I,K)+AINV(I,N)*AINV(N,K)
   15 CONTINUE
   10 AINV(I,N)=AINV(I,N)/D
      AINV(N,N)=1.0/D
   20 CONTINUE
      DO 25 I=1,NMAX
      DO 25 J=1,NMAX
   25 BINV(I,J)=AINV(I,J)
      RETURN
      END
C
C********************  S U B R O U T I N E   S T R E N G T H
C
      SUBROUTINE STRENG (ST1,ST2,SH,K)
      IMPLICIT REAL*8(A-H,O-Z)
      COMMON/FORC/STSLAM(100,6),SLAM(6),STSPLY(2,100,50),P,P2
     &  ,STG(5),R1(50)
      F11=1/(STG(1)*STG(2))
      F1=1/STG(1)-1/STG(2)
      F22=1/(STG(3)*STG(4))
      F2=1/STG(3)-1/STG(4)
      F66=1/STG(5)**2
      F12=-.5*SQRT(F11*F22)
      FIJ=F11*ST1**2+2*F12*ST1*ST2+F22*ST2**2+F66*SH**2
      FI=F1*ST1+F2*ST2
      RR=SQRT(FI**2+4*FIJ)
      R1(K)=(RR-FI)/(2*FIJ)
C      R2=(-RR-FI)/(2*FIJ)
      RETURN
      END
C
C     S U B R O U T I N E     R O T A T E
C
      SUBROUTINE ROTATE(T,K,NOL,N,ANG)
      IMPLICIT REAL*8(A-H,O-Z)
      DIMENSION T(N,N),ANG(50)
      T(1,1)=DCOS(ANG(K))*DCOS(ANG(K))
      T(1,2)=DSIN(ANG(K))*DSIN(ANG(K))
      T(1,3)=DSIN(ANG(K))*DCOS(ANG(K))*2.
      T(2,1)=T(1,2)
      T(2,2)=T(1,1)
      T(2,3)=-T(1,3)
      T(3,1)=T(2,3)/2
      T(3,2)=-T(3,1)
      T(3,3)=T(1,1)-T(1,2)
      RETURN
      END
C
```

```
C**** S U B R O U T I N E     M O D I F Y
C
      SUBROUTINE MODIFY(NOL,ARG)
      IMPLICIT REAL*8(A-H,O-Z)
      COMMON/COUNT/ICOUNT,IPOINT,LCOUNT,NNN,NOX,NOY,IDIR
      COMMON/STIF/ALF(3),QB(3,3),EE(2,100,50)
      COMMON/FORC/STSLAM(100,6),SLAM(6),STSPLY(2,100,50),P,P2
     &  ,STG(5),R1(50)
      WRITE(6,20) NNN
   20 FORMAT(//,10X,'*** LAMINATE PROPERTIES ARE MODIFIED AT POINT '
     &  ,I2,' ***',/)
      DO 10 K=1,NOL
      DO 10 J=1,2
      ARG=.010934084+4.2918D-8*STSPLY(J,NNN,K)
      IF(ARG.LE.0) THEN
      WRITE(6,100)
 100  FORMAT(10X,'*** MODIFICATION CAN NOT BE PERFORMED DUE TO HIGH',
     &' STRESSES (E=10) ***',/)
      EE(J,NNN,K)=10
      GOTO 10
      ENDIF
      EPS=(-.10456617+DSQRT(ARG))/2
      EE(J,NNN,K)=186402118*EPS+9745678
C     WRITE(6,*) EE(J,NNN,K)
   10 CONTINUE
  999 RETURN
      END
C
C********** S U B R O U T I N E     H O L E
C
      SUBROUTINE HOLE
C
C     COMPUTE STRESSES AROUND THE HOLE
C
      IMPLICIT REAL*8(A-H,O-Z)
      COMMON/PROP/EX,EY,VXY,GXY,TEMP,TH
      COMMON/FORC/STSLAM(100,6),SLAM(6),STSPLY(2,100,50),P,P2
     &  ,STG(5),R1(50)
      COMMON/COUNT/ICOUNT,IPOINT,LCOUNT,NNN,NOX,NOY,IDIR
      COMMON/XY/X1,Y1,X2,Y2,DELX,DELY,THETA1,THETA2,DTHETA,X(361),Y(361)
     &,THETAA(361),W,AA,BB,PATH
      COMPLEX*16 ZZ(2),ZETAB(2),PHIPRM(2),MU(2),AB(2),ZAB(2)
      COMPLEX*16 ALFAA,BETAA,II,EGV,FACT
      PI=4.*DATAN(1.D0)
C     EQUATION OF THE LINE FOR CHARACTERISTIC DISTANCES IS E+F*TH
      READ(5,200) PHI,AA,BB,W,PATH
 200  FORMAT(3(T50,F15.7,/),T50,F6.2,/,T50,F3.0)
      IF ((AA.EQ.0.0).AND.(BB.EQ.0.0)) GOTO 999
      IF(PATH.EQ.2) READ(5,*) THETA1,THETA2,DTHETA,CAA,CBB
C
```

```
C**** EITHER NOX OR NOY MUST BE NONZERO
C
      IF(PATH.EQ.1) READ(5,*) X1,Y1,X2,Y2,NOX,NOY,IDIR
      WRITE(6,10)
   10 FORMAT(/'********* HOLE PARAMETERS **********')
      WRITE(6,20)PHI,AA,BB
   20 FORMAT(//,1X,'PHI=',F6.2,5X,'SEMI-MAJOR AXIS=',F6.3,10X,
     &'SEMI-MINOR AXIS=',F6.3)
      WRITE(6,25) EX,EY,VXY,GXY
   25 FORMAT(/,1X,'EX=',E10.4,5X,'EY=',E10.4,5X,'VXY=',F6.3,5X,'GXY='
     &  ,E10.4)
      IF (PATH.EQ.1)  THEN
      IF(NOX.NE.0) THEN
      DELX=(X2-X1)/NOX
      ELSE
      DELX=0.D0
      ENDIF
      IF(NOY.NE.0) THEN
      DELY=(Y2-Y1)/NOY
      ELSE
      DELY=0.D0
      ENDIF
      WRITE(6,30) X1,Y1,X2,Y2,DELX,DELY
   30 FORMAT(1X,'X1=',F8.5,3X,'Y1=',F8.5,5X,'X2=',F8.5,3X,'Y2=',F8.5
     &,/,1X,'X INCREMENT=',F8.5,10X,'Y INCREMENT=',F8.5)
      ENDIF
      IF(PATH.EQ.2) WRITE(6,40) THETA1,THETA2,DTHETA
   40 FORMAT(1X,'THETA1=',F7.3,5X,'THETA2=',F7.3,5X,'THETA INCREMENT='
     &,F7.4)
      II=DCMPLX(0.D0,1.D0)
      EGV=DCMPLX(EX/GXY-2.*VXY,0.D0)
      EE=4.*EX/EY
      MU(1)=CDSQRT((-EGV+ CDSQRT(EGV**2-EE))/2.)
      MU(2)=CDSQRT((-EGV- CDSQRT(EGV**2-EE))/2.)
      IF(DIMAG(MU(1)).LT.0.D0) MU(1)=-MU(1)
      IF(DIMAG(MU(2)).LT.0.D0) MU(2)=-MU(2)
C     IF(DABS(DREAL(MU(1))).LT.1.D-5)  DREAL(MU(1))=0.D0
C     IF(DABS(DREAL(MU(2))).LT.1.D-5)  DREAL(MU(2))=0.D0
      WRITE(6,50) MU(1),MU(2)
   50 FORMAT(1X,'MU1=',E10.4,1X,E10.4,'I',10X,'MU2=',E10.4,1X,E10.4,'I')
      IF(PATH.EQ.2) GOTO 75
      WRITE(6,60)P
   60 FORMAT(/,5X,'STRESSES ALONG A LINE BETWEEN POINTS (X1,Y1) AND ',
     &'(X2,Y2)',/,5X,'FOR  P=',E10.4)
      IF(PATH.EQ.1) GOTO 85
   75 WRITE(6,80) CAA,CBB
   80 FORMAT(/,5X,'STRESSES ALONG AN ELLIPS OF SEMI-MAJOR AXIS=',F6.3,
     &5X,'SEMI-MINOR AXIS=',F6.3)
   85 PHI=PHI*4.*DATAN(1.D0)/180.
      FACT=P/2*(AA*DSIN(PHI)-II*BB*DCOS(PHI))
```

```
      ALFAA=-DSIN(PHI)*FACT
      BETAA=DCOS(PHI)*FACT
      IF (PATH.EQ.1) CALL LINE
      IF(PATH.EQ.2)  CALL ELLIPS(CAA,CBB)
      AB(1)=AA-II*MU(1)*BB
      AB(2)=AA-II*MU(2)*BB
      IF(PATH.EQ.1) WRITE(6,70)
   70 FORMAT(/,'POINT#',8X,'X',9X,'Y',8X,'SIGMA X',8X,'SIGMA Y',
     &8X,'TAU XY')
      IF(PATH.EQ.2) WRITE(6,91)
   91 FORMAT(/,'POINT#',3X,'THETA',4X,'X',7X,'Y',6X,'SIGMA X',7X,
     &'SIGMA Y',5X,'TAU XY')
      DO 100 J=1,IPOINT
      QUADR=1
      DO 95 I=1,2
      IF(X(J).LT.0) THEN
      QUADR=23
      X(J)=-X(J)
      Y(J)=-Y(J)
      ENDIF
      ZZ(I)=X(J)+MU(I)*Y(J)
      ZAB(I)=CDSQRT(ZZ(I)*ZZ(I)-AA**2-(MU(I)*BB)*(MU(I)*BB))
C     TO GET RID OF SINGULARITY DUE TO ELIMINATION OF HOLE "ZETAB" HAS
C     REPLACED ZETA
      ZETAB(I)=ZZ(I)+ZAB(I)
   95 CONTINUE
      PHIPRM(1)=AB(1)/ZAB(1)/(MU(1)-MU(2))*(MU(2)*ALFAA-BETAA)/ZETAB(1)
      PHIPRM(2)=AB(2)/ZAB(2)/(MU(1)-MU(2))*(BETAA-MU(1)*ALFAA)/ZETAB(2)
      STSLAM(J,1)=2.*REAL(MU(1)*MU(1)*PHIPRM(1)+MU(2)*MU(2)
     &*PHIPRM(2))+P*DCOS(PHI)**2
      IF(DABS(STSLAM(J,1)).LT.1.D-5)   STSLAM(J,1)=0.
      STSLAM(J,2)=2.*REAL(PHIPRM(1)+PHIPRM(2))+P*DSIN(PHI)**2
      IF(DABS(STSLAM(J,2)).LT.1.D-5)   STSLAM(J,2)=0.
      STSLAM(J,3)=-2.*REAL(MU(1)*PHIPRM(1)+MU(2)*PHIPRM(2))+
     &P*DSIN(PHI)*DCOS(PHI)
      IF(DABS(STSLAM(J,3)).LT.1.D-5)   STSLAM(J,3)=0.
      IF(QUADR.EQ.23) THEN
      X(J)=-X(J)
      Y(J)=-Y(J)
      ENDIF
      IF(PATH.EQ.1) WRITE(6,90) J,X(J),Y(J),(STSLAM(J,I),I=1,3)
   90 FORMAT(1X,I3,7X,2(F7.5,3X),3(E10.4,5X))
      IF(PATH.EQ.2) THEN
      THETAA(J)=THETAA(J)*180./PI
      WRITE(6,92)J,THETAA(J),X(J),Y(J),(STSLAM(J,I),I=1,3)
   92 FORMAT(1X,I3,3X,F6.2,3X,2(F7.3,3X),3(E10.4,3X))
      ENDIF
  100 CONTINUE
      DO 150 I=1,IPOINT
      DO 150 J=1,2
```

```
      STSLAM(I,J)=STSLAM(I,J)*(2+(1-2*AA/W)**3)/3/(1-2*AA/W)
  150 CONTINUE
  999 RETURN
      END
C
C ******  S U B R O U T I N E     E L L I P S
C
      SUBROUTINE ELLIPS(CAA,CBB)
      IMPLICIT REAL*8(A-H,O-Z)
      COMMON/XY/X1,Y1,X2,Y2,DELX,DELY,THETA1,THETA2,DTHETA,X(361),Y(361)
     &,THETAA(361),W,AA,BB,PATH
      COMMON/COUNT/ICOUNT,IPOINT,LCOUNT,NNN,NOX,NOY,IDIR
      IPOINT=0
      PI=4.*DATAN(1.D0)
      THETAA(1)=THETA1*PI/180.
      THETA2=THETA2*PI/180.
   10 IPOINT=IPOINT+1
      R=1/DSQRT(DCOS(THETAA(IPOINT))**2/CAA**2+DSIN(THETAA(IPOINT))
     &**2/CBB**2)
      X(IPOINT)=R*DCOS(THETAA(IPOINT))
      Y(IPOINT)=R*DSIN(THETAA(IPOINT))
      IF(THETAA(IPOINT).GE.THETA2) GOTO 999
      THETAA(IPOINT+1)=THETAA(IPOINT)+DTHETA*PI/180.
      GOTO 10
  999 RETURN
      END
C
C ******  S U B R O U T I N E     L I N E
C
      SUBROUTINE LINE
      IMPLICIT REAL*8(A-H,O-Z)
      COMMON/COUNT/ICOUNT,IPOINT,LCOUNT,NNN,NOX,NOY,IDIR
      COMMON/XY/X1,Y1,X2,Y2,DELX,DELY,THETA1,THETA2,DTHETA,X(361),Y(361)
     &,THETAA(361),W,AA,BB,PATH
      IPOINT=1
      X(1)=X1
      Y(1)=Y1
   10 IPOINT=IPOINT+1
      IF(DABS(X2-X1).LT.1.D-5.OR.NOX.EQ.0.) THEN
      Y(IPOINT)=Y(IPOINT-1)+DELY
      X(IPOINT)=Y(IPOINT)-Y1*(X2-X1)/(Y2-Y1)+X1
      IF(DABS(Y(IPOINT)).GE.(DABS(Y2)-DELY/5)) GOTO 999
      ELSE
      X(IPOINT)=X(IPOINT-1)+DELX
      Y(IPOINT)=(Y2-Y1)/(X2-X1)*(X(IPOINT)-X1)+Y1
      IF(DABS(X(IPOINT)).GE.(DABS(X2)-DELX/5)) GOTO 999
      ENDIF
      GOTO 10
  999 RETURN
```

```
      END
C
C***** S U B R O U T I N E    I N T E G
C
      SUBROUTINE INTEG(K,AVGSTS)
      IMPLICIT REAL*8(A-H,O-Z)
      COMMON/XY/X1,Y1,X2,Y2,DELX,DELY,THETA1,THETA2,DTHETA,X(361),Y(361)
     &,THETAA(361),W,AA,BB,PATH
      COMMON/FORC/STSLAM(100,6),SLAM(6),STSPLY(2,100,50),P,P2
     &  ,STG(5),R1(50)
      COMMON/COUNT/ICOUNT,IPOINT,LCOUNT,NNN,NOX,NOY,IDIR
      SLOPE=(Y2-Y1)/(X2-X1)
      IF(DABS(X2-X1).LT.1.D-5.OR.DELX.EQ.0.) THEN
      DELXY=DELY/DSIN(DATAN(SLOPE))
      ELSE
      DELXY=DELX/DCOS(DATAN(SLOPE))
      ENDIF
      WRITE(6,500) P2,DELXY
  500 FORMAT(1X,'SPECIFIED UNNOTCHED STRENGTH FOR COMPARISON= '
     & ,E10.4,10X,'DELXY=',F8.5)
      DO 10 L=3,IPOINT,2
      I=1
      IF(IDIR.LE.2) SUM=STSPLY(IDIR,I,K)
      IF(IDIR.GT.2) SUM=STSLAM(I,2)
      GOTO 5
    4 IF(I.EQ.L) THEN
      IF(IDIR.LE.2)  SUM=SUM+STSPLY(IDIR,I,K)
      IF(IDIR.GT.2)  SUM=SUM+STSLAM(I,2)
      GOTO 5
      ENDIF
      J=I/2
      AJ=I/2.
      IF((J+.1).GT.AJ)  THEN
      IF(IDIR.LE.2)  SUM=SUM+4*STSPLY(IDIR,I,K)
      IF(IDIR.GT.2)  SUM=SUM+4*STSLAM(I,2)
      GOTO 5
      ENDIF
      IF(IDIR.LE.2) SUM=SUM+2*STSPLY(IDIR,I,K)
      IF(IDIR.GT.2) SUM=SUM+2*STSLAM(I,2)
    5 I=I+1
      IF(I.LE.L) GOTO 4
      SUM=SUM*DELXY/3
      D=(I-2)*DELXY
      AVGSTS=SUM/D
      WRITE(6,50) L
   50 FORMAT(1X,'L=',I2)
      IF(DABS(AVGSTS).LE.DABS(P2)) GOTO 20
   10 CONTINUE
   20 IF(L.GE.IPOINT) WRITE (6,100)
  100 FORMAT(1X,'THE SPECIFIED DISTANCE IS NOT SUFFICIENT ')
```

```
    WRITE(6,550) D,AVGSTS
550 FORMAT(1X,'THE AVERAGE STRESS OVER DISTANCE ',F5.3,' INCHES FROM',
   &' THE HOLE IS ',E10.4)
999 RETURN
    END
```

Appendix B. Design Code

B.1 FMD Input Requirements

Title (20A4) = Title of the problem.

Next eleven lines of input are explained in the example input file shown in section B.2.

MICRO (T50,I1) = Flag for the choice of micromechanical equations to calculate bundle properties.

If MICRO=1, Tsai's micromechanical equations will be used.

If MICRO=2, Hashin's micromechanical equations will be used.

Next four lines of input are explained in the example input file shown in section B.2.

BL (T50,F10.5) = Unit length of a bundle explained in chapter 5 (L).

The repeating length of a bundle is equivalent to $0.75H_wL$

HW (T50,F10.5) = Harness number of the weave pattern.

Next two lines of input are explained in the input file shown at the end of the code.

FRX (T50,F10.5) = A factor which when multiplied by fiber diameter, results in the fiber kink length.

Next three lines of input are explained in the example input file shown in section B.2.

NOL (T50,I3) = Number of plies in the laminate.

LCOUNT (T50,I3) = Number of plies for which results are printed.

NUMPLY (T50,I3) = Ply number in which stresses are averaged.

STG(5) (T50,F10.2) = Shear strength of a ply.

Next NOL lines are ply properties for the classical lamination analysis, and have a free format.

E_1 E_2 G_{12} ν_{12} α_1 α_2 θ *thickness*

Next thirteen lines are information about the hole in the laminate.

PHI (T50,F15.7) = Angle in which the global compressive stress is applied to the laminate with respect to the hole axes. (figure 60).

AA (T50,F15.7) = Semi-major axis of the hole.

BB (T50,F15.7) = Semi-minor axis of the hole.

E (T50,F15.7) = The first term in the equation of the line E+F*TH which determines the characteristic distance.

F (T50,F15.7) = The second term in the equation of the line E+F*TH which determines the characteristic distance.

W (T50,F6.2) = Specimen width.

X1 (T50,F15.7) = X coordinate of the first point on the integration path.

X2 (T50,F15.7) = X coordinate of the first point on the integration path.

Y1 (T50,F15.7) = Y coordinate of the first point on the integration path.

Y2 (T50,F15.7) = Y coordinate of the first point on the integration path.

NOX = Number by which the X component of the line path will be divided. NOX must always be even because of the Modified Simpson's Rule used for the integration of stresses.

NOY = Number by which the Y component of the line path will be divided. NOY must always be even because of the Modified Simpson's Rule used for the integration of stresses.

Note: If NOX is none-zero, NOY will not be used.

Note: If NOX is zero, NOY will be used.

B.2 Input Example

```
CELION 3000/PMR15    (0,45,0,45)S
TRY AND ERROR STARTING LOAD (ARBITRARY).(TRYLOD):40000.
COMPRESSIVE STRENGTH OF A SINGLE FIBER..(FIBSTG):450000.
LONGITUDINAL ELASTIC MODULUS OF FIBER      (ELF):34000000.
TRANSVERESE MODULUS OF FIBER               (ETF):2000000.
LONGITUDINAL SHEAR MODULUS OF FIBER        (GLF):1650000.
TRANSVERSE SHEAR MODULUS OF FIBER          (GTF):700000.
LONGITUDINAL POISSON'S RATIO OF FIBER     (NULF):.20
TRANSVERSE POISSON'S RATIO OF FIBER       (NUTF):.25
NUMBER OF FIBERS IN A BUNDLE               (CEL):3000.
ELASTIC MODULUS OF MATRIX                   (EM):473000.
POISSON'S RATIO OF MATRIX                  (NUM):.36
MICRO-MECHANICAL EQ. (HASHIN=2) (TSAI=1) (MICRO):2
CONTIGUITY RATIO FOR TSAI (0 TO 1)         (CON):.5
SEMI-MAJOR AXIS OF BUNDLE                    (A):.0247
SEMI-MINOR AXIS OF BUNDLE                    (B):.003
INITIAL AMPLITUDE OF BUNDLE                (AMP):.00329
UNIT LENGTH OF BUNDLE (TOTAL=.75 HW*BL      (BL):.0638
HARNESS NUMBER OF THE WEAVE                 (HW):8.
SHEAR CORRECTION FACTOR                   (ALPHA):1.111
RADIUS OF FIBER                           (FRADI):.00014
LENGTH OF FIBER IN THE KINK=FRX*FRADI*2     (FRX):10.
MODE                                       (MODE): 5
ENDING POINT ON THE BUNDLE FOR CALCULATION (END):4.03
STEP FROM ZERO TO END                     (STEP):0.05
NUMBER OF PLIES IN THE LAMINATE             (NOL):  8
# OF LAYERS WHOSE STRESSES ARE PRINTED   (LCOUNT):  2
PLY # IN WHICH STRESSES ARE INTEGRATED   (NUMPLY):  1
SHEAR STRENGTH OF A PLY                   STG(5)  :18220.00
   E1         E2         G12      NU12   ALFA1 ALFA2 ANGLE    PLY TH.
9000000.   9000000.   850000.    .07     0.     0.     0.0     .0125
9000000.   9000000.   850000.    .07     0.     0.    45.0     .0125
9000000.   9000000.   850000.    .07     0.     0.     0.0     .0125
9000000.   9000000.   850000.    .07     0.     0.    45.0     .0125
9000000.   9000000.   850000.    .07     0.     0.    45.0     .0125
9000000.   9000000.   850000.    .07     0.     0.     0.0     .0125
9000000.   9000000.   850000.    .07     0.     0.    45.0     .0125
9000000.   9000000.   850000.    .07     0.     0.     0.0     .0125
DEGREE IN WHICH THE LOAD IS APPLIED        (PHI):90.
SEMI-MAJOR AXIS OF THE HOLE                (AA) :.1875
SEMI-MINOR AXIS OF THE HOLE                (BB) :.1875
E+F*TH=D  CHARACTERISTIC DISTANCE            (E):.05272
E+F*TH=D  CHARACTERISTIC DISTANCE            (F):.4399
SPECIMEN WIDTH                               (W):1.5
X CO. OF THE FIRST POINT ON THE INTEG. PATH (X1):.1875
```

```
Y CO. OF THE FIRST POINT ON THE INTEG. PATH (Y1):0.
X CO. OF THE SECOND POINT ON THE INTEG. PATH(X2):.3
Y CO. OF THE SECOND POINT ON THE INTEG. PATH(Y2):0.
NUMBER OF SEGMENTS IN THE X DIRECTION      (NOX):20
NUMBER OF SEGMENTS IN THE Y DIRECTION      (NOY):0
LOCAL DIRECTION OF STRESSES INTEGRATED    (IDIR):2
```

B.3 FMD Flow Chart

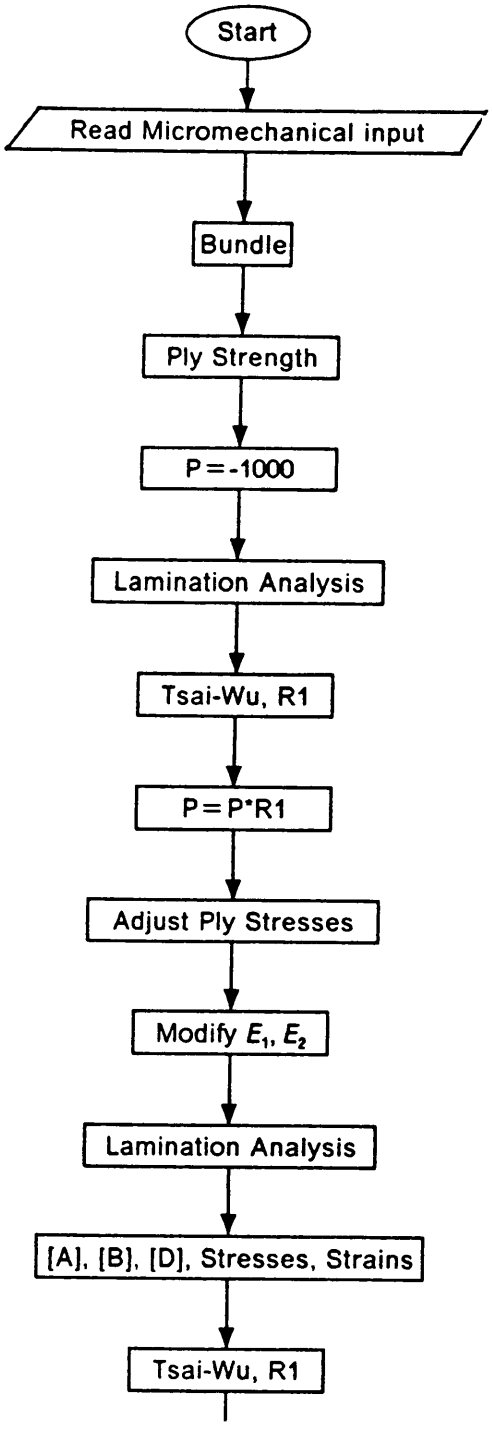

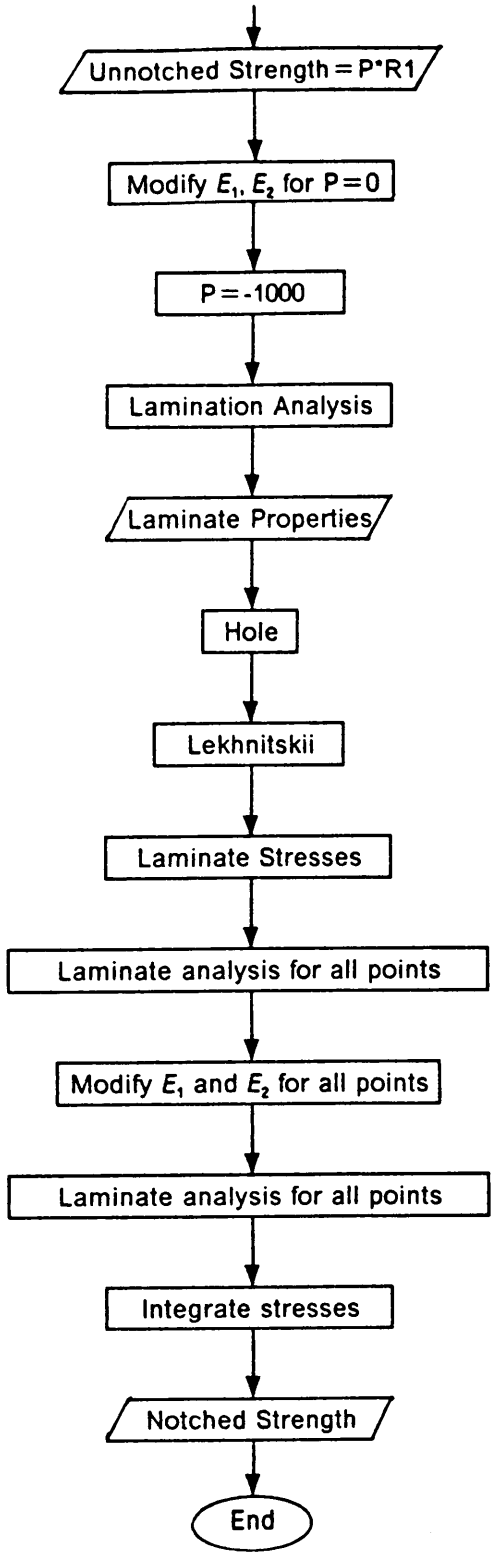
Unnotched Strength = P*R1
Modify E_1, E_2 for P=0
P=-1000
Lamination Analysis
Laminate Properties
Hole
Lekhnitskii
Laminate Stresses
Laminate analysis for all points
Modify E_1 and E_2 for all points
Laminate analysis for all points
Integrate stresses
Notched Strength
End

B.3 FMD

```
C*************************************************************************
c                            F M D                                       *
C          DESIGN OF WOVEN COMPOSITE LAMINATES                           *
C                             BY                                         *
C                       FARSHAD MIRZADEH                                 *
C      VIGINIA POLYTECHNIC INSTITUTE AND STATE UNIVERSITY               *
C*************************************************************************
C
C     VERSION 1.2  AUGUST 14, 1988  NEW INPUT STATEMENTS
C     THE PROGRAM IS CAPABLE OF DOING THE FOLOWING:
C
C     INPUT
C  1- BUNDLE GEOMETRY AND WEAVE GEOMETRY
C  2- FIBER AND MATRIX PROPERTIES
C  3- APPLIED REMOTE LOAD AND ITS DIRECTION WITH RESPECT TO THE HOLE
C  4- HOLE GEOMETRY
C
C****       THE FOLLOWING ARRAYS ARE USED
C
C A ....... "A" MATRIX
C ABD...... COMBINATION OF A,B AND D MATRICES
C ABHD..... INVERSE OF ABD MATRIX
C ALF...... COEFFICIENT OF THERMAL EXPANSION
C ANG...... PLY ANGLE
C AST ..... INVERSE OF "A" MATRIX
C B ....... "B" MATRIX
C BETA..... ARRAY OR NUMBER OF PLIES X COEFFICIENT OF MOISTURE EXPANSION
C EE....... PLY MODULUS OF ELASTICITY (STRESS DIRECTION X POINT NUMBER
C EK ...... STRAINS AND CURVATURES
C EOTH .... THERMAL STRAINS
C QB....... QBAR MATRIX
C QBAR..... QBAR MATRIX (JONES,S BOOK)
C QEBAR.... QE COLLECTED IN ONE MATRIX
C SB ...... (SBAR) COMPLIANCES
C STSLAM... ARRAY OF NUMBER OF POINTS X LAMINATE STRESSES AND MOMENTS
C           (AT THIS POINT NO MOMENTS ARE PRESENT)
C SLAM..... LAMINATE STRESSES AND MOMENTS TAKEN OUT OF STSLAM
C SNTH..... THERMAL STRAINS
C STSPLY .. PLY STRESSES AT EACH POINT
C STNTH.... THERMAL STRAINS OF PLIES
C ST12..... PLY STRESSES IN 1-2 DIRECTION
C STN...... PLY STRAINS AT EACH INTERFACE
C STNMEC... MECHANICAL STRAINS
C STG...... PLY STRENGTHS. 1,3=TENSION. 2,4=COMPRESSION.  5=SHEAR
C STS...... STRESSES ON TOP AND BOTTOM OF PLIES IN LAMINATE DIRECTIONS
C THICK.... PLY THICKNESS
C THLOD ... THERMAL LOAD
```

```
C X,Y..... COORDINATES OF POINTS
C Z..... DISTANCE OF PLY FROM THE MIDPLANE
C
C********  THE FOLLOWING SINGLE VARIABLES ARE USED
C
C A,B        MAJOR AND MINOR SEMI AXESS OF THE BUNDLE CROSS-SECTION
C AMP        AMPLITUDE OF BUNDLE
C ALPHA      SHEAR CORRECTION FACTOR
C BL         BUNDLE LENGTH
C CEL        TYPE OF CELION (3000 OR 6000 OR ....)
C DELX,DELY X AND Y INCREMENTS BETWEEN THE POINTS
C            X PLY NUMBER)
C DTHETA     INCREMENT OF THETA
C EM         MATRIX YOUNG'S MODULUS
C ELF        FIBER LONGITUDINAL MODULUS
C ETF        FIBER TRANSVERS MODULUS
C EX         LAMINATE MODULUS IN X DIRECTION
C EX         LAMINATE MODULUS IN Y DIRECTION
C FRADI      RADIUS OF FIBER
C FL         FIBER KINK LENGTH (EXPERIMENTAL)
C GF         FIBER SHEAR MODULUS
C GM         MATRIX SHEAR MODULUS
C GXY        LAMINATE SHEAR MODULUS
C IDIR       DIRECTION OF PLY STRESS WHICH IS INTEGRATED (1 OR 2) ONLY
C ICOUNT     COUNTER FOR DIFFERENT COMPUTATIONS
C IPOINT     NUMBER OF POINTS
C K1         LINEAR SPRING CONSTANT
C K2         TORSIONAL SPRING CONSTANT
C LCOUNT     PLY COUNTER FOR PRINTING PURPOSES ONLY
C NOX,NOY    NUMBER OF INCREMENTS BETWEEN THE BEGINNING AND THE END POINT
C NNN        INTEGER VARIABLE FOR NUMBER OF POINTS
C NUF        FIBER POISSON'S RATIO
C NUM        MATRIX POISSON'S RATIO
C P          APPLIED STRESS TO THE NOTCHED MATERIAL
C R1         A RATIO FROM TSI-WU FAILURE CRITERIA.  ULTIMATE LOAD=LOAD*R1
C THETA1     STARTING ANGLE FOR ELLIPTICAL PATH
C THETA2     ENDING ANGLE FOR ELLIPTICAL PATH
C THETAA     THETA COORDINATE OF EACH POINT
C TEMP       TEMPERATURE DIFFERENCE FROM STRESS FREE TEMPERATURE
C USTRGT     UNNOCHED STRENGTH OF THE MATERIAL
C VXY        LAMINATE POISSON'S RATIO
C X1,Y1      COORDINATES OF THE BEGINNING POINT OF THE LINE PATH
C X2,Y2      COORDINATES OF THE END POINT OF THE LINE PATH
C            IN LINE PATH. IF NOX IS NON ZERO THEN IT IS USED. IF NOX IS
C            ZERO THEN NOY IS OUTOMATICALLY USED.
C
C*****  M A I N  P R O G R A M
C*****************************************************************
      IMPLICIT REAL*8 (A-H,O-Z)
      REAL*8 INCLOD,NSTRGT
```

```
      REAL *8 KF,KM,NULF,NUM,NU12,NU23,M(100),NLOAD,
     & MAXST(100),MATVOL,NUTF,NU23UP,NU23LOW,KC
      DIMENSION  BETA(50,3),STNTH(50,3),ST12(102,3),STN(51,3),QEBAR(150)
     &,Z(51),QBAR(150,3),STNMEC(102,3),STS(102,3),ANG(50),THICK(50)
     &,FMAX(100),ITITLE(20)
      COMMON/PROP/EX,EY,VXY,GXY,TEMP,TH
      COMMON/COUNT/ICOUNT,IPOINT,IHOLE,LCOUNT,NNN,NUMPLY,NOX,NOY,IDIR
      COMMON/STIF/ALF(3),QB(3,3),EE(2,100,50)
      COMMON/FORC/STSLAM(100,6),SLAM(6),STSPLY(2,100,50),P,PNEW,USTRGT
     &,STMAX(50),STSMAX,STG(5),R1(50)
      COMMON/XY/X1,Y1,X2,Y2,DELX,DELY,THETA1,THETA2,DTHETA,X(361),Y(361)
     &,THETAA(361),DD
      COMMON/BMPROP/ELF,ETF,GLF,GTF,NULF,NUTF,CEL,EM,NUM,CON,
     & A,B,AMP,BL,ALPHA,FRADI,FRX,FL,START,END,STEP,S11,S12,S22,KK2
     & ,MICRO,NN,MODE
C **** DO LOOP TO CALCULATE THE COMPRESSIVE STRENGTH OF A BUNDLE
      READ(5,290)(ITITLE(I),I=1,20)
  290 FORMAT(20A4)
      READ(5,300) TRYLOD,FIBSTG,ELF,ETF,GLF,GTF,
     &  NULF,NUTF,CEL,EM,NUM,MICRO
     & ,CON,A,B,AMP,BL,ALPHA,FRADI,FRX,MODE,NN,START,END,STEP
     & ,S11,S12,S22,NOL,LCOUNT,NUMPLY,STG(5)
 300  FORMAT(11(T50,F15.2,/),T50,I1,/,T50,F5.3,/,7(T50,F10.5,/),
     & (T50,I2,/),2(T50,F5.3,/),3(T50,E10.3,/),T50,I3,/,
     & T50,I3,/,T50,I3,/,T50,F10.2,/)
      WRITE(6,145)(ITITLE(I),I=1,20)
  145 FORMAT(20A4,//)
      DO 50 IBEAM=1,5
      CALL BUNDLE (TRYLOD,FIBSTG,IBEAM,FIBMAX)
      TRYLOD=TRYLOD/FIBMAX*FIBSTG
   50 CONTINUE
C ***************************************************************
      PLYSTG=-TRYLOD
      STG(1)=-PLYSTG
      STG(2)=-PLYSTG
      STG(3)=-PLYSTG
      STG(4)=-PLYSTG
      WRITE(6,60) PLYSTG
   60 FORMAT ('PLY COMPRESSIVE STRENGTH=',F12.3,2X,'PSI')
      WRITE(6,150) NOL,TEMP
  150 FORMAT (5X,'NUMBER OF LAYERS=',I2,/,5X,'TEMPERATURE DIFFERENCE='
     &,F10.0,//)
      NOL3=NOL*3
      NOL22=NOL*2+2
      NOL1=NOL+1
C*****PERFORM LAMINATION ANALYSIS FOR  -1000. LBS
C
      LCNT2=LCOUNT*2
      NNN=1
      ICOUNT=1
```

```
      P=-1000.
      IPOINT=1
      CALL CLT (NOL,NOL1,NOL3,NOL22,LCNT2,STNTH,ST12,STN,QEBAR,QBAR,
     &STNMEC,STS,ANG,THICK,BETA,Z)
C
C***** CALCULATE THE REMOTE COMPRESSIVE STRESS WHICH MAKES THE MAXIMUM
C***** PLY STRESS IN THE FAILING PLY TO BE EQUAL TO PLY STRENGTH
       PNEW=P*R1(NUMPLY)
      WRITE(6,160) PNEW
  160 FORMAT('UNNOTCHED STRENGTH BEFOR MODIFICATION OF MODULI=',E10.3,/)
C
C*****CALCULATE PLY STRESSES FOR THE APPLIED LOAD  'PNEW'
      CALL ADJ (IPOINT,NOL)
C**** MODIFY PLY MODULI
      CALL MODIFY (NOL)
      ICOUNT=3
      P=PNEW
      CALL CLT (NOL,NOL1,NOL3,NOL22,LCNT2,STNTH,ST12,STN,QEBAR,QBAR,
     &STNMEC,STS,ANG,THICK,BETA,Z)
C***  CALCULATE STRENGTH USING THE TSI-WU CRITERIA
      USTRGT=PNEW*R1(NUMPLY)
      WRITE(6,45) USTRGT
   45 FORMAT(/,'UNNOTCHED STRENGTH=',F11.2,/)
C
C*****COMPUTE STRESS DISTRIBUTION AROUND THE HOLE IN THE LAMINATE
C*****FOR GLOBAL LOAD =P
C     DETERMINE PROPERTIES FOR NO LOAD SITUATION
      DO 26 IHOLE=1,2
      NNN=1
      DO 70 I=1,2
      DO 70 J=1,100
      DO 70 K=1,50
  70  STSPLY(I,J,K)=0.0
      P=-1000.0
      IF(IHOLE.EQ.2) THEN
      P=PNEW
      ICOUNT=3
      CALL MODIFY (NOL)
      CALL CLT (NOL,NOL1,NOL3,NOL22,LCNT2,STNTH,ST12,STN,QEBAR,QBAR,
     &STNMEC,STS,ANG,THICK,BETA,Z)
      ENDIF
      CALL MODIFY (NOL)
      CALL CLT (NOL,NOL1,NOL3,NOL22,LCNT2,STNTH,ST12,STN,QEBAR,QBAR,
     &STNMEC,STS,ANG,THICK,BETA,Z)
      LCOUNT=1
      CALL HOLE
C
C**** PERFORM CLT FOR EACH POINT OF INTEREST
C
      ICOUNT=4
```

```
      DO 30 NNN=1,IPOINT
      CALL CLT (NOL,NOL1,NOL3,NOL22,LCNT2,STNTH,ST12,STN,QEBAR,QBAR,
     &STNMEC,STS,ANG,THICK,BETA,Z)
   30 CONTINUE
      IF (IHOLE.EQ.2) THEN
C ****MODIFY PLY MODULY AT EVERY POINT OF INTEREST
      DO 11 NNN=1,IPOINT
      CALL MODIFY(NOL)
   11 CALL CLT (NOL,NOL1,NOL3,NOL22,LCNT2,STNTH,ST12,STN,QEBAR,QBAR,
     &STNMEC,STS,ANG,THICK,BETA,Z)
      ENDIF
C
C***** INTEGRATION OF PLY STRESSES IS PERFORMED ONLY FOR IDIR=1 OR
C***** IDIR=2 . IDIR=3 WILL AVERAGE THE LAMINATE STRESS
C
      DO 25 JJ=1,IPOINT
      WRITE(6,555) X(JJ) , STSPLY(2,JJ,NUMPLY),STSLAM(JJ,2)
  555 FORMAT(F10.6,10X,F11.2,10X,F11.2)
   25 CONTINUE
      CALL INTEG(IPOINT,NUMPLY,AVGSTS)
      PNEW=P*PLYSTG/AVGSTS
      WRITE(6,170) PNEW
  170 FORMAT('NOTCHED STRENGTH =',E10.3,/)
  26  CONTINUE
  999 STOP
      END
C
C*************** S U B R O U T I N E   C L T
C
      SUBROUTINE CLT(NOL,NOL1,NOL3,NOL22,LCNT2,STNTH,ST12,STN,QEBAR,QBAR
     &,STNMEC,STS,ANG,THICK,BETA,Z)
C     M A X I M U M  5 0  L A Y E R S
      IMPLICIT REAL*8(A-H,O-Z)
      DIMENSION  BETA(150),A(3,3),B(3,3),STNTH(50,3),ST12(102,3)
     &,D(3,3),ABD(6,6),EK(6),ABHD(6,6),STN(51,3),WK(6),THLOD(6)
     &,QE(3),QEBAR(150),SNTH(3),AST(3,3),EOTH(6),STRG(5),Z(51)
     &,QBAR(150,3),STNMEC(102,3),STS(102,3),ANG(50),THICK(50)
      COMMON/PROP/EX,EY,VXY,GXY,TEMP,TH
      COMMON/FORC/STSLAM(100,6),SLAM(6),STSPLY(2,100,50),P,PNEW,USTRGT
     &,STMAX(50),STSMAX,STG(5),R1(50)
      COMMON/COUNT/ICOUNT,IPOINT,IHOLE,LCOUNT,NNN,NUMPLY,NOX,NOY,IDIR
      COMMON/STIF/ALF(3),QB(3,3),EE(2,100,50)
      IF(ICOUNT.EQ.2.OR.ICOUNT.EQ.4) GOTO 7
C
C ****   ZERO ALL VARIABLES  *****************
C
      DO 1 J=1,3
      DO 1 I=1,NOL3
      QEBAR(I)=0
      QBAR(I,J)=0.
```

```
    1 CONTINUE
      DO 2 I=1,3
      DO 3 J=1,3
      QB(I,J)=0
      A(I,J)=0
      B(I,J)=0
      D(I,J)=0
    3 CONTINUE
      ALF(I)=0
      QE(I)=0
    2 SNTH(I)=0
      DO 4 I=1,6
      DO 5 J=1,6
      ABD(I,J)=0
    5 ABHD(I,J)=0
      EK(I)=0
      WK(I)=0
      THLOD(I)=0
    4 EOTH(I)=0
      TH = 0
      IF(ICOUNT.EQ.5) GOTO 11
      DO 6 I=1,100
      DO 6 J=1,6
    6 STSLAM(I,J)=0
C*************************************************************************
   11 WRITE (6,170)
  170 FORMAT(5X,'LAMINA  ANGLE(DEG)     THICKNESS          E1',
     +'          E2          G12       V12     V21      ALFA1      ALFA2',/)
      DO 10 K=1,NOL
C
C**** COMPUTE STIFFNESS MATRIX FOR EACH PLY
C
      CALL XYPROP(K,MODE,NOL,NOL1,NOL3,NOL22,ANG,THICK)
C
      DO 8 I=1,3
    8 SNTH(I)=TEMP*ALF(I)
C
      CALL MULT (QB,SNTH,QE,3)
C
      DO 9 J=1,3
    9 STNTH(K,J)=SNTH(J)
      J=3*K-2
      K3=3*K
      DO 20 I=J,K3
      N=I-J+1
      DO 20 M=1,3
      QBAR(I,M)=QB(N,M)
      QEBAR(I)=QE(N)
   20 CONTINUE
      TH=TH+THICK(K)
```

```
   10 CONTINUE
C
C                  G E N E R A T E  A,B,D  M A T R I C E S
C
      Z(1)=-TH/2
      DO 40 K=1,NOL
      L=K+1
      Z(L)=Z(K)+THICK(K)
      DO 30 II=1,3
      J=3*K-3+II
      II3=II+3
      THLOD(II)=THLOD(II)+QEBAR(J)*(Z(L)-Z(K))
      THLOD(II3)=THLOD(II3)+QEBAR(J)*(Z(L)*Z(L)-Z(K)*Z(K))/2
      DO 30 JJ=1,3
      A(II,JJ)=A(II,JJ)+QBAR(J,JJ)*(Z(L)-Z(K))
      B(II,JJ)=B(II,JJ)+QBAR(J,JJ)*(Z(L)*Z(L)-Z(K)*Z(K))/2
      D(II,JJ)=D(II,JJ)+QBAR(J,JJ)*(Z(L)**3-Z(K)**3)/3
   30 CONTINUE
C
C                  G E N E R A T E  ABD  M A T R I X
C
      DO 40 I=1,3
      DO 40 J=1,3
      ABD(I,J)=A(I,J)
      N=3+I
      M=3+J
      ABD(I,M)=B(I,J)
      ABD(N,M)=D(I,J)
      ABD(N,J)=B(I,J)
   40 CONTINUE
      DO 55 I=1,6
      DO 55 J=1,6
   55 IF (ABS(ABD(I,J)).LT..001) ABD(I,J)=0.
C
C                  P R I N T  ABD  M A T R I X
C
      IF(ICOUNT.EQ.3.OR.ICOUNT.EQ.4) GOTO 265
      WRITE (6,200)
  200 FORMAT (/,25X,'**** A MATRIX *****',35X,'**** B MATRIX ****',/)
      WRITE (6,220) (( ABD(I,J),J=1,6),I=1,3)
  220 FORMAT (6(5X,E14.7))
      WRITE (6,240)
  240 FORMAT( /,25X,'**** B MATRIX ****',35X,'**** D MATRIX ****'/)
      WRITE(6,260) (( ABD(I,J) ,J=1,6),I=4,6)
  260 FORMAT (6(5X,E14.7))
C
C***** ELASTIC PROPERTIES OF THE LAMINATE
C
  265 CALL INVERS(A,AST,3)
      DO 56 I=1,3
```

```
      DO 56 J=1,3
   56 AST(I,J)=AST(I,J)*TH
      EX=1/AST(1,1)
      EY=1/AST(2,2)
      VXY=-AST(1,2)/AST(1,1)
      VYX=-AST(1,2)/AST(2,2)
      GXY=1/AST(3,3)
      ETAXYX=AST(1,3)/AST(1,1)
      ETAXYY=AST(2,3)/AST(2,2)
      ETAXXY=AST(1,3)/AST(3,3)
      ETAYXY=AST(2,3)/AST(3,3)
C
C**** PRINT LAMINATE PROPERTIES
C
      WRITE(6,270)
  270 FORMAT(/,5X,'**********ELASTIC PROPERTIES OF LAMINATE**********')
      WRITE (6,280) EX,EY,GXY,VXY,VYX,ETAXYX,ETAXYY,ETAXXY,ETAYXY
  280 FORMAT(/,5X,'EX = ',E10.3,10X,'EY = ',E10.3,10X,'GXY = ',E10.3,
     *//,5X,'POISSON S RATIO XY = ',F10.6,10X,'POISSON S RATIO YX = ',
     *F10.6,//,5X,'ETA XY,X = ',F10.6,15X,'ETA XY,Y = ',F10.6,//,5X,
     *'ETA X,XY = ',F10.6,15X,'ETA Y,XY = ',F10.6,//)
C
C ***** I N V E R T  ABD  M A T R I X
C
      CALL INVERS(ABD,ABHD,6)
C
C***** P R I N T  A'B'H'D'  M A T R I X
C
      IF(ICOUNT.EQ.3.OR.ICOUNT.EQ.4) GOTO 375
      WRITE (6,300)
  300 FORMAT(/,25X,'**** A PRIME MATRIX ****',35X,'**** B PRIME MATRIX
     +****',/)
      WRITE (6,320) ((ABHD(I,J),J=1,6),I=1,3)
  320 FORMAT (6(5X,E14.7))
      WRITE (6,350)
  350 FORMAT(/,25X,'**** H PRIME MATRIX ****',35X,'**** D PRIME MATRIX
     +****',/)
      WRITE (6,370) ((ABHD(I,J) ,J=1,6),I=4,6)
  370 FORMAT (6(5X,E14.7))
C
C**** CALCULATE THERMAL PROPERTIES
C
  375 CALL MULT(ABHD,THLOD,EOTH,6)
      IF (TEMP.EQ.0.0) GOTO 7
      ALF(1)=EOTH(1)/TEMP
      ALF(2)=EOTH(2)/TEMP
      ALF(3)=EOTH(3)/TEMP
      WRITE (6,290) (ALF(I),I=1,3)
  290 FORMAT (5X,'COEFF. OF THERMAL EXPANSION   X= ',E10.3,/,35X,'Y= '
```

```
     *,E10.3,/,35X,'XY= ',E10.3,//)
C
C**** C A L C U L A T E   M I D P L A N E   S T R A I N S
C**** A N D   C U R V A T U R E S
C
    7 IF(ICOUNT.LE.3) THEN
      NNN=1
      STSLAM(NNN,2)=P
      ELSE
      WRITE (6,400) NNN
  400 FORMAT (//,10X,'POINT # ',I3,/)
      ENDIF
      DO 65 J=1,3
   65 SLAM(J)=STSLAM(NNN,J)*TH
C     WRITE(6,*)SLAM(J)
      DO 66 J=4,6
   66 SLAM(J)=0.
      CALL MULT (ABHD,SLAM,EK,6)
      WRITE (6,440)
  440 FORMAT (//,10X,'******* MIDPLANE STRAINS AND CURVATURES ******',/)
      WRITE (6,460) (EK(I),I=1,6)
  460 FORMAT (5X,'EPSX= ',E10.4,5X,'EPSY= ',E10.4,5X,'GAMAXY=',E10.4
     +,//,5X,'KX= ',E10.4,5X,'KY= ',E10.4,5X,'KXY= ',E10.4,/)
C
C************  C A L C U L A T E   S T R A I N S
C
      IF(LCOUNT.EQ.0) GOTO 999
      DO 70 K=1,NOL
      KK=2*K-1
      N=K+1
      DO 70 I=1,3
      II=I+3
      STN(K,I)=EK(I)+Z(K)* EK(II)
      STN(N,I)=EK(I)+Z(N)* EK(II)
      STNMEC(KK,I)=STN(K,I)-STNTH(K,I)
      STNMEC(KK+1,I)=STN(N,I)-STNTH(K,I)
   70 CONTINUE
C
C******C A L C U L A T E   S T R E S S E S
C
      CALL STRESS (NOL,NOL1,NOL3,NOL22,STRG,QBAR,LCNT2,STN,Z,ANG,STS
     &,ST12,THICK,TH,STNMEC)
  999 RETURN
      END
C
C             S U B R O U T I N E   X Y P R O P
C
C****  THIS SUBROUTINE WOULD CALCULATE PLY STIFFNESS AND COMPLIANCE
C****  MATRICES
      SUBROUTINE XYPROP (K,MODE,NOL,NOL1,NOL3,NOL22,ANG,THICK)
```

```
      IMPLICIT REAL*8(A-H,O-Z)
      DIMENSION ANG(50),THICK(50),SB(3,3),THETA(50)
      COMMON/STIF/ALF(3),QB(3,3),EE(2,100,50)
      COMMON/COUNT/ICOUNT,IPOINT,IHOLE,LCOUNT,NNN,NUMPLY,NOX,NOY,IDIR
      IF((ICOUNT.EQ.5).OR.(ICOUNT.EQ.3)) GOTO 5
      READ (5,*) EE(1,NNN,K),EE(2,NNN,K),G12,V12,AL1,AL2,THETA(K)
     &,THICK(K)
C
C*****C A L C U L A T E  R E D U C E D  S T I F F N E S S
C
    5 V21=V12*EE(2,NNN,K)/EE(1,NNN,K)
      WRITE(6,100) K,THETA(K),THICK(K),EE(1,NNN,K),EE(2,NNN,K),
     &G12,V12,V21,AL1,AL2
  100 FORMAT (5X,I2,5X,F7.2,10X,F5.3,6X,3(E10.3,2X),2(F5.3,2X),2(E10.3))
      Q11=EE(1,NNN,K)**2/(EE(1,NNN,K)-V12**2*EE(2,NNN,K))
      Q12=V12*EE(2,NNN,K)*EE(1,NNN,K)/(EE(1,NNN,K)- V12**2*EE(2,NNN,K))
      Q22=EE(2,NNN,K)*EE(1,NNN,K)/(EE(1,NNN,K)-V12**2*EE(2,NNN,K))
      Q66=G12
      PI=4.*DATAN(1.D0)
      ANG(K)=THETA(K)/180.*PI
      SI=DSIN(ANG(K))
      CO=DCOS(ANG(K))
      QB(1,1)=Q11*CO**4+(2*Q12+4*Q66)*(SI*CO)**2+Q22*SI**4
      QB(1,2)=(Q11+Q22-4*Q66)*(SI*CO)**2+Q12*(SI**4+CO**4)
      QB(2,1)=QB(1,2)
      QB(2,2)=Q11*SI**4+(2*Q12+4*Q66)*(SI*CO)**2+Q22*CO**4
      QB(1,3)=(Q11-Q12-2*Q66)*SI*CO**3+(Q12-Q22+2*Q66)*SI*SI*SI*CO
      QB(3,1)=QB(1,3)
      QB(2,3)=(Q11-Q12-2*Q66)*SI*SI*SI*CO+(Q12-Q22+2*Q66)*SI*CO**3
      QB(3,2)=QB(2,3)
      QB(3,3)=(Q11+Q22-2*Q12-2*Q66)*(SI*CO)**2+Q66*(SI**4+CO**4)
      DO 10  I=1,3
      DO 10  J=1,3
   10 IF (ABS(QB(I,J)).LT.1000.)  QB(I,J)=0.
      ALF(1)=AL1*CO**2+AL2*SI**2
      ALF(2)=AL1*SI**2+AL2*CO**2
      ALF(3)=(AL1-AL2)*CO*SI*2
C*****C A L C U L A T E  R E D U C E D  C O M P L I A N C E
  999 RETURN
      END
C
C*****************  S U B R O U T I N E  M U L T
C
      SUBROUTINE MULT (E,F,G,M)
      IMPLICIT REAL*8(A-H,O-Z)
      DIMENSION E(M,M),F(M),G(M)
      DO 5 II=1,M
    5 G(II)=0.
      DO 10 LL=1,M
      DO 10 JJ=1,M
```

```
      G(LL)=E(LL,JJ)*F(JJ)+G(LL)
   10 CONTINUE
      RETURN
      END
C
C***************** S U B R O U T I N E  S T R E S S
C
      SUBROUTINE STRESS (NOL,NOL1,NOL3,NOL22,STRG,QBAR,LCNT2,STN,Z,ANG
     &,STS,ST12,THICK,TH,STNMEC)
      IMPLICIT REAL*8(A-H,O-Z)
      DIMENSION   THICK(50),Z(51),ANG(50),STN(51,3)
     &,S1(3),S2(3),ST1(3),ST2(3),ST12(102,3),STS(102,3),
     &T(3,3),SL1(3),SL2(3),STRG(5),QBAR(150,3),STNMEC(102,3)
      COMMON/COUNT/ICOUNT,IPOINT,IHOLE,LCOUNT,NNN,NUMPLY,NOX,NOY,IDIR
      COMMON/STIF/ALF(3),QB(3,3),EE(2,100,50)
      COMMON/FORC/STSLAM(100,6),SLAM(6),STSPLY(2,100,50),P,PNEW,USTRGT
     &,STMAX(50),STSMAX,STG(5),R1(50)
      COMMON/XY/X1,Y1,X2,Y2,DELX,DELY,THETA1,THETA2,DTHETA,X(361),Y(361)
     &,THETAA(361),DD
C
C**** CALCULATE PLY STRESSES IN THE LAMINATE DIRECTIONS
C
      DO 40 K=1,NOL
      KP1=K+1
      KK=2*K-1
      KK1=KK+1
      DO 10 I=1,3
      II=K*3-3+I
      DO 10 J=1,3
   10 QB(I,J)=QBAR(II,J)
      DO 20 I=1,3
      S1(I)=STNMEC(KK,I)
   20 S2(I)=STNMEC(KK1,I)
      CALL MULT (QB,S1,ST1,3)
      CALL MULT (QB,S2,ST2,3)
      DO 30 I=1,3
      STS(KK,I)=ST1(I)
   30 STS(KK1,I)=ST2(I)
C
C**** CALCULATE PLY STRESSES ON THE PLY DIRECTIONS
C
      CALL ROTATE (T,K,NOL,3,ANG)
      CALL MULT (T,ST1,SL1,3)
      CALL MULT (T,ST2,SL2,3)
      DO 50 I=1,3
      ST12(KK,I)=SL1(I)
      ST12(KK1,I)=SL2(I)
   50 CONTINUE
C
C**** BENDING MOMENTS ARE NOT PRESENT AND LAMINATE IS
```

```
C**** ASSUMED TO BE SYMMETRIC. THEREFORE STRESSES IN EACH PLY ARE THE
C**** AVERAGES OF STRESSES ON TOP AND BOTTOM OF EACH PLY
      STK1=ST12(KK1,1)/2+ST12(KK,1)/2
      STK2=ST12(KK1,2)/2+ST12(KK,2)/2
      STK3=ST12(KK1,3)/2+ST12(KK,3)/2
      STSPLY(1,NNN,K)=STK1
      STSPLY(2,NNN,K)=STK2
C**** CALCULATE MAX. PLY STRESS (COMPRESSIVE)
      STMAX(K)=STK1
      IF (STK2.LT.STK1) STMAX(K)=STK2
   40 CONTINUE
C     FIND MAXIMUM COMPRESSIVE STRESS IN EACH PLY
C
      CALL MAX (NOL)
C********** P R I N T  S T R A I N S  AND  S T R E S S E S
C
      DO 60 K=1,LCOUNT
      KP1=K+1
      KK=2*K-1
      KK1=KK+1
      WRITE(6,100)
  100 FORMAT(5X,'TOTAL STRAINS IN X-Y SYSTEM',/,33X,'EX',12X,'EY',12X,
     +'GAMA XY')
      WRITE(6,150) K,(STN(K,I),I=1,3)
  150 FORMAT(5X,'TOP OF LAYER ',I2,3X,3(5X,E10.4))
      WRITE(6,200) K,(STN(KP1,I),I=1,3)
  200 FORMAT(5X,'BOTTOM OF LAYER ',I2,3(5X,E10.4),/)
      WRITE (6,250)
  250 FORMAT(5X,'MECHANICAL STRAINS IN X-Y SYSTEM',/,33X,'EX',12X,
     +'EY',12X,'GAMA XY')
      WRITE(6,150) K,(STNMEC(KK,I),I=1,3)
      WRITE(6,200) K,(STNMEC(KK1,I),I=1,3)
      WRITE(6,300)
  300 FORMAT(5X,'STRESSES IN X-Y SYSTEM',/,31X,'SIG X',12X,'SIG Y',12X,
     +'TAW XY')
      WRITE(6,350) K,(STS(KK,I),I=1,3)
  350 FORMAT(5X,'TOP OF LAYER ',I2,3X,3(5X,E11.5))
      WRITE(6,400) K,(STS(KK1,I),I=1,3)
  400 FORMAT(5X,'BOTTOM OF LAYER ',I2,3(5X,E11.5),/)
      WRITE (6,450)
  450 FORMAT(5X,'STRESSES IN 1-2 SYSTEM',/,31X,'SIG 1',12X,'SIG 2',10X
     +,'TAW 12')
      WRITE(6,350) K,(ST12(KK,I),I=1,3)
      WRITE (6,400) K,(ST12(KK1,I),I=1,3)
      STK1=ST12(KK1,1)/2+ST12(KK,1)/2
      STK2=ST12(KK1,2)/2+ST12(KK,2)/2
      STK3=ST12(KK1,3)/2+ST12(KK,3)/2
      CALL STRENG(STK1,STK2,STK3,K)
      WRITE(6,410)R1(K)
  410 FORMAT(5X,'SRENGTH RATIO IS',10X,'R1=',F10.4)
```

```
   60 CONTINUE
  999 RETURN
      END
C
C******************  S U B R O U T I N E   I N V E R S E **********
C
      SUBROUTINE INVERS (AINV,BINV,NMAX)
      IMPLICIT REAL*8(A-H,O-Z)
      DIMENSION AINV(NMAX,NMAX),BINV(NMAX,NMAX)
      DO 20 N=1,NMAX
      D=AINV(N,N)
      DO 5 J=1,NMAX
    5 AINV(N,J)=-AINV(N,J)/D
      DO 10 I=1,NMAX
      IF(N-I.EQ.0) GOTO 10
      DO 15 K=1,NMAX
      IF(N-K.EQ.0) GOTO 15
      AINV(I,K)= AINV(I,K)+AINV(I,N)*AINV(N,K)
   15 CONTINUE
   10 AINV(I,N)=AINV(I,N)/D
      AINV(N,N)=1.0/D
   20 CONTINUE
      DO 25 I=1,NMAX
      DO 25 J=1,NMAX
   25 BINV(I,J)=AINV(I,J)
      RETURN
      END
C
C*********************  S U B R O U T I N E   S T R E N G T H
C
      SUBROUTINE STRENG (ST1,ST2,SH,K)
      IMPLICIT REAL*8(A-H,O-Z)
      COMMON/FORC/STSLAM(100,6),SLAM(6),STSPLY(2,100,50),P,PNEW,USTRGT
     &,STMAX(50),STSMAX,STG(5),R1(50)
      F11=1/(STG(1)*STG(2))
      F1=1/STG(1)-1/STG(2)
      F22=1/(STG(3)*STG(4))
      F2=1/STG(3)-1/STG(4)
      F66=1/STG(5)**2
      F12=-.5*SQRT(F11*F22)
      FIJ=F11*ST1**2+2*F12*ST1*ST2+F22*ST2**2+F66*SH**2
      FI=F1*ST1+F2*ST2
      RR=SQRT(FI**2+4*FIJ)
      R1(K)=(RR-FI)/(2*FIJ)
C     R2=(-RR-FI)/(2*FIJ)
      RETURN
      END
C
C     S U B R O U T I N E     R O T A T E
C
```

```
      SUBROUTINE ROTATE(T,K,NOL,N,ANG)
      IMPLICIT REAL*8(A-H,O-Z)
      DIMENSION T(N,N),ANG(50)
      T(1,1)=DCOS(ANG(K))*DCOS(ANG(K))
      T(1,2)=DSIN(ANG(K))*DSIN(ANG(K))
      T(1,3)=DSIN(ANG(K))*DCOS(ANG(K))*2.
      T(2,1)=T(1,2)
      T(2,2)=T(1,1)
      T(2,3)=-T(1,3)
      T(3,1)=T(2,3)/2
      T(3,2)=-T(3,1)
      T(3,3)=T(1,1)-T(1,2)
      RETURN
      END
C
C**** S U B R O U T I N E     M O D I F Y
C
      SUBROUTINE MODIFY(NOL)
      IMPLICIT REAL*8(A-H,O-Z)
      COMMON/COUNT/ICOUNT,IPOINT,IHOLE,LCOUNT,NNN,NUMPLY,NOX,NOY,IDIR
      COMMON/STIF/ALF(3),QB(3,3),EE(2,100,50)
      COMMON/FORC/STSLAM(100,6),SLAM(6),STSPLY(2,100,50),P,PNEW,USTRGT
     &,STMAX(50),STSMAX,STG(5),R1(50)
      WRITE(6,55) NNN
   55 FORMAT(//,10X,'*** LAMINATE PROPERTIES ARE MODIFIED AT POINTS 1'
     &,' THRU ',I2,/)
      DO 10 K=1,NOL
      DO 10 J=1,2
      EPS=(-.10456617+DSQRT(.010934084+4.2918D-8*STSPLY(J,NNN,K)))/2
      EE(J,NNN,K)=186402118*EPS+9745678
   10 CONTINUE
      RETURN
      END
C
C     S U B R O U T I N E      B E A M
C
C
C********** S U B R O U T I N E     H O L E
C
      SUBROUTINE HOLE
C
C     COMPUTE STRESSES AROUND THE HOLE
C
      IMPLICIT REAL*8(A-H,O-Z)
      COMMON/PROP/EX,EY,VXY,GXY,TEMP,TH
      COMMON/FORC/STSLAM(100,6),SLAM(6),STSPLY(2,100,50),P,PNEW,USTRGT
     &,STMAX(50),STSMAX,STG(5),R1(50)
      COMMON/COUNT/ICOUNT,IPOINT,IHOLE,LCOUNT,NNN,NUMPLY,NOX,NOY,IDIR
      COMMON/XY/X1,Y1,X2,Y2,DELX,DELY,THETA1,THETA2,DTHETA,X(361),Y(361)
     &,THETAA(361),DD
```

```
      COMPLEX*16 ZZ(2),ZETAB(2),PHIPRM(2),MU(2),AB(2),ZAB(2)
      COMPLEX*16 ALFAA,BETAA,II,EGV,FACT
      PI=4.*DATAN(1.D0)
      IF(IHOLE.EQ.2) GOTO 2
C     EQUATION OF THE LINE FOR CHARACTERISTIC DISTANCES IS E+F*TH
      READ(5,200) PHI,AA,BB,E,F,W
 200  FORMAT(5(T50,F15.7,/),T50,F15.7)
      IF ((AA.EQ.0.0).AND.(BB.EQ.0.0)) GOTO 999
C
C**** EITHER NOX OR NOY MUST BE NONZERO
C
      READ(5,300) X1,Y1,X2,Y2,NOX,NOY,IDIR
 300  FORMAT(4(T50,F15.7,/),2(T50,I2,/),T50,I1)
   2  DD=E+F*TH
      Y1=0
      Y2=0
      X2=DD+X1
      NOY=0
      IDIR=1
      PHI=90
      WRITE(6,10)
  10  FORMAT(//'********** HOLE PARAMETERS **********')
      WRITE(6,20)PHI,AA,BB
  20  FORMAT(/,1X,'PHI=',F6.2,5X,'SEMI-MAJOR AXIS=',F6.3,10X,
     &'SEMI-MINOR AXIS=',F6.3)
      WRITE(6,25) EX,EY,VXY,GXY
  25  FORMAT(/,1X,'EX=',E10.4,5X,'EY=',E10.4,5X,'NUXY=',F6.3,5X,'GXY='
     &  ,E10.4)
      IF(NOX.NE.0) THEN
      DELX=(X2-X1)/NOX
      ELSE
      DELX=0.D0
      ENDIF
      IF(NOY.NE.0) THEN
      DELY=(Y2-Y1)/NOY
      ELSE
      DELY=0.D0
      ENDIF
      WRITE(6,30) X1,Y1,X2,Y2,DELX,DELY
  30  FORMAT(1X,'X1=',F8.5,3X,'Y1=',F8.5,5X,'X2=',F8.5,3X,'Y2=',F8.5
     &,/,1X,'X INCREMENT=',F8.5,10X,'Y INCREMENT=',F8.5)
      II=DCMPLX(0.D0,1.D0)
      EGV=DCMPLX(EX/GXY-2.*VXY,0.D0)
      EE=4.*EX/EY
      MU(1)=CDSQRT((-EGV+ CDSQRT(EGV**2-EE))/2.)
      MU(2)=CDSQRT((-EGV- CDSQRT(EGV**2-EE))/2.)
      IF(DIMAG(MU(1)).LT.0.D0) MU(1)=-MU(1)
      IF(DIMAG(MU(2)).LT.0.D0) MU(2)=-MU(2)
      WRITE(6,50) MU(1),MU(2)
  50  FORMAT(1X,'MU1=',E10.4,1X,E10.4,'I',10X,'MU2=',E10.4,1X,E10.4,'I')
```

```
      WRITE(6,60)P
   60 FORMAT(/,5X,'STRESSES ALONG A LINE BETWEEN POINTS (X1,Y1) AND ',
     &'(X2,Y2)',/,5X,'FOR  P=',E10.4)
   85 PHI=PHI*4.*DATAN(1.D0)/180.
      FACT=P/2*(AA*DSIN(PHI)-II*BB*DCOS(PHI))
      ALFAA=-DSIN(PHI)*FACT
      BETAA=DCOS(PHI)*FACT
      CALL LINE
      AB(1)=AA-II*MU(1)*BB
      AB(2)=AA-II*MU(2)*BB
      WRITE(6,70)
   70 FORMAT(/,'POINT#',8X,'X',9X,'Y',8X,'SIGMA X',8X,'SIGMA Y',
     &8X,'TAU XY')
      DO 100 J=1,IPOINT
      DO 95 I=1,2
      IF(X(J).LT.0) THEN
      X(J)=-X(J)
      Y(J)=-Y(J)
      ENDIF
      ZZ(I)=X(J)+MU(I)*Y(J)
      ZAB(I)=CDSQRT(ZZ(I)*ZZ(I)-AA**2-(MU(I)*BB)*(MU(I)*BB))
C     TO GET RID OF SINGULARITY DUE TO ELIMINATION OF HOLE "ZETAB" HAS
C     REPLACED ZETA
      ZETAB(I)=ZZ(I)+ZAB(I)
   95 CONTINUE
      PHIPRM(1)=AB(1)/ZAB(1)/(MU(1)-MU(2))*(MU(2)*ALFAA-BETAA)/ZETAB(1)
      PHIPRM(2)=AB(2)/ZAB(2)/(MU(1)-MU(2))*(BETAA-MU(1)*ALFAA)/ZETAB(2)
      STSLAM(J,1)=2.*REAL(MU(1)*MU(1)*PHIPRM(1)+MU(2)*MU(2)
     &*PHIPRM(2))+P*DCOS(PHI)**2
      IF(DABS(STSLAM(J,1)).LT.1.D-5)   STSLAM(J,1)=0.
      STSLAM(J,2)=2.*REAL(PHIPRM(1)+PHIPRM(2))+P*DSIN(PHI)**2
      IF(DABS(STSLAM(J,2)).LT.1.D-5)   STSLAM(J,2)=0.
      STSLAM(J,3)=-2.*REAL(MU(1)*PHIPRM(1)+MU(2)*PHIPRM(2))+
     &P*DSIN(PHI)*DCOS(PHI)
      IF(DABS(STSLAM(J,3)).LT.1.D-5)   STSLAM(J,3)=0.
      WRITE(6,90) J,X(J),Y(J),(STSLAM(J,I),I=1,3)
   90 FORMAT(1X,I3,7X,2(F7.5,3X),3(E10.4,5X))
      THETAA(J)=THETAA(J)*180./PI
  100 CONTINUE
  999 RETURN
      END
C
C ******   S U B R O U T I N E     L I N E
C
      SUBROUTINE LINE
      IMPLICIT REAL*8(A-H,O-Z)
      COMMON/COUNT/ICOUNT,IPOINT,IHOLE,LCOUNT,NNN,NUMPLY,NOX,NOY,IDIR
      COMMON/XY/X1,Y1,X2,Y2,DELX,DELY,THETA1,THETA2,DTHETA,X(361),Y(361)
     &,THETAA(361),DD
      IPOINT=1
```

```
      X(1)=X1
      Y(1)=Y1
   10 IPOINT=IPOINT+1
      IF(DABS(X2-X1).LT.1.D-5.OR.NOX.EQ.0.) THEN
      Y(IPOINT)=Y(IPOINT-1)+DELY
      X(IPOINT)=Y(IPOINT)-Y1*(X2-X1)/(Y2-Y1)+X1
      IF(DABS(Y(IPOINT)).GE.(DABS(Y2)-DELY/5)) GOTO 999
      ELSE
      X(IPOINT)=X(IPOINT-1)+DELX
      Y(IPOINT)=(Y2-Y1)/(X2-X1)*(X(IPOINT)-X1)+Y1
      IF(DABS(X(IPOINT)).GE.(DABS(X2)-DELX/5)) GOTO 999
      ENDIF
      GOTO 10
  999 RETURN
      END
C
C***** S U B R O U T I N E    I N T E G
C
      SUBROUTINE INTEG(IPOINT,K,AVGSTS)
      IMPLICIT REAL*8(A-H,O-Z)
      COMMON/XY/X1,Y1,X2,Y2,DELX,DELY,THETA1,THETA2,DTHETA,X(361),Y(361)
     &,THETAA(361),DD
      COMMON/FORC/STSLAM(100,6),SLAM(6),STSPLY(2,100,50),P,PNEW,USTRGT
     &,STMAX(50),STSMAX,STG(5),R1(50)
      SLOPE=(Y2-Y1)/(X2-X1)
      IF(DABS(X2-X1).LT.1.D-5.OR.DELX.EQ.0.) THEN
      DELXY=DELY/DSIN(DATAN(SLOPE))
      ELSE
      DELXY=DELX/DCOS(DATAN(SLOPE))
      ENDIF
      I=1
      IF(IDIR.LE.2) SUM=STSPLY(IDIR,I,K)
      IF(IDIR.GT.2) SUM=STSLAM(I,2)
      GOTO 5
    4 IF(I.EQ.IPOINT) THEN
      IF(IDIR.LE.2)  SUM=SUM+STSPLY(IDIR,I,K)
      IF(IDIR.GT.2)  SUM=SUM+STSLAM(I,2)
      GOTO 5
      ENDIF
      J=I/2
      AJ=I/2.
      IF((J+.1).GT.AJ)  THEN
      IF(IDIR.LE.2)  SUM=SUM+4*STSPLY(IDIR,I,K)
      IF(IDIR.GT.2)  SUM=SUM+4*STSLAM(I,2)
      GOTO 5
      ENDIF
      IF(IDIR.LE.2) SUM=SUM+2*STSPLY(IDIR,I,K)
      IF(IDIR.GT.2) SUM=SUM+2*STSLAM(I,2)
    5 I=I+1
      IF(I.LE.IPOINT) GOTO 4
```

```
      SUM=SUM*DELXY/3
      AVGSTS=SUM/(DELXY*(IPOINT-1))
      D=X2-X1
      WRITE(6,550) D,AVGSTS
  550 FORMAT(1X,'THE AVERAGE STRESS OVER DISTANCE ',F5.3,' INCHES FROM',
     &' THE HOLE IS ',E10.4)
  999 RETURN
      END
C
C**********   SUBROUTINE MAX
C
      SUBROUTINE MAX(NOL)
      IMPLICIT REAL*8 (A-H,O-Z)
      COMMON/FORC/STSLAM(100,6),SLAM(6),STSPLY(2,100,50),P,PNEW,USTRGT
     &,STMAX(50),STSMAX,STG(5),R1(50)
      STSMAX=STMAX(1)
      DO 10 J=1,NOL
      IF (DABS(STMAX(J)).GE.DABS(STSMAX))  STSMAX=STMAX(J)
   10 CONTINUE
      RETURN
      END
C
C**** SUBROUTINE  ADJUSTING THE STRESSES
C
      SUBROUTINE ADJ(IPOINT,NOL)
      IMPLICIT REAL*8 (A-H,O-Z)
      COMMON/FORC/STSLAM(100,6),SLAM(6),STSPLY(2,100,50),P,PNEW,USTRGT
     &,STMAX(50),STSMAX,STG(5),R1(50)
      WRITE(6,10)
   10 FORMAT(//,10X,'********** ADJUSTING STRESSES **********')
      DO 35 I=1,2
      DO 35 J=1,IPOINT
      DO 35 K=1,NOL
      STSPLY(I,J,K)=STSPLY(I,J,K)*PNEW/P
   35 CONTINUE
      DO 36 L=1,3
      DO 36 J=1,IPOINT
   36 STSLAM(J,L)=STSLAM(J,L)*PNEW/P
      RETURN
      END
C  ****  SUBROUTINE BUNDLE
C
C
      SUBROUTINE BUNDLE(TRYLOD,FIBSTG,IBEAM,FIBMAX)
      IMPLICIT REAL*8 (A-H,O-Z)
      DIMENSION XX(100),Y(100),Y1(100),QV(100),YPRIM(100),TLOAD(100),
     & QN(100),PF(11),B1(11),SIGMA(11),SF(11),HH(11),FMAX(100),
     & THETA(100)
      REAL *8 KF,KM,NULF,NUM,NU12,NU23,M(100),NLOAD,K1,K2,
     & MAXST(100),MATVOL,NUTF,NU23UP,NU23LOW,KC
```

```
      COMMON/BMPROP/ELF,ETF,GLF,GTF,NULF,NUTF,CEL,EM,NUM,CON,
     & A,B,AMP,BL,ALPHA,FRADI,FRX,FL,START,END,STEP,S11,S12,S22,KK2
     & ,MICRO,NN,MODE,HW
      IF(IBEAM.GT.1) GOTO 11
      PI=4.*DATAN(1.DO)
      BAREA=PI*A*B
      BI=PI*A*B**3/4.
      FL=FRADI*2*FRX
      FAREA=PI*FRADI**2
      FI=PI*FRADI**4/4.
      VF=CEL*FAREA/BAREA
      VM=1-VF
      GM=EM/2/(1+NUM)
      CAPR=FRADI* DSQRT(PI/VF/DCOS(PI/6))
      CC=CAPR-2*FRADI
C     WW=2*CAPR*DCOS(PI/6)-2*FRADI
      MATVOL=CAPR**2*DCOS(PI/6)*VM
      WRITE(6,100)ELF,ETF,GLF,GTF,NULF,NUTF,CEL
  100 FORMAT ('******************** FIBER PROPERTIES ********************',
     &  /,'EL=',E10.4,10X,'ET=',E10.4,5X,/,
     &  'GLT=',E10.4,9X,'GTT=',E10.4,/,'NULT=',F10.4,7X,
     &  'NUTT=',F10.4,/,'NUMBER OF FIBERS IN A BUNDLE=', F5.0 ,/)
      WRITE(6,110) EM,GM,NUM
  110 FORMAT ('********************* MATRIX PROPERTIES ********************',
     &  /,'E=',E10.4,11X,'G=',E10.4,11X,'NU=',F6.3,/)
      WRITE(6,120) BL,BAREA,BI,A,B,VF,ALPHA,AMP,HW
  120 FORMAT ('********************  MICRO GEOMETRY  ********************',
     &  /,'L=',F10.5,10X,'CROSS-SECTIONAL AREA OF BUNDLE=',E10.3,/,
     & 'MOMENT OF INERTIA ABOUT SEMI-MAJOR AXIS OF BUNDLE=',
     & E10.4,/,'SEMI-MAJOR AXIS=',F7.5,10X,'SEMI-MINOR AXIS=',F7.5,
     & /,'FIBER VOLUME FRACTION OF BUNDLE=',F5.3,10X,/,
     & 'SHEAR CORRECTION FACTOR=',F4.2,10X,'INITIAL AMPLITUDE= 2 * '
     &  ,F10.5,/,'HARNESS NUMBER=',F3.0,/)
      WRITE(6,130)FL,FAREA,FI,FRADI
  130 FORMAT('FIBER LENGTH IN THE KINK=',F7.5,10X,'FIBER AREA=',E10.4,/,
     & 'FIBER MOMENT OF INERTIA=',E10.4,10X,'FIBER RADIUS=',E10.4,/)
      WRITE(6,140)MODE,START,END,STEP
  140 FORMAT('MODE=',I2,5X,'START=',F5.3,5X,'END=',F5.3,
     &  5X,'STEP=',F5.3,/)
C********* CALCULATE BUNDLE PROPERTIES FROM ELASTICITY SOLUTION (TSAI)
      IF (MICRO.EQ.1) THEN
      WRITE(6,150)
  150 FORMAT(5X,'TSAI"S MICROMECHANICS EQUATIONS')
      KTF=ETF/2./(1-NUTF)
      KLF=ELF/2./(1-NULF)
      KM=EM/2./(1-NUM)
      E1=VF*ELF+VM*EM
      E2=2*(1-NULF+(NULF-NUM)*VM)*((1-CON)*(KTF*(2*KM+GM)-GM*
     &  (KTF-KM)*VM)/((2*KM+GM)+2*(KTF-KM)*VM)+
```

```
     &  CON*(KTF*(2*KM+GLF)+GLF+(KM-KTF)*VM)/((2*KM+GLF)-2*(KM-KTF)*VM))
C      NU12=(KTF*NULF*(2*KM+GM)*VF+KM*NUM*(2*KTF+GM)*VM)/
C     &  (KTF*(2*KM+GM)-GM*(KTF-KM)*VM)*(1-CON)+
C     &  CON*(KM*NUM*(2*KTF+GLF)*VM+KTF*NULF*(2*KM+GLF)*VF)/(KTF*(2*KM+GM
C     & )+GLF*(KM-KTF)*VM)
       NU12=NULF*VF+NUM*VM
       G12=(1-CON)*GM*(2*GLF-(GLF-GM)*VM)/(2*GM+(GLF-GM)*VM)
     &  +CON*GLF*((GLF+GM)-(GLF-GM)*VM)/((GLF+GM)+(GLF-GM)*VM)
       ENDIF
C********** CALCULATE BUNDLE PROPERTIES FROM ELASTICITY SOLUTION (HASHIN)
       IF(MICRO.EQ.2) THEN
        WRITE(6,160)
  160 FORMAT(5X,'HASHIN"S MICROMECHANICS EQUATIONS')
       KF=ETF/3/(1-2*NUTF)
       KM=EM/3/(1-2*NUM)
       E1=EM*VM+ELF*VF+4*(NULF-NUM)**2*VM*VF/(VM/KF+VF/KM+1/GM)
       NU12=NUM*VM+NULF*VF+(NULF-NUM)*(1/KM-1/KF)*VM*VF/
     &  (VM/KF+VF/KM+1/GM)
       G12=GM*(GM*VM+GLF*(1+VF))/(GM*(1+VF)+GLF*VM)
       BETA1=KM/(KM+2*GM)
       BETA2=KF/(KF+2*GTF)
       GAMMA=GTF/GM
       ALFA=(BETA1-GAMMA*BETA2)/(1+GAMMA*BETA2)
       RO=(GAMMA+BETA1)/(GAMMA-1)
       IF(GTF.GT.GM) THEN
       G23UP=GM*(1+(1+BETA1)*VF/(RO-VF*(1+3*BETA1*BETA1*VM*VM/(ALFA
     &  *VF*VF*VF+1))))
       G23LOW=GM+VF/(1/(GTF-GM)+(KM+2*GM)*VM/(2*GM*(KM+GM)))
       G23=(G23LOW+G23UP)/2
       ENDIF
       IF(GTF.LT.GM) THEN
       G23LOW=GM*(1+(1+BETA1)*VF/(RO-VF*(1+3*BETA1*BETA1*VM*VM/(ALFA
     &  *VF*VF*VF-BETA))))
       G23UP=GM+VF/(1/(GTF-GM)+(KM+2*GM)*VM/(2*GM*(KM+GM)))
       G23=(G23LOW+G23UP)/2
       ENDIF
       KC=(KM*(KF+GM)*VM+KF*(KM+GM)*VF)/((KF+GM)*VM+(KM+GM)*VF)
       AM=1+4*KC*NU12**2/E1
       E2UP=4*KC*G23UP/(KC+AM*G23UP)
       E2LOW=4*KC*G23LOW/(KC+AM*G23LOW)
       E2=(E2UP+E2LOW)/2
       NU23UP=(KC-AM*G23LOW)/(KC+AM*G23LOW)
       NU23LOW=(KC-AM*G23UP)/(KC+AM*G23UP)
       NU23=(NU23UP+NU23LOW)/2
       ENDIF
C  ************************************************************************
       IF(NU23.GE.NUM) THEN
       NU23=NU23LOW
       WRITE(6,170)
  170 FORMAT(10X,'*** LOWER BOUND POISSON S RATIO IS USED FOR NU23 ***')
```

```
      ENDIF
      S11P=1/E1
      S22P=1/E2
      S12P=-NU12/E1
      S21P=S12P*E2
      S23P=-NU23/E2
      S11=(S11P-S12P*S12P/S22P)
      S12=(S12P-S12P*S23P/S22P)
      S22=(S22P-S23P*S23P/S22P)
      BEZB=3*BL*PI*A*B/(PI*A+E2/E1*1.5*BL)
      EI=E1*BI
      WRITE(6,180) KF,KM
  180 FORMAT('FIBER BULK MODULUS=',E10.4,5X,'MATRIX BULK MODULUS='
     &  ,E10.4)
      WRITE(6,190) E1,E2UP,E2LOW,E2,NU12,NU23UP,NU23LOW,NU23,
     & G12,G23UP,G23LOW,G23
  190 FORMAT ('E1=',E10.4,5X,'E2UP=',E10.4,5X,'E2LOW=',E10.4,
     &  5X,'E2=',E10.4,/,
     &  'NU12=',F6.3,7X,'NU23UP=',F6.3,7X,'NU23LOW=',F6.3,7X,
     &  'NU23=',F6.3,/'G12=',E10.4,
     &  4X,'G23UP=',E10.4,4X,'G23LOW=',E10.4,4X,'G23=',E10.4,//)
      WRITE(6,200) S11,S12,S22
  200 FORMAT(/,'******** PLANE STRAIN COMPLIANCES OF FOUNDATION *******'
     & ,/,'S11=',E10.4,10X,
     & 'S12=',E10.4,10X,'S22=',E10.4)
      IF(MODE.EQ.1) GOTO 1000
    2 AG=BAREA*G12
      A13=-NU12/E1
      A66=1/G12
      A55=A66
      C=A/B
C
C********** CALCULATE BUNDLE RESULTANT FORCES AND DEFORMATIONS
C
   11 NLOAD=TRYLOD*BEZB
      WRITE(6,210)TRYLOD
  210 FORMAT(10X,'STARTING LOAD FOR TRIAL AND ERROR=',E10.4,/)
      SDENOM=-S11*S12+3*S11*S22-S12*S12-S12*S22
      i=0
      H=.75*HW
      X=START
    5 I=I+1
      XX(I)=X
      Y(I)=2*AMP/H
      YPRIM(I)=0
C     Y1PRIM(I)=0
C     Y1DPRIM(I)=0
      Y1(I)=0
      QV(I)=0
```

```
      M(I)=0
C START DO LOOP ON THE SUMMATION
      DO 10 N=1,NN
      LAMBDA=2*N*PI/H/BL
      K1=2*(2*A*LAMBDA*(B*LAMBDA*(S12+S22)+2*S11))/SDENOM
      K2= 2*(2*A*B*(2*B*LAMBDA*S22+S11+S12))/SDENOM
      IF(IBEAM.EQ.5)  THEN
      IF(N.EQ.1.AND.I.EQ.1) WRITE(6,220) K1,K2
      ENDIF
C 30  CONTINUE
  220 FORMAT(5X,'K1=',F15.2,20X,'K2=',F15.2)
      IF (2*N.LT.(H+.01).AND.2*N.GT.(H-.01)) GOTO 20
      AN=2*AMP/H*(H/N/PI*DSIN(2.*N*PI/H)+DSIN((1-2.*N/H)*PI)/
     & (1-2.*N/H)/PI+DSIN((1+2.*N/H)*PI)/(1+2.*N/H)/PI)
      GOTO 25
   20 AN=2*AMP/H*(H/N/PI*DSIN(2.*N*PI/H)+1+DSIN((1+2.*N/H)*PI)/
     &  (1+2.*N/H)/PI)
   25 DIN=(2.*N*PI/BL/H)**2*EI+(H/2./N*BL/PI)**2*K1+
     &   ALPHA*K1*EI/AG+K2-NLOAD
      CN=NLOAD*AN/DIN
      Y(I)=Y(I)+AN*(DIN+NLOAD)/DIN*DCOS(2.*N*PI*X/H)
      Y1(I)=Y1(I)+NLOAD*AN/DIN*DCOS(2.*N*PI*X/H)
   17 YPRIM(I)=YPRIM(I)-AN*(DIN+NLOAD)*(2.*N*PI/H/BL)/DIN*
     &   DSIN(2.*N*PI*X/H)
C     Y1PRIM(I)=Y1PRIM(I)-NLOAD*AN/DIN*2.*N*PI/H/BL*DSIN(2.*N*PI*X/H)
C     Y1DPRIM(I)=Y1DPRIM(I)-NLOAD*AN/DIN*(2.*N*PI/H/BL)**2
C    & *DCOS(2.*N*PI*X/H)
   18 M(I)=M(I)+AN*NLOAD*(EI*(2.*N*PI/BL/H)**2+ALPHA*K1*EI/AG)/DIN
     &*DCOS(2.*N*PI*X/H)
      QV(I)=QV(I)+AN*NLOAD*(H*BL/2./N/PI*K1)/DIN*
     &  DSIN(2.*N*PI*X/H)
      IF(MODE.NE.3) GOTO 10
      WRITE (6,230) N,Y(I),Y1(I),YPRIM(I),M(I),QV(I)
  230 FORMAT(5X,I3,5(E11.4,2X))
   10 CONTINUE
      IF(YPRIM(I).GE.0) THETA(I)=DACOS(1/DSQRT(YPRIM(I)**2+1))
      IF(YPRIM(I).LT.0) THETA(I)=-DACOS(1/DSQRT(YPRIM(I)**2+1))
C     WRITE(6,*) THETA(I)
C     QN(I)=(QV(I)+NLOAD*YPRIM(I))/(1+YPRIM(I)**2)**.5
C     TLOAD(I)=(NLOAD-QV(I)*YPRIM(I))/(1+YPRIM(I)**2)**.5
      X=X+STEP
      IF(X.LT.END) GOTO 5
      IF(IBEAM.EQ.5) WRITE (6,240)
  240 FORMAT('X',12X,'Y',12X,'Y1',12X,'M',12X,'QV',7X,'Y1/Y')
      II=(END-START)/STEP+1
      DO 60 I=1,II
      Y1OY=Y1(I)/(Y(I)-Y1(I))
      IF(IBEAM.EQ.5) WRITE(6,250)  XX(I),Y(I),Y1(I),M(I),QV(I),Y1OY
  250 FORMAT (F5.3,4X,4(E9.3,4X),E10.4)
```

```
   60 CONTINUE
C     WRITE (6,211)
C 211 FORMAT('X',10X,'QN',10X,'TLOAD',8X,'YPRIM',8X,'Y1PRIM',8X,
C    & 'Y1DPRIM')
C     DO 65 I=1,II
C     WRITE(6,260)  XX(I),QN(I),TLOAD(I),YPRIM(I)
C 260 FORMAT (F5.3,3X,3(E9.3,4X))
C 65  CONTINUE
C
C******* CALCULATE FIBER MAXIMUM STRESS
C
   51 L1=START/STEP+1
      L2=END/STEP+1
      HYPER=1.
      DO 50 L=L1,L2
      POINT=(L-1)*STEP-START
      IF(MODE.EQ.5) GOTO 271
      IF(IBEAM.EQ.5) WRITE(6,270)POINT,L
  270 FORMAT(//,5X,'STRESSES AT POINT ',F5.2,'L',5X,I2,/)
  271 CT=DCOS(THETA(L))
      ST=DSIN(THETA(L))
C     WRITE(6,*)CT,ST
   52 DO 55 I=1,11
      YY=B/10.*(I-1)
      SX=-NLOAD/BAREA*CT-DABS(M(L))*YY/CT/(PI*A*(B/CT)**3/4.)
      TXY=QV(L)/BAREA*CT
C     WRITE(6,*) SX,TXY
C TRANSFORM TO LOCAL COORDINATES
      SXLOC=SX*CT**2+2*TXY*ST*CT
      TXYLOC=-SX/2*DSIN(2*THETA(L))+TXY*DCOS(2*THETA(L))
C     WRITE(6,*) SXLOC,TXYLOC
C     YYMAX= B/A * DSQRT(A**2-ZZ**2)+B/50
C     PF(I)=(TLOAD(L)/BAREA+DABS(M(L)*(I-1)/10.*B/BI))*FAREA*ELF/E1
      PF(I)=DABS(SXLOC*FAREA*ELF/E1)
      B1(I)=((MATVOL*GM*(1+2*FRADI/CC)**2-PF(I))/ELF/FI)
C     *************************
      IF(B1(I).LT.0) THEN
      B1(I)=DSQRT(-B1(I))
      NQ=3
      HH(I)=-(DCOS(B1(I)*FL)-1)/DSIN(B1(I)*FL)/B1(I)
      ENDIF
C     *************************
      IF(B1(I).EQ.0.0) THEN
      HH(I)=0
      NQ=2
      ENDIF
C     ************************
      IF(B1(I).GT.0.0) THEN
      B1(I)=DSQRT(B1(I))
      IF(B1(I).GT.20) THEN
```

```
      HH(I)=1/B1(I)
      NQ=1
      ELSE
      HH(I)= ((DEXP(B1(I)*FL)+DEXP(-B1(I)*FL))/(DEXP(B1(I)*FL)-
     &DEXP(-B1(I)*FL))-2/(DEXP(B1(I)*FL)-DEXP(-B1(I)*FL)))/B1(I)
      NQ=1
      ENDIF
      ENDIF
C     ************************
C     WRITE (6,610) NQ
C 610 FORMAT(5X,'EQUATION NUMBER ',I1,' IS USED')
C     DO 55 J=1,11
C     YY=B/10.*(I-1)
C     ZZ=A/10.*(J-1)
C     YYMAX= B/A * DSQRT(A**2-ZZ**2)+B/50
C     SF(I,J)=DABS(QN(L)/BAREA)*FAREA
      SF(I)=DABS(TXYLOC)*FAREA
      IF(NQ.EQ.1.OR.NQ.EQ.3) SIGMA(I)=PF(I)/FAREA+SF(I)*FRADI/FI
     &*HH(I)
      IF(NQ.EQ.2) SIGMA(I)=PF(I)/FAREA+SF(I)*FRADI*FL/FI/2.
   55 CONTINUE
C     WRITE(6,650)(PF(I),I=1,11)
C 650 FORMAT (5X,'PF=',F10.4)
C     WRITE(6,651)(B1(I),I=1,11)
C 651 FORMAT (5X,'B1=',E10.4)
      FMAX(L)= SIGMA(1)
      DO 56 I=1,10
      II=I+1
      IF(SIGMA(II).GT.FMAX(L)) GOTO 57
      GOTO 56
   57 FMAX(L)=SIGMA(II)
   56 CONTINUE
      IF(IBEAM.EQ.5) WRITE(6,280) POINT,FMAX(L)
  280 FORMAT(F5.2,5X,E10.4)
      IF(MODE.EQ.5) GOTO 50
      IF(IBEAM.EQ.5) WRITE (6,290)(SIGMA(I),I=1,11)
  290 FORMAT(//,11(E10.4,1X))
   50 CONTINUE
      FIBMAX=FMAX(L1)
      DO 95 L=L1+1,L2
   95 IF(FMAX(L).GE.FIBMAX) FIBMAX=FMAX(L)
  102 CONTINUE
 1000 RETURN
      END
```

The vita has been removed from the scanned document